

## รายงานวิจัยฉบับสมบูรณ์

## โครงการ

วัสดุนาโนไฮบริดของเคลย์และสารที่มีสมบัติเชิงแสง Clay-photoactive species nanohybrid materials

หัวหน้าโครงการวิจัยผู้รับทุน รศ.ดร.นิธิมา เคารพาพงศ์ มหาวิทยาลัยขอนแก่น

## รายงานวิจัยฉบับสมบูรณ์

### โครงการ

วัสดุนาโนไฮบริดของเคลย์และสารที่มีสมบัติเชิงแสง Clay-photoactive species nanohybrid materials

หัวหน้าโครงการวิจัยผู้รับทุน รศ.ดร.นิธิมา เคารพาพงศ์ มหาวิทยาลัยขอนแก่น

สหับสนุนโดยสำหักงานสำหักงานกองทุนสหับสนุนการวิจัยและมหาวิทยาลัยขอนแก่น (ความเห็นในรายงานนี้เป็นของผู้วิจัย สกว. และมหาวิทยาลัยขอนแก่นไม่จำเป็นต้องเห็นด้วยเสมอไป)

#### บทคัดย่อ

ได้เตรียมวัสดุไฮบริดของแลดเมียมซิลิไนด์กับเลเยอร์อนินทรีย์ชนิดต่าง ๆ โดยการทำปฏิกิริยาใน สถานะของเหลว และพิสูจน์เอกลักษณ์ของวัสดุไฮบริด โดยเทคนิกการเลี้ยวเบนของรังสีเอกซ์ เทคนิก การวิเคราะห์เชิงความร้อน ฟูเรียทรานฟอร์มอินฟราเรดสเปกโทรสโกปี กล้องจุลทรรสน์อิเล็กตรอนแบบ ส่องผ่าน กล้องจุลทรรสน์อิเล็กตรอนแบบส่องกราด รามานสเปกโทรสโกปี ยูวีวิสิเบิลสเปกโทรสโกปี และโฟโตลูมิเนสเซนต์สเปกโทรสโกปี การเกิดอนุภาคแคดเมียมซิลิในด์ในวัสดุไฮบริดสามารถยืนยันได้ จากสเปกตรัมการดูดกลืนและสเปกตรัมเปล่งแสงของแคดเมียมซิลิในด์ในเลเยอร์อนินทรีย์ต่าง ๆ ได้แก่ มอนต์มอริลโลในต์ แมกกาดิไอด์ และออกโทซิลิเกต วัสดุไฮบริดที่ได้แสดงค่าเริ่มต้นของการดูดกลืน แสงในช่วง 521-593 นาโนเมตร เมื่อเปรียบเทียบค่าเริ่มต้นการดูดกลืนแสงของวัสดุไฮบริด กับแคดเมียม ซิลิในด์อิสระ ได้พบการเลื่อนตำแหน่งของค่าเริ่มต้นการดูดกลืนแสงไปยังค่าพลังงานที่มากขึ้น ซึ่งเป็น ลักษณะของปรากฏการณ์ควอนตัมคอนไฟน์เมนต์ที่เกิดกับอนุภาคแคดเมียมซิลิในด์ การปรากฏของค่า เปล่งแสงที่ 536-565 นาโนเมตรของวัสดุไฮบริด แสดงว่า เลเยอร์อนินทรีย์มีผลต่อการเปลี่ยนแปลงค่าการ เปล่งแสงของอนุภาคแคดเมียมซิลิในด์อนุภาคแคดเมียมซิลิในด์ที่เตรียมในเลเยอร์อนินทรีย์มีรูปร่างกลม แบบขนาดประมาณ 1.2-10 นาโนเมตร และมีการกระจายตัวที่สม่าเสมอในช่องว่างระหว่างเลเยอร์

คำสำคัญ วัสคุไฮบริค แคคเมียมซิลิในค์ มอนต์มอริลโลในต์ แมกกาดิไอค์ ออกโทซิลิเกต

#### **ABSTRACT**

Hybridization of cadmium selenide (CdSe) and layered inorganic solids was sucessfully investigated by conventional reaction. The hybrids were characterized by powder X-ray diffraction, thermal analysis, Fourier transmission infrared spectroscopy, transmission and scanning electron microscopies, as well as Raman, UV-Vis and photoluminescence spectroscopies. The formation of CdSe in the interlayer space of layered inorganic solids was confirmed by the spectroscopic observations. The diffuse reflectance absorption spectra of the hybrids of CdSe in layered inorganic solids (montmorillonite, magadiite, octosilicate and kanemite) showed the absorption onsets at 521-593 nm. By comparison with the bulk CdSe, the blue-shift of the absorption onset of the hybrids was ascribed to the quantum sized effect of CdSe nanoparticles. The photoluminescence spectra of CdSe in layered inorganic materials exhibited emission peaks at 536-565 nm. The round-shaped CdSe nanoparticles with the sizes of 1.2-10 nm were uniformly distributed in between the silicate layers of the hosts.

Keywords Hybrid material, cadmium selenide, montmorillonite, magadiite, octosilicate

DBG530004

## หน้าสรุปโครงการ (Executive Summary) โครงการ: วัสดนาโนไฮบริดของเคลย์และสารที่มีสมบัติเชิงแสง

### 1. วัตถุประสงค์ของโครงการ

- 1.1 ศึกษาวิธีการเตรียม อนุภาคนาโนของแคคเมียมซิลิในค์อิสระ อนุภาคนาโนของแคคเมียมซิลิในค์ที่ปรับปรุงผิว ด้วยสารลดแรงตึงผิว และวัสดุใฮบริดของอนุภาคนาโนของแคดเมียมซิลิในค์กับมอนต์มอริลโลในต์ ซึ่งเตรียมด้วยวิธี ต่าง ๆ
- 1.2 ศึกษาและวิเคราะห์อนุภาคนาโนของแคดเมียมซิลิในค์อิสระ อนุภาคนาโนของแคดเมียมซิลิในค์ ที่ปรับปรุงผิว และวัสคุใฮบริดของอนุภาคนาโนของแคดเมียมซิลิในค์กับมอนต์มอริลโลในต์ โดยเทคนิคการเลี้ยวเบนของรังสีเอกซ์ แบบผง (XRD) การวิเคราะห์เชิงความร้อน (TG-DTA) การถ่ายภาพด้วยกล้องจุลทรรศน์อิเล็กตรอนแบบส่องผ่าน (TEM) และการหาหมู่ฟังก์ชันในสารประกอบโดยเทคนิคอินฟราเรดและรามานสเปกโทรสโกปี
- 1.3 ศึกษาสมบัติเชิงแสง (optical properties) ของอนุภาคนาโนของแคดเมียมซิลิในค์อิสระ อนุภาคนาโนของ แคดเมียมซิลิในค์ที่ปรับปรุงผิว และวัสคุไฮบริดของอนุภาคนาโนของแคดเมียมซิลิในค์กับเลเยอร์อนินทรีย์ชนิดต่าง ๆ โดยเทคนิคอัลตราไวโอเลต-วิสิเบิลสเปกโทรสโกปี (UV-Vis spectroscopy) และโฟโตลูมิเนสเซนสเปกโทรสโกปี (PL spectroscopy)
  - 1.4 ศึกษาความเสถียรและประสิทธิภาพในการเร่งปฏิกิริยาเชิงแสงของผลิตภัณฑ์บางชนิคที่ได้

## 2. สิ่งที่ได้ดำเนินการไปอย่างย่อๆ และสิ่งที่ได้ค้นพบ

ทำการเตรียมแลดเมียมซิลิในด์-มอนต์มอริลโลในต์ โดยศึกษาผลของปริมาณของแลดเมียมซิลิในด์ต่อการเลิด อนุภาคนาโนในช่องว่างระหว่างเลเยอร์ของมอนต์มอริลโลในต์ หลังจากทำปฏิกิริยาการแลกเปลี่ยนใอออนระหว่าง HDTMA กับใอออนของโซเดียมในมอนต์มอริลโลในต์ โดยปริมาณของ HDTMA ที่ใช้เป็น 1, 2, 3 และ 4 เท่าของ ค่า ความสามารถในการแลกเปลี่ยนใอออน (cation exchange capacity, CEC) ได้ผลิตภัณฑ์ CdSe-HDTMA-montmorillonite(1), CdSe-HDTMA-montmorillonite(2), CdSe-HDTMA-montmorillonite(3) และ CdSe-HDTMA-montmorillonite(4) ที่มีลักษณะเป็นผงสีส้มแดง เมื่อนำผลิตภัณฑ์ที่ได้ไปศึกษาด้วยเทคนิคการเลี้ยวเบนรังสีเอ็กซ์แบบผง พบค่าระยะห่างระหว่างเลเยอร์ที่เพิ่มขึ้น แสดงว่า เมื่อเพิ่มอัตราส่วนโมลทำให้แคดเมียมซิลิในด์ สามารถแทรกเข้าไปใน ช่องว่างระหว่างเลเยอร์ของมอนต์มอริลโลในต์ได้มากขึ้น การศึกษาด้วยเทคนิคยูวี-วิสิเบิลและโฟโต-ลูมิเนสเซนต์ สเปกโทรสโกปี พบว่า เมื่อเพิ่มอัตราส่วนโดยโมลของแคดเมียมซิลิในด์เพิ่มขึ้น อนุภาคแคดเมียมซิลิ-ในด์แทรกเข้าไป ในช่องว่างระหว่างเลเยอร์ของออร์แกโนมอนต์มอริลโลในต์ได้มากขึ้น และอนุภาคมีขนาดใหญ่ขึ้น

การเตรียมวัสคุออร์แกโนเมกะดิไอต์ (HDTMA-magadiite) กับแกดเมียมซิลิในด์โดยใช้ปริมาณของแกดเมียม ซิลิ ในค์เป็น 0.25, 0.5 และ 1 เท่าของค่า CEC ของเมกะดิไอต์ ได้สารประกอบ CdSe-HDTMA-magaditte(0.25), CdSe-HDTMA-magaditte(0.5) และ CdSe-HDTMA-magaditte(1) นำผลิตภัณฑ์ที่ได้ไปศึกษาโดยเทคนิกการเลี้ยวเบนรังสี เอ็กซ์แบบผง พบว่าค่าระยะห่างระหว่างเลเยอร์เพิ่มขึ้น แสดงว่า มีการแทรกของ HDTMA และ CdSe ในช่องว่าง ระหว่างเลเยอร์ เมื่อเพิ่มปริมาณของแกดเมียมซิลิในด์ขึ้น ไม่พบการเพิ่มขึ้นของค่าระยะห่างระหว่างเล-เยอร์อย่างมี นัยสำคัญ ผลการศึกษา CdSe-HDTMA-octosilicate(n) แสดงว่า สามารถเตรียมสารประกอบ CdSe-HDTMA-octosilicate ได้โดยโดยปฏิกิริยาระหว่างของแข็งกับของเหลว การปรากฏของค่าเริ่มต้นของการคูดกลืน และการ เปล่งแสงของตัวอย่างทั้ง 3 ตัวอย่างนั้น แสดงให้เห็นการเกิดอนุภาคแคดเมียมซิลิในด์ในตัวอย่าง ซึ่งจากการทดลองใน ครั้งนี้ พบว่า การเตรียมวัสดุผสมโดยใช้เลเยอร์อนินทรีย์ชนิดต่าง ๆ สามารถควบคุมสมบัติเชิงแสงของแคดเมียมซิลิในด์ ได้ แม้ว่าผลิตภัณฑ์มีสมบัติเชิงแสงสูงแต่ไม่สามารถเร่งปฏิกิริยาเชิงแสงใด้ดีมาก

DBG530004

FI SEVIER

Contents lists available at ScienceDirect

## **Applied Clay Science**

journal homepage: www.elsevier.com/locate/clay



## Formation of ZnS and CdS in the interlayer spaces of montmorillonite

Nithima Khaorapapong a,\*, Areeporn Ontam a, Makoto Ogawa b

- a Department of Chemistry and Center of Excellence for Innovation in Chemistry, Faculty of Science, Khon Kaen University, Khon Kaen 40002, Thailand
- b Department of Earth Sciences and Graduate School of Creative Science and Engineering, Waseda University, Nishiwaseda 1-6-1, Shinjuku-ku, Tokyo 169-8050, Japan

#### ARTICLE INFO

Article history:
Received 15 January 2010
Received in revised form 11 June 2010
Accepted 15 June 2010
Available online 22 June 2010

Keywords: Intercalation Cadmium sulfide Montmorillonite Solid-solid reaction Zinc sulfide

#### ABSTRACT

Two types of semiconductor particles, ZnS and CdS, were formed in the interlayer spaces of montmorillonite by solid–solid reactions between Zn(II)– or Cd(II)–montmorillonite and Na<sub>2</sub>S at ambient temperature. The formation of the intercalation compounds was confirmed by powder XRD, TG–DTA and TG–MS. The *in situ* formation of ZnS and CdS nanoparticles in the interlayer spaces of montmorillonite was proved by UV–visible and photoluminescence spectroscopy. The diffuse reflectance absorption spectra of ZnS and CdS–montmorillonites exhibited the absorption onset at 345 and 541 nm, confirming the formation of ZnS and CdS nanoparticles in the interlayer spaces. The ZnS or CdS luminescence band at 583 nm for ZnS–montmorillonite or 529 nm for CdS–montmorillonite was weak due to the presence of quenching impurities in montmorillonite.

© 2010 Elsevier B.V. All rights reserved.

#### 1. Introduction

Intercalation is a method to construct functional low dimensional nanohybrid materials and has attracted interests from a wide range of scientific and industrial viewpoints (Whittingham, 1982; Ogawa, 2004). The possible ordered solids including the smectite group of layered clay minerals exhibit rich inclusion chemistry such as large specific surface area, swelling behavior, ion exchange and adsorption for organizing a wide variety of organic and inorganic guest species (Ogawa, 2004). Taking advantage of these characteristic features of smectites, the constructions, properties and applications of modified smectites have been extensively reported (Theng. 1974; Ogawa and Kuroda, 1995, 1997). The solid-solid reaction is one of the most suitable techniques to intercalate organic and inorganic guest species into the interlayer spaces of smectites. The surface modification of clay minerals with solid-state intercalation of both nonionic and cationic organic species have been described (Ogawa et al., 1989, 1990a,b, 1991, 1992a,b,c; Bujdák and Slosiariková, 1992). We have incorporated metal complexes into the interlayer spaces of smectites by solid-state intercalation of organic ligands and in situ complex formation at room temperature. Intercalation of 2,2'-bipyridine (Ogawa et al., 1991), 4,4'-bipyridine and 1,2-di(4-pyridine)ethylene (Khaorapapong et al., 2000, 2001), thioacetamide (Khaorapapong et al., 2002a), Na<sub>2</sub>S (Khaorapapong et al., 2008a,b, 2009) and 8hydroxyquinoline (Khaorapapong et al., 2002b; Khaorapapong and Ogawa, 2007, 2008) in smectites via solid–solid reactions and *in situ* formation has been reported.

The present paper deals with the formation of zinc sulfide and cadmium sulfide in the interlayer spaces of montmorillonite. Metal chalcogenides have gained increasing interest in the field of devices due to their size-dependent properties and great potential in the applications for optoelectronic devices such as solar cells, nonlinear optical devices, electroluminescent materials and so on (Henglein et al., 1986; Chin et al., 2001). Metal sulfide thin films have been prepared using various chemical methods for high efficiency devices (Su and Chov. 2000: Chavhan and Sharma, 2005: Öznülüer et al., 2006). The processing of the thin film, which is an ideal morphology for the optical applications, is not so simple that may result in less ordered films with low optical quality. The immobilization of metal sulfides in the restricted spaces including the interlayer spaces of smectites is attractive. The incorporation of metal sulfides into porous Vycor glass (Kuczynski and Thomas, 1985), mesoporous silicas (Hirai et al., 1999; Zhang et al., 2001), zeolites (Herron et al., 1989; Liu and Thomas, 1989), clay materials (Stramel et al., 1986; Katov et al., 1993), and polymers (Hirai et al., 2001; Antolini et al., 2005) and their optical properties have been reported so far. In our previous study, we prepared CdS in montmorillonite and reported the optical properties (Khaorapapong et al., 2008a). Nevertheless, the size and shape of the immobilized nanoparticles are not understood very well, and its solubility has never been studied yet. Therefore, further studies on the morphology and solubility are worth investigating.

Because the formation of metal sulfides in two dimensional layered materials may exhibit unique and enhanced properties, we report the intercalation of ZnS into the interlayer spaces of montmorillonite by solid-solid reactions and *in situ* formation between Zn(II)-montmorillonite and

<sup>\*</sup> Corresponding author.Tel.: +66 43 202222 41x12370 2; fax: +66 43 202373. E-mail address: nithima@kku.ac.th (N. Khaorapapong).

Na<sub>2</sub>S molecule at room temperature, morphology, and solubility in comparison with CdS-montmorillonite.

#### 2. Experimental

#### 2.1. Materials

Sodium montmorillonite (Kunipia F, Kunimine Industries Co., Ltd., the reference clay sample of the Clay Science Society of Japan) was used as a host material. The cation exchange capacity (CEC) of montmorillonite was 1.19 meq/g.  $Na_2S \cdot xH_2O$  (analytical grade) was obtained from Aldrich Co., Ltd. Zinc and cadmium chlorides supplied by Carlo Erba Agenti SpA, are also of analytical grade and used without further purification.

#### 2.2. Solid-solid reactions of Na<sub>2</sub>S with Zn(II)- and Cd(II)-montmorillonites

Zn(II)- and Cd(II)-montmorillonites were prepared by conventional ion exchange reactions in which an aqueous dispersion of montmorillonite was mixed with an aqueous solution of appropriate metal chloride, and the mixture was allowed to react for 1 day. After the ion exchange, the resulting solids were washed repeatedly with deionized water until the AgNO $_3$  test was negative. The samples were obtained and dried at 40 °C for 3 days. The amounts of the adsorbed cations were determined by inductively coupled plasma optical emission spectroscopy (ICP-OES) to confirm quantitative cation exchange. The amounts of exchanged cations were 1.15 and 1.09 meq/g of clay for Zn(II)- and Cd(II)-montmorillonites.

The reactions of  $Na_2S$  with Zn(II)- and Cd(II)-montmorillonites were carried out by solid–solid reactions as described before (Ogawa et al., 1991; Khaorapapong et al., 2000, 2001, 2002a,b, 2008a,b, 2009; Khaorapapong and Ogawa, 2007, 2008). The mixture of Zn(II)- or Z

#### 2.3. Characterization

Powder X-ray diffraction data were collected on a Bruker D8 ADVANCE diffractometer using monochromatic CuKα radiation. TEM images were taken on a JEOL JEM-2010 transition electron microscope with an accelerating voltage of 200 kV, Raman spectra were measured on a Jobin Yvon T64000 System Raman spectrometer with a 30 mW argon ion laser operating at 514 nm for excitation. Infrared spectra of the products were recorded on a Perkin Elmer Spectrum One FT-IR spectrophotometer by KBr disk method. Diffuse reflectance spectra of the solid samples were recorded on a Shimadzu UV-VIS-NIR-3101PC scanning spectrophotometer using an integrated sphere. TG-DTA curves were obtained on a Perkin Elmer Pyris Diamond TG-DTA instrument at a heating rate of 10 °C min<sup>-1</sup> under a dry air flow using  $\alpha$ -alumina ( $\alpha$ -Al<sub>2</sub>O<sub>3</sub>) as a standard material. Thermogravimetricmass spectroscopy analysis was performed on a Rigaku ThermoMass thermogravimetric-mass spectrometer (TG-DTA-MS) at a heating rate of 10 °C min<sup>-1</sup> under He flow. Inductively coupled plasma optical emission spectroscopic data were measured on a Perkin Elmer Optima 2100DV ICP-OES. Luminescence spectra were recorded on a Shimadzu RF-5301PC spectrofluorophotometer in the wavelength range of 300-900 nm with excitation at 320 nm.

#### 3. Results and discussion

#### 3.1. Reactions of Na<sub>2</sub>S with Zn(II)- and Cd(II)-montmorillonites

By the solid-solid reactions between Zn(II)-montmorillonite or Cd(II)-montmorillonite and  $Na_2S$  at the molar ratio of 1:1  $(Zn^2)$ -or

 $Cd^{2+}:S^{2-}$ ), the color (gray) and the basal spacings (d=1.54 nm for Zn(II)-montmorillonite and d = 1.49 nm for Cd(II)-montmorillonite) of the hydrated montmorillonites changed as shown in Table 1. The intercalation compounds were designated as Zn-montmorillonite-Na<sub>2</sub>S and Cd-montmorillonite-Na<sub>2</sub>S. The powder XRD pattern of Zn-montmorillonite-Na<sub>2</sub>S is shown in Fig. 1 together with that of Zn(II)-montmorillonite. After the solid-solid reactions, the basal spacing of Zn-montmorillonite-Na2S (Fig. 1b) was increased to 1.51 nm and that of Cd-montmorillonite-Na<sub>2</sub>S to 1.53 nm (Table 1). The X-ray diffraction pattern of Na<sub>2</sub>S powder was also measured (not shown) and strong reflections located at d = 0.19, 0.30, 0.31 and 0.93 nm were observed. The expansions of the interlayer spaces were determined to be 0.55 nm for Zn-montmorillonite-Na<sub>2</sub>S and 0.57 nm for Cd-montmorillonite-Na<sub>2</sub>S by subtracting the thickness of the silicate layer (0.96 nm) from the observed basal spacings. When the loading amounts of sulfide ion were increased (Zn<sup>2+</sup>or Cd<sup>2+</sup>:S<sup>2-</sup> was 1:2), the basal spacings did not increase further and the reflections due to the unreacted Na<sub>2</sub>S were detected in the X-ray diffraction patterns of the reacted products. The XRD patterns of Zn(II)-montmorillonite (Fig. 1c) and Cd(II)-montmorillonite (not shown) exhibited the basal spacings of ca. 1.5 nm, corresponding to bilayers of water molecules between the silicate layers (Clementz et al., 1973). The observed basal spacings were very similar to those obtained for the intercalation compounds, indicating that the intercalation of Na<sub>2</sub>S as well as the formation of metal sulfide did not affect the basal spacings, the color of Zn(II)-montmorillonite and Cd(II)-montmorillonite due to the hydrated interlayer metal ions changed by the solid-solid reactions, suggesting the changes in the coordination states of the Zn(II) and Cd(II) interlayer cations.

The intercalation compounds were heated at 200 °C for 1 h in air atmosphere. The observed basal spacing of the heated Zn-montmorillonite-Na<sub>2</sub>S was 1.23 nm (Fig. 1a), of the heated Cd-montmorillonite-Na<sub>2</sub>S 1.24 nm (Table 1), corresponding to the expansions of the interlayer spaces of 0.27 and 0.28 nm, respectively. The decrease of the basal spacings was attributed to the loss of the adsorbed as well as coordinated water molecules. We reported that the interlamellar distances of MnS- and NiS-montmorillonites were 0.31 and 0.32 nm (Khaorapapong et al., 2009). The expansion of the basal spacings of the heated intercalation compounds indicated the formation of ZnS or CdS with a particle height of ca. 0.3 nm. The crystal structure of the metal sulfides intercalated in montmorillonite is still difficult to be elucidated. Further investigation is necessary to clarify.

**Table 1**Changes in basal spacings (*d*), colors, emission bands and intensities of Znmontmorillonite-Na<sub>2</sub>S and Cd-montmorillonite-Na<sub>2</sub>S and those after heating.

Samples	Heating temperature (°C)	Basal spacing $(d_{001}, nm)$	Color	λ <sub>emiss</sub> (nm)	Intensity
Zn-montmorillonite	RT <sup>a</sup>	1.54	Gray	-	-
Zn-montmorillonite-	RT	1.51	Pale	583	41.2
Na <sub>2</sub> S	200	1.23	White	583	36.9
	400	1.22	Pale brown	576	12
	600	0.97	Bright brown	NDb	ND
	800	-	Bright brown	ND	ND
Cd-montmorillonite	RT	1.49	Gray	-	_
Cd-montmorillonite- Na <sub>2</sub> S	RT	1.53	Bright yellow	529	13
	200	1.24	Yellow	524	14
	400	1.22	Yellow	522	27
	600	0.96	Yellow	523	28
	800	0.96	Bright brown	519	8.5

- <sup>a</sup> Room temperature.
- b Not detected.

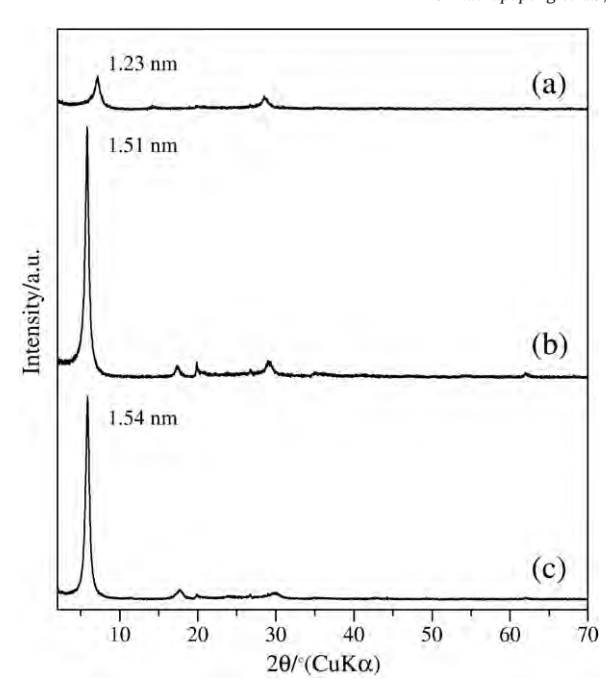
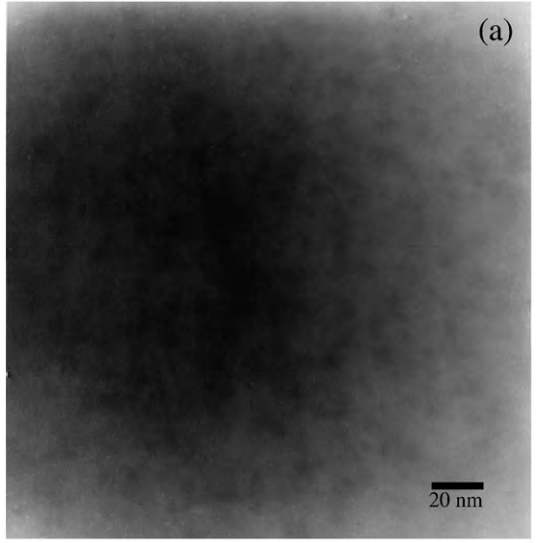


**Fig. 1.** XRD patterns of (a) Zn-montmorillonite-Na<sub>2</sub>S (200 °C), (b) Zn-montmorillonite-Na<sub>2</sub>S and (c) Zn(II)-montmorillonite.

When the two products were heated at 400 °C for 1 h in air, the basal spacings of the heated products (Table 1) were almost at the same (ca. 1.2 nm). The color of Zn-montmorillonite-Na<sub>2</sub>S slightly changed from white to pale brown, while that of Cd-montmorillonite-Na<sub>2</sub>S (yellow) did not significantly change, indicating the changes in the surrounding environments and/or crystal structures of the intercalated metal sulfides. After heating at 600 °C, the interlayer space of Zn-montmorillonite-Na<sub>2</sub>S (ca. 1.2 nm) collapsed, revealing the  $d_{001}$  of the dehydrated montmorillonite (ca. 1.0 nm) together with the new reflections located at around 48 and 58 (2 $\theta$ /degree) due to zinc blende ZnS (JCPDS 05-0566). The change of the basal spacings of the heated Cd-montmorillonite-Na<sub>2</sub>S was previously discussed in our report (Khaorapapong et al., 2008a).

After heating at 800 °C, the intensity of the 001 reflection with  $d={\rm ca.~1.0~nm}$  of Zn-montmorillonite-Na<sub>2</sub>S disappeared, while that of Cd-montmorillonite-Na<sub>2</sub>S decreased. The observed X-ray diffraction pattern indicated the collapse of the silicate layers due to the dehydroxylation of structural OH group. The reflections due to the deintercalated ZnS particles were absent, suggesting their decomposition. The FT-IR spectrum of the heated Zn-montmorillonite-Na<sub>2</sub>S (at 800 °C) did not show any absorption bands characteristic of the hydroxyl stretching and bending vibrations at around 3616 and 916 cm<sup>-1</sup>, confirming the dehydroxylation of the silicate layers (Tyagi et al., 2006). These observations were consistent with the thermogravimetric-mass analysis mentioned later.

Transmission electron micrographs of Zn-montmorillonite- $Na_2S$  (at 200 °C) and Cd-montmorillonite- $Na_2S$  (at 200 °C) are shown in Fig. 2. The images presented the immobilized ZnS or CdS nanoparticles (darker contrast), which were covered with thin films of the silicate layers (lighter contrast). Round shaped ZnS particles with an average size of ca. 2–7 nm and of CdS particles with 6–10 nm were well dispersed in the interlayer spaces of montmorillonite. The darker images of ZnS and CdS particles were probably due to overlapped particles and/or the formation of the metal sulfides on the external surface of montmorillonite. Taking the expansions of the interlayer spaces of the heated products (ca. 0.3 nm) into account, intercalated ZnS or CdS single particles probably were disk- or plate-shaped particles with a thickness of ca. 0.3 nm and a diameter of ca. 2–7 nm



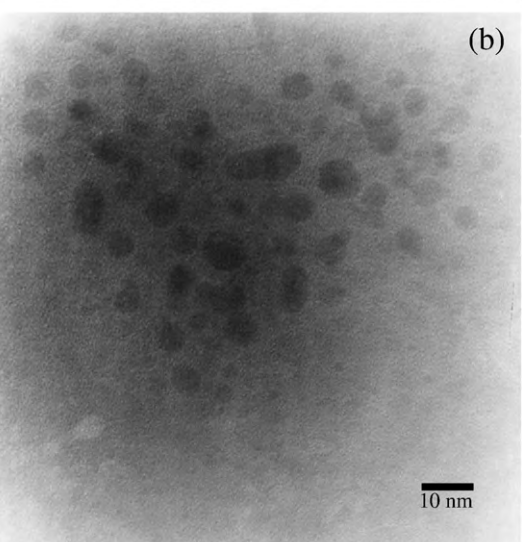


Fig. 2. TEM images of (a) Zn-montmorillonite-Na $_2$ S (200 °C), and (b) Cd-montmorillonite-Na $_2$ S (200 °C).

for ZnS and ca. 6–10 nm for CdS where the disk or plate plane was oriented parallel to the silicate layer.

The Raman spectrum of the heated Zn-montmorillonite-Na<sub>2</sub>S (at 200 °C) (Fig. 3a) revealed the characteristic bands of ZnS at 304 and 604 cm<sup>-1</sup> and that of the heated Cd-montmorillonite-Na<sub>2</sub>S showed the bands at 304 and 608 cm<sup>-1</sup> (Fig. 3b), which were ascribed to the 1LO and 2LO of CdS, respectively (Xu et al., 2002; Cao et al., 2006). The transverse optical phonon (TO), the first-harmonic longitudinal optical phonon (1LO), the second-harmonic longitudinal optical phonon (2LO) and the forth-harmonic longitudinal optical phonon (4LO) of ZnS were observed at 261, 335, 671, and 1336 cm<sup>-1</sup>, respectively (Zhang et al., 2006). The surface optical phonon (SO) of ZnS quantum dots embedded in a behenic acid was observed at  $316\ \mathrm{cm^{-1}}$  and no LO or TO confined optical phonons was seen in the Raman spectrum (Milekhin et al., 2002). The Raman spectrum of ZnS nanoparticles with air as the dielectric media exhibited 10 lines including the 1SO and 2SO bands at 322 and 611 cm<sup>-1</sup>, respectively (Abdulkhadar and Thomas, 1995). The Raman bands observed for the present samples supported the formation of ZnS and CdS particles in montmorillonite. The absence of the confined modes in the Raman spectrum was presumably due to the small size of the ZnS particles (Abdulkhadar and Thomas, 1995), while the vibration modes of ZnS in montmorillonite are still difficult to discuss at the present stage.

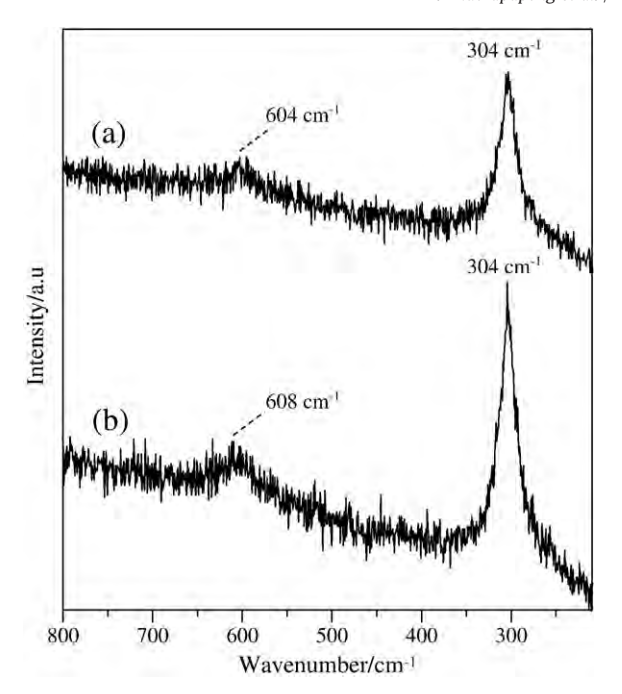


Fig. 3. Raman spectra of (a) Zn-montmorillonite-Na<sub>2</sub>S (200  $^{\circ}$ C), and (b) Cd-montmorillonite-Na<sub>2</sub>S (200  $^{\circ}$ C).

The TG–DTA curves of Zn-montmorillonite-Na<sub>2</sub>S are shown in Fig. 4 together with those of Zn(II)-montmorillonite and Na<sub>2</sub>S. The endothermic peaks due to melting and vaporization of Na<sub>2</sub>S crystals at around 52, 91 and 194 °C (Fig. 4f) were absent in the DTA curve of Zn-montmorillonite-Na<sub>2</sub>S (Fig. 4e), confirming that the unreacted Na<sub>2</sub>S crystals were absent. In the TG curve of Zn-montmorillonite-Na<sub>2</sub>S (Fig. 4b), three steps of mass losses were observed. The initial mass loss was observed between room temperature and 200 °C, which accompanied the endothermic peak at around 76 °C in the corresponding DTA curve and it was ascribed to the desorption of the adsorbed and coordinated water molecules (Guggenheim and van Groos, 2001). The TG–MS analysis (He flow) of Zn-montmorillonite-

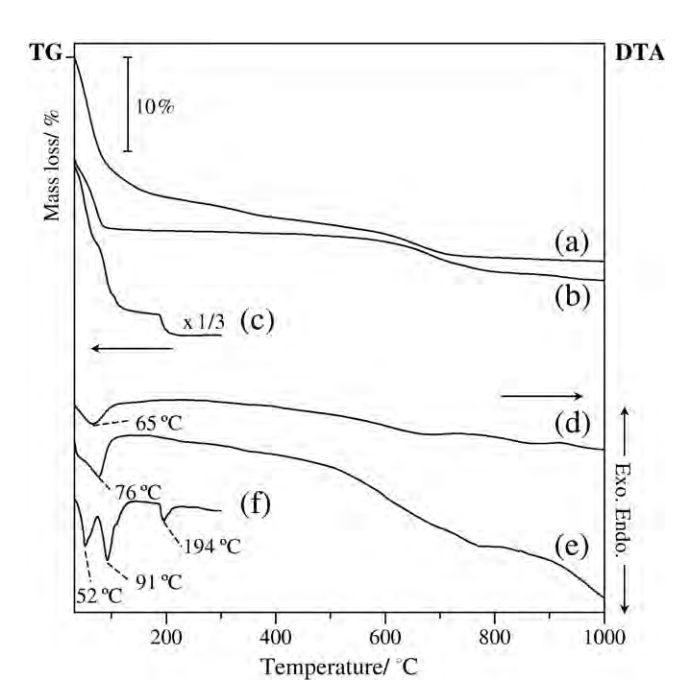


Fig. 4. TG–DTA curves of (a and d) Zn(II)-montmorillonite, (b and e) Zn-montmorillonite-Na $_2$ S, and (c and f) Na $_2$ S.

Na<sub>2</sub>S indicated that the gas evolved at around 76 °C was water. The second mass loss of Zn-montmorillonite-Na<sub>2</sub>S at 200-580 °C (Fig. 4b) was interpreted as the partial decomposition of ZnS and the dehydration of the retained water in the interlayer spaces (Guggenheim and van Groos, 2001). The desorption of water in this temperature range was also reported for Cd-montmorillonite-Na<sub>2</sub>S (Khaorapapong et al., 2008a). The mass spectra observed at around 285 and 565 °C showed the peak (m/z=64) due to the evolution of sulfur dioxide. It was reported that ZnS:Mn nanoparticles were unstable above 200 °C (Mu et al., 2005). In the DTG curve of Zn-montmorillonite-Na<sub>2</sub>S (not shown), the last mass loss between 580 and 875 °C showed the two steps, confirming the decomposition of the retained ZnS and dehydroxylation of structural OH groups of montmorillonite. On the other hand, in the DTG curve of Zn-montmorillonite, the last mass loss between 550 and 760 °C occurred in one step, indicating the dehydroxylation of structural hydroxyl groups of montmorillonite (Guggenheim and van Groos, 2001). The TG-MS data also confirmed that the gas evolved at around 300. 410 and 640 °C was water. Similar TG-DTG-DTA curves were observed for Cd-montmorillonite-Na<sub>2</sub>S (Khaorapapong et al., 2008a), confirming the formation of ZnS and CdS in the interlayer spaces of montmorillonite.

## 3.2. In situ formation and optical properties of zinc sulfide and cadmium sulfide

The diffuse reflectance spectra of Zn-montmorillonite-Na<sub>2</sub>S and Cd-montmorillonite-Na<sub>2</sub>S are shown in Fig. 5 together with those of montmorillonite and Na<sub>2</sub>S. The absorption spectrum of ZnS in montmorillonite (Fig. 5a) showed the onset at 345 nm, while the absorption onset of CdS in montmorillonite was observed at 541 nm (Fig. 5b). The absorption onsets were not observed for the absorption spectra of the starting materials (montmorillonite and Na<sub>2</sub>S; Fig. 5c and d). The absorption spectra of CdS and ZnS nanoparticles formed in the presence of organomontmorillonite, exhibited the onsets at around 480–525 nm and 337–410 nm (Dékány et al., 1995). The absorption edges of CdS–SiO<sub>2</sub> in ethanol–cyclohexane solution were observed at 455–500 nm, and those of CdS–SiO<sub>2</sub> and ZnS–SiO<sub>2</sub> in methanol–cyclohexane solution appeared at 495–507 nm and 311–320 nm (Dékány et al., 1996, 1997). The sharp bands of ZnS

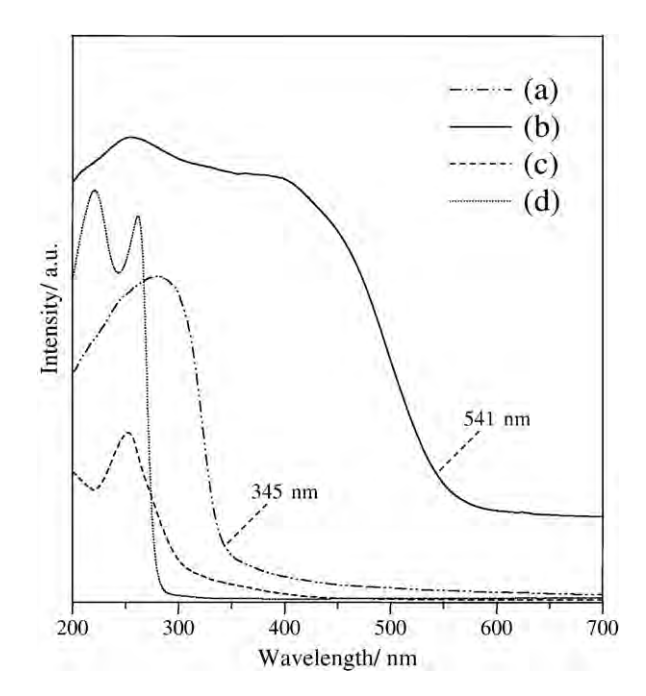


Fig. 5. Diffuse reflectance absorption spectra of (a) Zn-montmorillonite-Na $_2$ S, (b) Cd-montmorillonite-Na $_2$ S, (c) montmorillonite, and (d) Na $_2$ S.

and CdS nano/microspheres exhibited the absorption onsets at 298 and 448 nm, respectively (Deng et al., 2006). The ZnS and CdS powders showed the reflection edges at around 300 and 460 nm (Zhu et al., 2001). These observations clearly confirmed the formation of ZnS and CdS in the interlayer spaces of montmorillonite, which was consistent with the photoluminescence spectra described below.

The photoluminescence spectrum of Zn-montmorillonite-Na<sub>2</sub>S (Fig. 6a) showed the luminescence peak at 583 nm. The photoluminescence bands of Mn<sup>2+</sup>-activated ZnS nanocrystals (in which the Mn<sup>2+</sup> ions were distributed outside the ZnS nanocrystals) appeared at around 350 nm and that of Mn<sup>2+</sup>-doped ZnS nanocrystals (in which the Mn<sup>2+</sup> ions were incorporated) were observed at around 435 and 585 nm (Sooklal et al., 1996). The orange emission centered at 583 nm arose from the incorporation of trace amounts of Mn<sup>2+</sup> in the ZnS crystal lattice (Becker and Bard, 1983). Because the Mn<sup>2+</sup> ions (ca. 0.1%, determined by ICP-OES) was probably involved as an impurity in montmorillonite, the PL band of Zn-montmorillonite-Na<sub>2</sub>S (583 nm) can be ascribed to the formation of Mn<sup>2+</sup>-incorporated ZnS particles in the interlayer space, though further detailed characterization is required to claim this possibility.

The emission band of Cd-montmorillonite-Na $_2$ S was observed at 529 nm (Fig. 6b). The luminescence spectrum of montmorillonite was also measured (not shown) and the peak appeared at 471 nm. The photoluminescence spectra of CdS on Laponite showed the emission peaks at 450–580 nm (Stramel et al., 1986). The luminescence spectra of CdS-organomontmorillonite complexes showed the emission maxima in the 500–600 nm regions (Katov et al., 1993). Consequently, the luminescence band observed for the present Cd-montmorillonite-Na $_2$ S can be attributed to the formation of CdS particles in the interlayer spaces of montmorillonite. The weak photoluminescence spectra with the emission maxima of 583 nm for ZnS-montmorillonite and 529 nm for CdS-montmorillonite confirmed that the impurities such as iron ions quenched the luminescence of ZnS and CdS particles in montmorillonite (Ogawa and Kuroda, 1995).

Further changes in the absorption and photoluminescence spectra of the products by heating at different temperatures were measured to estimate the thermal stability of the intercalated products at 200, 400, 600 and 800 °C. The absorption spectrum of the heated ZnSmontmorillonite (not shown) showed the onset at 341–371 nm. With

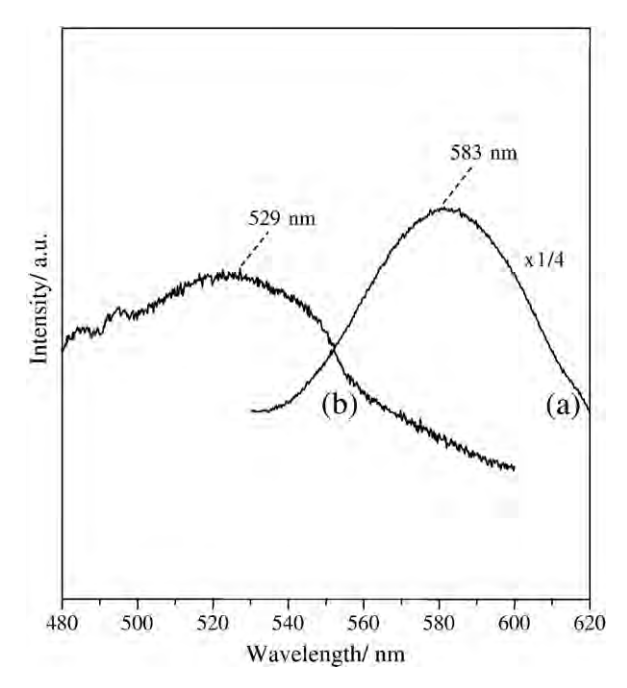


Fig. 6. Photoluminescence spectra of (a) Zn-montmorillonite- $Na_2S$ , and (b) Cd-montmorillonite- $Na_2S$ .

the increase of the heating temperature up to 400 °C, the absorption spectra of ZnS-montmorillonite slightly shifted toward the longer wavelength region, showing the growth of ZnS particles in the interlayer space (Wada et al., 2001). When the heating temperature was increased to 600–800 °C, the ZnS particles were damaged. The luminescence bands and intensity of the heated products are summarized in Table 1. The luminescence intensity of the heated ZnS-montmorillonite was decreased with increasing temperature up to 400 °C. The slight decrease of the PL intensity was observed for the heated ZnS-montmorillonite heated to 200 °C, suggesting the release of Mn<sup>2+</sup> ions from the ZnS structure (Mu et al., 2005). A further decrease in the intensity was observed for the sample heated at 400 °C, confirming the dehydration and partial evaporation of sulfur from ZnS particles. Above 600 °C, the emission peak of ZnS-montmorillonite disappeared, supporting the decomposition of the retained ZnS in the interlayer space.

The heated CdS-montmorillonite showed the absorption onset at 528–539 nm (not shown). The onset of CdS-montmorillonite slightly shifted toward a shorter wavelength region by the heat treatment at 200 and 400 °C, suggesting the presence of smaller particles of CdS (Khaorapapong et al., 2008a). After heating at 600-800 °C, the absorption onsets did not reveal a further change of the particle size of CdS. On the other hand, the luminescence intensity of CdSmontmorillonite was slightly increased by heating at 200, 400 and 600 °C, suggesting changes in the surrounding environment of the adsorbed CdS including the removal of water molecules from the interlayer space (Arnaud and Georges, 2003) and/or the decrease of the particle size of CdS (Loukanov et al., 2004) confirmed by the blue shift in the diffuse reflectance absorption spectra. On the heating to 800 °C, the luminescence intensity was decreased due to the deintercalation and decomposition of CdS. The luminescence bands of all the heated CdS-montmorillonites were almost pinned at the same wavelength (519-524 nm), only the intensities changed (Table 1), indicating the change of the particle size of CdS (Wada et al., 2001). Consequently, the temperature was found to play a key role in the size and stability of ZnS and CdS particles formed in the interlayer spaces of montmorillonite.

Because the metal sulfide-montmorillonite hybrids were prepared in solid-state, the removal of metal sulfide nanoparticles from the hybrids is worth investigating. Therefore, as-prepared and heated (at 200 °C) Zn-montmorillonite-Na<sub>2</sub>S, and as-prepared and heated (at 200 °C) Cd-montmorillonite-Na<sub>2</sub>S were magnetically stirred in waterethanol for 1 h and centrifugated to separate the solid material. The absorption spectra of the four supernatants were obtained. The samples did not clearly show any significant peak due to ZnS or CdS nanoparticles. No emission band owing to ZnS or CdS was observed in the supernatants of the as-prepared Zn-montmorillonite-Na<sub>2</sub>S and Cdmontmorillonite-Na<sub>2</sub>S, and the heated Cd-montmorillonite-Na<sub>2</sub>S. On the other hand, weak emission bands located at 416 and 431 nm were observed for the supernatant of the as-prepared Zn-montmorillonite-Na<sub>2</sub>S. The emission spectrum of the dispersed montmorillonite in water/ethanol solution was also measured and the emission peak was observed at 416 nm. The photoluminescence spectrum of dispersed ZnS in methanol solution showed an emission band at 435 nm (Sooklal et al., 1996). The luminescence band of colloidal ZnS appeared at 418 nm (Becker and Bard, 1983). Therefore, the emission band of the supernatant of the heated Zn-montmorillonite-Na2S observed at 431 nm confirmed the dispersion of free ZnS nanoparticles in the solution. Since the emission intensity was very weak, we thought that only small amounts of ZnS nanoparticles were removed from the interlayer space. This observation indicated the stability of the ZnS and CdS particles in montmorillonite.

#### 4. Conclusions

The formation of zinc sulfide and cadmium sulfide nanoparticles in the interlayer spaces of montmorillonite has been investigated by solid-solid reactions and in situ formation of Zn(II)- and Cd(II)montmorillonites with Na<sub>2</sub>S·xH<sub>2</sub>O. The absorption and luminescence bands showed the formation of zinc sulfide and cadmium sulfide. The wavelengths of the absorption bands varied compared to the isolated particles, indicating the change in size and size distribution of the intercalated species. The PL spectra of zinc sulfide and cadmium sulfide in montmorillonite showed the weak luminescence peaks at 583 and 529 nm, respectively, supporting the quenching impurities such as iron in montmorillonite. Formation of metal sulfides including ZnS and CdS in the constrained environments may lead to novel phase structures, size and size distribution, and photochemical and photophysical properties. The solid-solid reactions and in situ formation in the interlayer spaces of layered host materials are a promising way to fabricate metal chalcogenide layered silicate nanohybrids.

#### Acknowledgements

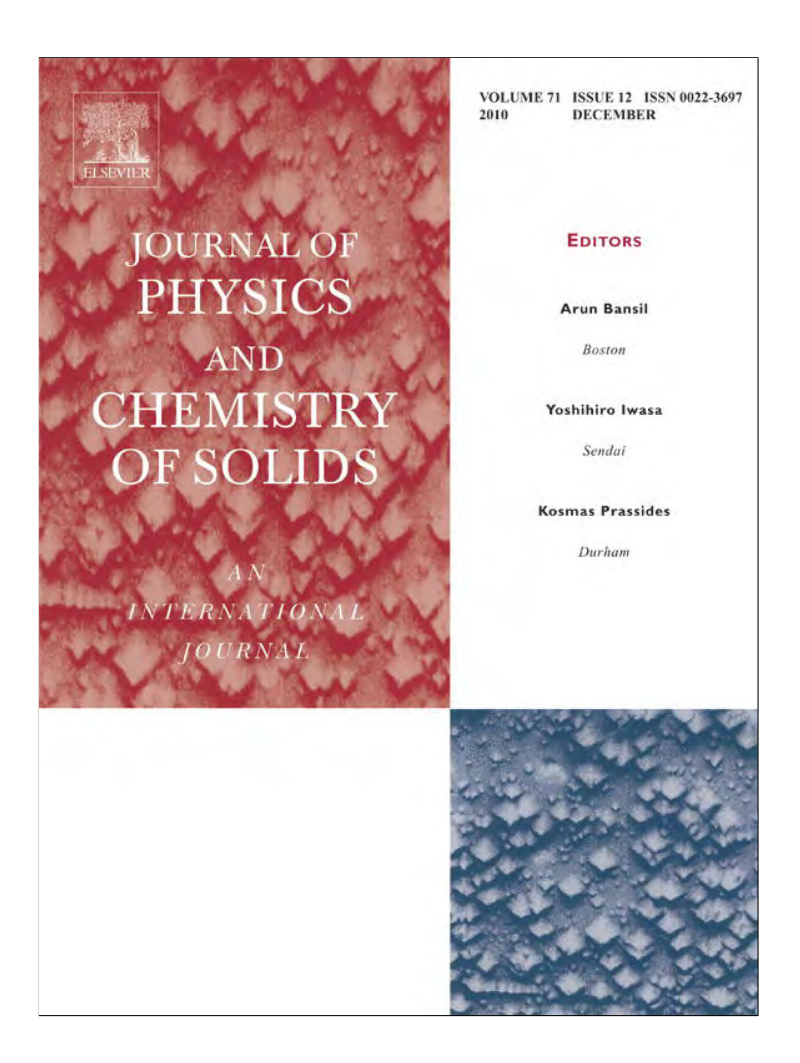
The authors appreciate the kind assistance of Mr. Akira Hachihama (Rigaku Co., Ltd. Japan) for performing TG-DTA-MS analysis. This project was financially supported by the Thailand Research Fund (TRF) and Khon Kaen University (grant no. DBG5380004), and the Center of Excellence for Innovation in Chemistry (PERCH-CIC), Commission on Higher Education, Ministry of Education, Thailand.

#### References

- Abdulkhadar, M., Thomas, B., 1995. Study of Raman spectra of nanoparticles of CdS and ZnS. Nanostruct. Mater. 5, 289-298.
- Antolini, F., Pentimalli, M., Di Luccio, T., Terzi, R., Schioppa, M., Re, M., Mirenghi, L., Tapfer, L., 2005. Structural characterization of CdS nanoparticles grown in polystyrene matrix by thermolytic synthesis. Mater. Lett. 59, 3181-3187.
- Arnaud, N., Georges, J., 2003. Comprehensive study of the luminescent properties and lifetimes of Eu<sup>3+</sup> and Tb<sup>3+</sup> chelated with various ligands in aqueous solutions: Influence of the synergic agent, the surfactant and the energy level of the ligand triplet. Spectrochim. Acta A 59, 1829-1840.
- Becker, W.G., Bard, A.J., 1983. Photoluminescence and photoinduced oxygen adsorption of colloidal zinc sulfide dispersions, I. Phys. Chem. 87, 4888-4893.
- Bujdák, J., Slosiariková, H., 1992. The reaction of montmorillonite with octadecylamine in solid and melted state. Appl. Clay Sci. 7, 263-269.
- Cao, H., Wang, G., Zhang, S., Zhang, X., Rabinovich, D., 2006. Growth and optical properties of wurtzite-type CdS nanocrystals. Inorg. Chem. 45, 5103-5108.
- Chavhan, S., Sharma, R.P., 2005. Growth, structural and optical transport properties of nanocrystal Zn $_{1-x}$ CdS thin films deposited by solution growth technique (SGT) for photosensor applications. J. Phys. Chem. Solids 66, 1721–1726.
- Chin, A.H., Calderón, O.G., Kono, J., 2001. Extreme midinfrared nonlinear optics in semiconductors. Phys. Rev. Lett. 86, 3292-3295.
- Clementz, D.M., Pinnavaia, T.J., Mortland, M.M., 1973. Stereochemistry of hydrate copper(II) ions on the interlamellar surface of layer silicates. An electron spin resonance study, J. Phys. Chem. B 101, 7786-7793.
- Dékány, I., Turi, L., Tombácz, E., Fendler, J.H., 1995. Preparation of size-quantized CdS and ZnS particles in nanophase reactors provided by binary liquids adsorbed at layered silicates. Langmuir 11, 2285-2292.
- Dékány, I., Nagy, L., Túri, L., Király, Z., Katov, N.A., Fendler, J.H., 1996. Preparation and characterization of CdS and ZnS particles in nanophase reactors provided by binary liquids adsorbed at colloidal silica particles. Langmuir 12, 3709–3715. Dékány, I., Turi, L., Galbács, G., Fendler, J.H., 1997. The effect of cadmium ion adsorption
- on the growth of CdS nanoparticles at colloidal silica particle interfaces in binary liquids. J. Colloid Interface Sci. 195, 307-315.
- Deng, H., Chen, C., Peng, Q., Li, Y., 2006. Formation of transition-metal sulfide microspheres or microtubes. Mater. Chem. Phys. 100, 224-229.
- Guggenheim, S., van Groos, A.F.K., 2001. Baseline studies of the Clay Minerals Society source clays: thermal analysis. Clays Clay Miner. 49, 433-443.
- Henglein, A., Kumar, A., Janata, E., Weller, H., 1986. Photochemistry and radiation chemistry of semiconductor colloids: reaction of the hydrated electron with CdS and non-linear optical effects. Chem. Phys. Lett. 132, 133-136.
- Herron, N., Wang, Y., Eddy, M.M., Stucky, G.D., Cox, D.E., Moller, K., Bein, T., 1989. Structure and optical properties of CdS supercluters in zeolite hosts. J. Am. Chem. Soc. 111, 530-540.
- Hirai, T., Okubo, H., Komasawa, I., 1999. Size-selective incorporation of CdS nanoparticles into mesoporous silica. J. Phys. Chem. B 103, 4228-4230.
- Hirai, T., Saito, T., Komasawa, I., 2001. Stabilization of CdS nanoparticles immobilized on thiol-modified polystyrene particles by encapsulation with polythiourethane. J. Phys. Chem. B 105, 9711-9714.
- Katov, N.A., Putyera, K., Fendler, J.H., Tombácz, E., Dékány, I., 1993. Cadmium sulfide particles in organomontmorillonite complexes. Colloids Surf. A 71, 317-326.
- Khaorapapong, N., Ogawa, M., 2007. Solid state intercalation of 8-hydroxyquinoline into Li(I)-, Zn(II)- and Mn(II)-montmorillonites. Appl. Clay Sci. 35, 31-38.

- Khaorapapong, N., Ogawa, M., 2008, *In situ* formation of bis(8-hydroxyguinoline) zinc(II) complex in the interlayer spaces of smectites by solid-solid reactions, I. Phys. Chem. Solids 69, 941-948.
- Khaorapapong N. Kuroda K. Hashizume H. Ogawa M. 2000 Solid state intercalation of 4,4'-bipyridine into the interlayer space of montmorillonites. Mol. Cryst. Liq. Cryst. 341, 351-356.
- Khaorapapong, N., Kuroda, K., Hashizume, H., Ogawa, M., 2001. Solid-state intercalation of 4.4'-bipyridine and 1,2-di(4-pyridine)ethylene into the interlayer spaces of Co(II)-, Ni(II)-, and Cu(II)-montmorillonites, Appl. Clay Sci. 19, 69-76.
- Khaorapapong, N., Kuroda, K., Ogawa, M., 2002a. Incorporation of thioacetamide into the interlayer space of montmorillonite by solid-solid reactions. Clay Sci. 11, 549–564. Khaorapapong, N., Kuroda, K., Ogawa, M., 2002b. Intercalation of 8-hydroxyquinoline
- into Al-smectites by solid-solid reactions. Clays Clay Miner. 50, 428-434.
- Khaorapapong, N., Ontam, A., Youngme, S., Ogawa, M., 2008a. Solid-state intercalation and in situ formation of cadmium sulfide in the interlayer space of montmorillonite. I. Phys. Chem. Solids 69, 1107-1111.
- Khaorapapong, N., Ontam, A., Ogawa, M., 2008b. Formation of MnS particles in the interlayer space of montmorillonite, Mater, Lett. 62, 3722-3723.
- Khaorapapong, N., Ontam, A., Khemprasit, J., Ogawa, M., 2009. Formation of MnS- and NiS-montmorillonites by solid-solid reactions. Appl. Clay Sci. 43, 238-242.
- Kuczynski, J., Thomas, J.K., 1985. Photophysical properties of cadmium sulfide deposited in porous Vycor glass. J. Phys. Chem. 89, 2720-2722.
- Liu, X., Thomas, J.K., 1989. Formation and photophysical properties of CdS in zeolites with cages and channels. Langmuir 5, 58-66.
- Loukanov, A.R., Dushkin, C.D., Papazova, K.I., Kirov, A.V., Abrashev, M.V., Adachi, E., 2004. Photoluminescence depending on the ZnS shell thickness of CdS/ZnS coreshell semiconductor nanoparticles. Colloids Surf. A Phys. Eng. Aspects 245, 9-14.
- Milekhin, A.G., Sveshnikova, L.L., Repinsky, S.M., Gutakovsky, A.K., Friedrich, M., Zahn, D.R.T., 2002. Optical vibrational modes in (Cd, Pb, Zn)S quantum dots embedded in Langmuir-Blodgett matrices. Thin Solid Films 422, 200-204.
- Mu, J., Gu, D., Xu, Z., 2005. Effect of annealing on the structural and optical properties of non-coated and silica-coated ZnS:Mn nanoparticles. Mater. Res. Bull. 40, 2198-2004.
- Ogawa, M., 2004. Photoprocess in clay-organic complexes. In: Auerbach, S.M., Carrado, K.A., Dutta, P.K. (Eds.), Handbook of Layered Materials. Marcel Dekker, New York, pp. 191-260.
- Ogawa, M., Kuroda, K., 1995. Photofunctions of intercalation compounds. Chem. Rev. 95, 399-438.
- Ogawa, M., Kuroda, K., 1997. Preparation of inorganic-organic nanocomposites through intercalation of organoammonium ions into layered silicates. Bull. Chem. Soc. Jpn 70, 2593-2618.
- Ogawa, M., Kuroda, K., Kato, C., 1989. Preparation of montmorillonite-organic intercalation compounds by solid-solid reactions. Chem. Lett. 1659-1662
- Ogawa, M., Kato, K., Kuroda, K., Kato, C., 1990a. Preparation of montmorillonitealkylamine intercalation compounds by solid-solid reactions. Clay Sci. 8, 31-36.
- Ogawa, M., Handa, T., Kuroda, K., Kato, C., 1990b. Formation of organoammoniummontmorillonites by solid-solid reactions. Chem. Lett. 71-74.
- Ogawa, M., Hashizume, T., Kuroda, K., Kato, C., 1991. Intercalation of 2,2'-bipyridine and complex formation in the interlayer space of montmorillonite by solid-solid reactions. Inorg. Chem. 30, 584-585.
- Ogawa, M., Nagafusa, Y., Kuroda, K., Kato, C., 1992a. Solid-state intercalation of acrylamide into smectites and Na-taeniolite. Appl. Clay Sci. 7, 291-302.
- Ogawa, M., Shirai, H., Kuroda, K., Kato, C., 1992b. Solid-state intercalation of naphthalene and anthracene into alkylammonium-montmorillonites. Clays Clay Miner. 40, 485-490.
- Ogawa, M., Hirata, M., Kuroda, K., Kato, C., 1992c. Selective solid-state intercalation of cis-trans isomers into montmorillonite. Chem. Lett. 365-368.
- Öznülüer, T., Erdoğan, İ., Demir, Ü., 2006. Electrochemically induced atom-by-atom growth of ZnS thin films: a new approach for ZnS co-deposition. Langmuir 22, 4415-4419
- Sooklal, K., Cullum, B.S., Angel, S.M., Murphy, C.J., 1996. Photophyical properties of ZnS nanoclusters with spatially localized Mn<sup>2+</sup>. J. Phys. Chem. 100, 4551–4555.
- Stramel, R.D., Nakamura, T., Thomas, J.K., 1986. Cadmium sulfide on synthetic clay. Chem. Phys. Lett. 130, 423-425.
- Su, B., Choy, K.L., 2000. Synthesis, microstructure and optical properties of ZnS films formed by electrostatic assisted aerosol jet deposition. J. Mater. Chem. 10, 949-952.
- Theng, B.K.G., 1974. The Chemistry of Clay-Organic Reactions. Adam Hilger, London.
- Tyagi, B., Chudasama, C.D., Jasra, R.V., 2006. Determination of structural modification in acid activated montmorillonite clay by FT-IR spectroscopy. Spectrochim. Acta A 64,
- Wada, Y., Kuramoto, H., Anand, J., Kitamura, T., Sakata, T., Mori, H., Yanagida, S., 2001. Microwave-assisted size control of CdS nanocrystallites. J. Mater. Chem. 11, 1936-1940.
- Whittingham, M.S., 1982. Intercalation chemistry: an introduction. In: Whittingham, M.S., Jacobson, A.J. (Eds.), Intercalation Chemistry. Academic Press, New York, pp. 1–18.
- Xu, W., Liao, Y., Akins, D.L., 2002. Formation of CdS nanoparticles within modified MCM-41 and SBA-15. J. Phys. Chem. B 106, 11127-11131.
- Zhang, Z., Dai, S., Fan, X., Blom, D.A., Pennycook, S.J., Wei, Y., 2001. Controlled synthesis of CdS nanoparticles inside ordered mesoporous silica using ion-exchange reaction. J. Phys. Chem. B 105, 6755-6758.
- Zhang, X., Song, H., Yu, L., Wang, T., Ren, X., Kong, X., Xie, Y., Wang, X., 2006. Surface states and its influence on luminescence in ZnS nanocrystallite. J. Lumin. 118, 251-256.
- Zhu, J., Zhou, M., Xu, J., Liao, X., 2001. Preparation of CdS and ZnS nanoparticles using microwave irradiation, Mater, Lett. 47, 25-29.

Provided for non-commercial research and education use. Not for reproduction, distribution or commercial use.



This article appeared in a journal published by Elsevier. The attached copy is furnished to the author for internal non-commercial research and education use, including for instruction at the authors institution and sharing with colleagues.

Other uses, including reproduction and distribution, or selling or licensing copies, or posting to personal, institutional or third party websites are prohibited.

In most cases authors are permitted to post their version of the article (e.g. in Word or Tex form) to their personal website or institutional repository. Authors requiring further information regarding Elsevier's archiving and manuscript policies are encouraged to visit:

http://www.elsevier.com/copyright

### **Author's personal copy**

Journal of Physics and Chemistry of Solids 71 (2010) 1644-1650



Contents lists available at ScienceDirect

## Journal of Physics and Chemistry of Solids

journal homepage: www.elsevier.com/locate/jpcs



# Formation of mono(8-hydroxyquinoline) lithium(I) complex in smectites by solid–solid reactions

Nithima Khaorapapong a,\*, Makoto Ogawa b

- <sup>a</sup> Department of Chemistry and Center of Excellence for Innovation in Chemistry, Faculty of Science, Khon Kaen University, Khon Kaen 40002, Thailand
- <sup>b</sup> Department of Earth Sciences, Waseda University, Nishiwaseda 1-6-1, Shinjuku-ku, Tokyo 169-8050, Japan

#### ARTICLE INFO

Article history:
Received 25 September 2009
Received in revised form
27 August 2010
Accepted 4 September 2010

Keywords:
A. Optical materials
C. X-ray diffraction
D. Luminescence

#### ABSTRACT

Lithium quinolate including mono(8-hydroxyquinoline) lithium(I) complex (Liq) formed in the interlayer spaces of two smectites via solid-solid reactions and *in situ* complex formation by reacting Li-smectites (Li(I)-synthetic saponite and Li(I)-montmorillonite) with 8-hydroxyquinoline at room temperature. The incorporation of 8-hydroxyquinoline into Li(I)-smectites was proved by powder X-ray diffraction, infrared spectroscopy, thermal and elemental (CHN) analysis. UV-vis absorption and photoluminescence spectra indicated that 8-hydroxyquinoline ligand formed Liq chelate in the interlayer spaces of smectites. The higher luminescence intensity of the Liq complex in synthetic saponite confirmed the very low content of quenching impurities such as iron in the synthetic saponite. The variation of the photoluminescence bands supported the difference in molecular packing and/or crystal structure of the complex formed in the interlayer spaces of smectites.

© 2010 Elsevier Ltd. All rights reserved.

#### 1. Introduction

Intercalation of organic guest species into layered inorganic materials is a way of producing ordered inorganic-organic assemblies with specific functions controlled by their microstructures [1]. Among possible layered solids, 2:1 layered clay minerals including smectites are attractive host materials because of their large surface area, ion exchange property, adsorptive property and swelling behavior for incorporating organic guest species in the interlayer spaces. The constructions, properties and applications of organic-inorganic nanohybrid based on smectites, which represented a new class of premier functional materials such as catalyst and optical properties, have been extensively reported [2,3].

Solid-solid reactions including mechanochemical procedure, which occur between powders in the solid state, are effective techniques for intercalation because of the facilitation of operation and the possibility to improve and functionalize the performances of compounds, which are not accessible from solutions, and so on [4,5]. The immobilization of organic species into three dimensional host materials such as zeolites [6], and two dimensional layered host materials including layered zirconium phosphate [7] as well as layered clay minerals [8–11] by solid-solid reactions was studied so far.

We have successfully prepared metal chelates in the interlayer spaces of smectites via solid-solid reactions between metal exchanged smectites with organic ligands and *in situ* complex formation. Incorporation of 2,2'-bipyridine, 4,4'-bipyridine and 1,2-di(4-pyridine)ethylene and thioacetamide in montmorillonites [12–14], 8-hydroxyquinoline in smectites [15–17] as well as sulfide ion [18–21] through solid-state intercalation and *in situ* formation was already reported.

In the present paper, we report the intercalation of 8-hydroxyquinoline (abbreviated as 8Hq, the molecular structure is shown in Scheme 1a) in the interlayer spaces of lithium(I) exchanged smectites (abbreviated as Li-smectites). Metal quinolate complexes including mono(8-hydroxyquinoline) lithium(I) (abbreviated as Liq, the molecular structure is shown in Scheme 1b) have intensively used in the organic light emitting devices (OLEDs) [22-28] because of their high electroluminescence efficiency and capability of emitting many color throughout the visible spectrum. Developments in design and use of thin films of metal quinolate complexes deposited by vapor phase processes as organic electroluminescent materials for light emitting device applications has been investigated [22]. In order to optimize the performance as emitting materials for OLEDs, metal quinolate must be isolated and thermally stable [22-26]. The incorporation of metal quinolate complexes on solid surfaces or in polymers may be a way to improve isolation and thermal stability, which lead to controlled fluorescent property as well as thin film fabrication. Bis(8-hydroxyquinoline) manganese(II) complex (Mnq2) was immobilized in zeolites including NaY, KL, Naβ and Na-ZSM-5, and mesoporous material (MCM-41) by heating the manganese-exchanged zeolites with excess 8Hq ligands at 120 °C in argon atmosphere for one day [29]. Incorporation of bis(8-hydroxyquinoline) zinc(II) complex (Znq<sub>2</sub>) in a poly(vinylcarbazole) was done and the thin film was

<sup>\*</sup> Corresponding author. Tel.: +66 4320 2222 41x12370 2; fax: +66 4320 2373. E-mail address: nithima@kku.ac.th (N. Khaorapapong).

**Scheme 1.** The molecular structures of 8-hydroxyquinoline (a) and mono (8-hydroxyquinoline) lithium(I) (b).

fabricated by spin-coating technique [30]. Polystyrene containing zinc quinolate complexes in the backbone was prepared as an emitting layer of OLEDs [31]. The effects of the host-guest interactions are worth investigating further for controlling stability, emission efficiency and wavelength.

The previous successes in the solid-solid reactions of layered silicates with organic species have been applied for the immobilization of metal quinolate complexes, which are difficult to be intercalated in the interlayer spaces of smectites by conventional ion exchange methods because of their ionically neutral property [15–17]. In the present study, we carried out the solid-solid reactions between Li-smectites and 8-hydroxyquinoline to prepare new luminescent nanohybrid materials.

#### 2. Experimental

#### 2.1. Materials

Na-synthetic saponite (Sumecton SA, the reference clay sample of the Clay Science Society of Japan, obtained from Kunimine Industries Co., Ltd. synthesized by a hydrothermal reaction) and Na-montmorillonite (Kunipia F, obtained from Tsukinuno Mine, Kunimine Industries Co., Ltd., Japan) were used as the host materials. The cation exchange capacities (CEC) of Na-synthetic saponite and Na-montmorillonite were 70 and 120 meq /100 g of host, respectively. 8-Hydroxyquinoline was obtained from Junsei Chemical Co., Ltd. Lithium chloride was purchased from May&Baker Ltd. All chemicals were reagent grade and used without further purification.

## 2.2. Preparation of Li-smectites by a conventional ion exchange method

Li-smectites (synthetic saponite and montmorillonite) were synthesized by a conventional ion exchange method. Powders of Na-smectites were mixed with a fresh aqueous solution of lithium chloride and the mixtures were magnetically stirred at room temperature for one day. After the ion exchange reactions, the resulting solids were recovered with a centrifugal separator and washed with deionized water repeatedly until a negative AgNO<sub>3</sub> test was obtained. The amounts of the exchanged lithium cations were determined by inductively coupled plasma atomic emission spectroscopy (ICP-AES) to be 55 and 98 meq/100 g of clay mineral for Li-synthetic saponite and Li-montmorillonite, respectively.

## 2.3. Solid-state intercalation of 8Hq into the interlayer spaces of Li-smectites

The intercalation of 8Hq into Li-smectites was carried out by solid-solid reactions according to the method described in our previous reports [12–20]. The mixtures of Li-smectites and 8Hq were manually ground with a pestle and an agate mortar at room

temperature for 10–15 min. The molar ratios of the lithium interlayer cation to 8Hq were 1:1, 1:2 and 1:3.

#### 2.4. Characterization

Powder X-ray diffraction patterns were taken on a Bruker D8-ADVANCE diffractometer using monochromatic CuKα radiation. Visible absorption spectra of the samples were obtained on a Shimadzu UV-VIS-NIR-3101PC scanning spectrophotometer. Diffuse reflectance spectra of the solid samples were collected using an integrated sphere. Infrared spectra of the samples were recorded between 4000 and 400 cm<sup>-1</sup> on a Perkin Elmer Spectrum One FT-IR spectrophotometer by KBr disk method. TG-DTG-DTA data were obtained on a Perkin Elmer Pyris Diamond TG-DTA instrument at a heating rate of 10 °C min<sup>-1</sup> under a dry air atmosphere using  $\alpha$ -alumina ( $\alpha$ -Al<sub>2</sub>O<sub>3</sub>) as the standard material. Luminescence spectra were recorded on a Shimadzu RF-5301PC spectrofluorophotometer in the wavelength range of 400-650 nm with the excitation at 360 nm. The composition of the intercalation compounds were analyzed for C and N contents on a Perkin Elmer 2400 series II CHNS/O analyzer. The amounts of lithium(I) cation were determined by inductively coupled plasma atomic emission spectroscopy (ICP-AES) (Perkin Elmer Optima 2100DV spectrometer).

#### 3. Results and discussion

#### 3.1. Intercalation of 8Hq in the interlayer spaces of Li-smectites

The changes in the basal spacings and color of hydrated smectites by the solid–solid reactions between Li-smectites (Li-synthetic saponite and Li-montmorillonite) and 8Hq at the molar ratios (Li:8Hq) of 1:1, 1:2 and 1:3 are summarized in Table 1. Hereafter, the intercalated products are denoted as Li-smectites-8Hq(n), where n in the parenthesis indicated the molar ratio of 8Hq to interlayer lithium cation (8Hq/Li).

The powder X-ray diffraction patterns of the intercalation compounds prepared by the reactions of Li-synthetic saponite with 8Hq at the molar ratio of 1:1, 1:2 and 1:3 (Li:8Hq) are shown in Fig. 1 together with that of 8Hq. The basal spacings of Li-synthetic saponite-8Hq(1) and Li-montmorillonite-8Hq(1) intercalation compounds were 1.30 (Fig. 1a and Table 1) and 1.66 nm (Table 1) [16], respectively. The gallery heights were calculated by subtracting the thickness of a silicate layer (0.96 nm) from the observed basal spacings (1.30 and 1.66 nm) to be 0.34 and 0.70 nm for Li-synthetic saponite-8Hq(1) and Li-montmorillonite-8Hq(1), respectively. The XRD pattern of 8Hq powder was collected, where the diffraction peaks were located at

Basal spacings and colors of hydrated smectites and the intercalation compounds prepared by solid-solid reactions with 8-hydroxyquinoline.

Host	Molar ratio (Li/8Hq)	Hydrated		After the reaction with 8Hq	
		d (nm)	Color	d (nm)	Color
Synthetic saponite	1:0 1:1 1:2 1:3	1.26 - -	White - -	- 1.30 1.34, 1.69 1.67	- Bright yellow Bright yellow Bright yellow
Montmorillonite	1:0 1:1 1:2 1:3	1.46 - -	White	- 1.66 1.68 1.68	- Yellow-green Yellow-green Yellow-green

d=0.94, 0.62 and 0.38 nm (Fig. 1d). The XRD patterns of Li-synthetic saponite-8Hq(1) and Li-montmorillonite-8Hq(1) did not show any reflection of 8Hq crystal. The X-ray diffraction patterns of Li-montmorillonite-8Hq(2) and Li-montmorillonite-8Hq(3), which were reported in our previous work [10], showed the sharp diffraction peaks with the basal spacing of 1.68 nm (Table 1) and the corresponding higher order reflections. Further increase in the basal spacing (ca. 1.7 nm) was not observed for Li-montmorillonite-8Hq(2) and Li-montmorillonite-8Hq(3), and the reflections due to the free 8Hq molecule were detected in the XRD patterns. On the other hand, the basal spacings of Li-synthetic saponite-8Hq(2) (Fig. 1b) and Li-synthetic saponite-8Hq(3) (Fig. 1c) were 1.34 and 1.69, and 1.67 nm (Table 1), respectively. No reflection of 8Hq crystal was observed in the XRD patterns of Li-synthetic saponite-8Hq(2) and Li-synthetic saponite-8Hq(3). We reported that the gallery heights of Alq3-synthetic saponite and Alq3-montmorillonite were determined to be 0.45 and 0.68 nm, respectively [15], being approximately consistent with the present products. The result confirmed the intercalation of 8Hq molecules.

To study the stability of the intercalation compounds, only the products without any unreacted 8Hq including Li-synthetic saponite-8Hq(1), Li-synthetic saponite-8Hq(2), Li-synthetic saponite-8Hq(3) and Li-montmorillonite-8Hq(1) were allowed to stand at room temperature for longer periods (more than 6 months). The diffraction peaks ( $d_{001}$ ) of Li-synthetic saponite-8Hq(1) and Li-montmorillonite-8Hq(1) were maintained at the same d values, while those of Li-synthetic saponite-8Hq(2) and Li-synthetic saponite-8Hq(3) were slightly shifted toward the higher  $2\theta$  region, indicating the deintercalation of 8Hq. This observation supported that the intercalation compounds (Li-synthetic saponite-8Hq(1) and Li-montmorillonite-8Hq(1)) were stable under the ambient

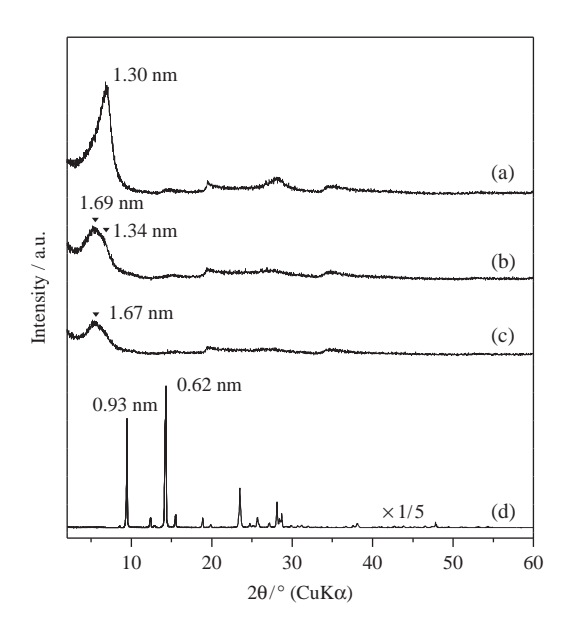


Fig. 1. XRD patterns of Li-synthetic saponite-8Hq(1) (a), Li-synthetic saponite-8Hq(2) (b), Li-synthetic saponite-8Hq(3) (c) and 8Hq (d).

conditions. Therefore, further characterizations of only the two products were obtained.

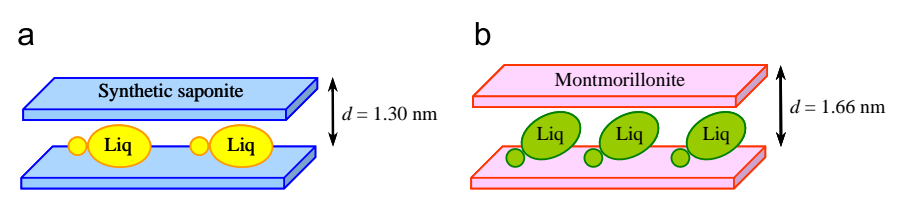
In order to prove thermal stability of the two products, Li-synthetic saponite-8Hq(1) and Li-montmorillonite-8Hq(1) were heated at 200  $^{\circ}$ C for 1 h in air atmosphere. The basal spacings of the heat-treated products (from 1.30 to 1.28 nm for Li-synthetic saponite-8Hq and from 1.66 to 1.63 nm for Li-montmorillonite-8Hq(1)) were very similar to those of the original samples and the diffraction peaks due to the ligand were not observed, supporting the intercalation of 8Hq in the interlayer spaces of smectites and the thermal stability of the intercalation compounds.

As a result of the solid–solid reactions, the change in the color (from colorless to bright yellow and yellow–green color for Li-synthetic saponite-8Hq and Li-montmorillonite-8Hq, respectively) suggested the formation of complex in the interlayer spaces. Since the interlayer lithium cations of two smectites were surrounded by water molecules at ambient temperature, the increase in the basal spacings was thought to be caused by the intercalation of 8Hq via ligand displacement reactions between water and 8Hq molecule.

Because the gallery height (0.70 nm) of Li-montmorillonite-8Hq(1) was larger than that observed for Li-synthetic saponite-8Hq(1) (0.34 nm), the intercalated Liq complex was thought to have a different molecular structure and/or molecular packing in the interlayer spaces. The coordinated 8Hq of Li-synthetic saponite-8Hq(1) and Li-montmorillonite-8Hq(1) formed a monolayer arrangement with the different molecular packing in the interlayer spaces due to the different in CEC of the two clay minerals (Scheme 2a and b). The gallery height (0.70 nm) of Li-synthetic saponite-8Hq(3) was very similar to that observed for Alq<sub>3</sub>-montmorillonite [15]. The 8Hq ligands were thought to take a bilayer arrangement in the interlayer spaces of synthetic saponite similar to Alq<sub>3</sub>-montmorillonite. The gallery heights (0.36 and 0.70 nm) of Li-synthetic saponite-8Hq(2) were attributed to the two different arrangements (a monolayer (0.36 nm) and a bilayer (0.70 nm) arrangements) of 8Hq took place in the interlayer space of synthetic saponite. Since the CEC of montmorillonite was higher than that of synthetic saponite, the difference in the arrangements of 8Hq ligand, which coordinated to lithium interlayer cation of two smectites, should be observed. Because no octahedrally coordinated complex ion of Liq3 was reported, the coordination of unsymmetrical bidentate ligand (8Hq) to Li(I) interlayer cation might form the unstable Liq<sub>3</sub> complex ion, or Liq and/or Liq<sub>2</sub> together with the free 8Hq molecule adsorbed in the interlayer space of synthetic saponite. This result was consistent with the shift in the diffraction peaks of Li-synthetic saponite-8Hq(2) and Li-synthetic saponite-8Hq(3) intercalation compounds after storage more than 6 months as mentioned above.

#### 3.2. The amounts of adsorbed 8Hq in smectites

The chemical compositions were determined by CHN analysis. The carbon and nitrogen contents of the intercalation compounds (Table 2) were 7.83% and 1.02% for Li-synthetic saponite-8Hq(1) and 12.38% and 1.65% for Li-montmorillonite-8Hq(1) [16]. The C:N ratios of the samples (8.96:1 for Li-synthetic saponite-8Hq(1) and 8.76:1 for Li-montmorillonite-8Hq(1)) were in good



Scheme 2. The schematic structures of Li-synthetic saponite-8Hq(1) (a) and Li-montmorillonite-8Hq(1) (b).

Table 2
Chemical compositions of the intercalation compounds before and after washing with ethanol

Host	C/mass %	N/mass %	C:N
Synthetic saponite Before washing After washing	7.83 3.53	1.02 0.76	8.96:1 5.42:1
Montmorillonite Before washing After washing	12.38 11.27	1.65 1.54	8.76:1 8.54:1

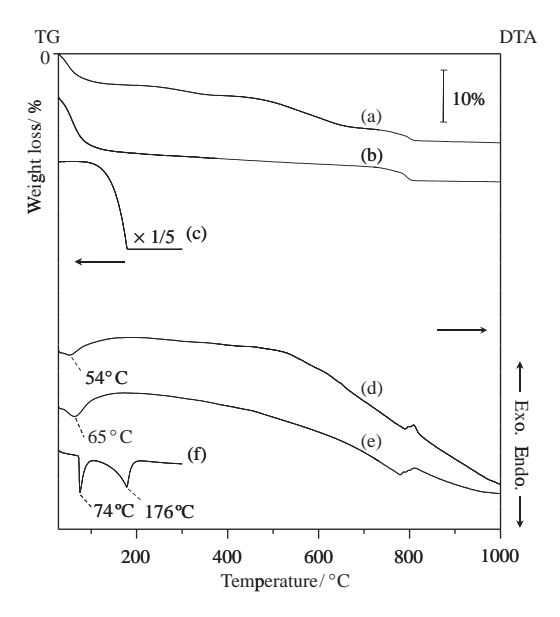


**Fig. 2.** TGA and DTA curves of Li-synthetic saponite-8Hq(1) (a, d), Li-synthetic saponite (b, e) and 8-hydroxyquinoline (c, f).

agreement with that of 8Hq molecule (9:1), indicating that no decomposition of 8Hq molecule occurred during the solid-solid reactions. The ratios of intercalated 8Hq to lithium ion in the interlayer spaces of smectites were estimated to be ca. 1:1, based on the C contents. Thus, the intercalated species were thought to form complex with the formula of Liq [23–25].

The TG-DTA curves of Li-synthetic saponite-8Hq(1) are shown in Fig. 2 together with those of Li-synthetic saponite and 8Hq molecule. The DTG curves of Li-synthetic saponite-8Hq(1) and Li-montmorillonite-8Hq(1) are also displayed in Fig. 3 together with those of the layered host materials. The endothermic peaks due to the melting and vaporization of 8Hq crystal at around 74 and 176 °C (Fig. 2f) were not observed in the DTA curves of the intercalation compounds (Li-synthetic saponite-8Hq(1) and Li-montmorillonite-8Hq(1)), indicating that unreacted 8Hq crystal were not involved in the two products. The endothermic peak at 54 °C of Li-synthetic saponite-8Hq (Fig. 2d), which accompanied the weight loss, was attributed to elimination of adsorbed water. Since the product was ground at ambient temperature, a small amount of water should adsorb on the solid surfaces. The TG-MS analysis (He flow) of Alq<sub>3</sub>-montmorillonite revealed that the gas evolved at 57 °C was water [15]. In the TG and DTG curves (Figs. 2 and 3), the second weight loss of Li-synthetic saponite-8Hq(1) was observed at the temperature range of 196-393 °C without significant exothermic and endothermic peak (Fig. 2d) and that of Li-montmorillonite-8Hq(1) (Fig. 3b) at the temperature range 188-344 °C, corresponding to the endothermic peak at 259 °C [16], were attributed to the dehydration of the coordinated water of the intercalated complex in agreement with the

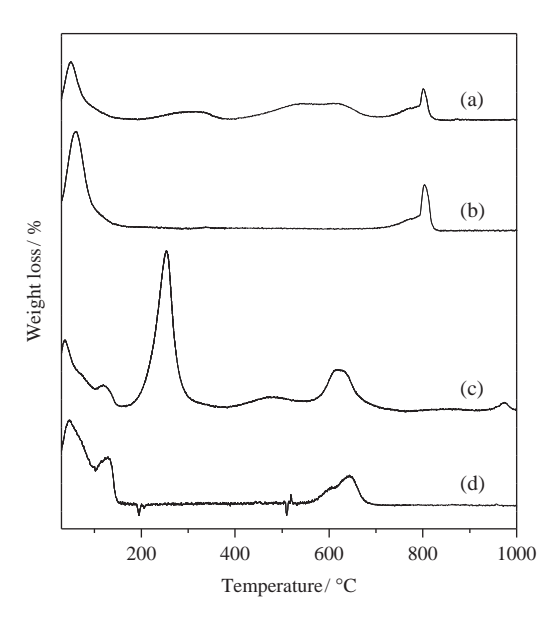


**Fig. 3.** DTG curves of Li-synthetic saponite-8Hq(1) (a), Li-synthetic saponite (b), Li-montmorillonite-8Hq(1) (c) and Li-montmorillonite (d).

proposed geometries mentioned above and/or the partial decomposition of the lithium quinolate complex [16,17]. It was reported that the crystallization water of Liq was eliminated by drying the complex at 200 °C [23]. In the DTG curves (Fig. 3), the third weight losses between 393 and 580 °C for Li-synthetic saponite-8Hq(1) and 344 and 545 °C for Li-montmorillonite-8Hq(1) were ascribed to the decomposition and partial oxidation of coordinated 8Hq [16,17]. The last weight losses between 580 and 850 °C for Li-synthetic saponite-8Hq(1) (Fig. 2d) and 541 and 1000 °C for Li-montmorillonite-8Hq(1) were attributed to the final pyrolysis of 8Hq [32,33], the oxidation of the charcoal [33] and the dehydroxylation of the structural layers of the smectites [34]. By comparison with the TG-DTG-DTA curves of the host materials, the thermal behavior of the intercalation compounds was ascribed to the decomposition of the intercalated 8Hq. However the detail of reaction at each temperature is still difficult to be separated and elucidated. This finding supported the formation of Liq in the interlayer spaces of smectites. As we know, no thermal analysis of Liq complex was reported so far. We reported that the thermal decomposition of Znq<sub>2</sub> in smectites occurred at the higher temperature if compared with the free Znq<sub>2</sub> · 2H<sub>2</sub>O complex [17]. These present intercalation compounds were also thought to be thermally more stable than the free complex of similar composition. This observed property is attributed to the silicate shielding of intercalated Liq complex in the interlayer spaces of smectites.

#### 3.3. Formation of Liq in smectites

Fourier transform infrared, UV-vis absorption and photoluminescence spectra of Li-synthetic saponite-8Hq(1) and Li-montmorillonite-8Hq(1) were recorded to examine the adsorbed states of 8Hq. The characteristic wavenumbers observed in the FT-IR spectra of Li-synthetic saponite-8Hq(1) are summarized in Table 3 together with those of Li-montmorillonite-8Hq(1) reported in our previous work [16], the absorption bands due to 8Hq such as the C-H out of plane bending modes with strong relative intensities at around 742, 781 and 818 cm<sup>-1</sup> [35] were also observed in the FT-IR spectra of the products. The bands in the regions were found to shift slightly toward the higher frequency ranges in the intercalation compounds when compared

Table 3 Wavenumbers  $(cm^{-1})$  of infrared bands of the intercalation compounds and their assignments.

Assignments	8Hq [35]	Li-saponite-8Hq(1)	Li-montmorillonite-8Hq(1)
Ring stretching	1625	-	=
Ring stretching	1593	-	=
Ring stretching	1580	1563	1579
Ring stretching	1509	-	1517
Ring stretching	1499	1503	1502
Ring stretching	1473	1472	1469
Ring stretching	1434	=	1435
+CH bending	1410	=	1421
CH bending	1398	1389	1384
+Ring stretching	1380	=	_
CH bending+	1372	-	_
Ring stretching	1355	-	1325
CH bending	1286	1278	1270
CH bending	1257	=	_
CH stretching+	1245	=	_
CH bending			
CH stretching+	1223	=	_
CH bending			
C-O stretching+	1100	=	_
CH bending			
CH waging	818	825	820
Ring deformation	807	_	_
CH waging	781	790	787
CH waging	742	750	750
		-	713

with those observed for the free 8Hq molecule, confirming the coordination between 8Hq molecule and lithium interlayer cation of synthetic saponite and montmorillonite. The FT-IR spectra of the products did not show any additional absorption band due to decomposed species, proving no decomposition of 8Hq molecule.

The UV-vis diffuse reflectance absorption spectra of Li-synthetic saponite-8Hq(1), Li-montmorillonite-8Hq(1) and 8Hq were obtained and shown in Fig. 4 together with that of 8Hq. The absorption band due to  $\pi$  to  $\pi^*$  charge transfer from electron-rich phenoxide ring to the electron-deficient pyridyl ring of 8Hq unit [27], was observed at 366 nm ( $\lambda_{max}$ ) for Li-synthetic saponite-8Hq(1) (Fig. 4a) and at 318 nm ( $\lambda_{max}$ ) for Li-montmorillonite-8Hq(1) (Fig. 4b). The bands were not detected for the absorption spectra of Li-synthetic saponite (not shown), Li-montmorillonite (not shown) and 8Hq (Fig. 4c). The absorption bands of Liq in solid film appeared at 259 and 365 nm [23], at 315 nm in thin film [27] and that of Liq in DMF solution showed at 420 nm [36]. The absorption spectra of lithium-2-methyl-8hydroxyquinolinolate complex (LiMeq) in solid film also gave some major bands at 259 and 365 nm [23]. Accordingly, the bands observed for Li-synthetic saponite-8Hq(1) and Li-montmorillonite-8Hq(1) can be ascribed to Liq formed in the interlayer spaces of smectites. This result was consistent with PL spectra described below. The absorption band of Li-synthetic saponite-8Hq(1) (366 nm) was different from that observed for Li-montmorillonite-8Hq(1) (318 nm), indicating the different microstructures and/or molecular packing of Liq formed in the interlayer spaces of synthetic saponite and montmorillonite.

The PL spectra (with excitation at 360 nm) of the intercalation compounds are shown in Fig. 5. In the luminescence spectra, intense luminescence was observed at around 509 nm for Li-synthetic saponite-8Hq(1) (Fig. 5a) or at 532 nm for Li-montmorillonite-8Hq(1) (Fig. 5b). The PL band of Liq showed at 485 nm in solid film [23], at 550 nm in a DMF solution [36] and at 501 nm in thin film [27]. The luminescence spectrum of LiMeq film was also observed at 485 nm [23]. These observations supported the formation of Liq in the interlayer spaces of smectites. The difference in luminescence intensity of

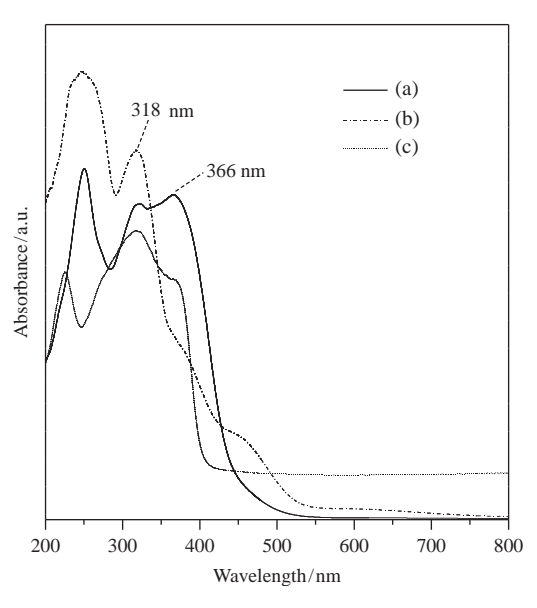


**Fig. 4.** Diffuse reflectance absorption spectra of Li-synthetic saponite-8Hq(1) (a), Li-montmorillonite-8Hq(1) (b) and 8-hydroxyquinoline (c).

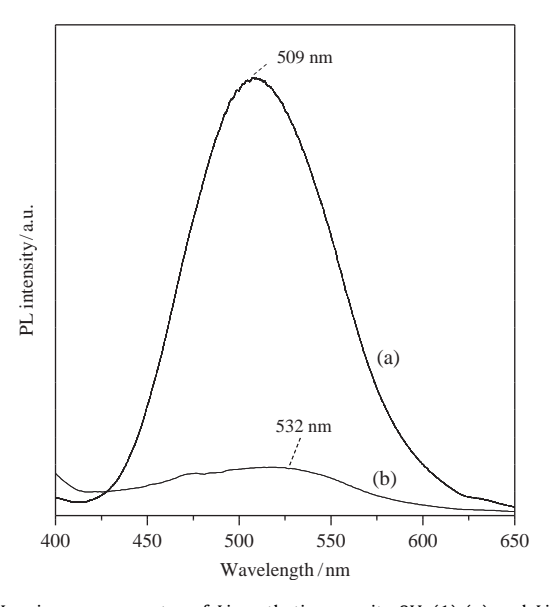


Fig. 5. Luminescence spectra of Li-synthetic saponite-8Hq(1) (a) and Li-mont-morillonite-8Hq(1) (b).

Li-smectites-8Hq systems was similar to that observed between Alq $_3$ -synthetic saponite and Alq $_3$ -montmorillonite systems [17]. Since the cation exchange capacities of the two smectites used in this present work are 70 meq/100 g of clay for synthetic saponite and 120 meq/100 g of clay for montmorillonite, the proximity of the adjacent complexes should be different. As a result, the molecular structure and packing of Liq formed in smectites varied to reveal the slight difference in the wavelength of PL spectra.

The two products, Li-synthetic saponite-8Hq(1) and Li-montmorillonite-8Hq(1), were washed with ethanol at room temperature for 1 h. The amount of the desorbed Liq was determined by the luminescence spectra of the supernatants, where the luminescence bands owing to Liq was detected at 496 nm for Li-synthetic saponite-8Hq(1) and at 511 nm Li-montmorillonite-8Hq(1). It was reported that  $Znq_2 \cdot 2H_2O$  can be transformed into  $(Znq_2)_4$  by the heat treatment under vacuum and reversed transformation can be occurred by the dissociation of the complex

in chloroform and ethanol [37]. Moreover, we have found that anhydrous  $\rm Znq_2$  and  $\rm Znq_2 \cdot 2H_2O$  in smectites can be partially transformed to  $\rm Znq_2 \cdot nH_2O$  by interacting with ethanol [17] to shift the luminescence maxima toward a shorter wavelength region. The computational studies on Liq cluster also showed that the various structures of the complex ( $\rm Li_nq_n$ ;  $n\!=\!1$ , 2, 3, 4 and 6) were easily visualized [38]. Thus, the shifts in the emission bands of the supernatants from 509 to 496 nm for Li-synthetic saponite-8Hq(1) and 532–511 nm for Li-montmorillonite-8Hq(1) were thought to result from the variation of the molecular structure of the Liq complex. The CHN data of the washed products are shown together with those of the original ones in Table 2. The desorbed amount of Liq from montmorillonite was so small, since the chemical composition of the solid did not change significantly.

The advantage of the present complexation with montmorillonite was the stability toward washing with ethanol, while that of the complex with the synthetic saponite was the luminescence intensity. The photoluminescence intensity of Liq in synthetic saponite (Fig. 5a) was 9.3 times higher than that of Liq-montmorillonite (Fig. 5b). This observation indicated that the impurities including iron in montmorillonite quenched the luminescence of Liq. The Fe<sub>2</sub>O<sub>3</sub> composition of natural montmorillonite used in this work was reported to be 1.9 wt% [39], while there was no iron contained in the synthetic saponite. The wavelength of the UV-vis absorption and luminescence bands of the complex varied slightly depending on the hosts, confirming the difference in molecular structures and packing of the intercalated complex.

#### 4. Conclusions

8-Hydroxyquinoline was successfully introduced in the interlayer spaces of Li-smectites via solid-solid reactions at ambient temperature. The intercalated 8-hydroxyquinoline ligand formed mono(8-hydroxyquinoline) lithium(I) complex (Liq) in the interlayer spaces of smectites. The optical properties of the complex were influenced by the nature of the two smectites. High photoluminescence intensity of the complex was observed, when synthetic saponite was used as the host material. The selection of host–guest systems is also very effective to be used for functionalizing ionically neutral species in the interlayer spaces by this solid-state intercalation.

#### Acknowledgements

The financial supports from the Thailand Research Fund and Khon Kaen University (Grant no. DBG5380004), and the Center of Excellence for Innovation in Chemistry, Commission on Higher Education, Ministry of Education, Thailand are kindly acknowledged. N.K. also wishes to thank Ms. Areeporn Ontam, Ms. Sawanya Luamlam, Ms. Niracha Pilahom and Mr. Naranyu Jantarawongsa for experimental assistances.

#### References

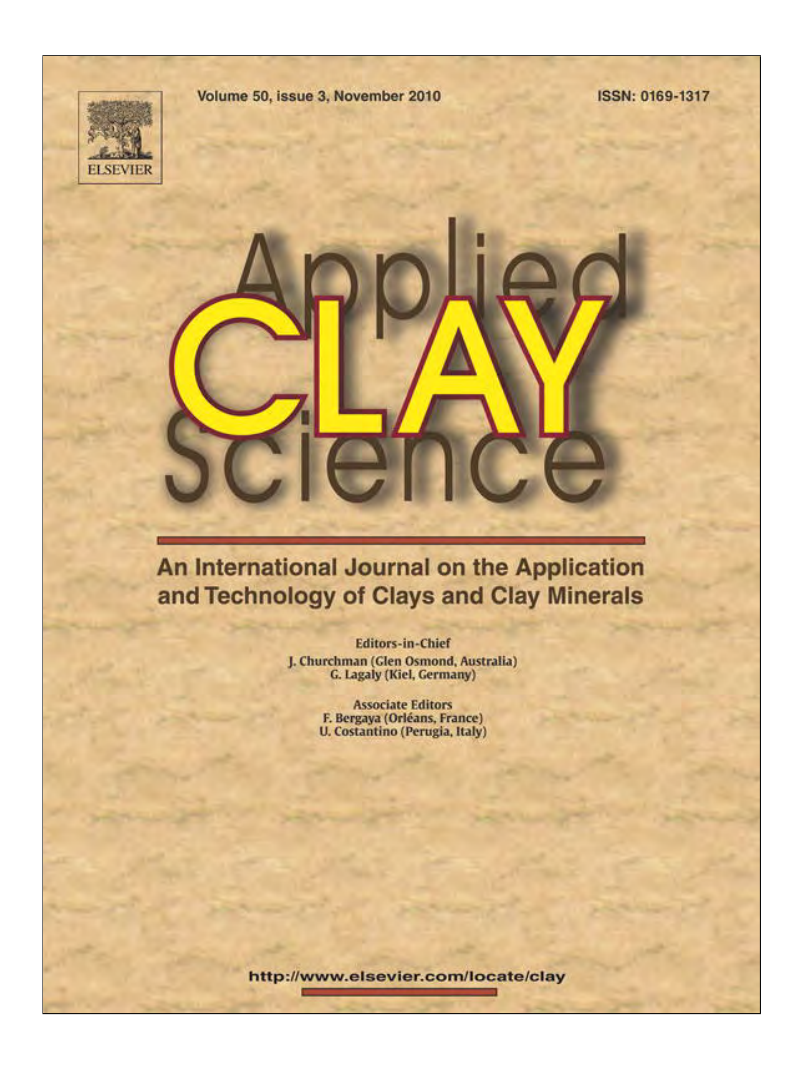
- M. Ogawa, Photoprocesses in clay-organic complexes, in: S.M. Auerbach, K.A. Carrado, P.K. Dutta (Eds.), Handbook of Layered Materials, Marcel Dekker, New York, 2004, pp. 191–260.
- [2] M. Ogawa, K. Kuroda, Photofunctions of intercalation compounds, Chem. Rev. 95 (1995) 399–438.
- [3] M. Ogawa, K. Kuroda, Preparation of inorganic-organic nanocomposites through intercalation of organoammonium ions into layered silicates, Bull. Chem. Soc. Jpn. 70 (1997) 2593–2618.
- [4] A.O. Patil, D.Y. Curtin, I.C. Paul, Solid-state formation of quinhydrones from their components: use of solid-solid reactions to prepare compounds not accessible from solution, J. Am. Chem. Soc. 106 (1984) 348–353.

- [5] F. Toda, K. Tanaka, A. Sekikawa, Host-guest complex formation by a solid-solid reaction, J. Chem. Soc., Chem. Commun. (1987) 279–280.
- [6] K. Lázár, G. Pál-Borbély, H.K. Beyer, H.G. Karge, Solid-state ion exchange in zeolites, J. Chem. Soc., Faraday Trans. 90 (1994) 1329–1334.
- [7] A. Clearfield, J.M. Troup, Ion exchange between solids, J. Phys. Chem. 74 (1970) 2578–2580.
- [8] M. Ogawa, K. Kuroda, C. Kato, Preparation of montmorillonite-organic intercalation compounds by solid-solid reactions, Chem. Lett. (1989) 1659–1662.
- [9] M. Ogawa, T. Handa, K. Kuroda, C. Kato, Formation of organoammoniummontmorillonites by solid-solid reactions, Chem. Lett. (1990) 71-74.
- [10] M. Ogawa, T. Aono, K. Kuroda, C. Kato, Photophysical probe study of alkylammonium-montmorillonites, Langmuir 9 (1993) 1529–1533.
- [11] J. Bujdák, H. Slosiariková, The reaction of montmorillonite with octadecylamine in solid and melted state, Appl. Clay Sci. 7 (1992) 263–269.
- [12] M. Ogawa, T. Hashizume, K. Kuroda, C. Kato, Intercalation of 2,2'-bipyridine and complex formation in the interlayer space of montmorillonite by solidsolid reactions, Inorg. Chem. 30 (1991) 584–585.
- [13] N. Khaorapapong, K. Kuroda, H. Hashizume, M. Ogawa, Solid-state intercalation of 4,4'-bipyridine and 1,2-di(4-pyridine)ethylene into the interlayer spaces of Co(II)-, Ni(II)-, and Cu(II)-montmorillonites, Appl. Clay Sci. 19 (2001) 69–76.
- [14] N. Khaorapapong, K. Kuroda, M. Ogawa, Incorporation of thioacetamide into the interlayer space of montmorillonite by solid-solid reactions, Clay Sci. 11 (2002) 549–564.
- [15] N. Khaorapapong, K. Kuroda, M. Ogawa, Intercalation of 8-hydroxyquinoline into Al-smectites by solid-solid reactions, Clays Clay Miner. 50 (2002) 428-434.
- [16] N. Khaorapapong, M. Ogawa, Solid-state intercalation of 8-hydroxyquinoline into Li(I)-, Zn(II)- and Mn(II)-montmorillonites, Appl. Clay Sci. 35 (2007) 31–38.
- [17] N. Khaorapapong, M. Ogawa, *In situ* formation of bis(8-hydroxyquinoline) zinc(II) complex in the interlayer spaces of smectites by solid-solid reactions, J. Phys. Chem. Solids 69 (2008) 941–948.
- [18] N. Khaorapapong, A. Ontam, S. Youngme, M. Ogawa, Solid-state intercalation and in situ formation of cadmium sulfide in the interlayer space of montmorillonite, J. Phys. Chem. Solids 69 (2008) 1107–1111.
- [19] N. Khaorapapong, A. Ontam, M. Ogawa, Formation of MnS particles in the interlayer space of montmorillonite, Mater. Lett. 62 (2008) 3722–3723.
- [20] N. Khaorapapong, A. Ontam, J. Khemprasit, M. Ogawa, Formation of MnS- and NiS-montmorillonites by solid-solid reactions, Appl. Clay Sci. 43 (2009) 238–242.
- [21] N. Khaorapapong, A. Ontam, M. Ogawa, Formation of ZnS and CdS in the interlayer spaces of montmorillonite. Appl. Clay Sci., in press, doi:10.1016/j. clay.2010.06.013.
- [22] C.H. Chen, J. Shi, Metal chelates as emitting materials for organic electroluminescence. Coord. Chem. Rev. 171 (1998) 161–174.
- luminescence, Coord. Chem. Rev. 171 (1998) 161–174.
   [23] C. Schmitz, H.-W. Schmidt, M. Thelakkat, Lithium-quinolate complexes as emitter and interface materials in organic light-emitting diodes, Chem. Mater. 12 (2000) 3012–3019.
- [24] Z. Liu, O.V. Salata, N. Male, Improved electron injection in organic LED with lithium quinolate/aluminium cathode, Synth. Met. 128 (2002) 211–214.
- [25] J. Endo, T. Matsumoto, J. Kido, Organic electroluminescent devices having metal complexes as cathode interface layer, Jpn. J. Appl. Phys. 41 (2002) L-800-L803.
- complexes as cathode interface layer, Jpn. J. Appl. Phys. 41 (2002) L-800-L803. [26] M. Ghedini, M. La Deda, I. Aiello, A. Grisolia, Synthesis and photophysical characterisation of soluble photoluminescent metal complexes with substituted 8-hydroxyquinolines, Synth. Met. 138 (2003) 189-192.
- [27] A. Jaafari, V. Ouzeau, M. Ely, F. Rodriguez, A. Yassar, J.J. Aaron, P. Benalloul, C. Barthou, Fine-tuning the optical properties of aluminium and lithium quinolates through oligothiophene substituents in 2-position, Synth. Met. 147 (2004) 175–182.
- [28] X. Zheng, Y. Wu, R. Sun, W. Zhu, X. Jiang, Z. Zhang, S. Xu, Efficiency improvement of organic light-emitting diodes using 8-hydroxy-quinolinato lithium as an electron injection layer, Thin Solid Films 478 (2005) 252–255.
- [29] R. Ganesan, B. Viswanathan, Redox properties of bis(8-hydroxyquinoline) manganese(II) encapsulated in various zeolites, J. Mol. Catal., A Chem. 223 (2004) 21–29.
- [30] T.A. Hopkins, K. Meerholz, S. Shaheen, M.L. Anderson, A. Schmidt, B. Kippelen, A.B. Padias, H.K. Hall Jr., N. Peyghambarian, N.R. Armstrong, Substituted aluminum and zinc quinolates with blue-shifted absorbance/luminescence bands: synthesis and spectroscopic, photoluminescence, and electroluminescence characterization, Chem. Mater. 8 (1996) 344–351.
- [31] X. Xia, J. Lu, H. Li, S. Yao, L. Wang, Zn(II) based mixed complex with 8-hydroxyquinoline end group functionalized PSt and the study of fluorescent properties, Opt. Mater. 27 (2005) 1350–1357.
- [32] S.A. Juiz, M.I.G. Leles, A.C.F. Caires, N. Boralle, M. Ionashiro, Thermal decomposition of the magnesium, zinc, lead and niobium chelates derived from 8-quinolinol, J. Therm. Anal. 50 (1997) 625–632.
- [33] I.A. Pastre, I.D.N. Oliveria, A.B.S. Moitinho, G.R. de Souza, E.Y. Ionashiro, F.L. Fertonani, Thermal behaviour of intercalated 8-hydroxyquinoline (oxine) in montmorillonite clay, J. Therm. Anal. Calorim. 75 (2004) 661–669.
- [34] F. Dellisanti, V. Minguzzi, G. Valdrè, Thermal and structural properties of Ca-rich montmorillonite mechanically deformed by compaction and shear, Appl. Clay Sci. 31 (2006) 282–289.
- [35] B. Marchon, L. Bokobza, G. Cote, Vibrational study of 8-quinolinol and 7-(4-ethyl-1-methyloctyl)-8-quinolinol (Kelex 100), two representative members of an important chelating agent family, Spectrochim. Acta 42A (1986) 537-542.

N. Khaorapapong, M. Ogawa / Journal of Physics and Chemistry of Solids 71 (2010) 1644–1650

- [36] F.E. Lytle, D.R. Storey, M.E. Juricich, Systematic atomic number effects in
- [36] F.E. Eyler, D.R. Storey, M.E. Jurictit, Systematic atomic funition complexes exhibiting ligand luminescence, Spectrochim. Acta 29A (1973) 1357–1369.
  [37] B.-S. Xu, Y.-Y. Hao, H. Wang, H.-F. Zhou, X.-G. Liu, M.-W. Chen, The effects of crystal structure on optical absorption/photoluminescence of bis(8-hydroxyquinoline) zinc, Solid State Commun. 136 (2005) 318–322.
- [38] M. Rajeswaran, W.J. Begley, L.P. Olson, S. Huo, Steric effects of substituted quinolines on lithium coordination geometry, Polyhedron 26 (2007) 3653–3660.
   [39] Y. Sugahara, K. Kuroda, C. Kato, Synthesis of β-sialon from a montmorillonite-polyacrylonitrile intercalation compound by carbothermal reduction, J. Am. Ceram. Soc. 67 (1984) C-247–C-248.

Provided for non-commercial research and education use. Not for reproduction, distribution or commercial use.



This article appeared in a journal published by Elsevier. The attached copy is furnished to the author for internal non-commercial research and education use, including for instruction at the authors institution and sharing with colleagues.

Other uses, including reproduction and distribution, or selling or licensing copies, or posting to personal, institutional or third party websites are prohibited.

In most cases authors are permitted to post their version of the article (e.g. in Word or Tex form) to their personal website or institutional repository. Authors requiring further information regarding Elsevier's archiving and manuscript policies are encouraged to visit:

http://www.elsevier.com/copyright

### **Author's personal copy**

Applied Clay Science 50 (2010) 414-417



Contents lists available at ScienceDirect

## **Applied Clay Science**

journal homepage: www.elsevier.com/locate/clay



Note

## In situ complexation of thiourea in the interlayer space of copper(II)-montmorillonite

#### Nithima Khaorapapong \*

Department of Chemistry and Center of Excellence for Innovation in Chemistry, Faculty of Science, Khon Kaen University, Khon Kaen 40002, Thailand

#### ARTICLE INFO

Article history:
Received 20 June 2010
Received in revised form 12 August 2010
Accepted 22 August 2010
Available online 31 August 2010

Keywords: Copper(I) thiourea Intercalation Montmorillonite Solid-solid reaction

#### ABSTRACT

Intercalation of thiourea into the interlayer space of Cu(II)-montmorillonite was performed by solid-solid reaction at room temperature. The successful intercalation was proved by powder X-ray diffraction data and spectroscopic results. The basal spacing of the intercalation compound at the molar ratio 1:6 for copper(II) ion to thiourea was ca. 1.7 nm and the value was larger than that of the starting host material. The absence of the electron spin resonance signal of the product indicated that the copper(II) interlayer cation was reduced to copper(I) cation which remained in the interlayer space as a copper(I) thiourea complex. Both elemental (CHN) and thermogravimetry analyses, as well as Raman and infrared spectroscopy of the intercalation compound supported the presence of the copper(I) thiourea complex in the interlayer space montmorillonite.

© 2010 Elsevier B.V. All rights reserved.

#### 1. Introduction

Intercalation of organic and inorganic species into layered host materials, which is an effective way of constructing ordered inorganic-organic or inorganic-inorganic assemblies with unique microstructures and properties, has drawn increasing interest in a wide variety of scientific and industrial studies (Ogawa, 2004; Lagaly et al., 2006). The smectite group of clay minerals provides attractive features including large surface area, swelling behavior, adsorption and ion exchange. Smectites have been extensively used as the host materials and the other possible applications because of their attractive properties and ability to accommodate various kinds of organic and inorganic guest species (Ogawa and Kuroda, 1995, 1997). The so-called solid-solid reaction has attracted attention due to the facile operation and possibility to prepare compounds not accessible from solution (Patil et al., 1984; Toda et al., 1987). The adsorption of neutral molecules (Ogawa et al., 1992, 1993, 1995a), cation exchange of organoammonium ions (Ogawa et al., 1995b), in situ complexation (Ogawa et al., 1991; Khaorapapong and Ogawa, 2007; Khaorapapong et al., 2001, 2002a,b), as well as in situ sulfidation of metal sulfides (Khaorapapong et al., 2009, 2010) into the interlayer spaces of smectites using solid-solid reaction as a synthetic method were reported.

The transition metal interlayer cations of smectites can form metal complexes with appropriate organic ligands. The metal complex–clay mineral intercalation compounds have been increasingly studied because of their unique properties such as the possibility of fixation of catalytically active sites (Pinnavaia, 1983;

Ozin and Gil, 1989) and construction of low dimensional nanomaterials with novel functional surfaces, and so on. Thiourea is an excellent ligand for transition metals and exhibits redox activity with reducible metal ions to make the reaction systems complicated. In this paper, the study on solid-state intercalation was investigated to incorporate thiourea into the interlayer space of Cu(II)-montmorillonite. Numerous copper(I) thiourea complexes including monomers, dimers, polymers and clusters were reported over the last 50 years (Yamaguchi et al., 1958; Swaminathan and Irving, 1964; Taylor et al., 1974; Johnson and Steed, 1998; Bott et al., 1998). Incorporation of a gold thiourea complex  $(Au(TU)_2^+)$  in beidellite (Stievano et al., 1998) and a silver thiourea complex  $(Ag(TU)_2^+)$  in the interlayer spaces of sodium, calcium and aluminium montmorillonites (Pleysier and Cremers, 1975) by the ion exchange reactions of the complex cations was investigated. Thiourea can donate both nitrogen and/or sulfur atoms to coordinate with transition metals as well as the reaction between copper(II) and thiourea can generate both copper(I)- and copper(II) thiourea complexes (Bott et al., 1998). Although Cu(II)-montmorillonite has been widely used as a host material for intercalation, the solid-state intercalation of thiourea into the interlayer spaces of Cu(II)-montmorillonite has never been studied. Here the solid-solid reaction between Cu(II)montmorillonite and thiourea is reported because the unique way of assembling copper thiourea complex on a solid surface may lead to a low dimensional nanohybrid materials with novel microstructures and properties.

#### 2. Experimental

Montmorillonite used as a host material in this study was Kunipia F (JCSS-3101) supplied by Kunimine Industries Co., Ltd. Japan. Copper(II) chloride (CuCl<sub>2</sub> 2H<sub>2</sub>O) and thiourea (NH<sub>2</sub>CSNH<sub>2</sub>)

<sup>\*</sup> Tel.: +66 43 202222 41x12370 2; fax: +66 43 202373. E-mail address: nithima@kku.ac.th.

were obtained from Junsei Chemical Co., Ltd. and used as received. Cu(II)-montmorillonite was prepared by ion exchange reaction. The content of copper in Cu(II)-montmorillonite was determined to be 1.18 meq/g of clay mineral by inductively coupled plasma atomic emission spectroscopy (ICP-AES). The intercalation of thiourea into Cu(II)-montmorillonite was carried out by solid-solid reactions according to the method described previously (Khaorapapong and Ogawa, 2007; Khaorapapong et al., 2002b, 2009). The mixtures of Cu(II)-montmorillonite and thiourea were ground manually with an agate mortar and a pestle in air at room temperature for 10–15 min. The molar ratio of thiourea to the copper(II) interlayer cation was varied from 6:1 to 1:1.

X-Ray powder diffraction data were collected with monochromatic CuKα radiation on a Mac Science MXP<sup>3</sup> diffractometer. Infrared spectra of the samples in KBr disks were recorded on a Perkin Elmer FT-IR 1640 spectrophotometer. Raman spectra were recorded on a Perkin Elmer system 2000NIR FT-Raman spectrometer equipped with a Perkin Elmer diode pumped Nd:YAG laser. CHN analysis was performed on a Perkin Elmer PE-2400II instrument. Electron spin resonance spectra of the randomly oriented powder samples were recorded at room temperature on a JEOL RE-2XG ESR spectrometer using 100 kHz magnetic field modulations. TG-DTA analysis was performed on a Mac Science TG-DTA 2000S instrument at a heating rate of 10 °C min<sup>-1</sup> using  $\alpha$ -alumina ( $\alpha$ -Al<sub>2</sub>O<sub>3</sub>) as a standard material. Thermogravimetric-mass spectroscopy analysis was performed on a Rigaku Thermo plus MS/IF (a TG model) equipped with a Shimadzu GCMS-QP5050A gas chromatograph mass spectrometer at a heating rate of 10 °C min<sup>-1</sup> under a He flow. Inductively coupled plasma atomic emission spectroscopic (ICP-AES) data were taken on a Nippon Jarrell-Ash ICAP-575 Mark II instrument.

#### 3. Results and discussion

The color changes of the products obtained from Cu(II)-montmorillonite and thiourea are listed in Table 1. By the solid–solid reactions between Cu(II)-montmorillonite and thiourea at the molar ratios of 6:1, 5:1 and 4:1 for thiourea to the interlayer cation, the white solids were obtained. While the mixtures of the white and blue solids were observed in the products with the molar ratios of 3:1, 2:1 and 1:1, suggesting that the unreacted Cu(II)-montmorillonite was involved in the products. Hereafter, the intercalation compounds were designated as Cu-montmorillonite-TU(n), where n in the parenthesis indicated the molar ratio of thiourea to copper(II) cation ( $TU/Cu^{2+}$ ).

The X-ray diffraction pattern of Cu(II)-montmorillonite-TU(6) gave a sharp reflection with the basal spacing of ca. 1.7 nm (Fig. 1g). The expansion of the interlayer space was determined to be ca. 0.7 nm by subtracting the thickness of the silicate layer (ca. 1.0 nm) from the observed basal spacing. No further increase of the basal spacing was observed when a large amount of thiourea was added. The change of the color and the expansion of the interlayer space of montmorillonite

**Table 1**Colors and basal spacings of the products prepared by solid-solid reaction and conventional adsorption process between Cu(II)-montmorillonite with thiourea.

Molar	Solid-solid reaction		Reaction in H <sub>2</sub> O		Reaction in EtOH	
ratio (TU/Cu <sup>2+</sup> )	Color	d <sub>001</sub> (nm)	Color	d <sub>001</sub> (nm)	Color	d <sub>001</sub> (nm)
0:1	Blue	1.24	Blue	1.24	Blue	1.24
1:1	White-blue	1.43 <sup>a</sup>	White-green	1.27 <sup>a</sup>	Dark green	1.24 <sup>b</sup>
2:1	White-blue	1.51 <sup>a</sup>	_	_	_	_
3:1	White-blue	1.62 <sup>a</sup>	White-green	1.32 <sup>a</sup>	White-brown	1.39 <sup>a</sup>
4:1	White	1.65 <sup>a</sup>	-	_	_	_
5:1	White	1.67 <sup>a</sup>	_	_	_	_
6:1	White	1.70	White	1.60	White-gray	1.47

<sup>&</sup>lt;sup>a</sup> Broad and asymmetric reflection.

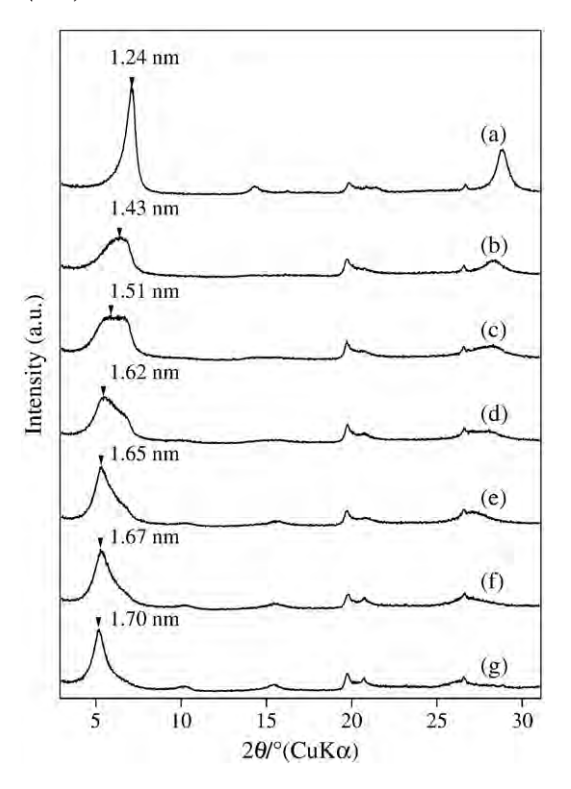


**Fig. 1.** XRD patterns of Cu(II)-montmorillonite (a), Cu(II)-montmorillonite-TU at the molar ratios of thiourea to copper(II) interlayer cation were 1:1 (b), 2:1 (c), 3:1 (d), 4:1 (e), 5:1 (f) and 6:1 (g).

indicated the intercalation of thiourea and *in situ* complexation of copper thiourea complex. On the other hand, the  $d_{001}$  reflections of the products, which the molar ratios of thiourea to copper(II) interlayer cation were lower than 6:1, showed the broad reflection (Fig. 1f), or the broad and subsidiary reflections (Fig. 1b, c, d, e) with the basal spacings below 1.7 nm, confirming the partial complexation of the interlayer cation.

In order to study the effect of the reaction processes and reacting solvents, the in situ complexation of thiourea was also performed by a conventional adsorption process in aqueous and ethanol with the molar ratios of 6:1, 3:1 and 1:1 for thiourea to the interlayer cation. The basal spacings (Table 1) were observed at 1.60, 1.32 and 1.27 nm for the product prepared in aqueous with the molar ratios of 6:1, 3:1 and 1:1 and at 1.47, 1.39 and 1.24 nm in ethanol. The products obtained at the molar ratio of 6:1 in aqueous and ethanol showed the basal spacings lower than that prepared by the solid-solid reaction. The other products prepared by the conventional reactions indicated the incomplete intercalation, excluding the 1:1 product prepared in ethanol showed the basal spacing of 1.24 nm, which was similar to the pristine montmorillonite, suggesting that the intercalation of thiourea did not occur in the resulting solid. It was reported that the reaction of copper(II) with thiourea in aqueous and non-aqueous solutions, thiourea reduced copper(II) to copper(I) and was oxidized to formamimide disulfide (Kratochvil et al., 1966; Doona and Stanbury, 1996). The difference of the observed basal spacings for the products investigated by the solid-solid reactions and conventional adsorption processes indicated that the intercalation mechanisms and products involved in both solid-solid and solid-liquid processes were different. For the products prepared by the conventional processes, thiourea was thought to form formamimide disulfide in the solutions. Only the remained thiourea molecules could be intercalated in the interlayer spaces, corresponding to the smaller expansion of the interlayer spaces. Thus, the reaction of thiourea in the solid-state was different from the ones in the solutions. The mechanism occurred in the solid-

b Strong reflection (no intercalation of thiourea).

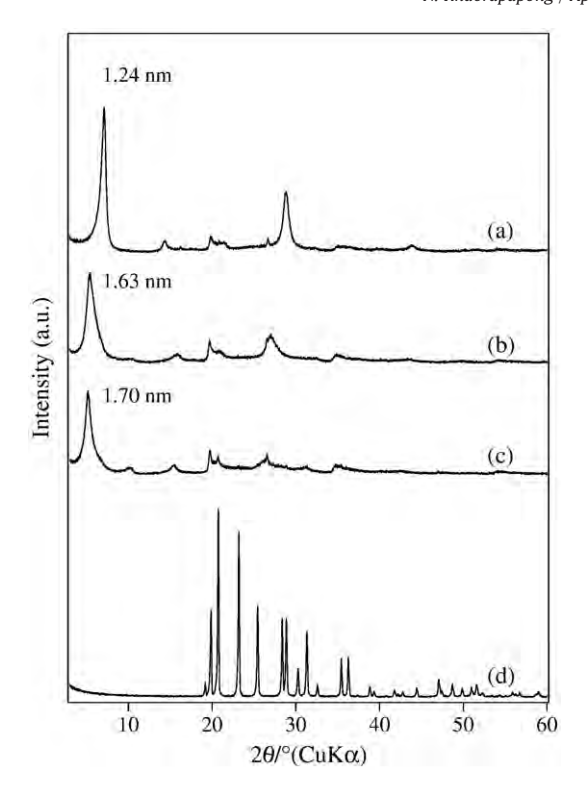


**Fig. 2.** XRD patterns of Cu(II)-montmorillonite (a), Cu(II)-montmorillonite-TU at the molar ratio of thiourea to copper(II) interlayer cation was 6:1 after (b), and before (c) washing, and thiourea (d).

state might be more complicated than those occurred in the solutions. It is still not clear at the present study.

The stability of Cu-montmorillonite-TU(6) was studied by washing the product with acetone in a Soxhlet's extractor for 1 h. Hereafter, the washed product was denoted as Cu-montmorillonite-TU(w). The basal spacing of Cu-montmorillonite-TU(w) (Fig. 2b) was gradually reduced to ca. 1.6 nm, which corresponded to the expansion of the interlayer space of ca. 0.6 nm. However, the  $d_{001}$  reflection of Cu-montmorillonite-TU(w) was slightly broad and asymmetry, indicating the deintercalation of some thiourea, copper thiourea complex and/or formamimide disulfide. This observation suggested that the Cu(II)-montmorillonite-TU(6) intercalation compound or intercalated formamimide disulfide was unstable in acetone.

The C:N ratios of 1:1.9 for Cu-montmorillonite-TU(6) and 1:1.7 for Cu-montmorillonite-TU(w) determined by CHN analysis were in good agreement with that of thiourea (1:2), confirming that no decompo-

sition of thiourea occurred during the solid-solid reaction and washing procedure. Considering the expansion of the interlayer space (ca. 0.7 nm) and the molecular size and geometry of thiourea molecule, the intercalated copper thiourea complex was thought to form a monolayer complex in between the silicate sheets.

In TG-DTA curves of Cu-montmorillonite-TU(6) (not shown), the endothermic peaks due to the melting and vaporization of thiourea at 179 and 230 °C were absent in the DTA curve, indicating that the unreacted thiourea was not contained in the product. The endothermic reaction started from room temperature, which corresponded to a mass loss at the temperature range, was attributed to desorption of the adsorbed water. The exothermic peaks observed at around 200–350 °C were attributed to the oxidative decomposition of the intercalated thiourea. The TG-MS analysis (He flow) showed that the gas evolved at around 60 °C was water. The mass spectra observed in the temperature range beyond 180 °C indicated the peaks due to the ligand, suggesting the decomposition of thiourea and/or copper thiourea complex. These observations confirmed the intercalation of thiourea in the interlayer space.

The electron spin resonance (ESR) spectrum of Cu(II)-montmorillonite exhibited a resonance signal with a g value of 2.05. This resonance was believed to be due to the paramagnetic copper(II) interlayer cation of montmorillonite (Clementz et al., 1973). The absence of the resonance signal at g = 2.05 in the ESR spectrum of the product indicated that thiourea reacted with the copper(II) interlayer cation and reduced Cu(II) to Cu(I) (Kratochvil et al., 1966; Doona and Stanbury, 1996) remained in the interlayer space as a diamagnetic copper(I) thiourea complex, which was ESR silent.

In IR spectrum of the product (Table 2), the absorption bands due to thiourea including NH $_2$  stretching ( $\nu_{\rm NH}$ ) at around 3100–3400 cm $^{-1}$  $NH_2$  bending ( $\delta_{NH2}$ ) at around 1617 cm<sup>-1</sup>, composed bands of  $NH_2$ rocking ( $\rho_{NH2}$ ), N–C–N stretching ( $\nu_{CN}$ ) and C=S stretching ( $\nu_{CS}$ ) at around 1476 and 1398 cm $^{-1}$ , as well as C=S stretching ( $\nu_{\rm CS}$ ) at around 717 cm<sup>-1</sup> (Yamaguchi, et al., 1958; Swaminathan and Irving, 1964; Bott et al., 1998) were slightly shifted compared to those of thiourea molecules, confirming the intercalation of thiourea and in situ complexation between thiourea and the interlayer cation. The absorption band at 1474 cm<sup>-1</sup> of thiourea was slightly shifted towards higher frequency (at  $1476 \text{ cm}^{-1}$ ). The band due to C=S stretching of the product appeared at 717 cm<sup>-1</sup> was shifted to the frequency lower than that of thiourea (at 730 cm<sup>-1</sup>). The shifts of the absorption bands observed for the product were attributed the increased double bond character of the C-N bond (Bott et al., 1998) and the reduced double bond character of the C=S bond (Yamaguchi et al., 1958), suggesting that the bonding between copper and sulfur was predominant in the intercalation compound.

Raman spectrum of the product revealed the bands assigned to thiourea such as N–C–N stretching ( $\nu_{\rm CN}$ ) at 1091 cm<sup>-1</sup>, C=S stretching

**Table 2**Observed frequencies (cm<sup>-1</sup>) in infrared and Raman spectra of thiourea and the product prepared at the molar ratio of 6:1 for thiourea to copper(II) interlayer cation.

Assignment	Thiourea <sup>a</sup>		Thiourea		Cu(II)-montmorillonite-TU(6)	
	IR	R	IR	R	IR	R
$\nu_{ m NH}$	3375	=	3382	_	3355	=
	3273	_	3275	_	3303	_
	3172	_	3177	_	3187	_
$\delta_{NH_2}$	1615	_	1618	_	1617	_
$v_{CN}$	1472	_	1474	_	1476	_
$\rho_{NH2}$ , $\nu_{CN}$ , $\nu_{CS}$	1410	1383	1413	1385	1398	_
$\nu_{\rm CN}$ , $\rho_{\rm NH_2}$ and $\nu_{\rm CS}$	1083	1092	1084	1095	_	1091
$\nu_{CS}$	728	732	730	736	717	721
$\delta_{SCN}$	480	476	488	482	_	474
$\delta_{NCN}$	_	413	_	410	_	437, 430, 422
$v_{\text{CuS}}$ (3-coord Cu) <sup>a</sup>	_	_	_	_	_	249
$v_{\text{CuS}}$ (4-coord Cu) <sup>a</sup>	-	-	-	-	=	221

<sup>&</sup>lt;sup>a</sup> Bott et al., 1998.

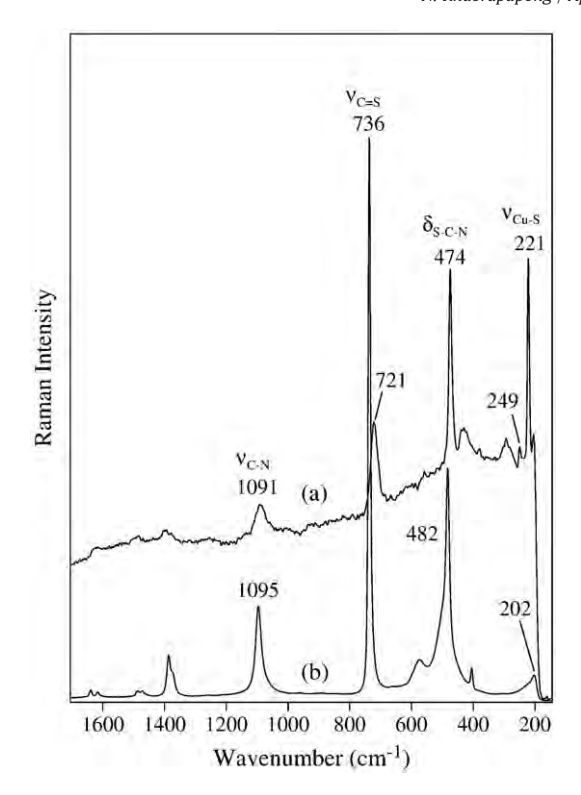


Fig. 3. Raman spectra of Cu(II)-montmorillonite-TU at the molar ratio of thiourea to copper(II) interlayer cation was 6:1 (a) and thiourea (b).

 $(\nu_{CS})$  at 721  $cm^{-1},$  as well as S–C–N bending  $(\delta_{SCN})$  and N–C–N bending ( $\delta_{NCN}$ ) at around 500–400 cm<sup>-1</sup> and they were slightly shifted to the lower wavenumbers compared to those of the thiourea molecules (Fig. 3 and Table 2), supporting the in situ complexation. In the region below 300 cm $^{-1}$ , the bands due to Cu–S linkage ( $\nu_{\text{CuS}}$ ) were observed at 221 (s) and 249 (w) cm<sup>-1</sup>, confirming the formation of copper thiourea complex via sulfur atom. It was reported that the Raman bands of a four-coordinate copper appeared below 230 cm<sup>-1</sup> and that of a three-coordinate copper occurred in the higher region (Bott et al., 1998) (Table 2). The clear observation of the Raman band at 221 cm<sup>-1</sup> indicated that the four-coordinate copper,  $[Cu^{I}(TU)_{4}]^{+}$ , formed as a major product and that at 249 cm<sup>-1</sup> interpreted to the three-coordinate copper,  $[Cu^I(TU)_3]^+$ , obtained as a minor one in the interlayer space (Doona and Stanbury, 1996). The molecular geometry of the intercalated copper(I) thiourea complexes is still not clear at the present.

#### 4. Conclusions

Thiourea was successfully immobilized in the interlayer space of Cu(II)-montmorillonite by solid-solid reaction at room temperature. The copper(II) interlayer cation was reduced to copper(I) and formed the copper(I) thiourea complexes in the interlayer space of montmorillonite. The solid-state intercalation and in situ complexation reported in the present paper was proved to be a way to prepare layered silicate-copper(I) thiourea hybrid.

#### Acknowledgements

The author appreciates the kind assistance and support of Professor Dr. Kazuyuki Kuroda, Waseda University, Japan. Thanks also go to Miss Kanda Saosoong and Mr. Uthit Yaowarit for experimental assistance. The financial support from the Hitachi Scholarship Foundation, Japan, the Thailand Research Fund and Khon Kaen University (grant no. DBG5380004), and the Center of Excellence for Innovation in Chemistry (PERCH-CIC), Commission on Higher Education, Ministry of Education, Thailand were gratefully acknowledged.

#### References

Bott, R.C., Bowmaker, G.A., Davis, C.A., Hope, G.A., Jones, B.E., 1998. Crystal structure of [Cu<sub>4</sub>(tu)<sub>7</sub>](SO<sub>4</sub>)<sub>2</sub>·H<sub>2</sub>O and vibrational spectroscopic studies of some copper(I) thiourea complexes. Inorg. Chem. 37, 651–657.

Clementz, D.M., Pinnavaia, T.J., Mortland, M.M., 1973. Stereochemistry of hydrated copper(II) ions on the interlamellar surfaces of layer silicates. An electron spin resonance study. J. Phys. Chem. 77, 196-200.

Doona, C.J., Stanbury, D.M., 1996. Equilibrium and redox kinetics of copper(II)-thiourea complexes, Inorg, Chem. 35, 3210-3216.

Johnson, K., Steed, J.W., 1998. Effect of non-molecular forces on molecular structure in tris(thiourea)copper(I). J. Chem. Soc., Dalton Trans. 2601-2602

Khaorapapong, N., Ogawa, M., 2007. Solid state intercalation of 8-hydroxyquinoline into Li(I)-, Zn(II)- and Mn(II)-montmorillonites. Appl. Clay Sci. 35, 31-38.

Khaorapapong, N., Kuroda, K., Hashizume, H., Ogawa, M., 2001. Solid state intercalation of 4, 4'-bipyridine and 1, 2-di(4-pyridine)ethylene into the interlayer space of Co (II)-, Ni(II)-, and Cu(II)-montmorillonites. Appl. Clay Sci. 19, 69-76.

Khaorapapong, N., Kuroda, K., Ogawa, M., 2002a. Incorporation of thioacetamide into the interlayer space of montmorillonite by solid-solid reactions. Clay Sci. 11, 549-564

Khaorapapong, N., Kuroda, K., Ogawa, M., 2002b. Intercalation of 8-hydroxyquinoline into Al-smectites by solid-solid reactions. Clays Clay Miner. 50, 428-434

Khaorapapong, N., Ontam, A., Khemprasit, J., Ogawa, M., 2009. Formation of MnS- and NiS-montmorillonites by solid-solid reactions. Appl. Clay Sci. 43, 238-242

Khaorapapong, N., Ontam, A., Ogawa, M., 2010. Formation of ZnS and CdS in the interlayer spaces of montmorillonite. Appl. Clay Sci. 50, 19-24.

Kratochvil, B., Zatko, D.A., Markuszewski, R., 1966. Copper(II) as an analytical oxidant in acetonitrile. Anal. Chem. 38, 770–772. Lagaly, G., Ogawa, M., Dékány, I., 2006. Clay mineral organic intercalation. In: Bergaya,

F., Theng, B.K.G., Lagaly, G. (Eds.), Handbook of Clay Sciences. : Developments in Clay Science, 1. Elsevier, The Netherlands, pp. 309-377.

Ogawa, M., 2004. Photoprocesses in clay-organic complexes. In: Auerbach, S.M., Carrado, K.A., Dutta, P.K. (Eds.), Handbook of Layered Materials. Marcel Dekker, New York, pp. 191-260.

Ogawa, M., Kuroda, K., 1995. Photofunctions of intercalation compounds. Chem. Rev. 95, 399-438.

Ogawa, M., Kuroda, K., 1997. Preparation of inorganic-organic nanocomposites through intercalation of organoammonium ions into layered silicates. Bull. Chem. Soc. Jpn 70, 2593-2618.

Ogawa, M., Hashizume, T., Kuroda, K., Kato, C., 1991. Intercalation of 2, 2'-bipyridine and complex formation in the interlayer space of montmorillonite by solid-solid reactions. Inorg. Chem. 30, 584–585.

Ogawa, M., Nagafusa, Y., Kuroda, K., Kato, C., 1992. Solid-state intercalation of

acrylamide into smectites and Na-taeniolite. Appl. Clay Sci. 7, 291-302.

Ogawa, M., Aono, T., Kuroda, K., Kato, C., 1993. Photophysical probe study of alkylammonium-montmorillonites. Langmuir 9, 1529-1533.

Ogawa, M., Wada, T., Kuroda, K., 1995a. Intercalation of pyrene into alkylammoniumexchanged swelling layered silicates: the effects of the arrangements of the interlayer alkylammonium ions on the states of adsorbates. Langmuir 11, 4598-4600.

Ogawa, M., Hagiwara, A., Handa, T., Kato, C., Kuroda, K., 1995b. Solid state ion exchange reactions between homoionic-montmorillonites and organoammonium salts. J. Porous Mater. 1, 85-89.

Ozin, G.A., Gil, C., 1989. Intrazeolite organometallics and coordination complexes: internal versus external confinement of metal guests. Chem. Rev. 89, 1749-1764

Patil, A.O., Curtin, D.Y., Paul, I.C., 1984. Solid-state formation of quinhydrones from their components. Use of solid-solid reactions to prepare compounds not accessible from solution. J. Am. Chem. Soc. 106, 348-353.

Pinnavaia, T.J., 1983. Intercalated clay catalysts. Science 220, 365-371.

Pleysier, J., Cremers, A., 1975. Stability of silver-thiourea complexes in montmorillonite clay. J. Chem. Soc., Faraday Trans. 71, 256-264.

Stievano, L., Calogero, S., Storaro, L., Lenarda, M., Wagner, F.E., 1998. Metal complexes in a constrained environment. J. Chem. Soc., Faraday Trans. 94, 2627-2632

Swaminathan, K., Irving, H.M.N.H., 1964. Infra-red absorption spectra of complexes of

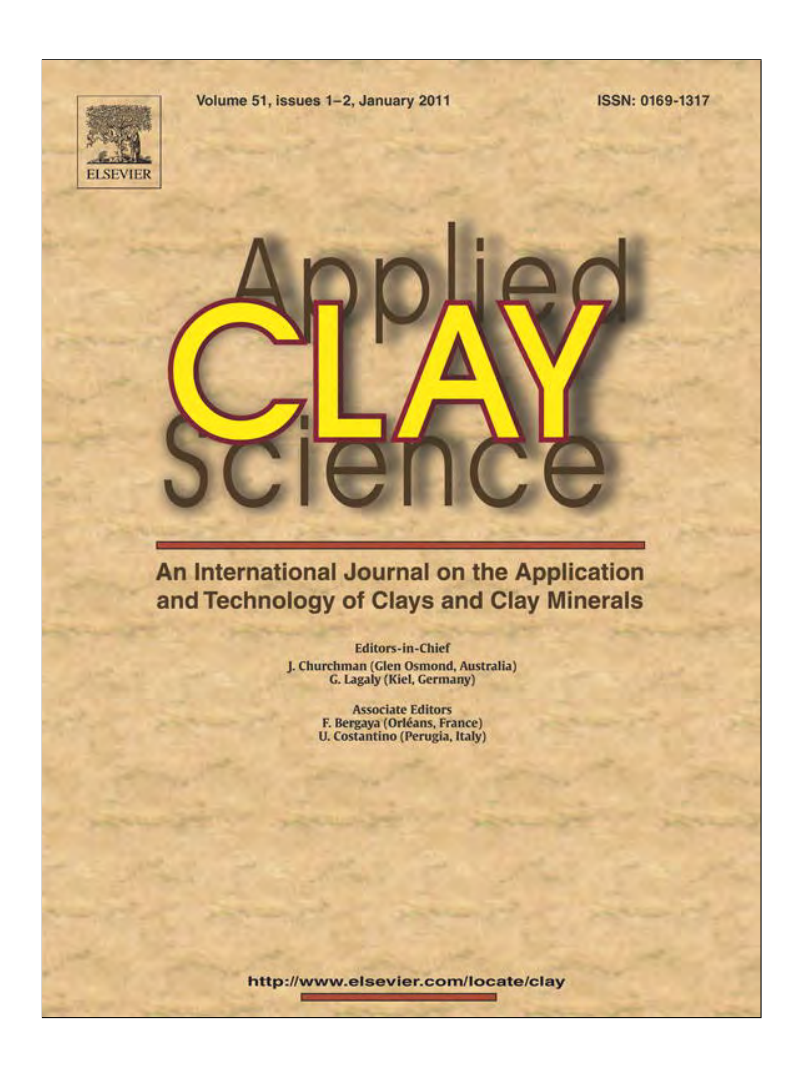
thiourea. J. Inorg. Nucl. Chem. 26, 1291–1294.

Taylor, I.F., Weininger, M.S., Amma, E.L., 1974. Preparation, crystal structure, and bonding of the dimers of tris(thiourea)copper(I) tetrafluoroborate and tris(sdimethylthiourea)copper(I) tetrafluoroborate. Inorg. Chem. 13, 2835–2842

Toda, F., Tanaka, K., Sekikawa, A., 1987. Host-guest complex formation by a solid-solid reaction. J. Chem. Soc., Chem. Commun. 279-280.

Yamaguchi, A., Penland, R.B., Mizushima, S., Lane, T.J., Curran, C., Quagliano, J.V., 1958. Infrared absorption spectra of inorganic coordination complexes. XIV. Infrared studies of some metal thiourea complexes. J. Am. Chem. Soc. 80, 527–529. Provided for non-commercial research and education use.

Not for reproduction, distribution or commercial use.



This article appeared in a journal published by Elsevier. The attached copy is furnished to the author for internal non-commercial research and education use, including for instruction at the authors institution and sharing with colleagues.

Other uses, including reproduction and distribution, or selling or licensing copies, or posting to personal, institutional or third party websites are prohibited.

In most cases authors are permitted to post their version of the article (e.g. in Word or Tex form) to their personal website or institutional repository. Authors requiring further information regarding Elsevier's archiving and manuscript policies are encouraged to visit:

http://www.elsevier.com/copyright

## **Author's personal copy**

Applied Clay Science 51 (2011) 182-186



Contents lists available at ScienceDirect

## **Applied Clay Science**

journal homepage: www.elsevier.com/locate/clay



Note

# Very slow formation of copper sulfide and cobalt sulfide nanoparticles in montmorillonite

Nithima Khaorapapong a,\*, Areeporn Ontam a, Makoto Ogawa b

- a Department of Chemistry and Center of Excellence for Innovation in Chemistry, Faculty of Science, Khon Kaen University, Khon Kaen 40002, Thailand
- b Department of Earth Sciences and Graduate School of Creative Science and Engineering, Waseda University,1-6-1 Nishiwaseda, Shinjuku-ku, Tokyo 169-8050, Japan

#### ARTICLE INFO

Article history:
Received 12 June 2010
Received in revised form 28 October 2010
Accepted 29 October 2010
Available online 16 November 2010

Keywords: Copper sulfide Cobalt sulfide Montmorillonite Solid–solid reactions Intercalation

#### ABSTRACT

Intercalation of semiconductor nanoparticles, copper sulfide or cobalt sulfide, into montmorillonite was carried out by solid-solid reactions of Cu(II)- or Co(II)-montmorillonite with sodium sulfide at room temperature. The intercalation compounds were characterized by X-ray diffraction, thermal analysis, transmission electron microscopy, Raman, UV-visible and photoluminescence spectroscopy. The photoluminescent copper sulfide and cobalt sulfide nanoparticles in the interlayer spaces formed after the sample storage at room temperature for several months.

© 2010 Elsevier B.V. All rights reserved.

#### 1. Introduction

Intercalation of organic and inorganic guest species in the interlayer spaces of inorganic layered materials had attracted increasing interest from a wide range of fundamental and practical viewpoints (Lagaly et al., 2006; Ogawa, 2004). Among possible layered inorganic materials, smectites were studied widely for designing organic-inorganic and inorganic-inorganic hybrids because of its stability and ability to accommodate a wide variety of organic and inorganic species (Ogawa and Kuroda, 1995, 1997). To design novel host-guest systems for possible applications, new or modified preparation procedures are of the interested topics in this field. We were interested in solid-solid reactions because of the ease of operation and the possibility to prepare compounds not accessible from solutions (Patil et al., 1984; Toda et al., 1987). Solid-state intercalation of metal chelates into smectites was previously studied (Khaorapapong and Ogawa, 2007, 2008; Khaorapapong et al., 2000, 2001, 2002a, 2002b; Ogawa et al., 1991). As an extension of the solidsolid reactions, we recently reported the solid-state reactions and in situ formation of ZnS, CdS, MnS and NiS into montmorillonite (Khaorapapong et al., 2008a,b, 2009, 2010).

Semiconductor particles such as copper sulfide and cobalt sulfide have attracted much attention due to their unique optical and electrical properties. The property, morphologies and stoichiometric compositions of the metal sulfides including CuS, Cu<sub>2</sub>S, Cu<sub>9</sub>S<sub>8</sub>, Cu<sub>7</sub>S<sub>4</sub>,

CoS, Co<sub>9</sub>S<sub>8</sub>, Co<sub>3</sub>S<sub>4</sub> and CoS<sub>2</sub> (Chen et al., 2007; Eze and Okeke, 1997; Jiang et al., 2000; Kalyanikutty, et al., 2006; Kore et al., 2001; Qian et al., 1998; Wang et al., 1999, 2005) were affected by the synthetic routes. In addition, the shape, size and dispersion of nanoparticles in the solid samples depended on the nature of layered host materials and host-guest interactions as well as the way of preparation (Németh et al., 2003; Papp et al., 2001, 2004). CuS nanowire arrays were fabricated in anodic alumina membranes by electrodeposition (Wu et al., 2008). Ternary CoS nanoparticles were obtained inside and outside of mesoporous silica (AlMCM-41) (Sohrabnezhad et al., 2008a). The encapsulation of CoS in mordenite by sulfidation (Sadjadi et al., 2007) and in Y-zeolite by hydrothermal reaction (Zhai et al., 2002) was accomplished. Since the properties of copper sulfide and cobalt sulfide are strongly dependent on the particle shape, size, distribution and surface properties, the crystal structure and optoelectronic properties of the metal sulfides may be varied depending on the microenvironment of layered inorganic matrices.

In this study, the solid–solid reactions between Cu(II)– or Co(II)–montmorillonite and sodium sulfide at room temperature and subsequent heating at 200 °C were investigated to form copper sulfide– and cobalt sulfide–montmorillonite hybrids. The long term stability of the composite materials should be of interest in materials chemistry since reactions at room temperature for long periods were scarcely investigated.

#### 2. Experimental

Montmorillonite, Kunipia F (Kunimine Industries), was used as the host material. The cation exchange capacity (CEC) was 1.19 meq/g.

<sup>\*</sup> Corresponding author. Tel.: +66 43 202222 41x12370 2; fax: +66 43 202373. E-mail address: nithima@kku.ac.th (N. Khaorapapong).

Sodium sulfide  $(Na_2S \cdot xH_2O)$  was purchased from Aldrich. Cobalt chloride  $(CoCl_2 \cdot 6H_2O)$  and copper chloride  $(CuCl_2 \cdot 2H_2O)$  were supplied by Univar and BDH. All chemicals were of analytical grade and were used without further purification. Cu(II)- and Co(II)-montmorillonites were prepared by conventional ion exchange. The reactions of sulfide ions (from  $Na_2S$ ) with Cu(II)- and Co(II)-montmorillonites were carried out by solid-solid reactions as reported previously (Khaorapapong et al., 2008a,b, 2009). The molar ratio of sulfide ions to Cu(II) or Co(II) was 1:1. After the reactions, all samples were heated at 200 °C for 1 h in air and allowed to stand in a desiccator with silica gel at room temperature.

XRD patterns were obtained on a Bruker D8 ADVANCE diffractometer using monochromatic CuK $\alpha$  radiation. TEM images were taken on a JEOL JEM-2010 transmission electron microscope with an accelerating voltage of 200 kV. The Raman spectra were recorded on a Jobin Yvon T64000 System Raman spectrometer with a 30 mW argon ion laser operating at 514 nm for excitation. Diffuse reflectance spectra were recorded with a Shimadzu UV-VIS-NIR-3101PC scanning spectrophotometer using an integrated sphere. TG-DTA curves were performed with a Perkin Elmer Pyris Diamond TG-DTA at a heating rate of 10  $^{\circ}$ C min $^{-1}$  under dry air flow using  $\alpha$ -Al $_2$ O $_3$  as a standard material. Inductively couple plasma data were obtained with a Perkin Elmer Optima 2100DV ICP-OES. Luminescence spectra were carried out on Shimadzu RF-5301PC spectrofluorophotometer with the excitation at 340 nm.

#### 3. Results and discussion

The mixture of Cu(II)-montmorillonite or Co(II)-montmorillonite with Na<sub>2</sub>S gave green and black powders with basal spacings ( $d_{001}$ ) of 1.26 and 1.25 nm (Table 1) after the solid–solid reactions. The products were abbreviated as Cu-montmorillonite-Na<sub>2</sub>S and Co-montmorillonite-Na<sub>2</sub>S.

By heating at 200 °C, the basal spacings of the heated Cumontmorillonite-Na<sub>2</sub>S and heated Co-montmorillonite-Na<sub>2</sub>S became 1.15 and 1.19 nm, indicating the expansions of the interlayer spaces. The color changes and the increased basal spacings were ascribed to the intercalation of sulfide ions and *in situ* formation of copper sulfide or cobalt sulfide particles in the interlayer spaces. After storage (4 months), the basal spacings of the heated Cu-montmorillonite-Na<sub>2</sub>S (Fig. 1a) and heated Co-montmorillonite-Na<sub>2</sub>S (Fig. 1b) were 1.21 and 1.19 nm. No reflections due to CuS or CoS, Na<sub>2</sub>S and other compounds were seen in the XRD patterns of the heated products, suggesting that deintercalation did not occur after storage.

The TEM micrographs of the heated products (4 months) showed the platy morphology of the silicate layers (lighter contrast) covered with the copper sulfide or cobalt sulfide particles, which exhibited darker contrast than the silicate layer. The intercalated copper sulfide and cobalt sulfide formed round shaped particles with an average diameter of ca. 2–9 nm. We believed that the darker characteristic images of the particles (Fig. 2b) should be caused by overlapping particles compared with the lighter images of the isolated particles and/or the formation of the metal sulfide particles on the external surface of montmorillonite. Taking the expansion of the interlayer

**Table 1** Basal spacings of hydrated montmorillonites, as-synthesized, heated (200  $^{\circ}$ C) and stored (4 months) products.

Sample	Basal spacing, $d_{001}$ (nm)			
	After reaction <sup>a</sup>	After heating	After 4 months	
Cu(II)-montmorillonite	1.26	-	-	
Co(II)-montmorillonite	1.48	_	_	
Cu-montmorillonite-Na <sub>2</sub> S	1.26	1.15	1.21	
Co-montmorillonite-Na <sub>2</sub> S	1.25	1.19	1.19	

<sup>&</sup>lt;sup>a</sup> At room temperature.

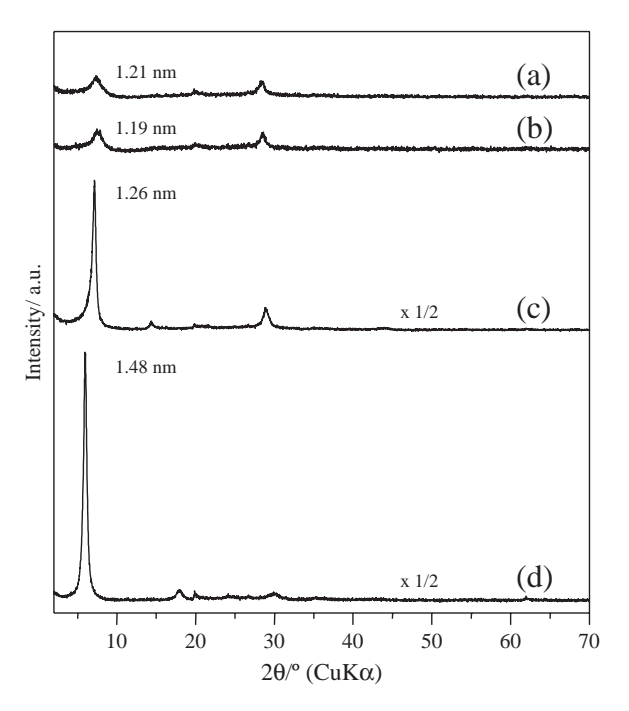


Fig. 1. XRD patterns of (a) heated Cu-montmorillonite- $Na_2S$  (4 months), (b) heated Co-montmorillonite- $Na_2S$  (4 months), (c) Cu(II)-montmorillonite, (d) Co(II)-montmorillonite.

spaces ( $d_{001}$ ) of the heated products (ca. 0.2 nm) and the average size of the particles (2–9 nm) into account, the intercalated copper sulfides and cobalt sulfides formed disk or plate-shape particles with the thicknesses of ca. 0.2 nm and diameters of ca. 2–9 nm.

After 4 months, the heated Cu-montmorillonite-Na $_2$ S showed a sharp and strong Raman band at 423 cm $^{-1}$  (Fig. 3), while no Raman band was observed for the heated Co-montmorillonite-Na $_2$ S. The copper sulfide thin film exhibited a strong and sharp Raman band due to the lattice vibration of CuS at 474 cm $^{-1}$  (Minceva-Sukarova et al., 1997). The MnS particles in montmorillonite showed a characteristic Raman band at 510 cm $^{-1}$  (Khaorapapong et al., 2008b, 2009). The shift of the Raman band of copper sulfides in montmorillonite to lower wavenumbers and the disappearance of the corresponding band for cobalt sulfide were probably caused by the changes in the microenvironment and/or microstructure of copper sulfide and cobalt sulfide particles.

Two stages of mass losses were observed in the TG curves of the two products (not shown). The first stage was observed below 225 °C for Cumontmorillonite-Na $_2$ S or below 200 °C for Co-montmorillonite-Na $_2$ S. The corresponding DTA curves showed the endothermic peaks at 70 °C for Cu-montmorillonite-Na $_2$ S, and at 46 °C and 77 °C for Co-montmorillonite-Na $_2$ S, indicating the removal of adsorbed water. The second stage observed between 225–782 °C for Cu-montmorillonite-Na $_2$ S and 200–793 °C for Co-montmorillonite-Na $_2$ S was ascribed to the decomposition of copper sulfide (Dunn and Muzenda, 2001) or cobalt sulfide (Qian et al., 1998) and dehydroxylation of structural OH groups of montmorillonite (Guggenheim and Koster van Groos, 2001). This thermal behavior confirmed the formation of copper sulfide and cobalt sulfide.

The absorption spectrum of the as-prepared Cu-montmorillonite-Na<sub>2</sub>S showed an onset at 558 nm, a small band at 448 nm, and a broad band beyond 800 nm (Fig. 4a). All the UV-visible spectra of various CuS nanostructures showed a broad band in the region between 300 and 650 nm with a small shoulder and the increased near-IR band (Xu et al., 2006; Zhang and Gao, 2003; Zhang and Wong, 2009; Zhao et al., 2009). The broad absorption band in near-IR region of green CuS sample was attributed to overlapping d–d transitions of copper(II) in a trigonal coordination (Silvester et al., 1991) and/or charge transfer from a valence band of the CuS core to a middle-gap state of the Cu–O shell due to surface

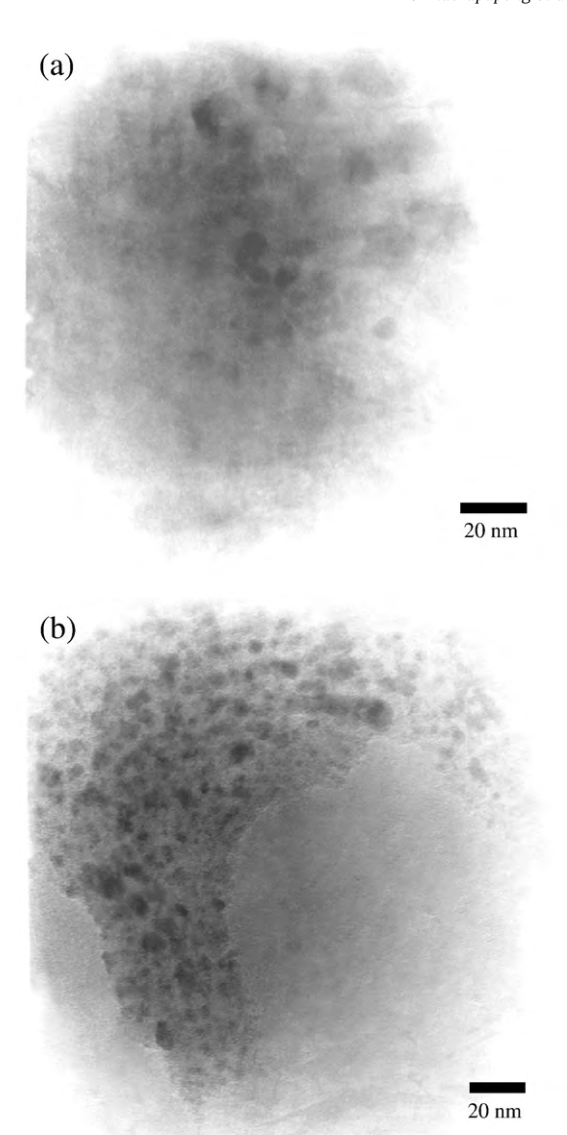


Fig. 2. TEM images of (a) heated Cu-montmorillonite-Na<sub>2</sub>S (4 months), (b) heated Co-montmorillonite-Na<sub>2</sub>S (4 months).

oxidation (Brelle et al., 2000). The absorption spectrum of the as-prepared Co-montmorillonite- $Na_2S$  revealed an onset at 317 nm (not shown). CoS bulk evinced the absorption edge at 347 nm, while CoS in mordenite showed the absorption edge at 322 nm (Sadjadi et al., 2007; Sohrabnezhad et al., 2008b). No emission band was observed for the as-prepared products. CuS fibres did not show a PL signal at 400–800 nm (Jiang et al., 2000). This observation was attributed to the formation of non-luminescent CuS and CoS in the interlayer spaces.

After heating at 200 °C, the absorption onset remained at the same position (558 nm) and the broad absorbance from 350 to 550 nm as well as the near-IR band of the heated Cu-montmorillonite-Na<sub>2</sub>S were seen accompanied by the shift of a weak absorption band at 448 nm to 471 nm. The absorption intensity of the near-IR region beyond 800 nm was decreased, indicating that the amount of intercalated CuS particles was reduced by heating (Drummond et al., 1999). The red shift of the weak band indicated that the dehydrated clay mineral surface provided a different polarity environment compared with the hydrated surface, or the difference in morphology and/or the appearance of a new phase. The absorbance of the heated Co-montmorillonite-Na<sub>2</sub>S also showed the weakening of the broad maximum at 300–800 nm, suggesting changes of the composition of heated Co-montmorillonite-Na<sub>2</sub>S. No emission

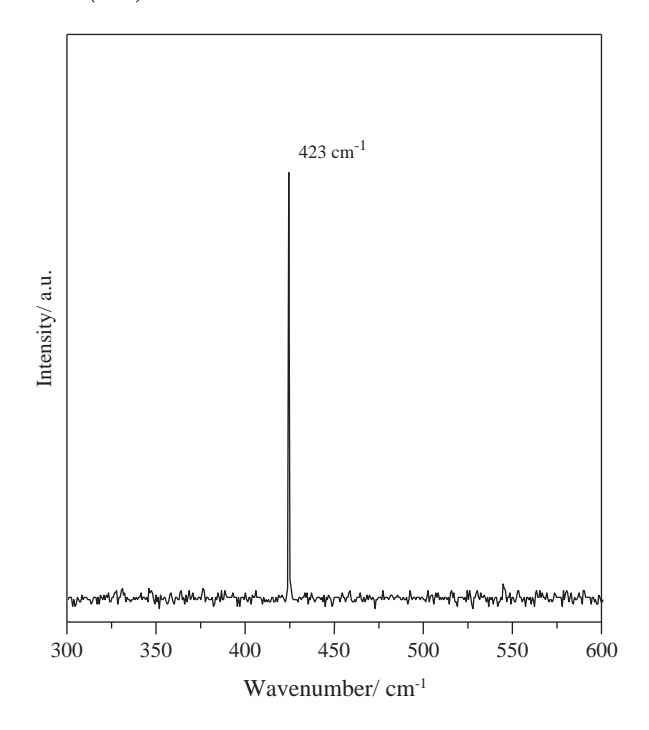
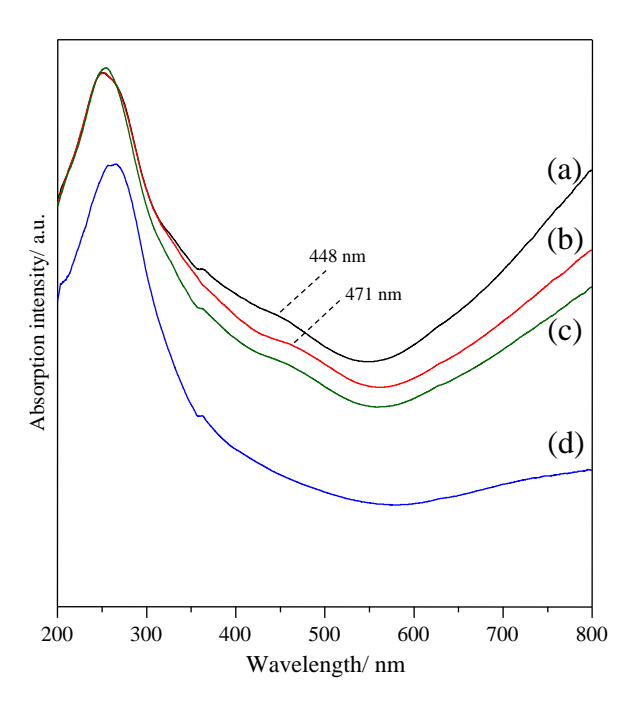


Fig. 3. Raman spectrum of heated Cu-montmorillonite-Na<sub>2</sub>S (4 months).

band was observed for the heated Co-montmorillonite- $Na_2S$ , while weak intensity of the emission band at 439 nm was seen for the heated Cu-montmorillonite- $Na_2S$  (Fig. 5e). This result suggested that the luminescent phase of copper sulfides or cobalt sulfides did not formed by heating, and/or the iron ions as impurity in montmorillonite acted as quenching agent to the new luminescent phases of copper sulfides or cobalt sulfides that formed only small amounts.

After 4 months, the absorption onset (558 nm) and peak (471 nm) were observed at the same wavelength of the heated Cu-montmorillonite- $Na_2S$  (Figs. 4c and 5a). The absorption of the near-IR band and



**Fig. 4.** Diffuse reflectance absorption spectra of (a) as-prepared Cu-montmorillonite-Na<sub>2</sub>S, (b) heated Cu-montmorillonite-Na<sub>2</sub>S, (c) heated Cu-montmorillonite-Na<sub>2</sub>S (4 months), (d) heated Cu-montmorillonite-Na<sub>2</sub>S (16 months).

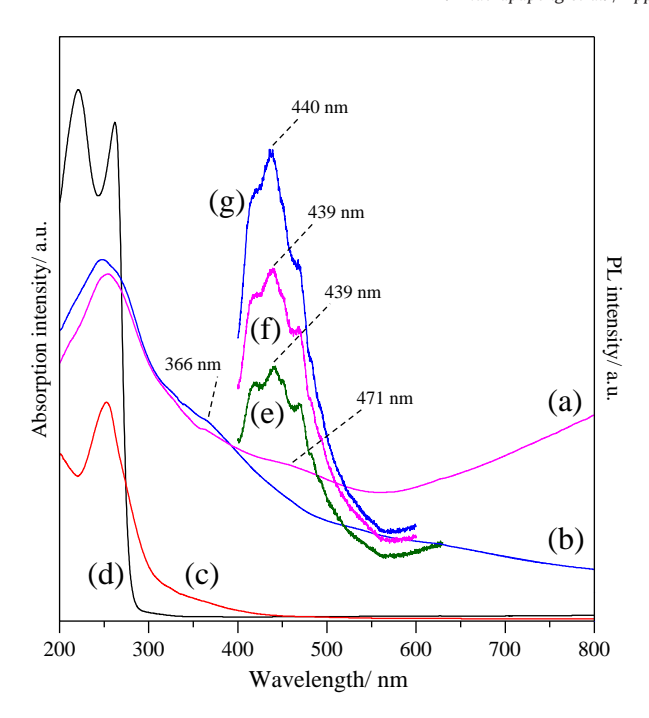


**Fig. 5.** Diffuse reflectance absorption spectra of (a) heated Cu-montmorillonite-Na<sub>2</sub>S (4 months), (b) heated Co-montmorillonite-Na<sub>2</sub>S (4 months), (c) montmorillonite, (d) Na<sub>2</sub>S, and luminescence spectra of (e) heated Cu-montmorillonite-Na<sub>2</sub>S (f) heated Cu-montmorillonite-Na<sub>2</sub>S (4 months), (g) heated Co-montmorillonite-Na<sub>2</sub>S (4 months).

broad absorption at 300–550 nm were further weakened. The small absorption peak at 366 nm was also seen in UV–visible spectrum of the heated Co-montmorillonite-Na<sub>2</sub>S (4 months) (Fig. 5b). The absorbance of Cu<sub>7</sub>S<sub>4</sub> nanoparticles at 450–550 nm (Behboudnia and Khanbabaee, 2007) as well as that of Cu<sub>9</sub>S<sub>8</sub> and Cu<sub>7</sub>S<sub>4</sub> showed small peaks at 440 and 443 nm (Jiang et al., 2000). The change of the absorption spectrum suggested the change of morphology and/or composition of the intercalated metal sulfide particles.

The emission peaks at 439 nm for the heated Cu-montmorillonite-Na<sub>2</sub>S (4 months) (Fig. 5f) and at 440 nm for the heated Comontmorillonite-Na<sub>2</sub>S (4 months) (Fig. 5g) were clearly observed. The luminescence band of CuS nanowires showed at 423 nm (Zhang and Wong, 2009), and those of CuS nanorods revealed at 515 nm (Roy and Srivastava, 2007), as well as at 414 and 437.5 nm (Ou et al., 2005). To the best of our knowledge, no PL spectrum of CoS was reported so far. We reported that the structure of smectites provided two electron-donating sites on the smectite surfaces (Kakegawa et al., 2003). Therefore, the appearance of new luminescent phases of the sulfides as indicated in the absorption and emission spectra of the heated products was thought to be caused by the electron-donating ability of montmorillonite. In the absence of coordinated water and presence of sodium ions, the non-stoichiometric copper sulfides or cobalt sulfides such as  $Cu_{2-x}S$  or  $Co_{2-x}S$  were thought to form as intermediary phases and then slowly transformed into Cu<sub>2</sub>S (Débart, et al., 2006) or Co<sub>2</sub>S, according to the reactions:

$$2CuS + 2Na^{+} \rightarrow Cu_2S + Na_2S$$

$$2\text{CoS} + 2\text{Na}^+ \rightarrow \text{Co}_2\text{S} + \text{Na}_2\text{S}$$

The morphology of copper sulfide or cobalt sulfide particles in the interlayer spaces could be only parallel to the silicate layers while free metal sulfides would aggregate in all directions. This may be the cause of the very slow PL appearance of the emissive copper sulfides or cobalt sulfides.

The absorption spectra of the heated Cu-montmorillonite-Na<sub>2</sub>S (16 months) showed the onset at 532 nm (Fig. 4d). In addition, the absence of the band at 471 nm, and the steep decrease of the near-IR band and absorbance between 300 and 650 nm were observed. The UV-visible spectra of the sulfides in many compounds such as Cu<sub>2</sub>S (Zhang and Gao, 2003),  $Cu_{2-x}S$  (x = 0.2, 0.03) (Zhao et al., 2009), Cu<sub>9</sub>S<sub>8</sub> and Cu<sub>7</sub>S<sub>4</sub> (Jiang et al., 2000) exhibited the absence of the near-IR band. As the onset of heated Cu-montmorillonite-Na<sub>2</sub>S (4 months) at 558 nm was shifted to 532 nm for heated Cu-montmorillonite-Na<sub>2</sub>S (16 months), the size of copper sulfide particles was reduced. In contrast to the absorption spectrum of heated Co-montmorillonite-Na<sub>2</sub>S (16 months) the onset and the band due to cobalt sulfide remained at 317 nm and at 366 nm but the absorbance at 300-800 nm was reduced. The decrease of the absorbance of the heated products (16 months), and the absence of the band at 471 nm and the extremely decreased intensity of the near-IR band of heated Cumontmorillonite-Na<sub>2</sub>S (16 months) may be a consequence of the reduced amounts of CuS and CoS nanoparticles and/or the formation of the other sulfide phases in the interlayer spaces, as well as the change in the composition and/or morphology.

The emission bands of the heated products (16 months) were almost remained at the same wavelength. The luminescence intensity of the heated Co-montmorillonite-Na<sub>2</sub>S (16 months) was slightly increased, whereas the intensity of the luminescence band of heated Cu-montmorillonite-Na<sub>2</sub>S (16 months) was 5 times higher than that of the 4 months product. We assume that the intercalated cobalt sulfide particles were stabilized at the composition formed within 4 months, while the structure and size of the immobilized copper sulfides still further changed. It was reported that the emission intensity of copper sulfide nanoparticles was higher than that of the larger particles because of the increase in the oxygen vacancy on the solid surface and/or defects with decreasing size (Lou et al., 2003). This result was consistent with the blue shift of the absorption onset from 558 nm for Cu-montmorillonite-Na $_2$ S (4 months) to 532 nm for Cu-montmorillonite-Na<sub>2</sub>S (16 months) in the absorption spectra, which was due to the quantum size effect (Roy and Srivastava, 2007). The increase of the emission maximum of the heated products (16 months) was possibly due to the decrease of the size and/or increase of the amount of luminescent phases of sulfide particles.

To study the optical properties of the free nanoparticles, the intercalated nanoparticles were removed by stirring the products (16 months) in 1:1 water/ethanol for 1 h. The emission bands of the dispersed copper sulfide and cobalt sulfide nanoparticles located at 437 and 438 nm (not shown), and a higher intensity was observed than for the dispersed copper sulfide particles. The emission maxima of the dispersed sulfide particles were located almost at the same wavelength compared to the heated products in solid-state (16 months). We assume that similar crystalline structures were responsible for this effect.

#### 4. Conclusions

The immobilization of copper sulfide and cobalt sulfide nanoparticles in the interlayer spaces of montmorillonite was investigated via solid–solid reactions and  $in\ situ$  formation between Cu(II)- or Co(II)-montmorillonite and sodium sulfide, and subsequent heating at 200 °C. The appearance of the absorption and emission bands after 4 months was attributed to the formation of new luminescent phases in the interlayer spaces. The change of morphology and microstructure of copper sulfides or cobalt sulfides were achieved by the host–guest complexation of the sulfides and montmorillonite.

#### Acknowledgements

The financial supports from the Thailand Research Fund (TRF) and Khon Kaen University (grant no. DBG5380004), the Center of Excellence for Innovation in Chemistry (PERCH-CIC), Commission on Higher

Education, Ministry of Education and the Integrated Nanotechnology Research Center, Khon Kaen University, Thailand are gratefully acknowledged.

#### References

- Behboudnia, M., Khanbabaee, B., 2007. Investigation of nanocrystalline copper sulfide Cu<sub>7</sub>S<sub>4</sub> fabricated by ultrasonic radiation technique. J. Cryst. Growth 304, 158–162.
- Brelle, M.C., Torres-Martinez, C.L., McNulty, J.C., Mehra, R.K., Zhang, J.Z., 2000. Synthesis and characterization of CuxS nanoparticles. Nature of the infrared band and charge-
- carrier dynamics. Pure Appl. Chem. 72, 101–117. Chen, X., Zhang, Z., Qiu, Z., Shi, C., Li, X., 2007. Hydrothermal fabrication and characterization of polycrystalline linneite (Co<sub>3</sub>S<sub>4</sub>) nanotubes based on the Kirkendall effect. J. Colloid Interface Sci. 308, 271–275.
- Débart, A., Depont, L., Patrice, R., Tarascon, J.-M., 2006. Reactivity of transition metal (Co, Ni, Cu) sulphides versus lithium: the intriguing case of the copper sulphide. Solid State Sci. 8, 640-651.
- Drummond, K.M., Grieser, F., Healy, T.W., 1999. Steady-state radiolysis study of the reductive dissolution of ultrasmall colloidal CuS. Langmuir 15, 6637-6642
- Dunn, J.G., Muzenda, C., 2001. Thermal oxidation of covellite (CuS). Thermochim. Acta
- Eze, F.C., Okeke, C.E., 1997. Chemical-bath-deposited cobalt sulphide films: preparation effects. Mater. Chem. Phys. 47, 31-36.
- Guggenheim, S., Koster van Groos, A.F., 2001. Baseline studies of the Clay Minerals
- Society source clays: thermal analysis. Clays Clay Miner, 49, 433–443.

  Jiang, X., Xie, Y., Lu, J., He, W., Zhu, L., Qian, Y., 2000. Preparation and phase transformation of nanocrystalline copper sulfides (Cu<sub>9</sub>S<sub>8</sub>, Cu<sub>7</sub>S<sub>4</sub> and CuS) at low temperature. J. Mater. Chem. 10, 2193-2196.
- Kakegawa, N., Kondo, T., Ogawa, M., 2003. Variation of electron-donating ability of smectites as probed by the photoreduction of methyl viologen. Langmuir 19, 3578-3582
- Kalyanikutty, K.P., Nikhila, M., Maitra, U., Rao, C.N.R., 2006. Hydrogel-assisted synthesis of nanotubes and nanorods of CdS, ZnS and CuS, showing some evidence for oriented attachment. Chem. Phys. Lett. 432, 190-194.
- Khaorapapong, N., Ogawa, M., 2007. Solid-state intercalation of 8-hydroxyquinoline into Li(I)-, Zn(II)- and Mn(II)-montmorillonites. Appl. Clay Sci. 35, 31-38.
- Khaorapapong, N., Ogawa, M., 2008. In situ formation of bis(8-hydroxyquinoline) zinc (II) complex in the interlayer spaces of smectites by solid-solid reactions. J. Phys. Chem. Solids 69, 941-948.
- Khaorapapong, N., Kuroda, K., Hashizume, H., Ogawa, M., 2000. Solid state intercalation of 4, 4'-bipyridine into the interlayer space of montmorillonites. Mol. Cryst. Liq. Cryst. 341, 351-356.
- Khaorapapong, N., Kuroda, K., Hashizume, H., Ogawa, M., 2001. Solid-state intercalation of  $\dot{\bf 4}$ ,  $\dot{\bf 4}'$ -bipyridine and 1, 2-di(4-pyridine)ethylene into the interlayer spaces of Co (II)-, Ni(II)- and Cu(II)-montmorillonites. Appl. Clay Sci. 19, 69–76.
- Khaorapapong, N., Kuroda, K., Ogawa, M., 2002a. Incorporation of thioacetamide into the interlayer space of montmorillonite by solid-solid reactions. Clay Sci. 11, 549-564.
- Khaorapapong, N., Kuroda, K., Ogawa, M., 2002b. Intercalation of 8-hydroxyquinoline
- into Al-smectites by solid-solid reactions. Clays Clay Miner. 50, 428–434. Khaorapapong, N., Ontam, A., Youngme, S., Ogawa, M., 2008a. Solid-state intercalation and in situ formation of cadmium sulfide in the interlayer space of montmorillonite. J. Phys. Chem. Solids 69, 1107–1111.
- Khaorapapong, N., Ontam, A., Ogawa, M., 2008b. Formation of MnS particles in the interlayer space of montmorillonite. Mater. Lett. 62, 3722-3723.
- Khaorapapong, N., Ontam, A., Khemprasit, J., Ogawa, M., 2009. Formation of MnS and
- NiS-montmorillonites by solid-solid reactions. Appl. Clay Sci. 43, 238–242. Khaorapapong, N., Ontam, A., Ogawa, M., 2010. Formation of ZnS and CdS in the interlayer spaces of montmorillonite. Appl. Clay Sci. 50, 19-24.
- Kore, R.H., Kulkarni, J.S., Haram, S.K., 2001. Effect of nonionic surfactants on the kinetics of disproportion of copper sulfide nanoparticles in the aqueous sols. Chem. Mater. 13, 1789-1793.
- Lagaly, G., Ogawa, M., Dékány, I., 2006. Clay mineral organic intercalation. In: Bergaya, F., Theng, B.K.G., Lagaly, G. (Eds.), Handbook of Clay Sciences, Developments in Clay Science, vol. 1. Elsevier Science, Amsterdam, pp. 309–377.

- Lou, Y., Chen, X., Samia, A.C., Burda, C., 2003. Femtosecond spectroscopic investigation of the carrier lifetimes in digenite quantum dots and discrimination of the electron and hole dynamics via ultrafast interfacial electron transfer. J. Phys. Chem. B 107,
- Minceva-Sukarova, B., Najdoski, M., Grozdanov, I., Chunnilall, C.J., 1997. Raman spectra of thin solid films of some metal sulfides. J. Mol. Struct. 410-411, 267-270.
- Németh, J., Dékány, I., Süvegh, K., Marek, T., Klencsár, Z., Vértes, A., Fendler, J.H., 2003. Preparation and structural properties of tin oxide montmorillonite nanocomposites. Langmuir 19, 3762-3769.
- Ogawa, M., 2004. Photoprocess in clay-organic complexes. In: Auerbach, S.M., Carrado, K.A., Dutta, P.K. (Eds.), Handbook of Layered Materials. Marcel Dekker, New York, pp. 191-260.
- Ogawa, M., Kuroda, K., 1995. Photofunctions of intercalation compounds. Chem. Rev. 95. 399-438.
- Ogawa, M., Kuroda, K., 1997. Preparation of inorganic-organic nanocomposites through intercalation of organoammonium ions into layered silicates. Bull. Chem. Soc. Jpn. 70, 2593-2618.
- Ogawa, M., Hashizume, T., Kuroda, K., Kato, C., 1991. Intercalation of 2, 2'-bipyridine and complex formation in the interlayer space of montmorillonite by solid-solid reactions. Inorg. Chem. 30, 584-585.
- Ou, S., Xie, Q., Ma, D., Liang, J., Hu, X., Yu, W., Qian, Y., 2005. A precursor decomposition route to polycrystalline CuS nanorods. Mater. Chem. Phys. 94, 460-466.
- Papp, S., Szücs, A., Dékány, I., 2001. Preparation of Pd<sup>0</sup> nanoparticles stabilized by polymers and layered silicate. Appl. Clay Sci. 19, 155-172.
- Papp, S., Szél, J., Oszkó, A., Dékány, I., 2004. Synthesis of polymer-stabilized nanosized rhodium particles in the interlayer space of layered silicates. Chem. Mater. 16, 1674-1685.
- Patil, A.O., Curtin, D.Y., Pual, I.C., 1984. Solid-state formation of quinhydrones from their components. Use of solid-solid reactions to prepare compounds not accessible from solution. J. Am. Chem. Soc. 106, 348-353.
- Qian, X.F., Zhang, X.M., Wang, C., Tang, K.B., Xie, Y., Qian, Y.T., 1998. Solvent-thermal preparation of nanocrystalline pyrite cobalt disulfide. J. Alloy. Compd. 278, 110-112
- Roy, P., Srivastava, S.K., 2007. Low-temperature synthesis of CuS nanorods by simple wet chemical method. Mater. Lett. 61, 1693-1697.
- Sadjadi, M.S., Pourahmad, A., Sohrabnezhad, Sh., Zare, K., 2007. Formation of NiS and CoS semiconductor nanoparticles inside mordenite-type zeolite. Mater. Lett. 61, 2923-2926
- Silvester, E.J., Grieser, F., Sexton, B.A., Healy, T.W., 1991. Spectroscopic studies on copper sulfide sols. Langmuir 7, 2917–2922.

  Sohrabnezhad, Sh., Pourahmad, A., Sadjadi, M.S., Sadeghi, B., 2008a. Nickel cobalt
- sulfide nanoparticles grown on AlMCM-41 molecular sieve. Physica E 40, 684-688.
- Sohrabnezhad, Sh., Pourahmad, A., Sadjadi, M.S., Zanjanchi, M.A., 2008b. Growth and characterization of NiS and NiCoS nanoparticles in mordenite zeolite host. Mater.
- Sci. Eng. C 28, 202–205. Toda, F., Tanaka, K., Sekikawa, A., 1987. Host-guest complex formation by a solid–solid reaction. J. Chem. Soc. Chem. Commun. 279-280.
- Wang, C., Zhang, X.M., Qian, X.F., Xie, Y., Qian, Y.T., 1999. A low temperature route to nanocrystalline Co<sub>9</sub>S<sub>8</sub>. J. Phys. Chem. Solids 60, 2005–2008.
- Wang, Q., Xu, Z., Yin, H., Nie, Q., 2005. Fabrication of transition metal sulfides nanocrystallites via an ethylenediamine-assisted route. Mater. Chem. Phys. 90,
- Wu, C., Shi, J.-B., Chen, C.-J., Chen, Y.-C., Lin, Y.-T., Wu, P.-F., Wei, S.-Y., 2008. Synthesis and optical properties of CuS nanowires fabricated by electrodeposition with anodic alumina membrane. Mater. Lett. 62, 1074-1077.
- Xu, H., Wang, W., Zhu, W., 2006. Sonochemical synthesis of crystalline CuS nanoplates via an in situ template route. Mater. Lett. 60, 2203-2206.
- Zhai, Q.-Z., Jiang, T.-Ś., Hu, W.-H., Guan, X., Wang, W., Qiu, S., 2002. Preparation, characterization, and luminescence of host (Y zeolite)-guest (FeS, CoS, NiS) nanocomposite materials. Mater. Res. Bull. 37, 1837–1842.
- Zhang, P., Gao, L., 2003. Copper sulfide flakes and nanodisks. J. Mater. Chem. 13, 2007-2010.
- Zhang, F., Wong, S.S., 2009. Controlled synthesis of conducting metal sulfide nanowires. Chem. Mater. 21, 4541-4554.
- Zhao, Y., Pan, H., Lou, Y., Qiu, X., Zhu, J., Burda, C., 2009. Plasmonic Cu<sub>2 x</sub>S nanocrystals: optical and structural properties of copper-deficient copper(I) sulfides. J. Am. Chem. Soc. 131, 4253-4261.

Provided for non-commercial research and education use.

Not for reproduction, distribution or commercial use.



This article appeared in a journal published by Elsevier. The attached copy is furnished to the author for internal non-commercial research and education use, including for instruction at the authors institution and sharing with colleagues.

Other uses, including reproduction and distribution, or selling or licensing copies, or posting to personal, institutional or third party websites are prohibited.

In most cases authors are permitted to post their version of the article (e.g. in Word or Tex form) to their personal website or institutional repository. Authors requiring further information regarding Elsevier's archiving and manuscript policies are encouraged to visit:

http://www.elsevier.com/copyright

## Author's personal copy

Materials Letters 65 (2011) 657-660



Contents lists available at ScienceDirect

### Materials Letters

journal homepage: www.elsevier.com/locate/matlet



## Preparation of zinc oxide-montmorillonite hybrids

Nithima Khaorapapong a,\*, Nuttaporn Khumchoo a, Makoto Ogawa b

- a Department of Chemistry and Center of Excellence for Innovation in Chemistry, Faculty of Science, Khon Kaen University, Khon Kaen 40002, Thailand
- b Department of Earth Sciences and Graduate School of Creative Science and Engineering, Waseda University, Nishiwaseda 1-6-1, Shinjuku-ku, Tokyo 169-8050, Japan

#### ARTICLE INFO

Article history: Received 6 July 2010 Accepted 23 November 2010 Available online 26 November 2010

Keywords:
Montmorillonite
Organophilic-montmorillonite
Zinc oxide
Optical properties

#### ABSTRACT

The new hybrid materials of zinc oxide with montmorillonite were synthesized by a reaction between the aqueous solutions of the reactants of zinc oxide (zinc chloride and sodium hydroxide solutions) and montmorillonite or hexadecyltrimetylammonium—montmorillonite. The hybrids were characterized by powder X-ray diffraction, Fourier transform-infrared, UV-visible and photoluminescence spectroscopies. The diffuse reflectance absorption spectra of the hybrids exhibited the absorption onsets at 375 nm for zinc oxide—montmorillonite and at 378 nm for zinc oxide—hexadecyltrimetylammonium—montmorillonite, respectively, confirming the formation of zinc oxide in the hybrid materials. The photoluminescence bands of both hybrids, which can be attributed to singly ionized oxygen vacancy in zinc oxide, were observed at 548 nm. The enhancement in emission intensity of the zinc oxide hybrids may be probably due to increase in oxygen vacancies defect arose by the surrounding environment of montmorillonite.

© 2010 Elsevier B.V. All rights reserved.

#### 1. Introduction

The preparation of inorganic nanoparticles with controlled structures, morphologies in solid matrices is an interesting topic from basic scientific and practical studies [1]. Smectites, a 2:1 type layered silicate, including montmorillonite exhibit beneficial properties, such as large surface area, swelling behavior, adsorptive property and ion exchange property [2]. The surface of montmorillonite can be used to prevent the guest particles from aggregation. Taking advantages of smectites for nanoparticle preparation and immobilization, the hybrid materials of smectite-semiconductor particles including metal [3], metal oxides [4–6], and metal sulfides have been successfully prepared and evaluated [7–11]. Organophilic-smectites, which are long-chain organoammonium exchanged smectites, are also known to support inorganic nanoparticles to form hybrids.

In this paper, we report the preparation of zinc oxide in the aqueous clay suspension. Zinc oxide (ZnO) is one of semiconductors studied most extensively because of its interesting characteristics such as a direct band gap (ca. 5.3 eV) at 300 K, large exciton binding energy (ca. 60 meV), high melting temperature (2248 K) and so on [12]. It has been reported that inorganic–organic or inorganic–inorganic hybridized in nanometer scale may provide a combination of properties of both species and have advanced functions depending on the compositions [13,14]. The nanostructures of ZnO hybrid materials dominated by the mesoporous silica and clay mineral were reported [15–17]. Zinc oxide nanoparticles coated with titania/polydimethylsiloxane hybrid were synthesized by co-hydrolysis and co-condensation [18]. Due to the

interesting properties and potential applications of ZnO nanostructures and hybrids that differ from those of bulk crystals, novel efficient synthesis method and/or hybrided species are required. Here, we report the preparation and the optical properties of ZnO–montmorillonite hybrids.

#### 2. Experimental

The sodium montmorillonite used in the present study was Kunipia F (the reference clay sample of the Clay Science Society of Japan) obtained from Kunimine Industries, Japan. The cation exchange capacity (CEC) of Na–montmorillonite is 119 meq/100 g of clay. Zinc chloride (ZnCl<sub>2</sub>) and sodium hydroxide (NaOH) were obtained from Carlo Erba Reagenti. Hexadecyltrimetylammonium (HDTMA) bromide was purchased from Sigma-Aldrich. All chemicals were used without further purification.

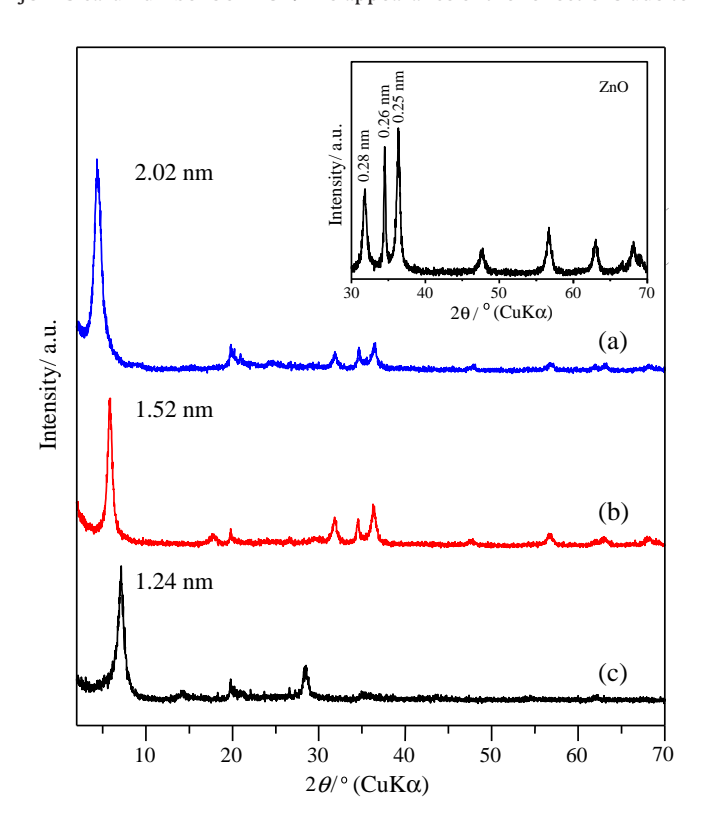
ZnO was synthesized by the reaction between zinc chloride and sodium hydroxide at the molar ratio of Zn<sup>2+</sup>:OH<sup>-</sup> was 1:15. The aqueous solution of zinc chloride was mixed with sodium hydroxide solution and vigorously stirred at 70 °C for 24 h. HDTMA exchanged montmorillonite was prepared by a conventional ion exchange reaction of Na-montmorillonite and aqueous solution of HDTMA bromide [19]. ZnO-montmorillonite and ZnO-HDTMA-montmorillonite were prepared by adding the aqueous mixture of zinc chloride and sodium hydroxide solutions into the suspension of Na-montmorillonite or organomontmorillonite with continuous stirring at 70 °C and the mixture was allowed to react for 24 h. The amount of zinc oxide in each sample was 0.0610 g per 0.1 g of clay. The resulting solids were separated by centrifugation, washed several times with deionized water, and dried at 50 °C for 3 days.

<sup>\*</sup> Corresponding author. Tel.: +66 43 202222 41x12370 2; fax: +66 43 202373. E-mail address: nithima@kku.ac.th (N. Khaorapapong).

X-ray diffraction (XRD) data were obtained on a Bruker D8 ADVANCE diffractometer using monochromatic CuKα radiation. SEM micrographs were carried out on a Hitachi-52380N scanning electron microscope. TEM images were taken on the Hitachi H-8100A and H-7650 transmission electron microscopes. Fourier transform-infrared (FT-IR) spectra were recorded on a Perkin-Elmer Spectrum One FT-IR spectrometer using KBr pellet method. Raman spectra were performed on Renishaw inVia Raman microscope. Diffuse reflectance absorption spectra of the solid samples were performed on a Shimadzu UV-VIS-NIR-3101PC scanning spectrophotometer using an integrated sphere. Photoluminescence spectra were measured on a Shimadzu RF-5301PC spectrofluorophotometer in the wavelength range of 300–900 cm<sup>-1</sup> with the excitation wavelength at 350 nm.

#### 3. Results and discussions

The XRD patterns of ZnO-montmorillonite and ZnO-HDTMAmontmorillonite hybrids are shown in Fig. 1 together with that of Namontmorillonite. The reflections of ZnO crystal as shown in the inset of Fig. 1 located at d = 0.28, 0.26 and 0.25 nm, while the basal spacing  $(d_{001})$  of Na-montmorillonite was observed at low angle region  $(2\theta < 10^\circ, d = 1.24 \text{ nm})$  (Fig. 1c). After the reactions, the  $d_{001}$  peak of ZnO-montmorillonite and ZnO-HDTMA-montmorillonite shifted towards to lower angle side when compared with Na-montmorillonite and the reflections due to ZnO were also seen at higher angle region. The basal spacing of ZnO-montmorillonite and ZnO-HDTMAmontmorillonite were 1.52 (Fig. 1b) and 2.02 nm (Fig. 1a), respectively. The gallery heights were determined to be 0.56 for ZnOmontmorillonite and 1.06 nm for ZnO-HDTMA-montmorillonite by subtracting the thickness of the silicate layer (0.96 nm) [4], showing the expansion of the interlayer spaces that may thought to be caused by the intercalation of ZnO particles and/or organic species. All of the reflections at d = 0.28, 0.26 and 0.25 nm of ZnO and the hybrids are well confirmed to a ZnO hexagonal wurtzite lattice, according to JCPDS card number 36-1451. The appearance of the reflections due to



 $\label{eq:fig.1.} \textbf{Fig. 1.} \ \textbf{XRD patterns of (a) ZnO-HDTMA-montmorillonite, (b) ZnO-montmorillonite, and (c) Na-montmorillonite and (inset) ZnO crystal.$ 

ZnO crystal in the XRD patterns of ZnO-montmorillonite and ZnO-HDTMA-montmorillonite was ascribed to the formation of ZnO on the solid surfaces.

Morphologies of the products were examined by SEM and TEM analyses. The images of ZnO (Fig. 2a,d) showed flower like microstructures (averaged diameter of ca. 1.5 µm) composed of hexagonal ZnO rods. The flower-shaped structures with the average diameter ca. 1.2 and 1.4 µm were seen on the external surface of clay mineral for ZnO-montmorillonite (Fig. 2b,e) and ZnO-HDTMA-montmorillonite (Fig. 2c), respectively. The presence of some ZnO nanoparticles embedded in the interlayer space of montmorillonite was also seen on the edge of silicate layers for ZnO-montmorillonite (not shown) and ZnO-HDTMA-montmorillonite (Fig. 2f). The images of the hybrid materials indicated the decrease of size and size distribution ZnO particles on the surface of clay mineral, which were consistent with the blue shift of the absorption onsets and increase of PL intensities mentioned below.

The Raman spectrum of ZnO (Fig. 3) showed a sharp and strong Raman active peak at  $441~\text{cm}^{-1}$ , which can be attributed to the optical phonon  $\text{E}_2$ mode of hexagonal wurtzite ZnO and the Raman peaks at 338 and  $1122\,\mathrm{cm^{-1}}$  correlated to  $\mathrm{E_{2H}}\mathrm{-E_{2L}}$  (multiple-phonon scattering process), and  $2A_{1L}$  or  $2E_{1L}$  modes [20,21]. In addition, the Raman band at around 576 cm<sup>-1</sup> assigned to the E<sub>1L</sub> mode was caused by the impurities and defects in ZnO such as oxygen vacancies and zinc interstitials [20]. On the other hand, the Raman spectra ZnO-montmorillonite and ZnO-HDTMAmontmorillonite (not shown) did not show any Raman lines in the wavenumber of  $200-1200~\text{cm}^{-1}$ ; we assume that the products exhibited the extremely strong luminescence, which covered the weak Raman signals [22]. In FT-IR spectrum of ZnO-HDTMA-montmorillonite, the characteristic bands due to asymmetric and symmetric -CH<sub>2</sub> stretching vibrations modes of amine [23] were slightly shifted to higher frequency regions at 2923 and 2851 cm<sup>-1</sup>, respectively, when compared to those observed for HDTMA (at around 2918 and 2850 cm<sup>-1</sup>), indicating the formation of HDTMA in montmorillonite. The Zn-O stretching vibration bands (at around 429–547 cm<sup>-1</sup>) [24] were not seen in the FT-IR spectra of the two hybrids because of the overlapping with the absorption bands due to Si-O-Si bending vibration of montmorillonite appeared at 522 and 467 cm<sup>-1</sup> [25]. The FT-IR spectra of the products did not shown any additional bands, suggesting that no other species was formed during the

The diffuse reflectance absorption spectra of ZnO, ZnO hybrids and Na-montmorillonite were obtained. The UV-visible spectrum of ZnO showed an absorption onset at 383 nm (3.31 eV) (Fig. 4a). The characteristic onsets of ZnO-montmorillonite and ZnO-HDTMAmontmorillonite appeared at 375 (ca. 3.33 eV) (Fig. 4b) and 378 nm (ca. 3.39 eV) (Fig. 4c), respectively. The absorption edge of ZnO nanoparticles dispersed in DMSO was found at 348 nm and those of ZnO nanoparticles in the presence of montmorillonite revealed at 272.2, 277.7 and 365.1 nm [26]. The absorption onsets of calcined ZnO/LDHs were reported at around 390 nm [27]. The absorption band at around 350 nm was observed for zinc oxide in mesoporous silica [28]. This observation was attributed to the formation of ZnOmontmorillonite and ZnO-HDTMA-montmorillonite hybrids. The absorption onsets of the hybrids were slightly blue shifted with respected to the ZnO phase, indicating the slight decrease of the size and size distribution of ZnO formed in the hybrids.

The photoluminescence band of ZnO was observed at 544 nm (Fig. 4g) and those of ZnO hybrids were remarked at 548 nm (Fig. 4e,f). The luminescence band in UV region of ZnO showed at 380 nm and the green emission exhibited at 515 nm [29]. The emission band of colloidal ZnO appeared at around 526 nm and those of mesoporous silicamodified ZnO and ZnO-coated polystyrene were observed at around 520 nm [30]. It is well known that ZnO reveals four emission bands in PL spectrum: (1) near band edge emission (UV emission) corresponding to free-exciton recombination appeared at around 380 nm, (2) blue emission due to intrinsic defects such as oxygen and zinc interstitials exhibited at around 460 nm, (3) green emission caused by impurities, a

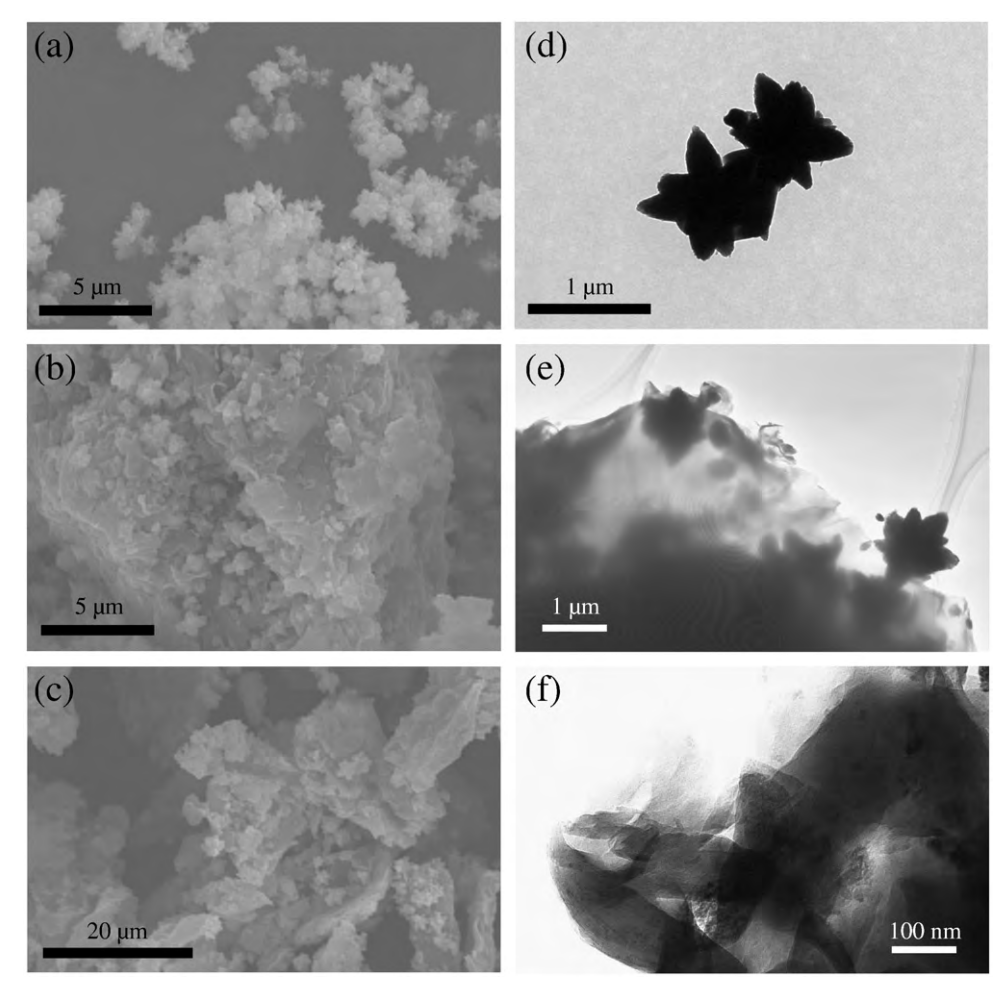


Fig. 2. SEM and TEM images of (a, d) ZnO, (b, e) ZnO-montmorillonite, and (c, f) ZnO-HDTMA-montmorillonite.

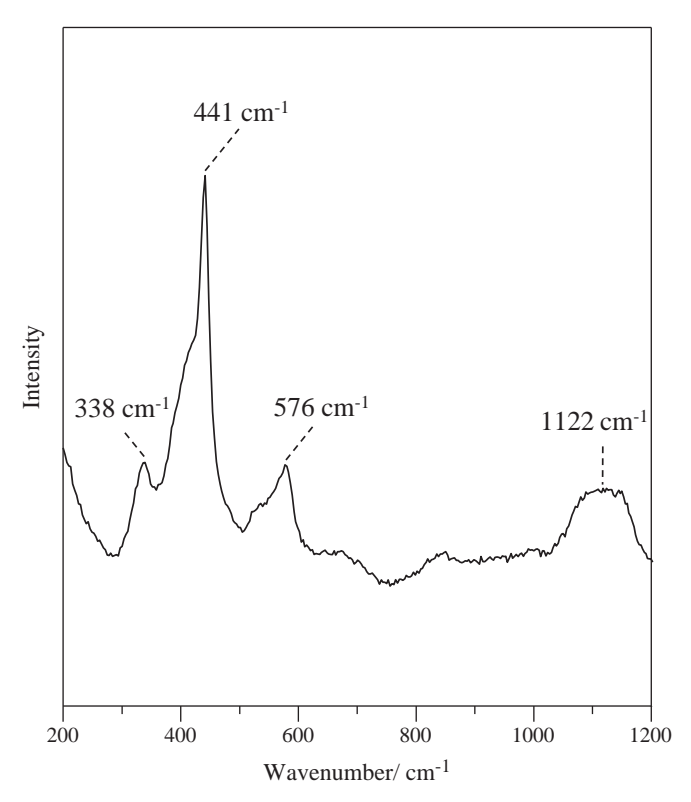


Fig. 3. Raman spectrum of ZnO.

structural defects in the crystal such as oxygen vacancies, zinc interstitials and so on showed at around 540 nm and (4) red emission owing to oxygen and zinc anti-sites arose at around 630 nm [31]. The photoluminescent enhancement due to the concentration and energy transfer from polyaniline to ZnO, and blue shifted emission band caused by chemical interaction between NH groups of polyaniline chains and surface zinc ions were significantly observed in the PL spectra of ZnOpolyaniline film [32]. These observations suggested that the green emission observed at around 548 nm for both products can be expected for the formation of ZnO in the hybrids materials. By comparison with PL intensity of ZnO (Fig. 4g), the enhancement in green emission intensity of ZnO hybrids was thought to be due to the increase in oxygen vacancies and/or the decrease of size as well as size distribution of ZnO particles created by the surrounding environment of montmorillonite or HDTMA-montmorillonite. The highest emission intensity took place in the PL spectrum of ZnO-HDTMA-montmorillonite was attributed to passivation of the ionized oxygen on ZnO surface by electrostatic interaction between ZnO and the surfactant on the surface [33] and/or prevention of the aggregation ZnO by HDTMA on the silicate layers.

The optical properties of ZnO are influenced by organically modified and pristine montmorillonite surface. Further studies on the formation of metal oxide hybrids by changing compositions, method and/or layered inorganic solids are worth investigating to construct novel low dimensional nanohybrid materials with useful properties.

#### 4. Conclusions

Zinc oxide-montmorillonite hybrids were prepared by simply synthetic method at low temperature. The powder diffraction data N. Khaorapapong et al. / Materials Letters 65 (2011) 657-660

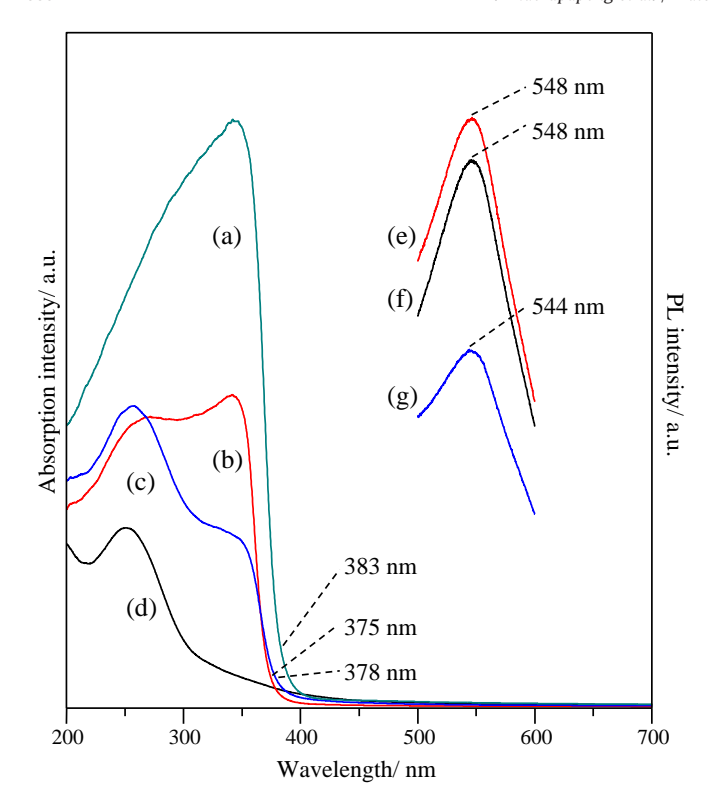


Fig. 4. Diffuse reflectance absorption spectra of (a) ZnO, (b) ZnO-montmorillonite, (c) ZnO-HDTMA-montmorillonite, (d) Na-montmorillonite and photoluminescence spectra of (e) ZnO-HDTMA-montmorillonite, (f) ZnO-montmorillonite and (g) ZnO.

and the absorption and luminescence spectra confirmed the formation of zinc oxide. The increase in green emission intensity of zinc oxide in hybrid materials was caused by the surrounding environment of montmorillonite or HDTMA-montmorillonite. The highest emission intensity of ZnO in HDTMA-montmorillonite is due to spatial separation and/or interfacial effect of the surfactant adsorbed on the solid surface.

#### Acknowledgements

The present work was supported by the Thailand Research Fund (TRF) and Khon Kaen University (grant no. DBG5380004), the Center of Excellence for Innovation in Chemistry (PERCH-CIC), Commission on Higher Education, Ministry of Education, and the National Research Project, Khon Kaen University, Thailand. We would like to thank the Hitachi High-technologies for partial support on TEM instrument.

#### References

- [1] Ogawa M. Photoprocess in clay-organic complexes. In: Auerbach SM, Carrado KA, Dutta PK, editors. Handbook of Layered Materials. New York: Marcel Dekker; 2004. p. 191-260.
- [2] Lagaly G, Ogawa M, Dékány I. Clay Mineral Organic Interactions. In: Bergaya F, Theng BKG, Lagaly G, editors. Handbook of Clay Science, Developments in Clay Science, volume 1. Amsterdam: Elsevier; 2006. p. 309-77.
- Ravindranathan P, Malla PB, Komarneni S, Roy R. Catal Lett 1990;6:401-8.
- Miyoshi H, Yoneyama H. J Chem Soc, Faraday Trans 1989;85:1873-80.
- Yoneyama H, Haga S, Yamanaka S. J Phys Chem 1989;93:4833-7.
- Yamanaka S, Makita K. J Porous Mater 1995;1:29–41.
- Stramel RD, Nakamura T, Thomas JK. Chem Phys Lett 1986;130:423-5.
- Liu X, Thomas JK. J Colloid Inter Sci 1989;129:476-82.
- Khaorapapong N, Ontam A, Youngme S, Ogawa M. J Phys Chem Solids 2008;69: 1107-11.
- [10] Khaorapapong N, Ontam A, Ogawa M. Mater Lett 2008;62:3722-3.
- Khaorapapong N, Ontam A, Khemprasit J, Ogawa M. Appl Clay Sci 2009;43:
- Shan FK, Shin BC, Jang SW, Yu YS. J Eur Ceram Soc 2004;24:1015-8.
- Ogawa M, Kuroda K. Chem Rev 1995;95:399-438.
- Ogawa M, Kuroda K. Bull Chem Soc Jpn 1997;70:2593-618.
- Zhang WH, Shi JL, Wang LZ, Yan DS. Chem Mater 2000;12:1408–13. Xiong Y, Zhang LZ, Tang GQ, Zhang GL, Chen WJ. J Lumin 2004;110:17–22.
- Hur SG, Kim TW, Hwang SJ, et al. J Phys Chem B 2006;110:1599–604. Nakade M, Ogawa M. J Mater Sci 2007;42:4254–9.
- He H, Frost RL, Bostrom T, et al. Appl Clay Sci 2006;31:262-71.
- Mohajerani MS, Mazloumi M, Lak A, et al. J Cryst Growth 2008;310:3621-5. [20]
- Gao YJ, Zhang WC, Wu XL, et al. Appl Surf Sci 2008;255:1982–7. Fleger Y, Nagli L, Gaft M, Rosenbluh M. J Lumin 2009;129:979–83.
- Guo H, Jing X, Zhang L, Wang J. J Mater Sci 2007;42:6951-5.
- Wang YD, Zhang S, Ma CL, Li HD. J Lumin 2007;126:661-4.
- Ŝontevska V, Jovanovski G, Makreski P. J Mol Struct 2007;834-836:318-27.
- Németh J, Rodríguez-Gattorno G, Díaz D, Vázquez-Olmos AR, Dékány I. Langmuir 2004:20:2855-60.
- Yuan S, Li Y, Zhang Q, Wang H. Colloids Surf A 2009;348:76–81.
- Vaishnavi TS, Haridoss P, Vijayan C. Mater Lett 2008;62:1649-51. [28]
- Wahab R, Ansari SG, Kim YS, et al. Mater Res Bull 2007;42:1640-8.
- Zhang JJ, Gao G, Zhang M, et al. J Colloid Interface Sci 2006;301:78-84.
- Ghosh A, Deshpande NG, Gudage YG, et al. J Alloy Compd 2009;469:56-60. Zheng ZX, Xi YY, Dong P, et al. Phys Chem Comm 2002;5:63-5.
- [33] Usui H. Mater Lett 2009;63:1489-92.

FISEVIER

Contents lists available at ScienceDirect

## Journal of Colloid and Interface Science

www.elsevier.com/locate/jcis



#### **Short Communication**

## Simple preparation of a cadmium selenide-montmorillonite hybrid

Areeporn Ontam<sup>a</sup>, Nithima Khaorapapong<sup>a,\*</sup>, Makoto Ogawa<sup>b</sup>

- a Department of Chemistry and Center of Excellence for Innovation in Chemistry, Faculty of Science, Khon Kaen University, Khon Kaen 40002, Thailand
- b Department of Earth Sciences and Graduate School of Creative Science and Engineering, Waseda University, 1-6-1 Nishiwaseda, Shinjuku-ku, Tokyo 169-8050, Japan

#### ARTICLE INFO

Article history: Received 29 December 2010 Accepted 5 February 2011 Available online 12 February 2011

Keywords: Cadmium selenide Hybrid Montmorillonite Nanoparticle Optical properties Self-assembly

#### ABSTRACT

The immobilization of organically modified cadmium selenide on montmorillonite was investigated by the reaction of modified cadmium selenide nanoparticles with montmorillonite. The intercalation of the nanoparticles was indicated by the expansion of the interlayer space and spectroscopic observations. The diffuse reflectance absorption spectrum of the product showed absorption onset at 567 nm. In comparison to the bulk cadmium selenide, the blue shift of the absorption onset of the hybrid was ascribed to the quantum size effect of the modified cadmium selenide nanoparticles. This study provides a new method for introducing nanoparticles into the interlayer space of layered inorganic materials.

© 2011 Elsevier Inc. All rights reserved.

#### 1. Introduction

Intercalation of guest species into layered inorganic solids is a way of producing ordered inorganic-organic hybrids with unique multilayered nanostructures controlled by host-guest and guest-guest interactions [1,2]. Smectite is one of the layered hosts studied most extensively owing to the stability of its structure and ability to accommodate a wide variety of organic and inorganic species [3]. Besides the molecular species, polymers and inorganic nanoparticles have been intercalated into the interlayer space of smectites. The spatial distribution and orientation of the guest species in the hybrids can improve their physicochemical properties that potentially can be used as advanced materials. Polymer-clay composites have been utilized to replace various plastics [4]. In addition, inorganic particles have been synthesized in the interlayer space to produce inorganic-inorganic hybrids with potential for catalysts and adsorbents [5–7]. Since the progress of nanoparticle syntheses, the intercalation of presynthesized nanoparticles into the interlayer space has been a topic of interest because the *in situ* particle formation in the interlayer space requires careful experimentation and, as far as we know, it is difficult to precisely control the shape and the size of the forming nanoparticles.

Among functional hybrids, those with optical applications have been investigated extensively partly because the nanostructures significantly affect their performances. Accordingly, the organization of photoactive species, including molecular species, polymers, and semiconductor particles, on the surfaces of organic and inorganic materials has been conducted [7–20]. Cadmium selenide (CdSe), one of the useful II–VI group semiconductors, has attracted much interest because of its unique optical and electronic properties that may find applications as photocatalysts and photoluminescent materials [21,22]. Since the characteristic features of the hybrids are achieved by host–guest systems [3–6], the organization of CdSe semiconductors on the inorganic materials is worth the tailoring of the size, shape, and unique optical properties of the nanoparticles.

In this study, we investigated the incorporation of hexadecyltrimethylammonium-capped cadmium selenide into the interlayer space of montmorillonite. The hydrophilic surface of montmorillonite is often not suitable for adsorbing poorly water-soluble organic or inorganic guest species, while the organically modified montmorillonite is a possible adsorbent for poorly water-soluble species. Here the preparation of a cadmium selenide-hexadecyltrimethylammonium-montmorillonite hybrid was carried out by the reaction between cadmium selenide-hexadecyltrimethylammonium and montmorillonite. The spectroscopic properties of the hybrid were investigated to show the merit of the present product and the preparative method.

#### 2. Materials and methods

#### 2.1. Materials

Na-montmorillonite used in the present study was Kunipia F obtained from Kuminine Industries, Japan. Hexadecyltrimethylammonium (HDTMA) bromide ( $C_{19}H_{42}NBr$ ) and selenium (Se)

<sup>\*</sup> Corresponding author. Fax: +66 43 202373. E-mail address: nithima@kku.ac.th (N. Khaorapapong).

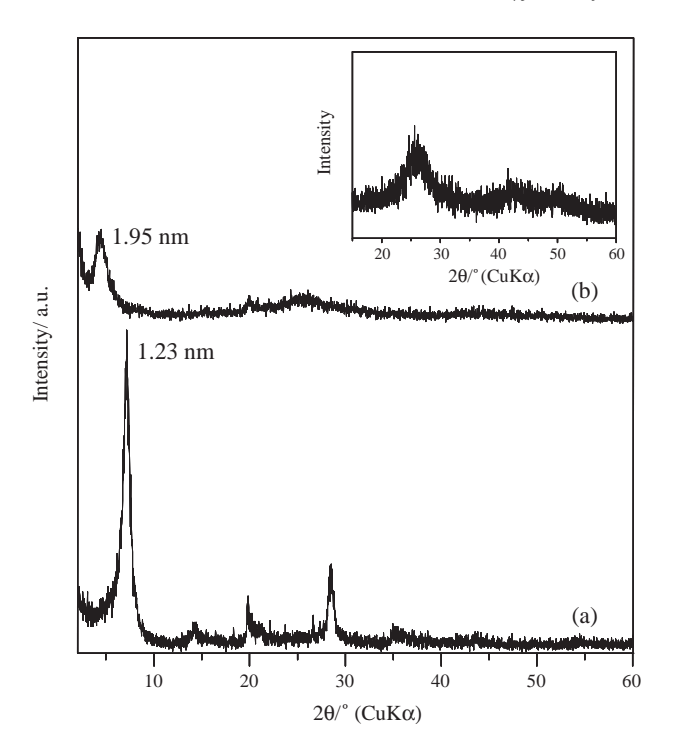


**Fig. 1.** X-ray diffraction patterns of (a) montmorillonite, (b) CdSe-HDTMA-montmorillonite, (inset) CdSe-HDTMA.

powder were purchased from Sigma–Aldrich. Cadmium sulfate (CdSO<sub>4</sub>·8H<sub>2</sub>O) was obtained by Carlo Erba Reagenti. Sodium sulfite (Na<sub>2</sub>SO<sub>3</sub>) was supplied by APS Finechem. All chemicals are analytical grade and were used without further purification.

#### 2.2. Preparation of cadmium selenide-hexadecyltrimethylammonium

The transparently orange solution of CdSe was prepared by a reaction between an aqueous sodium selenosulfite ( $Na_2SeSO_3$ ) synthesized by refluxing the aqueous solution of  $Na_2SO_3$  and Se powder under stirring for 1 day, as well as an aqueous solution of cadmium sulfate [23]. Then, a fresh solution of CdSe was added into the hexadecyltrimethylammonium bromide solution. The mixture was ultrasonicated for 3 h in order to produce the colloidal cadmium selenide–hexadecyltrimethylammonium (abbreviated as CdSe–HDTMA).

#### 2.3. Intercalation of CdSe-HDTMA into montmorillonite

The dispersion of montmorillonite was poured into the colloidal CdSe–HDTMA solution and the mixture was kept statically at 10 °C for 1 day. Afterward, the bright orange solid was precipitated. The resulting solid was separated by centrifugation, washed with ethanol for several times, and dried in a desiccator for 5 days. The product was denoted as CdSe–HDTMA–montmorillonite.

#### 2.4. Characterization

X-ray diffraction (XRD) data were performed on a Bruker D8 ADVANCE diffractometer using monochromatic Cu K $\alpha$  radiation. A TEM image was taken on a Hitachi H-7650 transmission electron microscope with an accelerating voltage of 120 kV. Raman spectrum was recorded on a Jobin Yvon T64000 System Raman spectrometer with a 30 mW argon ion laser, operating at 514.5 nm. Diffuse reflectance absorption spectra of the solid samples were measured on a Shimadzu UV-VIS-NIR-3101PC

scanning spectrophotometer using an integrated sphere. Photoluminescence (PL) spectra were recorded on a Hitachi F-4500 fluorescence spectrophotometer at a temperature between 77 and 398 K with the excitation wavelength of 450 nm. The temperature was controlled by a closed-cycle liquid nitrogen cryostat system with a programmable temperature controller (Oxford DN-1704).

#### 3. Results and discussion

After self-organization, the color of montmorillonite changed from gray to bright orange. The X-ray diffraction pattern of CdSe-HDTMA-montmorillonite is shown in Fig. 1 together with those of montmorillonite and CdSe-HDTMA. The reflection appearing at  $2\theta$  = 25, 42, and 49° for CdSe–HDTMA (Fig. 1, inset) was ascribed to cubic CdSe (ICPDS 19191). No other diffraction peaks were observed in the XRD pattern of CdSe-HDTMA, indicating that the crystal structure of CdSe was not changed by capping with HDTMA. The basal spacing of CdSe-HDTMA-montmorillonite (Fig. 1b) was 1.95 nm, being increased from 1.23 nm for the hydrated montmorillonite (Fig. 1a). The gallery height of the hybrid was determined to be 0.99 nm by subtracting the thickness of the silicate layer (0.96 nm) from the observed basal spacing. No diffraction peak due to CdSe particles was seen in the XRD pattern of CdSe-HDTMA-montmorillonite, implying that the modified CdSe particles did not form outside the interlayer space and/or another possibility is that only small amounts of CdSe-HDTMA were trapped on the outer surface of montmorillonite. Therefore, the change in the color and the expansion of the interlayer space were ascribed to the formation of the organically modified CdSe in the interlayer space of montmorillonite. The hydrophilic interaction between the CdSe-HDTMA and the interlayer sodium ions was thought to be a driving force for the intercalation.

The morphology and the size of CdSe particle were investigated by TEM measurements. The sheet-like morphology of montmorillonite, which covered CdSe nanoparticles, was clearly observed (Fig. 2a). The round-shaped nanoparticles with sizes of 3-6 nm were uniformly distributed on the solid surface. Taking the expansion of the interlayer space of CdSe-HDTMAmontmorillonite (ca. 0.99 nm) into account, the intercalated CdSe nanoparticles probably were disk- or plate-shaped nanoparticles with a thickness of ca. 0.99 nm and a diameter of ca. 3-6 nm, where the disk or plate plane was oriented parallel to the silicate layer. The Raman peak due to a longitudinal-optical mode of CdSe exhibited at 206 cm<sup>-1</sup> for CdSe-HDTMA-montmorillonite (Fig. 2b). Raman spectra of CdSe nanocrystals with particle sizes of 3.52 and 2.26 nm showed the peak positions at 204.8 and 201.4 nm [24]. These observations confirmed the formation of CdSe particles in montmorillonite.

The diffuse reflectance absorption spectra of CdSe-HDTMAmontmorillonite, CdSe-HDTMA, and montmorillonite are shown in Fig. 3. The absorption onset of CdSe-HDTMA-montmorillonite was observed at 567 nm (Fig. 3a) and that of CdSe-HDTMA appeared at 592 nm (Fig. 3b). The absorption onsets were not evident in the absorption spectrum of montmorillonite (Fig. 3c). From the absorption onsets of CdSe-HDTMA-montmorillonite (567 nm) and CdSe-HDTMA (592 nm), the band gaps were calculated to be 2.22 and 2.05 eV, respectively. The absorption onset of bulk CdSe was observed at 698 nm (1.78 eV) [25]. Other prior reports clearly showed the blue shift of the absorption onsets at 619 nm for CdSe nanoparticles [26], at 580 nm for starch-capped CdSe nanoparticles [9], and at 622 nm for CdSe in mesoporous SBA-15 [18] compared to that of the bulk CdSe. Thus, the characteristic absorption onsets observed at 567 nm for CdSe-HDTMAmontmorillonite and at 592 nm for CdSe-HDTMA indicated the

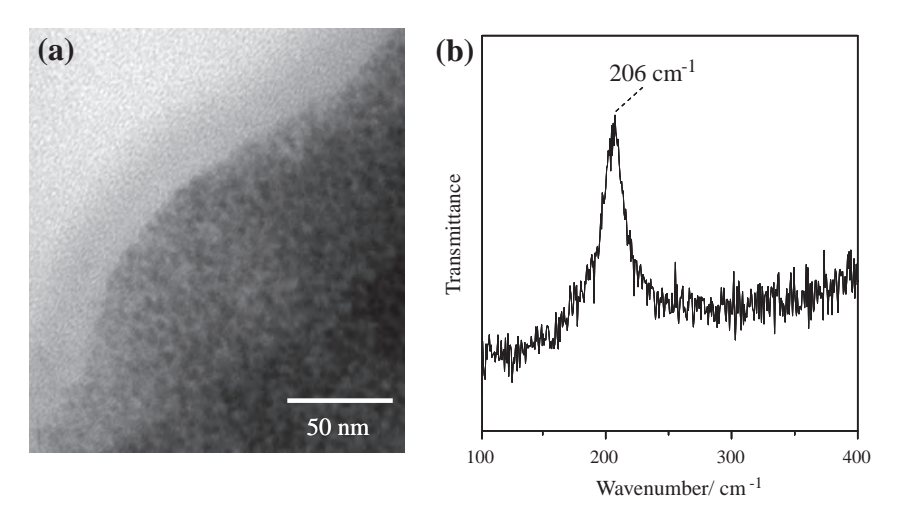
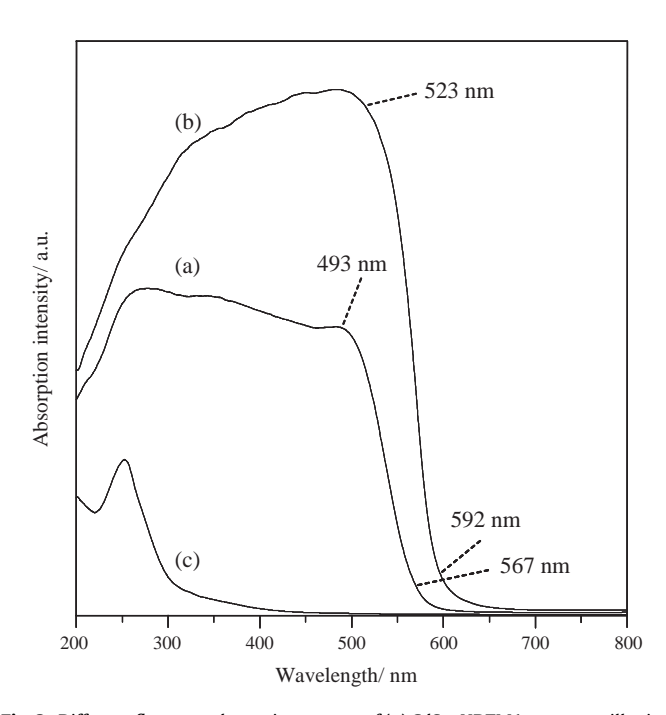
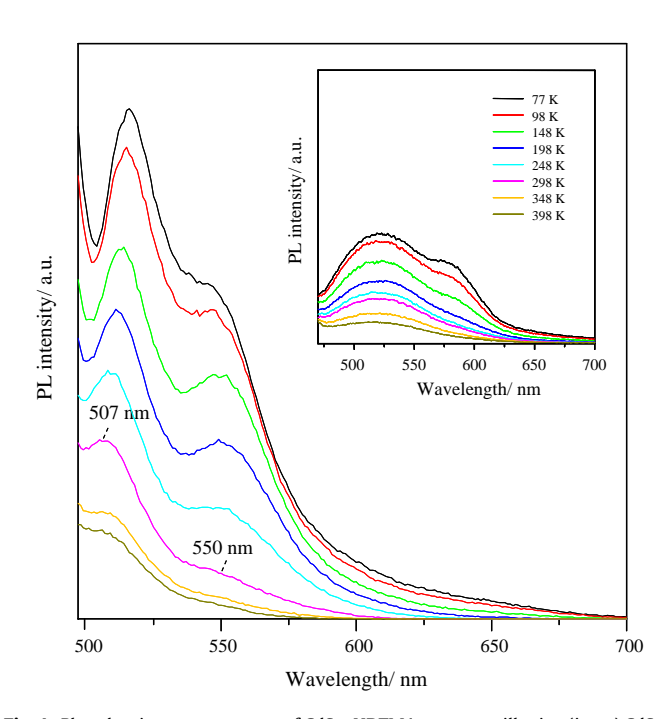


Fig. 2. (a) TEM image, (b) Raman spectrum of CdSe-HDTMA-montmorillonite.



 $\label{eq:Fig.3.} \textbf{Fig. 3.} \ \ \textbf{Diffuse reflectance absorption spectra of (a) CdSe-HDTMA-montmorillonite,} \\ \textbf{(b) CdSe-HDTMA, (c) montmorillonite.}$ 



**Fig. 4.** Photoluminescence spectra of CdSe–HDTMA–montmorillonite, (inset) CdSe–HDTMA at a temperature range of 77–398 K.

formation of CdSe nanoparticles. The CdSe-HDTMA-montmorillonite exhibited an absorption onset at wavelengths lower than that of CdSe-HDTMA, suggesting that the subsequent aggregation of CdSe nanoparticles was interrupted by the restricted environment of montmorillonite. Moreover, an ionic interaction between organically modified CdSe nanoparticles and layered silicate may also prevent the interaction between CdSe nanoparticles.

The photoluminescence spectrum of CdSe–HDTMA–montmorillonite measured at 298 K showed a strong emission peak at 507 nm with a full width at half-maximum (FWHM) of 30 nm, as well as a weak emission peak at 550 nm with a FWHM of 49 nm (Fig. 4). The PL bands of the other hybrid systems of cadmium selenide such as starch-capped CdSe, cysteine-capped CdSe nanoparticle, CdSe–polymers, and CdSe–mesoporous materials were also observed at a wavelength of 400–700 nm [8–13]. The emission

peaks of CdSe–HDTMA–montmorillonite due to the near band-edge (507 nm) and deep-trap (550 nm) emissions can be attributed to the presence of CdSe nanoparticles in the hybrid material [10,17]. On the other hand, the PL spectrum at 298 K of CdSe–HDTMA (Fig. 4, inset) revealed only a weak emission peak due to the band-edge emission at 523 nm with a FWHM of 89 nm. By comparison, the FWHM of the emission band of CdSe–HDTMA–montmorillonite was narrower and the PL intensity was two times higher than those of CdSe–HDTMA, indicating the uniform shape, size, and size distribution of CdSe formed in the interlayer space of montmorillonite [10,27,28]. The blue shift of the near band-edge emission of CdSe–HDTMA–montmorillonite (507 nm) with respect to the band-edge emission of CdSe–HDTMA (523 nm) was thought to originate from the effects of quantum confinement and/or the rigid nature of the silicate layer [29], and the trap emission of the

modified CdSe in montmorillonite was arisen from the surface defects and/or site-substituted impurities of the nanoparticles, which were assumed to be caused by the clay mineral. These observations presented that montmorillonite is an effective matrix that precisely controls the size, excessive aggregation, and dispersity of the nanoparticles.

The photoluminescence spectra of CdSe-HDTMA-montmorillonite at varying temperatures from 77 to 398 K showing the near band-edge and deep-trap emission maxima in the ranges of 507-516 and 548-550 nm are displayed in Fig. 4 together with those of CdSe-HDTMA. The intensities of the emission bands of both samples were gradually quenched as the temperature increased, because the competitive nonradiation process occurring in CdSe particles became effective [12,27]. It has been reported that the red shift of the emission peak for a semiconductor with increasing temperature involved shrinking of the energy band gap and exiton-phonon coupling [30]. Interestingly, the PL spectrum of CdSe-HDTMA-montmorillonite did not track as expected for band-gap reduction. The blue shift of the near band-edge emission was observed on heating from 77 to 248 K, implying a thermal redistribution of excited electrons in the surface defects of CdSe nanoparticles and their relaxation processes [31,32]. This result was likely related to the rigid nature of the microenvironment of CdSe. But the deep-trap emission of CdSe-HDTMA-montmorillonite almost remained at the same wavelength or displayed a very small shift (1-2 nm) on temperature (Fig. 4), indicating that the defect state was not associated with quantum size effects [28].

On the other hand, the band-edge emission of CdSe-HDTMA (Fig. 4 inset) without clay was hardly changed at higher temperatures up to 398 K. Since the small size nanocrystal usually has properties different from the larger one, the spectral shift occurred only in the growth interruption; namely the near band edge of CdSe-HDTMA-montmorillonite revealed the blue shift with increasing temperature as noted above [31,32]. No spectral shift of the band was observed in the PL spectrum of CdSe-HDTMA; it was complicatedly due to the formation of large size semiconductor particles in CdSe-HDTMA. These observations supported that the restricted environment of montmorillonite played an essential role in the temperature-dependent behavior of CdSe nanoparticles. The present process is a promising way to improve the PL properties and tune the visible emission wavelengths of CdSe semiconductors via the intercalation using the layered clay mineral as a controlling material.

#### 4. Conclusions

Surfactant-modified cadmium selenide nanoparticles were immobilized on montmorillonite as shown by the absorption onsets in the visible absorption spectra and the photoluminescence. The successful preparation of well-dispersed CdSe nanoparticles in montmorillonite suggested that the growth and distribution of CdSe particles, which directly correlate with their optical properties, can be controlled by the interactions with the silicate layer.

#### Acknowledgments

One of the authors (A.O.) thanks the Office of the Higher Education Commission. Thailand, for supporting by a grant fund under the program Strategic Scholarships for Frontier Research Network for the Join Ph.D. Program Thai Doctoral degree for this research. This project was financially supported by the Thailand Research fund (TRF) and Khon Kaen University (Grant DBG5380004), and the Center of Excellence for Innovation in Chemistry (PERCH-CIC), Commission on Higher Education, Ministry of Education, Thailand. We kindly thank Hitachi High-Technologies for partial support of the TEM instrument.

#### References

- [1] M.S. Whittingham, in: M.S. Whittingham, A.J. Jacobson (Eds.), Intercalation Chemistry, Academic Press, New York, 1982, p. 1.
- M. Ogawa, in: S.M. Auerbach, K.A. Carrado, P.K. Dutta (Eds.), Handbook of Layered Materials, Dekker, New York, 2004, p. 191.
- [3] M. Ogawa, K. Kuroda, Chem. Rev. 95 (1995) 399.
- E. Ruiz-Hitzky, A. van Meerbeek, in: F. Bergaya, B.K.G. Theng, G. Lagaly (Eds.), Handbook of Clay Science, vol. 1, Elsevier Science, Amsterdam, 2006, p. 583.
- S. Nir, Y. El Nahhal, T. Undabeytia, G. Rytwo, T. Polubesova, Y. Mishael, U. Rabinovitz, B. Rubin, in: F. Bergaya, B.K.G. Theng, G. Lagaly (Eds.), Handbook of Clay Science, vol. 1, Elsevier Science, Amsterdam, 2006, p. 677.
- (a) T.J. Pinnavaia, Science 220 (1983) 365; (b) N. Hu, J.F. Rusling, Anal. Chem. 63 (1991) 2163.
- K. Rajeshwar, N.R. de Tacconi, C.R. Chenthamarakshan, Chem. Mater. 13 (2001) 2765.
- S.O. Oluwafemi, N. Revaprasadu, A.J. Ramirez, J. Cryst. Growth 310 (2008) 3230.
- [9] J.H. Li, C.L. Ren, X.Y. Liu, Z.D. Hu, D.S. Xue, Mater. Sci. Eng. A 458 (2007) 319.
- [10] P.K. Khanna, P. More, B.G. Bharate, A.K. Vishwanath, J. Lumin. 130 (2010) 18.
- [11] S.H. Liu, X.F. Qian, J.Y. Yuan, J. Yin, R. He, Z.K. Zhu, Mater. Res. Bull. 38 (2003)
- [12] T. Trindade, M.C. Neves, A.M.V. Barros, Scr. Mater. 43 (2000) 567.
- [13] J.D. Kehlbeck, M.E. Hagerman, B.D. Cohen, J. Eliseo, M. Fox, W. Hoek, D. Karlin, E. Leibner, E. Nagle, M. Nolan, I. Schaefer, A. Toney, M. Topka, R. Uluski, C. Wood, Langmuir 24 (2008) 9727.
- [14] I. Dékány, L. Turi, E. Tombácz, J.H. Fendler, Langmuir 11 (1995) 2285.
- [15] G. Cao, L.K. Rabenberg, C.M. Nunn, T.E. Mallouk, Chem. Mater. 3 (1991) 149.
- [16] P. Wang, Y. Zhu, X. Yang, C. Li, H.L. Du, Acta. Mater. 56 (2008) 1144. [17] E.A. Turner, Y. Huang, J.F. Corrigan, Eur. J. Inorg. Chem. (2005) 4465.
- [18] Y. Shan, L. Gao, S. Zheng, Mater. Chem. Phys. 88 (2004) 192.
- [19] H. Parala, H. Winkler, M. Kolbe, A. Wohlfart, R.A. Fischer, R. Schmechel, H. von Seggern, Adv. Mater. 12 (2000) 1050.
- [20] (a) N. Khaorapapong, A. Ontam, J. Khemprasit, M. Ogawa, Appl. Clay Sci. 43 (2009) 238:
  - (b) N. Khaorapapong, A. Ontam, M. Ogawa, Appl. Clay Sci. 50 (2010) 19;
  - (c) N. Khaorapapong, A. Ontam, M. Ogawa, Appl. Clay Sci. 51 (2011) 182.
- [21] R. Garuthara, M. Tomkiewicz, R. Tenne, Phys. Rev. B 31 (1985) 7844
- [22] D. Beydoun, R. Amal, G. Low, S. McEvoy, J. Nanoparticle Res. 1 (1999) 439.
- [23] S. Yochelis, G. Hodes, Chem. Mater. 16 (2004) 2740.
- [24] Y.-T. Nien, B. Zaman, J. Ouyang, I.-G. Chen, C.-S. Hwang, K. Yu, Mater. Lett. 62 (2008) 4522
- [25] Y.-L. Yan, Y. Li, X.-F. Qian, J. Yin, Z.-K. Zhu, Mater. Sci. Eng. B 103 (2003) 202.
- [26] X. Zheng, Y. Xie, L. Zhu, X. Jiang, A. Yan, Ultrason. Sonochem. 9 (2002) 311.
- [27] S. Santhi, E. Bernstein, F. Paille, J. Lumin. 117 (2006) 101.
- [28] R. He, H. Gu, Colloids Surf. A 272 (2006) 111.
- [29] M. Ogawa, M. Inagaki, N. Kodama, K. Kuroda, C. Kato, J. Phys. Chem. 97 (1993) 3819
- [30] P. Jing, J. Zheng, M. Ikezawa, X. Liu, S. Lv, X. Kong, J. Zhao, Y. Masumoto, J. Phys. Chem. C 113 (2009) 13545.
- [31] T. Arai, K. Matsuishi, J. Lumin. 70 (1996) 281.
- [32] H.-P. Tranitz, H.P. Wagner, R. Engelhardt, U.W. Pohl, D. Bimberg, Phys. Rev. B 65 (2002) 035325.

## **Dalton Transactions**

Dynamic Article Links

Cite this: Dalton Trans., 2011, 40, 5964

**PAPER** www.rsc.org/dalton

### Formation of mixed-ligand zinc(II) complex-montmorillonite hybrids by solid-solid reactions†

Nithima Khaorapapong,\*\*\* Patcharaporn Pimchan\*\* and Makoto Ogawa\*\*

Received 10th December 2010, Accepted 28th March 2011 DOI: 10.1039/c0dt01736a

Two luminescent hybrids, Znqb- and Znqp-montmorillonites (q = 8-hydroxyquinoline, b = 2,2'-bipyridine, p = 1,10-phenanthroline), were prepared by solid-solid reactions between Zn(II)-montmorillonite and two ligands (8-hydroxyquinoline and 2,2'-bipyridine or 1,10-phenanthroline) at room temperature. The intercalation and in situ complex formation of the two ligands into an interlayer space of Zn(II)-montmorillonite were confirmed by powder XRD, TG-DTA, as well as FT-IR, UV-vis and photoluminescence spectroscopies. The emission band of Znqb-montmorillonite was red-shifted compared to that of the mixture of Znq-montmorillonite and Znb-montmorillonite, confirming the formation of Znqb complex in montmorillonite. The photoluminescence intensity of Znqb-montmorillonite was higher than that of Znqp-montmorillonite, indicating that 2,2'-bipyridine enhanced the emission intensity of zinc(8-hydroxyquinoline) complex in montmorillonite, while the coordination of 1,10-phenanthroline quenched the intensity of the immobilized chelate.

#### Introduction

The organization of photo and electroluminescent metal complexes within ordered structures has attracted great attention because of the excellent luminescent properties towards the scientific study and potential application for light emitting diodes (LEDs).1 The hybrid materials of various inorganic substances containing metal complexes such as [Ru(bpy)<sub>3</sub>]<sup>2+</sup>-niobates and titanates,<sup>2</sup> [Co(NH<sub>3</sub>)<sub>6</sub>]<sup>3+</sup>- and [Co(NH<sub>3</sub>)<sub>5</sub>Cl]<sup>2+</sup>-manganese oxide,<sup>3</sup> [Eu(bpy)<sub>2</sub>]<sup>3+</sup>-bentonite,<sup>4</sup> [Ru(bpy)<sub>3</sub>]<sup>2+</sup>-zeolite Y,<sup>5</sup> [Al(8hydroxyquinoline)<sub>3</sub>]-mesoporous silica<sup>6,7</sup> have been synthesized, and their properties and applications have been proposed so far. The confinements of metal complexes in nanospace have been done by utilizing in situ complex formation and/or immobilization of pre-synthesized metal complexes into the inorganic solids.

Layered clay minerals act as a scaffold for immobilizing metal complexes. Smectite, a group of 2:1 layered clay minerals, provides such attractive properties as ion exchange property, large surface area, and two dimensional expandable interlayer spaces for accommodating guest species. 1,8 Accordingly, intercalation compounds of smectites with various metal complexes including copper(II)-arene, [Ni(phen)] [2+, 10 [Fe(phen)] [2+, 11 [Rh(PPh])] [1+ (PPh])

and  $[Rh(PPh_3)_3]^+$   $(PPh_3 = triphenylphosphine),^{12} [Fe((N-methyl-$ 4-pyridiniumyl)porphyrin) $_4$ ]<sup>3+</sup>, <sup>13</sup> as well as [Ru(bpy) $_3$ ]<sup>2+14-16</sup> have been prepared and the properties of the intercalates have been examined extensively.

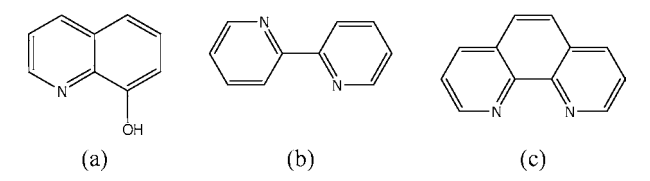
For the preparation of metal complex-smectite hybrids, we have found that the solid-solid reaction is one of the suitable method, due to the ease of operation and possibility to prepare the compounds, which are not accessible from solutions and so on. 17,18 We have successfully prepared metal chelates in the interlayer spaces of smectites including montmorillonite by solidsolid reaction and in situ complex formation. 19-23 Because of the advantages of the synthetic methodology, the effect of solidstate intercalation of metal complexes in clay minerals on their structures and properties is worth investigating for constructing novel low dimensional nanohybrid materials.

In the present study, we examined the preparation of mixed-ligand zinc(II) complexes, zinc(8-hydroxyquinoline)(2,2'bipyridine) and zinc(8-hydroxyquinoline)(1,10-phenanthroline), in the interlayer spaces of montmorillonite, and their optical properties as well as thermal stability were studied. Among the luminescent materials for LEDs, metal complexes of 8-hydroxyquinoline (abbreviated as 8hq, Scheme 1a) and its derivatives have been investigated to adjust the emitting colour.24,25 The synthesis and molecular design of the metal complexes depend on both the selection of metal ion center and organic ligand. The substitutions of 8hq including replacement with monodentate ligand are effected to the emission of complexes.<sup>25,26</sup> Due to their relatively high thermal stability and electroluminescent property for LEDs application, renewed interest is currently focused on the chemistry of mixedligand complexes. The mixed-ligand complexes containing neutral

<sup>&</sup>lt;sup>a</sup>Department of Chemistry and Center of Excellence for Innovation in Chemistry, Faculty of Science, Khon Kaen University, Khon Kaen 40002, Thailand. E-mail: nithima@kku.ac.th; Fax: +66-4320-2373; Tel: +66-4320-

<sup>&</sup>lt;sup>b</sup>Department of Earth Sciences and Graduate School of Creative Science and Engineering, Waseda University, Nishiwaseda 1-6-1, Shinjuku-ku, Tokyo 169-8050, Japan

<sup>†</sup> Electronic supplementary information (ESI) available: TG-DTG curves and FT-IR data. See DOI: 10.1039/c0dt01736a



Scheme 1 The molecular structures of 8-hydroxyquinoline (a), 2,2'-bipyridine (b) and 1,10-phenanthroline (c).

N,N' bidentate ligands including 2,2'-bipyridine (abbreviated as bpy, Scheme 1b) and 1,10-phenanthroline (abbreviated as phen, Scheme 1c) and their optical properties have been recently reported.27-29

The two ligands, 8-hydroxyquinoline and diimines, were selected because of the unique optical properties of their metal complexes.<sup>27–29</sup> Segregation is a phenomenon associating the host– guest complexation.<sup>30,31</sup> When two guest species are allowed to react with hosts at the same time, guests often segregate resulting in the mixture of two intercalation compounds. Here, solidsolid reaction was applied to promote the complex formation between Zn(II)-montmorillonite and 8-hydroxyquinoline, as well as co-ligand (bpy or phen) to form zinc(8-hydroxyquinoline)(2,2'bipyridine) and zinc(8-hydroxyquinoline)(1,10-phenanthroline) complexes in the interlayer spaces of montmorillonite.

#### **Experimental**

#### **Materials**

Na-montmorillonite (Kunipia F, obtained from Tsukinuno Mine, Kunimine Industries Co., Ltd., Japan) was used as a host material. The cation exchange capacity (CEC) of Na-montmorillonite was 119 meq per 100 g of clay. Zinc chloride (ZnCl<sub>2</sub>) was purchased from Carlo Erba Reagenti SpA. 8-Hydroxyquinoline was obtained from Junsei Chemical Co., Ltd. 2,2'-Bipyridine and 1,10-phenanthroline were purchased from Tokyo Kasei Kogyo Co., Ltd. and Fisher Chemical Co., Ltd., respectively. All the reagents are analytical grade and were used as received.

#### Preparation of mixed-ligand zinc(II)-montmorillonite

The hybrid materials were prepared via solid-solid reactions at room temperature as reported previously.<sup>23,32,33</sup> Firstly, the parent product, zinc(8-hydroxyquinoline)-montmorillonite was investigated by manual grinding between Zn(II)-montmorillonite and 8hq at the molar ratio of 1:1 (Zn(II):8hq) for 10-15 min in air at room temperature. The amount of the adsorbed zinc(II) cation in Zn(II)-montmorillonite prepared by cation exchange reactions<sup>20,21</sup> was 105 meg per 100 g of clay. Then the solid-solid reactions between the parent product and co-ligand (bpy or phen) at the molar ratio of 1:1 (Zn(II): bpy or phen) were performed at the same conditions. After the reactions, the two products, zinc(8-hydroxyquinoline)(2,2'bipyridine)-montmorillonite and zinc(8-hydroxyquinoline)(1,10phenanthroline)-montmorillonite were obtained.

#### Characterization

Powder X-ray diffraction (XRD) patterns were obtained on a Bruker D8 ADVANCE diffractometer using monochromatic Cu-Kα radiation. Diffuse reflectance spectra of the solid samples were collected on a Shimadzu UV-VIS-NIR-3101PC scanning spectrophotometer using an integrated sphere. Infrared spectra of the samples were performed on a Perkin Elmer Spectrum One FT-IR spectrophotometer by KBr disk method. TG-DTG-DTA data were measured on a Perkin Elmer Pyris Diamond TG-DTA instrument at a heating rate of 10 °C min-1 under a dry air atmosphere using  $\alpha$ -alumina ( $\alpha$ -Al<sub>2</sub>O<sub>3</sub>) as a standard material. Photoluminescence spectra were recorded on a Shimadzu RF-5301PC spectrofluorophotometer in the wavelength range of 300– 800 nm with the excitation at 360 nm. Inductively coupled plasma optical emission spectroscopic (ICP-OES) data were taken with a Perkin Elmer Optima 2100DV ICP-OES.

#### **Results and discussion**

#### Solid-state intercalation of mixed-ligand zinc(II)-montmorillonite

The basal spacings and colours of the hydrated Zn(II)montmorillonite, the parent product and the final products are summarized in Table 1. After the solid-solid reaction between Zn(II)-montmorillonite and 8-hydroxyquinoline (abbreviated as Znq-montmorillonite), the colour of the hydrated Zn(II)montmorillonite (Fig. 1a) changed from white to green (Fig. 1b). This product was referred to as Zng-montmorillonite and used as a parent product to react with the co-ligands in solidstate. When Znq-montmorillonite was ground with powder of bpy (abbreviated as Znqb-montmorillonite) or phen (abbreviated as Znqp-montmorillonite), a little bit change in the colour of

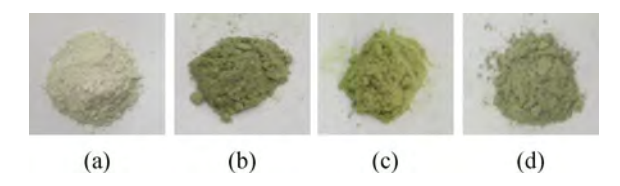


Fig. 1 Colours of Zn(II)-montmorillonite (a), Znq-montmorillonite (b), Znqb-montmorillonite (c) and Znqp-montmorillonite (d).

Table 1 Basal spacings (doot), colours, luminescence bands and intensities of starting material and products

Substance	d <sub>001</sub> /nm	Colour	$\lambda_{ m emission}/ m nm$	Intensity
Zn(II)-montmorillonite	1.49	White	_	_
Zng-montmorillonite	1.56	Green	496	63
Znq <sub>2</sub> -montmorillonite	1.56	Green	506	87
Zngb-montmorillonite	1.77	Yellowish green	507	334
Zngp-montmorillonite	1.75	Pale green	495	56
Znbq-montmorillonite	1.77	Yellowish green	510	435
Znpq-montmorillonite	1.75	Pale green	497	78

Zng-montmorillonite was observed (Fig. 1c and 1d). Therefore, the change in the colour of Zn(II)-montmorillonite suggested the change in the coordination state of Zn(II) interlayer cation.

The X-ray diffraction patterns of the products are shown in Fig. 2. The broad diffraction peak  $(d_{001})$  of the parent product, Zng-montmorillonite, was observed at 1.56 nm (Fig. 2c). When the added amount of 8hq was increased (molar ratio of Zn(II): 8hq = 1:2), the basal spacing was slightly shifted to larger d value (1.65 nm). Therefore, the basal spacing of Zng-montmorillonite (1.56 nm) was described to the formation of Znq, Znq<sub>2</sub> and/or hydrated Zn(II) that homogeneously distributed in the interlayer space of montmorillonite. After the parent product was reacted with bpy or phen, the basal spacings increased to 1.77 and 1.75 nm for Zngb- and Zngp-montmorillonites (Fig. 2b and 2a), respectively. The gallery heights were determined by subtracting the thickness of the silicate layer (0.96 nm) from the observed basal spacings (1.77 and 1.75 nm) to be 0.81 nm for Znqbmontmorillonite and 0.79 nm for Znqp-montmorillonite. The XRD patterns of the products did not show any reflections due to 8hg (d = 0.94, 0.62 and 0.38 nm), bpy (d = 0.58, 0.51 and 0.49 nm) or phen (d = 0.89, 0.61 and 0.51 nm) crystals, indicating that 8hq and the co-ligand molecules (bpy and phen) were intercalated into the interlayer spaces of montmorillonite. The  $d_{001}$  reflection shifted to larger d values when the ligands were introduced into montmorillonite and the reflections characteristic to the organic ligands (as mentioned above) and/or two mixedligand complexes (as mentioned below) were not observed. It is noteworthy that no segregation phenomenon was observed (single phase XRD pattern), probably due to the stabilities of the mixed-ligand complexes formed in the interlayer space of montmorillonite. The XRD results and the changes in the colour of the products supported the solid-state intercalation and in

1.75 nm (a) 1.77 nm Intensity/ a.u. (b) 1.56 nm (c) 1.49 nm (d) 10 40 50 20 30 60 2θ/° (CuKα)

Fig. 2 XRD patterns of Znqp-montmorillonite (a), Znqb-montmorillonite (b), Znq-montmorillonite (c) and Zn(II)-montmorillonite (d).

situ complex formation of the mixed-ligand zinc complexes in montmorillonite. Taking the gallery height (ca. 0.8 nm) into account, it is worthwhile to mention that the mixed-ligand zinc complexes formed a monolayer arrangement in between the silicate layers, in agreement with the results reported for Znq<sub>2</sub>montmorillonite<sup>20</sup> and Alq<sub>3</sub>-montmorillonite.<sup>23</sup>

In comparison, the intercalation of pre-synthesized complexes, zinc(2,2'-bipyridine)(8-hydroxyquinoline) (bright yellow powder, abbreviated as Znbq) and zinc(1,10-phenanthroline)(8hydroxyquinoline) (green powder, abbreviated as Znpq), prepared by the methods reported previously, 28,29 into Na-montmorillonite (the molar ratio of Znbq or Znpq: Na(I) = 1:1) was investigated by two different methods. One was the cation exchange reaction of the Znbq or Znpq complex cation and the other was solidsolid reaction between Na-montmorillonite and the Znbq or Znpq complex. The products prepared by the cation exchange reactions were abbreviated as Na-montmorillonite-Znbg(1) and Na-montmorillonite-Znpq(1) and those prepared by solid-solid reactions were denoted as Na-montmorillonite-Znbq(2) and Namontmorillonite-Znpq(2).

The X-ray diffraction patterns of Na-montmorillonite-Znbq(1) and Na-montmorillonite-Znbq(2) are displayed in Fig. 3 together with that of Znbq complex. Na-montmorillonite-Znbq(1) and Namontmorillonite-Znbq(2) showed the reflections due to unreacted Na-montmorillonite (d = ca. 1.2-1.4 nm) that overlapped with the strong diffraction peak of Znbq complex (d = 1.27 nm) including the peaks at d = 0.55, 0.47, 0.42, 0.25 nm. The diffraction peaks at d = 1.27, 0.78, 0.65, 0.42, 0.25 nm due to Znpq complex were also observed in the XRD patterns of Na-montmorillonite-Znpq(1) and Na-montmorillonite-Znpq(2). The results demonstrated that the free mixed-ligand zinc complexes cannot be directly intercalated in the interlayer spaces of

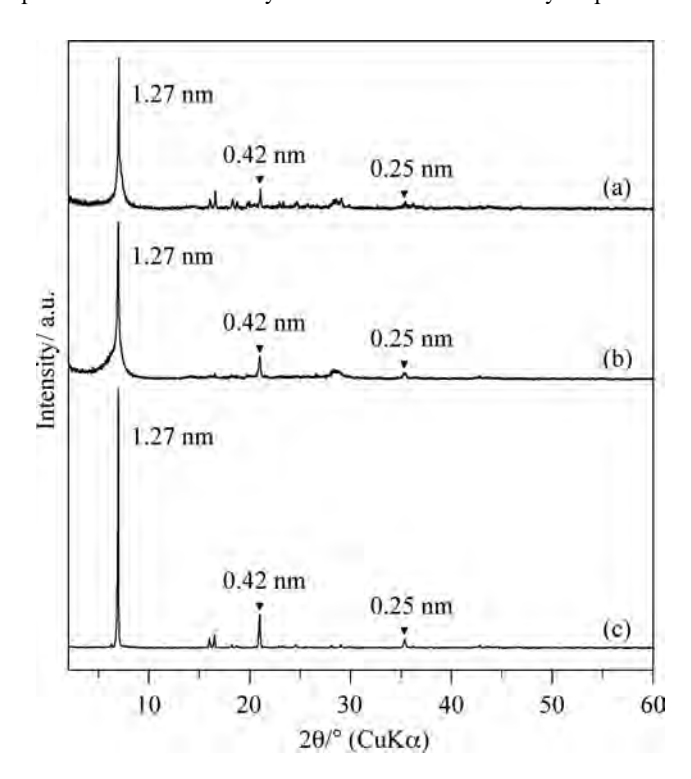
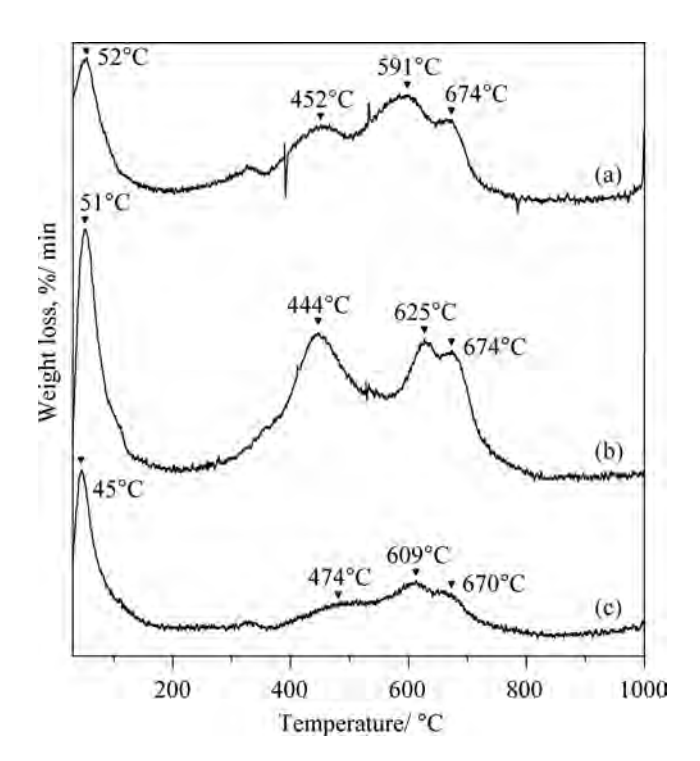


Fig. 3 XRD patterns of Na-montmorillonite-Znbq(2) (a), Na-montmorillonite-Znbq(1) (b) and Znbq complex (c).

Na-montmorillonite and the products contained two phases that have the basal spacings of 1.2–1.4 nm corresponding to the hydrated montmorillonite and 1.27 nm corresponding to free complexes. These indicated that it is rather difficult to incorporate the pre-synthesized mixed-ligand complexes in the interlayer spaces of the layered inorganic solids due to their molecular sizes and/or neutral charges.

The endothermic peaks due to the melting and vaporization of the ligands (Fig. S1, ESI)† were absent, suggesting that the free ligands were not maintained in the products. The first step of mass loss of Zng-montmorillonite, Zngb-montmorillonite or Zngpmontmorillonite (Fig. S2, ESI)† starting from room temperature up to around 200 °C, which accompanied the endothermic reactions in the DTA curves, was ascribed to the dehydration. Thermal decompositions of two organic ligands in the intercalation compounds observed after the dehydration (Fig. 4 and S2)† were interpreted to the partial oxidation and evaporation of ligand (8hq) and co-ligand (bpy or phen) of the complexes formed in the interlayer spaces, as well as final pyrolysis of 8hq and/or coligands and degradation of ZnO.34-37 In the DTG curves of the products (Fig. 4), the final stage of the decomposition observed at around 670 °C was ascribed to the oxidation of charcoal and dehydroxydation of the structural OH.38 It has been reported that the first degradation step of Znq<sub>2</sub> revealed at 114–156 °C, and the decomposition of bpy in  $Zn(bpy)_2(RCOO)_2 \cdot 2H_2O(R = C_2H_5)$  and phen in Zn(phen)(HCOO)<sub>2</sub>·2H<sub>2</sub>O occurred at 120–375 °C and 180-335 °C, respectively. 35,36 Znqb-montmorillonite and Znqpmontmorillonite intercalation compounds were decomposed at the temperature higher than those of the free complexes, showing that the thermal stability of the complexes was enhanced by immobilizing in the interlayer spaces of the clay mineral. These result interpreted that the host matrix probably enhanced the



**Fig. 4** DTG curves of Znqp-montmorillonite (a), Znqb-montmorillonite (b) and Znq-montmorillonite (c).

thermal stability of the intercalated mixed-ligand complexes. The higher thermal stability of the hybrids is an advantage property for getting greater longevity use.

## Formation of Znqb and Znqp complexes in the interlayer spaces of montmorillonite

The in situ complex formation of zinc(II) interlayer cation and mixed ligands (8hq and bpy or phen) was determined by FT-IR, UV-vis and PL spectroscopies. In FT-IR spectra (Table S1, ESI),† the absorption bands due to C-H out of plane bending modes of 8hq were observed at around 840, 820, and 800 cm<sup>-1</sup> for all the products. The bands of the products in the regions were slightly shifted to higher frequency when compared to those observed for free 8hq molecule (817, 781 and 741 cm<sup>-1</sup>), confirming the coordination of 8hq with the zinc interlayer cation.<sup>39</sup> FT-IR spectrum of Zngb-montmorillonite showed the pyridine ring frequencies of bpy at 1606 and 1444 cm<sup>-1</sup>. The aromatic bending characteristic bands of phen were observed at 870 and 760 cm<sup>-1</sup> for Znqp-montmorillonite. The characteristic bands of the two products in the regions were also slightly shifted to higher frequency compared to those observed for the neat molecules (at 1599 and 1443 cm<sup>-1</sup> for bpy and at 854 and 739 cm<sup>-1</sup> for phen), proving the coordination between co-ligands and zinc(II) interlayer cation in montmorillonite. 36,40,41 This observation indicated the formation of Zngb or Zngp complex in the interlayer space of montmorillonite. Because the homogenous mixture of zinc(8-hydroxyquinoline) and zinc(2,2'-bipyridine) or zinc(1,10-phenanthroline) complexes in the hybrids may exhibit the shifts in the IR spectra, the further characterizations of UV-vis and PL spectroscopies were also used to confirm the in situ complex formation of the mixed-ligand complexes in montmorillonite.

The diffuse reflectance absorption spectra of the products are shown in Fig. 5 together with that of the layered host material. The absorption spectra of the ligands were also obtained (not shown) and the bands were seen at 222, 325 and 360 (sh) nm for 8hg, at 230 (sh), 264 and 317 nm for bpy and at 219 (sh), 255, 293 (sh) and 329 nm for phen. In the UV region, the absorption band observed at 252 nm for Zn(II)-montmorillonite (Fig. 5d) was attributed to charge transfer from oxo (O2-, OH-, OH2) to ferric ion (Fe³+) in clay mineral. 42 The bands due to  $\sigma$  to  $\pi^*$  and  $\pi$  to  $\pi^*$ transitions of aromatic ring in 8hq were reported at 270 and 300-320 nm, respectively.<sup>43</sup> Therefore, the bands observed at around 252 nm for Znq-montmorillonite (Fig. 5c), Znqb-montmorillonite (Fig. 5b), and the weakly separated band at 267 nm for Znqpmontmorillonite (Fig. 5a) were suggested to the overlapping bands between charge transfer from oxo to ferric ion in the clay and  $\sigma$  to  $\pi^*$  transition of 8hq. The absorption bands appeared at 297 and 302 nm for Znqp- and Znqb-montmorillonites were assigned to phen and bpy and/or the quinoline superimposed to diimine transitions.<sup>27</sup> The shoulder appeared at 310 nm for Znqmontmorillonite was interpreted to  $\pi$  to  $\pi^*$  transition of 8hq.<sup>43</sup>

In the visible region, the absorption maxima from  $\pi$  to  $\pi^*$  transition of aromatic ring was observed at 366 nm for Znq-montmorillonite. In the spectra of Znqp- and Znqb-montmorillonites, the intensity of the bands observed at around 366 nm were decreased and shifted to 380 nm, indicating the transformation in the microstructure of the former complex to the new mixed-ligand complexes. It has been reported that the

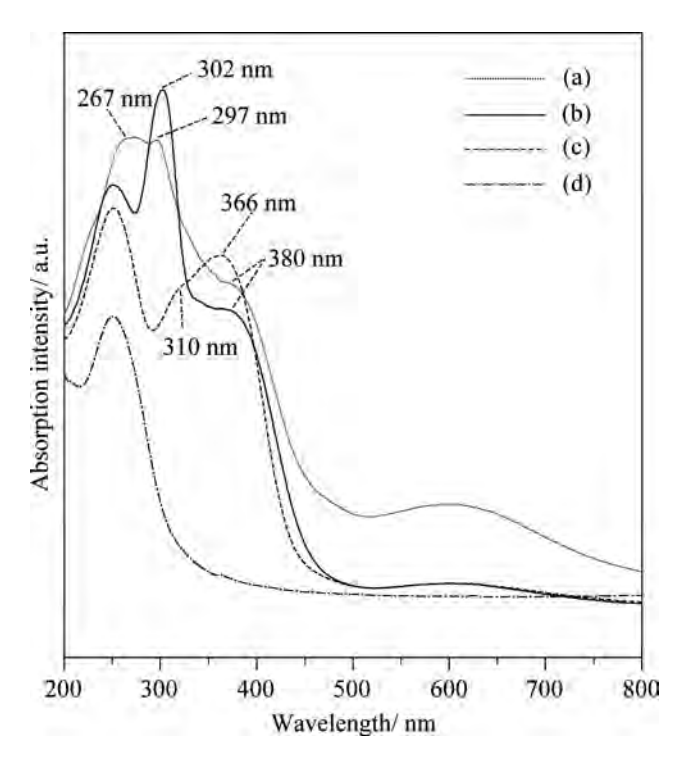


Fig. 5 Diffuse reflectance absorption spectra of Znqp-montmorillonite (a), Znqb-montmorillonite (b), Znq-montmorillonite (c) and Zn(II)-montmorillonite (d).

absorption bands of Znbq complex in toluene appeared at 382 and 342 nm.<sup>29</sup> The absorption spectra of [Q'<sub>2</sub>Ga(bpy)][X] and  $[Q'_2Ga(phen)][X](HQ'=2-methyl-8-hydroxyquinoline; X=NO_3^-,$ PF<sub>6</sub><sup>-</sup>) in dichloromethane and acetone solutions gave the characteristic bands between 260–365 nm and 260–372 nm, respectively.<sup>27</sup> Consequently, the bands observed for Zngb- and Zngpmontmorillonites were attributed to Znqb and Znqp complexes formed in the interlayer spaces of montmorillonite, which were consistent with the photoluminescence spectra described below.

Since the intercalation compound of zinc(8-hydroxyquinoline) examined in this study gave the highest luminescence intensity when it was excited at 360 nm, therefore all products were excited at the same wavelength in order to study the enhancement and quenching of the co-ligands. The emission band due to the  $\pi$  to  $\pi^*$ transition of Zng-montmorillonite was observed at 496 nm (Fig. 6c). The PL band of Znqb-montmorillonite showed the higher intensity band at 507 nm (Fig. 6b), while Znqp-montmorillonite showed the weaker emission band at 495 nm (Fig. 6a). The strong PL band of Znqb-montmorillonite (507 nm) was identical with that of Zng<sub>2</sub>-montmorillonite (506 nm) (not shown). Thus, the emission band observed for Znqb-montmorillonite can be assigned to the  $\pi$  to  $\pi^*$  transition, which was the electronic charge partially transferred from the electron rich phenoxide ring to the electron deficient pyridyl ring of 8hq.27 The powders of Znbq and Znpq complexes prepared according to the previous reports<sup>28,29</sup> also showed the emission bands at 502 and 498 nm, respectively. While the luminescence bands of those complexes in ethanol: acetone displayed at 545 nm. The PL band of Znbq complex in toluene was observed at 545 nm.<sup>29</sup> The emitting band of OLEDs using Znbq or Znpq as an emitting material was observed at 545 or 542 nm.<sup>28,29</sup> The blue shift of the emission bands of the

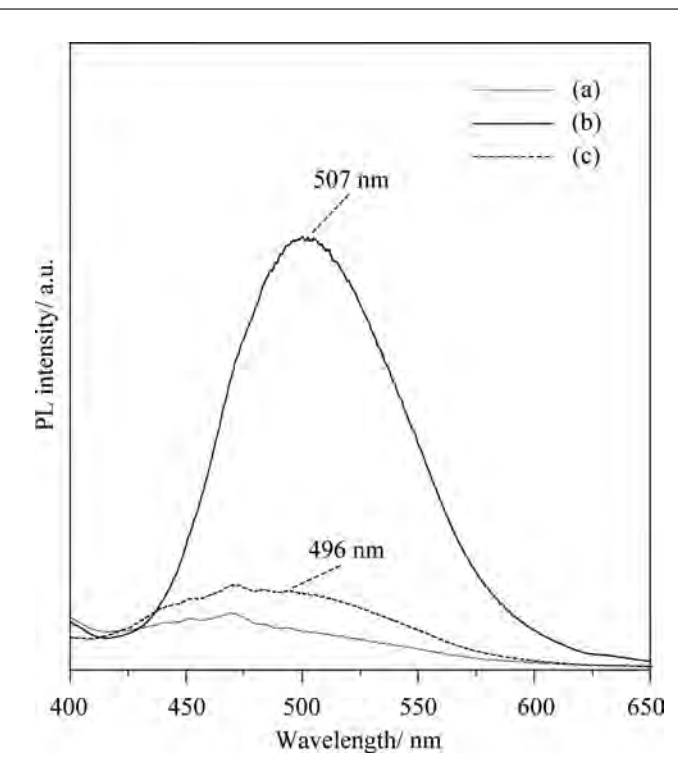


Fig. 6 Photoluminescence spectra of Znqp-montmorillonite (a), Znqbmontmorillonite (b) and Znq-montmorillonite (c).

mixed-ligand complexes in montmorillonite compared to those of the free mixed-ligand complexes may potentially due to the constrained geometry of the host, and the arrangements of the complexes in the interlayer spaces as well as the increased intermolecular interaction between adjacent molecules in solid-state.<sup>31</sup> These observations supported the in situ complex formation of mixed-ligand zinc complexes (zinc(8-hydroxyquinoline)(2,2'bipyridine) or zinc(8-hydroxyquinoline)(1,10-phenanthroline)) in the interlayer spaces of montmorillonite. The emission intensity of Zngb-montmorillonite was significantly higher than that of Znq-montmorillonite, while that of Znqp-montmorillonite was found to be lower, indicating that bpy was enhancing the emission intensity of the complex and phen was quenching.27 Similar difference were also reported in the luminescence intensities of [O'<sub>2</sub>Ga(bpy)][X] and [O'<sub>2</sub>Ga(phen)][X] complexes due to the differences of molecular and crystal packing, which were rational to the structural differences between the ground state and excited state geometries of the complexes. 27,45

Since the observed emission spectra of the products can be thought to be caused by the sum of the luminescence of the two complexes (zinc(8-hydroxyquinoline), and zinc(2,2'-bipyridine) or zinc(1,10-phenanthroline)) formed in the interlayer spaces of montmorillonite. In order to exclude this possibility, the PL spectra of the other two products prepared by the two different routes were also examined. One was the product prepared by grinding Zn(II)montmorillonite and the two ligands (bpy and 8hq) together at the same time (abbreviated as Zn(bpy/8hq)-montmorillonite) and the other was that of the mixed complex product investigated by grinding Zn(II)-montmorillonite with each ligand (bpy or 8hq), separately and subsequently blended the two zinc complexmontmorillonites (zinc(2,2'-bipyridine)-montmorillonite

zinc(8-hydroxyquinoline)-montmorillonite) together, the product was called as Zn-bpy/Zn-8hq-montmorillonite. The weak emission band of Zn(bpy/8hg)-montmorillonite (503 nm) was blue shifted relative to Znq<sub>2</sub>-montmorillonite (506 nm), suggesting the segregation of zinc(8-hydroxyquinoline) and zinc(2,2'bipyridine) complexes in the interlayer space of montmorillonite.<sup>31</sup> The PL band of the mixture of Zn-bpy/Zn-8hq-montmorillonite was observed at 501 nm and the intensity was lower than that of the starting compound of Znq<sub>2</sub>- montmorillonite (506 nm), indicating that the emission band of the mixture was blue shifted and zinc(2,2'-bipyridine) complex quenched the emission band of zinc(8-hydroxyquinoline) in the mixture of the intercalation compounds (Zn-bpy/Zn-8hq). Therefore, the red shift of the luminescent band of Zngb-montmorillonite (507 nm) relative to those of Zn(bpy/8hq)-montmorillonite (503 nm) and Znbpy/Zn-8hq-montmorillonite (501 nm), confirming the formation of zinc(8-hydroxyquinoline)(2,2'-bipyridine) (Znqb) complex in the interlayer space of montmorillonite.

In addition, the PL intensities of Zngb- and Zngpmontmorillonite were weaker than those of the products prepared by the solid-solid reactions between Zn(II)-montmorillonite and the co-ligands (bpy and phen) and subsequent grinding with 8hq (abbreviated as Znbq- and Znpq-montmorillonite, respectively). The emission intensities of the mixed-ligand zinc complexes in montmorillonite prepared by the difference in the order of the added ligands are showed in Table 1. This observation indicated that the sequence of addition ligand affected the molecular structure and/or packing of the complexes formed in montmorillonite. The highest PL intensity and red shift of Znbq-montmorillonite supported that the mixed-ligand complexes were major phase and more stable than the mixtures of the two complexes. PL spectra of the products washed with ethanol were also examined. The emission maxima maintained at the same wavelengths as those of the as-prepared samples, supporting that the unreacted ligands was not included in the products obtained by the solid-solid reactions. The solid-solid reactions present a successful preparation of the hybrids of the mixed-ligand complex-montmorillonites that may create the opportunities to use these hybrids in designing novel optical materials.

#### **Conclusions**

The hybrids of mixed ligands (8-hydroxyquinoline and 2,2'bipyridine or 1,10-phenanthroline) zinc complexes, zinc(8hydroxyquinoline)(2,2'-bipyridine)-montmorillonite and zinc(8hydroxyquinoline)(1,10-phenanthroline)-montmorillonite, were successfully prepared by solid-state intercalation at room temperature. The luminescence intensity of zinc(8-hydroxyquinoline)(1,10phenanthroline)-montmorillonite was lower than that of zinc(8hydroxyquinoline)(2,2'-bipyridine)-montmorillonite, associating that the co-ligands remarkably affected the emission intensities of the mixed-ligand complexes in montmorillonite. 2,2'-Bipyridine co-ligand was enhancing the emission of zinc(8-hydroxyquinoline) complex while 1,10-phenanthroline was quenching. The studies on solid-solid reaction and in situ complex formation by using other mixed-ligand complexes are worth investigating to construct novel nanohybrid materials with precisely controlled properties.

#### Acknowledgements

Funding for this work is provided by the Thailand Research Fund (TRF) and Khon Kaen University (grant no. DBG5380004), the Center of Excellence for Innovation in Chemistry (PERCHCIC), Commission on Higher Education, Ministry of Education, Thailand and the Hitachi Scholarship Foundation, Japan.

#### References

- 1 M. Ogawa, Photoprocess in Clay-Organic Complexes, in Handbook of Layered Materials, ed., S. M. Auerbach, K. A. Carrado and P. K. Dutta, Marcel Dekker, New York, 2004, p. 191.
- 2 T. Nakato, K. Kusunoki, K. Yoshizawa, K. Kuroda and M. Kaneko, J. Phys. Chem., 1995, 99, 17896.
- 3 Z.-H. Liu, X. Yang and K. Ooi, *J. Colloid Interface Sci.*, 2003, **265**, 115.
- 4 A. Sánchez, Y. Echeverría, C. M. Sotomayor Torres, G. González and E. Benavente, *Mater. Res. Bull.*, 2006, **41**, 1185.
- 5 P. Lainé, M. Lanz and G. Calzaferri, Inorg. Chem., 1996, 35, 3514.
- 6 N. Li, X. Li, W. Wang, W. Geng and S. Qiu, Mater. Chem. Phys., 2006, 100, 128.
- 7 M. Tagaya and M. Ogawa, Phys. Chem. Chem. Phys., 2008, 10, 6849.
- 8 G. Lagaly, M. Ogawa and I. Dékány, *Clay Mineral Organic Intercalation, in Handbook of Clay Science, Developments in Clay Science*, vol. 1, ed., F. Bergaya, B. K. G. Theng and G. Lagaly, Elsevier Science, Amsterdam, 2006, p. 309.
- 9 T. J. Pinnavaia and M. M. Mortland, J. Phys. Chem., 1971, 75, 3957.
- 10 A. Yamagishi, J. Chem. Soc., Chem. Commun., 1984, 119.
- 11 V. E. Berkheiser and M. M. Mortland, Clays Clay Miner., 1977, 25, 105
- 12 T. J. Pinnavaia, R. Raythatha, J. G.-S. Lee, L. J. Halloran and J. F. Hoffman, J. Am. Chem. Soc., 1979, 101, 6891.
- 13 K. A. Carrado, P. Thiyagarajan, R. E. Winans and R. E. Botto, *Inorg. Chem.*, 1991, 30, 794.
- 14 G. Villemure, Clays Clay Miner., 1990, 38, 622.
- 15 T. Okada, T. Morita and M. Ogawa, Appl. Clay Sci., 2005, 29, 45.
- 16 N. Kakegawa and M. Ogawa, *Langmuir*, 2004, **20**, 7004.
- 17 A. O. Patil, D. Y. Curtin and I. C. Paul, J. Am. Chem. Soc., 1984, 106, 348.
- 18 F. Toda, K. Tanaka and A. Sekikawa, J. Chem. Soc., Chem. Commun., 1987, 279.
- 19 M. Ogawa, T. Hashizume, K. Kuroda and C. Kato, *Inorg. Chem.*, 1991, 30 584
- 20 N. Khaorapapong and M. Ogawa, Appl. Clay Sci., 2007, 35, 31.
- 21 N. Khaorapapong and M. Ogawa, J. Phys. Chem. Solids, 2008, 69, 941.
- 22 N. Khaorapapong, K. Kuroda, H. Hashizume and M. Ogawa, Appl. Clav Sci., 2001, 19, 69.
- 23 N. Khaorapapong, K. Kuroda and M. Ogawa, *Clays Clay Miner.*, 2002, 50 428
- 24 L. S. Sapochak, P. E. Burrows, D. Garbuzov, D. M. Ho, S. R Forrest and M. E. Thompson, *J. Phys. Chem.*, 1996, **100**, 17766.
- 25 L. S. Sapochak, A. Padmaperuma, N. Washton, F. Endrino, G. T. Schmett, J. Marshall, D. Fogarty, P. E. Burrows and S. R. Forrest, J. Am. Chem. Soc., 2001, 123, 6300.
- 26 L. M. Leung, W. Y. Lo, S. K. So, K. M. Lee and W. K. Choi, J. Am. Chem. Soc., 2000, 122, 5640.
- 27 A. Crispini, M. Ghedini, I. De Franco, I. Aiello, M. La Deda, N. Godbert and A. Bellusci, *Dalton Trans.*, 2008, 1186.
- 28 D.-E. Kim, W.-S. Kim, B.-S. Kim, B.-J. Lee and Y.-S. Kwon, *Colloids Surf.*, A, 2008, 313–314, 320.
- 29 V. K. Rai, R. Srivastava, G. Chauhan, K. Saxena, R. K. Bhardwaj, S. Chand and M. N. Kamalasanan, *Mater. Lett.*, 2008, 62, 2561.
- 30 P. K. Ghosh and A. J. Bard, J. Phys. Chem., 1984, 88, 5519.
- 31 M. Ogawa, M. Inagaki, N. Kodama, K. Kuroda and C. Kato, *J. Phys. Chem.*, 1993, 97, 3819.
- 32 N. Khaorapapong, A. Ontam, J. Khemprasit and M. Ogawa, *Appl. Clay Sci.*, 2009, **43**, 238.
- 33 N. Khaorapapong, A. Ontam and M. Ogawa, Appl. Clay Sci., 2010, 50, 19
- 34 D. Czakis-Sulikowska, A. Czylkowska, J. Radwańska-Doczekalska, R. Grodzki and E. Wojciechowska, J. Therm. Anal. Calorim., 2007, 90, 557.

- 35 D. Czakis-Sulikowska, J. Radwańska-Doczekalska, M. Markiewicz and M. Pietrzak, J. Therm. Anal. Calorim., 2008, 93, 789.
- 36 M. E. Mahmoud, S. S. Haggag and T. M. Abdel-Fattah, Polyhedron, 2009, 28, 181.
- 37 S. A. Juiz, M. I. G. Leles, A. C. F. Caires, N. Boralle and M. Ionashiro, J. Therm. Anal., 1997, 50, 625.
- 38 I. A. Pastre, I. D. N. Oliveira, A. B. S. Moitinho, G. R. de Souza, E. Y. Ionashiro and F. L. Fertonani, J. Therm. Anal. Calorim., 2004, 75, 661.
- 39 B. Marchon, L. Bokobza and G. Cote, Spectrochim. Acta, Part A, 1986, **42**, 537.
- 40 F. E. Lytle and D. M. Hercules, J. Am. Chem. Soc., 1969, 15, 253.
- 41 D. M. Boghaei and M. Gharagozlou, Spectrochim. Acta, Part A, 2007,
- 42 S. W. Karickhoff and G. W. Bailey, Clays Clay Miner., 1973, 21, 59.
- 43 M. Ghedini, M. La Deda, I. Aiello and A. Grisolia, *J. Chem. Soc., Dalton Trans.*, 2002, 3406.
- 44 X. Ouyang, H. Zeng and Y. Xie, Chem. China, 2007, 2, 407.
- 45 A. Crispini, I. Aiello, M. La Deda, I. De Franco, M. Amati, F. Lelj and M. Ghedini, Dalton Trans., 2006, 5124.

ST STATE

Contents lists available at SciVerse ScienceDirect

#### **Applied Clay Science**

journal homepage: www.elsevier.com/locate/clay



#### Note

# Preparation of a series of group XIII metal–quinolate complexes in natural and synthetic smectites

Patcharaporn Pimchan <sup>a</sup>, Nithima Khaorapapong <sup>a,\*</sup>, Makoto Ogawa <sup>b</sup>

- a Department of Chemistry and Center of Excellence for Innovation in Chemistry, Faculty of Science, Khon Kaen University, Khon Kaen 40002 Thailand
- b Department of Earth Sciences and Graduate School of Creative Science and Engineering, Waseda University, Nishiwaseda 1-6-1, Shinjuku-ku, Tokyo 169-8050 Japan

#### ARTICLE INFO

Article history:
Received 8 February 2011
Received in revised form 19 April 2011
Accepted 11 September 2011
Available online 10 October 2011

Keywords: 8-Hydroxyquinoline Optical properties Montmorillonite Saponite Solid-state intercalation

#### ABSTRACT

The preparation of metal–quinolate complexes,  $Mq_3$  (M = Al(III), Ga(III) and In(III); q = 8-hydroxyquinoline) in the interlayer spaces of smectites (natural montmorillonite and synthetic saponite), as well as their optical properties were investigated. The basal spacings of the products increased through solid–solid reactions between M(III)-smectites and 8-hydroxyquinoline, indicating the intercalation of 8-hydroxyquinoline. The photoluminescence maxima and intensities of the intercalation compounds varied depending on the metal ions and nature of clay minerals. The PL intensities of  $Mq_3$  complexes in synthetic saponite were higher than those of the complexes in montmorillonite because of the difference in molecular structure and/or molecular packing, as well as the presence of the quenching impurities in montmorillonite.

© 2011 Elsevier B.V. All rights reserved.

#### 1. Introduction

The intercalation of organic guest species into layered inorganic solids is an elegant process of constructing nanocomposite materials based on the combination of vast varieties of inorganic and organic substances (Lagaly et al., 2006; Ogawa, 2004). Smectite, a 2:1 type layered clay mineral, possesses various attractive features such as swelling behavior, large surface area, ion exchange and adsorptive properties for organizing photoactive species. Solid–solid reaction is one of the most suitable modification techniques of organic–inorganic hybrid materials due to the ease of operation and possibility to prepare the compounds, which are not accessible from solutions and so on (Patil et al., 1984; Toda et al., 1987). The solid-state intercalation of both nonionic and cationic species into layered zirconium phosphate (Clearfield and Troup, 1970), zeolites (Lázár et al., 1994) and layered clay minerals (Ogawa et al., 1989, 1990, 1991, 1992a, 1992b; Wada, 1961) was reported so far.

In our previous efforts to explore novel intercalation compounds with unique microstructures and properties, our interests have been focused in organic molecular materials and inorganic species including metal complexes and semiconductor nanoparticles because of the useful luminescence properties especially for organic light emitting devices (OLEDs) and electro-optical materials. We successfully prepared metal chelates (diimine and/or quinolate complexes) and metal chalcogenide nanoparticles (CdS, ZnS, MnS, etc.) in the interlayer spaces of smectites by solid–solid reactions and *in situ* 

formations (Khaorapapong, 2010; Khaorapapong and Ogawa, 2007, 2008, 2010; Khaorapapong et al., 2000, 2001, 2002a, 2002b, 2008a, 2008b, 2009, 2010, 2011a, 2011b; Ogawa et al., 1991). Because of the advantages of the synthetic methodology such as the facile operation and low possibility of the desorption, the effect of solid-state intercalation of metal complexes in clay minerals on their structures and properties is worth investigating for producing novel low dimensional nanohybrid materials.

Metal–quinolate complexes, Mq $_3$  (where M = Al(III), Ga(III), and In(III); q=8-hydroxyquinoline) are excellent electroluminescent materials for organic light emitting devices (Burrows et al., 1994, 1996). The capability of emitting many colors throughout the visible spectrum and luminescent efficiency of metal–quinolate complexes were governed by the molecular structure and packing of the metal complexes (Chen and Shi, 1998; Higginson et al., 1998). Here, a series of metal–quinolate complexes of group XIII elements (Al, Ga and In) was prepared in the interlayer spaces of smectites. The differences in the metal complexing ions and type of clay minerals may affect the emission intensity and/or color of each compound. In the present study, Alq $_3$ , Gaq $_3$  and Inq $_3$  complexes were prepared in the interlayer spaces of smectites by solid–solid reactions and *in situ* complex formations. The effects of the type of metal ions and nature of clay minerals with optical properties of the products were investigated.

#### 2. Experimental

Two smectites, natural montmorillonite (Reference clay sample of the Clay Science Society of Japan, JCSS-3101, Kunipia F, obtained from Tsukinuno mine, Japan) and synthetic saponite (Reference clay sample

<sup>\*</sup> Corresponding author. Tel.: +66 4320 2222 41x12370 2; fax: +66 4320 2373. E-mail address: nithima@kku.ac.th (N. Khaorapapong).

**Table 1**Basal spacings  $(d_{001})$  and colors of the hydrated smectites and the products prepared by solid–solid reactions.

Substance	Hydrated smectite	Hydrated smectite		After the reaction with 8-hydroxyquinoline	
	d <sub>001</sub> (nm)	Color	d <sub>001</sub> (nm)	Color	the interlayer space (nm)
Al(III)-montmorillonite	1.53	white	1.70	green	0.74
Al(III)-synthetic saponite	1.45	white	1.50	yellowish green	0.54
Ga(III)-montmorillonite	1.53	white	1.67	green	0.71
Ga(III)-synthetic saponite	1.43	white	1.53	yellowish green	0.57
In(III)-montmorillonite	1.58	white	1.71	green	0.75
In(III)-synthetic saponite	1.45	white	1.53	yellowish green	0.57

of the Clay Science Society of Japan, JCSS-3501, Sumecton SA, synthesized hydrothermally by Kunimine Industries Co., Japan) were used as the host materials. The cation exchange capacities (CEC) of the clay minerals were 1.19 and 0.70 meq/g for montmorillonite and synthetic saponite. Aluminum chloride (AlCl $_3$ ·6H $_2$ O) and gallium nitrate (Ga (NO $_3$ ) $_3$ ·xH $_2$ O) were obtained by Ajax Finechem Pty. Ltd. and Aldrich Chemical Co. Ltd. Indium chloride (InCl $_3$ ) was supplied by Fisher Chemical Co., Ltd. 8-Hydroxyquinoline (C $_9$ H $_7$ NO) was purchased from Junsei Chemical Co., Ltd. All the reagents are analytical grade and were used without further purification.

Al(III)-, Ga(III)- and In(III)-smectites (Al(III)-, Ga(III)- and In(III)montmorillonites, and synthetic saponites) were synthesized by a conventional ion exchange method. Smectite was mixed with an aqueous solution of each metal salt and the mixture was stirred at room temperature for 1 day. After the ion exchange reaction, the resulting solids were collected by centrifugation and washed repeatedly with deionized water until no chloride or nitrate ion was detected in the supernatants. The yields of the exchanged cations (Al(III), Ga(III) and In(III)) in smectites determined by inductively coupled plasma optical emission spectroscopy (ICP-OES) were 98-100%. The mixture of Al(III)-, Ga(III)- or In(III)-smectites and 8hydroxyquinoline was ground manually in an agate mortar at room temperature for 10-15 min. The molar ratio of 8-hydroxyquinoline to the interlayer cation was 3:1. The products were abbreviated as Mq3-montmorillonites or Mq3-synthetic saponites, where M was Al (III), Ga(III) or In(III).

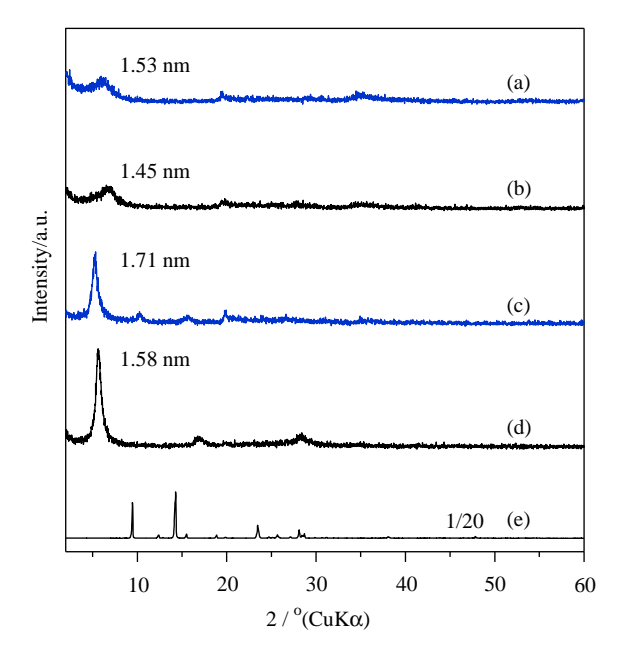
Powder X-ray diffraction patterns (XRD) were obtained on a Bruker D8 ADVANCE diffractometer using monochromatic Cu K $\alpha$  radiation. Diffuse reflectance spectra were collected on a Shimadzu UV–VIS–NIR–3101PC scanning spectrophotometer using an integrated sphere. Infrared spectra were performed by KBr disk method on a Perkin-Elmer Spectrum One FT-IR spectrophotometer. TG-DTG-DTA data were measured on a Perkin Elmer Pyris Diamond TG-DTA instrument at a heating rate of 10 °C/min under a dry air atmosphere using  $\alpha$ -alumina ( $\alpha$ -Al<sub>2</sub>O<sub>3</sub>) as a standard material. Photoluminescence spectra were recorded on a Shimadzu RF-5301PC spectrofluorophotometer in the wavelength range of 300–800 nm with the excitation at 360 nm and slit widths were 1.5 for excitation and 5 for emission. Inductively coupled plasma optical emission spectroscopic (ICP-OES) data were taken with Perkin Elmer Optima 2100DV ICP-OES.

#### 3. Results and discussion

By the solid–solid reactions of M(III)–smectites with 8-hydroxy-quinoline, the yellowish green to green products were obtained. The basal spacings ( $d_{001}$ ) and the colors of the hydrated smectites and the final products were summarized in Table 1. The basal spacings of Mq<sub>3</sub>–montmorillonites were ca. 1.7 nm and those of Mq<sub>3</sub>–synthetic saponites were ca. 1.5 nm. The expansions of the interlayer spaces obtained by subtracting the thickness of a silicate layer (0.96 nm) from the observed basal spacings were determined to be 0.5–0.8 nm. The reflections due to 8-hydroxyquinoline at d=0.94, 0.62, 0.38 and 0.31 nm were absent in the XRD patterns of the products

(Fig. 1). Gaq<sub>3</sub>- or Inq<sub>3</sub>-smectites were heated at 200 °C in air for 2 h in order to confirm that the XRD patterns of the heated products were not different from those of the as-prepared compounds and the reflections due to 8-hydroxyquinoline crystal were not observed. The change in the colors and the expansion of the interlayer spaces were in accordance with those reported for Alq3-montmorillonite and Alg<sub>3</sub>-synthetic saponite (Khaorapapong et al., 2002b), as well as Znq<sub>2</sub>-montmorillonite and Znq<sub>2</sub>-synthetic saponite (Khaorapapong and Ogawa, 2008), suggesting the intercalation of 8-hydroxyquinoline and the formation of Mq3 complexes in situ in the interlayer spaces. The expansions of the interlayer spaces of Mg<sub>3</sub>-montmorillonites were larger than those of Mg<sub>3</sub>-synthetic saponites, which were thought to be derived from the difference in the molecular structure and/or molecular packing of Mq3 complexes in montmorillonite and synthetic saponite. Because the cation exchange capacities of montmorillonite and synthetic saponite used in this work are 1.19 and 0.70 meq/g, the distance between the adjacent cation exchange sites is different. Therefore, the geometry and/or packing of the intercalated Mq<sub>3</sub> complexes varied to result in the difference of the interlayer expansions. The intercalation of 8-hydroxyquinoline into smectites took place by the ligand displacement processes between 8-hydroxyquinoline molecule and the coordinated water.

In the DTA curves of Mq<sub>3</sub>-smectites, the endothermic peaks due to the melting and vaporization of 8-hydroxyquinoline at around 75 and 185 °C were absent as reported previously for Alq<sub>3</sub>-smectites (Khaorapapong et al., 2002b), suggesting that 8-hydroxyquinoline crystal was not present in the products. From the TG-DTA curves of the products (Figs. S1 and S2, Supporting Information), the initial



 $\label{eq:fig.1.} \textbf{Fig. 1.} \ \textbf{XRD patterns of } Inq_3\text{-synthetic saponite (a), } In(III)\text{-synthetic saponite (b), } Inq_3\text{-montmorillonite (c), } In(III)\text{-montmorillonite (d) and } 8\text{-hydroxyquinoline (e).}$ 

mass losses observed from room temperature to at around 130 °C were ascribed to the desorption of the adsorbed water (Juiz et al., 1997). In the DTA curves, the exothermic peaks in the temperature range of ca. 300-700 °C accompanied the mass losses in the TG and DTG curves (Figs. S3 and S4, Supporting Information) were interpreted to the oxidative decomposition and evaporation of the coordinated 8-hydroxyguinoline (Juiz et al., 1997; Mahmoud et al., 2009). The last mass losses of the intercalation compounds observed at higher temperatures were attributed to the oxidation of carbonaceous residue and the dehydroxydation of the structural OH (Pastre et al., 2004). It was reported that the beginning of mass loss of Alq<sub>3</sub> revealed at around 300 °C (Wang et al., 2007). The decompositions of Alq<sub>3</sub> and Gaq<sub>3</sub> were observed in the temperature range of 320-500 °C (Sapochak et al., 2001). The observations confirmed the intercalation of 8-hydroxyquinoline in smectites by solid-solid reactions. The difference of thermal behaviors supported that the molecular geometry and/or packing of the complexes in smectites were different.

The *in situ* complex formation of Mq<sub>3</sub>-smectites was confirmed by FT-IR, UV-vis and PL spectroscopies. The characteristic absorptions of 8-hydroxyquinoline (Marchon et al., 1986) including the C-H out of plane bending vibrations at 817, 781 and 741 cm<sup>-1</sup> were clearly observed in the FT-IR spectra of the products. The absorption bands of all the products were shifted to higher frequency by comparison with those observed for the neat 8-hydroxyquinoline (Table S1, Supporting Information), indicating the chelations between 8-hydroxyquinoline and the interlayer metal cations (Al(III), Ga(III) and In (III)) of the layered host materials.

The diffuse reflectance absorption spectra of the products and M (III)-smectites were shown in Figs. 2 and 3. In the absorption spectrum of 8-hydroxyquinoline (data not shown), the corresponding bands were seen at 222, 325 and 360 (sh) nm. The absorption bands due to charge transfer from oxo (O<sup>2-</sup>, OH<sup>-</sup>, OH<sub>2</sub>) to ferric ion (Fe<sup>3+</sup>) (Karickhoff and Bailey, 1973) of M(III)-montmorillonites were observed at ca. 250 nm. The bands of M(III)-synthetic saponites appeared at 253 and 256 nm were interpreted to the oxo to metal cations–either as structural elements or exchangeable cations charge transfer transitions (Karickhoff and Bailey, 1973; Kshirsagar et al., 2009). The diffuse reflectance spectra of the products exhibited

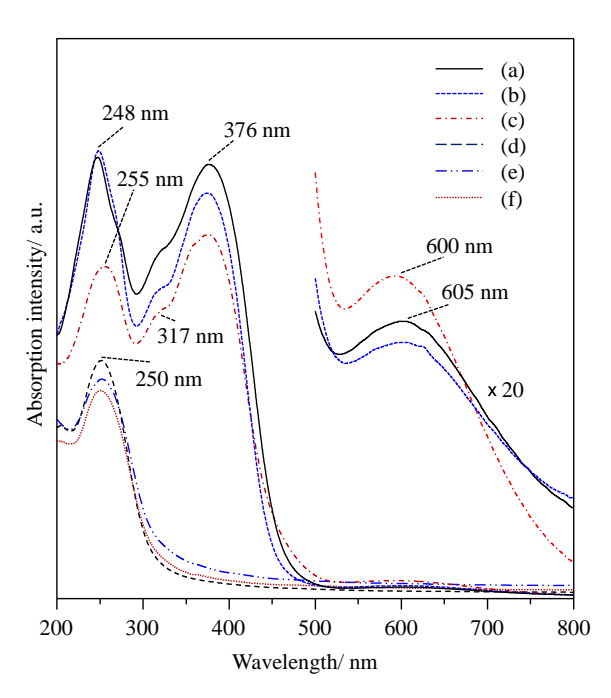


**Fig. 2.** Diffuse reflectance absorption spectra of Inq<sub>3</sub>-montmorillonite (a), Gaq<sub>3</sub>-montmorillonite (b), Alq<sub>3</sub>-montmorillonite (c), In(III)-montmorillonite (d), Ga(III)-montmorillonite (e) and Al(III)-montmorillonite (f).

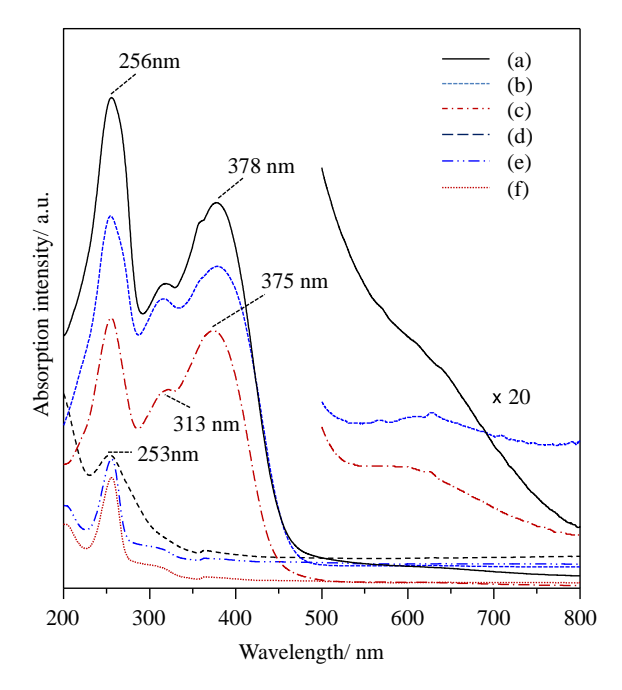


**Fig. 3.** Diffuse reflectance absorption spectra of Inq<sub>3</sub>-synthetic saponite (a), Gaq<sub>3</sub>-synthetic saponite (b), Alq<sub>3</sub>-synthetic saponite (c), In(III)-synthetic saponite (d), Ga(III)-synthetic saponite (e) and Al(III)-synthetic saponite (f).

three absorption bands with the maxima of 248 or 255, 317 (sh) and 376 nm for Mg<sub>3</sub>-montmorillonites (Fig. 2), 256, 313 (sh) and 375 or 378 nm for Mq<sub>3</sub>-synthetic saponites (Fig. 3). The bands due to  $\sigma$  to  $\pi^*$  and  $\pi$  to  $\pi^*$  transitions of aromatic ring in the metal-quinolate complexes were reported at 270 and 300-320 nm, respectively (Ghedini et al., 2002). Thus, the bands observed at around 248-256 nm for Mq3-smectite intercalation compounds were ascribed to the overlapping bands between the charge transfer from the oxo to ferric ion or metal cations in the clay minerals and the  $\sigma$ to  $\pi^*$  transition of 8-hydroxyguinoline. The shoulders appeared at 313-317 nm in the absorption spectra of all the products and the absorption maxima revealed at 375-378 nm were attributed to the  $\pi$  to  $\pi^*$  transition of the aromatic ring of metal-quinolate complexes (Ghedini et al., 2002; Ouyang et al., 2007). The absorption bands of Alg<sub>3</sub> and Gag<sub>3</sub> in a dilute chloroform solution appeared at 388 nm and at 392 nm (Sapochak et al., 2001). The UV-visible spectra of Alg<sub>3</sub>, Gag<sub>3</sub> and Ing<sub>3</sub> in DMSO showed the absorption bands at 386, 390 and 390 nm (Ghedini et al., 2003). It was reported that the absorption bands of Alg<sub>3</sub> and Ing<sub>3</sub> solid films were majorly observed at 390 nm (Shukla and Kumar, 2007; Shukla et al., 2006). Consequently, the bands observed for Alq<sub>3</sub>-, Gaq<sub>3</sub>- and Inq<sub>3</sub>-smectites were ascribed to the formation of Alq<sub>3</sub>, Gaq<sub>3</sub> and Inq<sub>3</sub> complexes in montmorillonite and synthetic saponite, which were consistent with the photoluminescence spectra described below.

The photoluminescence spectra of the intercalation compounds were shown in Fig. 4 and the emission intensities were summarized in Table 2. Since 8-hydroxyquinoline gave the absorption maxima in the visible region at 360 nm and the PL spectra of Alq<sub>3</sub>-smectites (Khaorapapong et al., 2002b) were also recorded at the same wavelength, in order to exclude the effect of the excitation wavelength, therefore, all the products were excited at 360 nm. The luminescent emissions of metal–quinolate complexes due to the electronic  $\pi$  to  $\pi^*$  transition, which involved charge transfer from the filled  $\pi$  orbitals on the phenoxide side (HOMO) to the unfilled  $\pi^*$  orbitals on the pyridyl side (LUMO) (Chen and Shi, 1998; Halls and Schlegel, 2001), were observed at 508 nm for Alq<sub>3</sub>-montmorillonite and at 510 nm for Alq<sub>3</sub>-synthetic saponite. The emission bands of Alq<sub>3</sub> in DMSO as well as in DMF solution were observed at 516 and 520 nm (Burrows

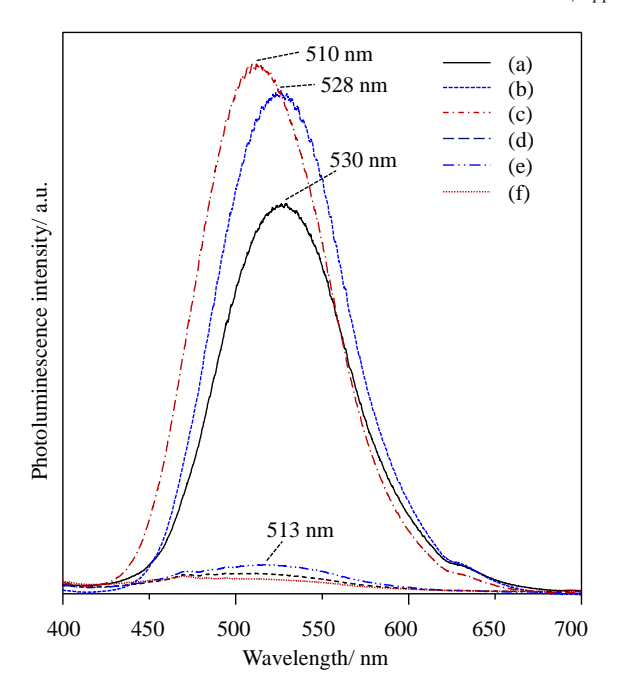


**Fig. 4.** Photoluminescence spectra of Inq<sub>3</sub>-synthetic saponite (a), Gaq<sub>3</sub>-synthetic saponite (b), Alq<sub>3</sub>-synthetic saponite (c), Inq<sub>3</sub>-montmorillonite (d), Gaq<sub>3</sub>-montmorillonite (e) and Alq<sub>3</sub>-montmorillonite (f).

et al., 1994; Ghedini et al., 2003). The emission wavelength of Alq<sub>3</sub> complex was blue-shifted as the polarity of the solvents decreased along DMF and DMSO (Table 2). The photoluminescence bands of Alg<sub>3</sub>, Gag<sub>3</sub> and Ing<sub>3</sub> complexes in montmorillonite were blue-shifted compared to those in synthetic saponite. Since the substitution in the tetrahedral sites of synthetic saponite generates higher polarity than that in the octahedral sites of montmorillonite (Kakegawa et al., 2003), the blue-shifts of the emission band of Alq3, Gaq3 and Inq3 complexes in montmorillonite were thought to be caused by the effect of the polarity of surrounding environments. The blue-shifts of photoluminescence bands of the Mq<sub>3</sub> complexes in montmorillonite supported the higher polarity of synthetic saponite. The PL bands of solid film were observed at 520 nm for Alq3, at 541 nm for Gaq3 and at 540 nm for Inq<sub>3</sub> (Burrows et al., 1994). This observation confirmed the in situ formation of Alq<sub>3</sub>, Gaq<sub>3</sub> and Inq<sub>3</sub> complexes in smectites.

The photoluminescence intensities of Alq<sub>3</sub>-, Gaq<sub>3</sub>- and Inq<sub>3</sub>-synthetic saponites varied depending on the atomic number of metal ions due to the heavy atom quenching; namely the PL efficiencies of the complexes in synthetic saponite decreased in the order Alq<sub>3</sub>>Gaq<sub>3</sub>>Inq<sub>3</sub>. For montmorillonite system, the emission intensity of Alq<sub>3</sub>-montmorillonite was lower than those of Gaq<sub>3</sub>- and Inq<sub>3</sub>-montmorillonites. This result which occurred from the side reactions of impurities, such as oxygen and water, led to the failure of Mq<sub>3</sub> complexes, which was indicated by the appearance of the absorption bands observed at around 600 nm due to n to  $\pi^*$  transition of quinones and *N*-oxides, or the presence of impurity such as non-emissive species (Papadimitrakopoulos et al., 1996). The absorption bands

**Table 2** Luminescence bands of the Mq<sub>3</sub> complexes in different matrices.

Matrix	PL, λ <sub>emi</sub>	ss (nm)	References	
	Alq <sub>3</sub>	$Gaq_3$	Inq <sub>3</sub>	
Montmorillonite	508	513	520	this work
Synthetic saponite	510	528	530	this work
DMSO solution	516	525	525	Ghedini et al. (2003)
DMF solution	520	542	541	Burrows et al. (1994)

owing to n to  $\pi^*$  transition were observed at 600 nm for Alq<sub>3</sub>-montmorillonite and at 605 nm for Gaq<sub>3</sub>- and Inq<sub>3</sub>-montmorillonites (Fig. 2), while those bands were not clearly seen for the synthetic saponite system (Fig. 3), indicating the degradation of the intercalated complexes and/or the formation of non-emissive species due to the larger amount water contained in montmorillonite. Additionally, the PL intensities of Mq<sub>3</sub> complexes in montmorillonite were lower than those of the complexes in synthetic saponite ca. 40 times for Alq<sub>3</sub> or Inq<sub>3</sub> and ca. 20 times for Gaq<sub>3</sub>, supporting the degradation of the intercalated metal–quinolate complexes and/or quenching impurities in montmorillonite. Our results showed the important roles of cation size and nature of clay mineral to the PL intensities and spectral shifts. The heavy atom reduced PL intensities in Mq<sub>3</sub>-synthetic saponites, while impurities played a dominant role on the quenching in Mq<sub>3</sub>-montmorillonites.

#### 4. Conclusions

The high electroluminescent metal–quinolate complexes, Alq<sub>3</sub>, Gaq<sub>3</sub> and Inq<sub>3</sub>, were successfully intercalated into the interlayer spaces of natural and synthetic smectites by solid–solid reactions at room temperature. The blue–shift of emission bands and the decrease of emission intensities of Mq<sub>3</sub>–smectites took place as the decrease of cation size along the series of Inq<sub>3</sub>, Gaq<sub>3</sub> and Alq<sub>3</sub> and the nature of smectites. The luminescence intensities of the metal–quinolate complexes in synthetic saponite were higher than those in natural montmorillonite, indicating the degradation of the complexes and quenching impurities in natural montmorillonite. The studies on the series of group XIII metal–quinolate complexes in smectites are important for understanding the effects of the type of metal ions and nature of clay minerals to construct novel nanohybrid materials with precisely controlled required properties.

Supplementary materials related to this article can be found online at doi:10.1016/j.clay.2011.09.002.

#### Acknowledgments

One of the other authors (PP) thanks for her Ph.D. scholarship from the Higher Education Research Promotion and National Research University Project of Thailand, Office of the Higher Education Commission, through the Advanced Functional Materials Cluster of Khon Kaen University, the authors gratefully acknowledge the financial supports from the Thailand Research Fund (TRF) and Khon Kaen University (Grant no. DBG5380004), the Center of Excellence for Innovation in Chemistry (PERCH-CIC), Commission on Higher Education, Ministry of Education, Thailand.

#### References

Burrows, P.E., Sapochak, L.S., McCarty, D.M., Forrest, S.R., 1994. Metal ion dependent luminescence effects in metal tris-quinolate organic heterojunction light emitting devices. Applied Physics Letters 64, 2718–2720.

Burrows, P.E., Shen, Z., Bulovic, V., McCarty, D.M., Forrest, S.R., Cronin, J.A., Thompson, M.E., 1996. Relationship between electroluminescence and current transport in organic heterojunction light-emitting devices. Journal of Applied Physics 79, 7991–8006.

Chen, C.H., Shi, J., 1998. Metal chelates as emitting materials for organic electroluminescence. Coordination Chemistry Reviews 171, 161–174.

Clearfield, A., Troup, J.M., 1970. Ion exchange between solids. Journal of Physical Chemistry 74, 2578–2580.

Ghedini, M., La Deda, M., Aiello, I., Grisolia, A., 2002. Synthesis and photophysical characterisation of luminescent zinc complexes with 5-substituted-8-hydroxyquinolines. Journal of the Chemical Society, Dalton Transactions 3406–3409.

Ghedini, M., La Deda, M., Aiello, I., Grisolia, A., 2003. Synthesis and photophysical characterisation of soluble photoluminescent metal complexes with substituted 8-hydroxyquinolines. Synthetic Metals 138, 189–192.

Halls, M.D., Schlegel, H.B., 2001. Molecular orbital study of the first excited state of the OLED material tris(8-hydroxyquinoline)aluminum(III). Chemistry of Materials 13, 2632–2640.

- Higginson, K.A., Zhang, X.-M., Papadimitrakopoulos, F., 1998. Thermal and morphological effects on the hydrolytic stability of aluminum tris(8-hydroxyquinoline) (Alq<sub>3</sub>). Chemistry of Materials 10, 1017–1020.
- Juiz, S.A., Leles, M.I.G., Caires, A.C.F., Boralle, N., Ionashiro, M., 1997. Thermal decomposition of the magnesium, zinc, lead and niobium chelates derived from 8-quinolinol. Journal of Thermal Analysis 50, 625–632.
- Kakegawa, N., Kondo, T., Ogawa, M., 2003. Variation of electron-donating ability of smectites as probed by photoreduction of methyl viologen. Langmuir 19, 3578–3582.
- Karickhoff, S.W., Bailey, G.W., 1973. Optical absorption spectra of clay minerals. Clays and Clay Minerals 21, 59–70.
- Khaorapapong, N., 2010. *In situ* complexation of thiourea in the interlayer space of copper(II)-montmorillonite. Applied Clay Science 50, 414–417.
- Khaorapapong, N., Ogawa, M., 2007. Solid-state intercalation of 8-hydroxyquinoline into Li(I)-, Zn(II)- and Mn(II)-montmorillonites. Applied Clay Science 35, 31–38.
- Khaorapapong, N., Ogawa, M., 2008. In situ formation of bis(8-hydroxyquinoline) zinc (II) complex in the interlayer spaces of smectites by solid-solid reactions. Journal of Physics and Chemistry of Solids 69, 941–948.
- Khaorapapong, N., Ogawa, M., 2010. Formation of mono(8-hydroxyquinoline) lithium (I) complex in smectites by solid-solid reactions. Journal of Physics and Chemistry of Solids 71, 1644–1650.
- Khaorapapong, N., Kuroda, K., Hashizume, H., Ogawa, M., 2000. Solid state intercalation of 4,4'-bipyridine into the interlayer space of montmorillonites. Molecular Crystals and Liquid Crystals 341, 351–356.
- Khaorapapong, N., Kuroda, K., Hashizume, H., Ogawa, M., 2001. Solid-state intercalation of 4,4'-bipyridine and 1,2-di(4-pyridine)ethylene into the interlayer spaces of Co(II)-, Ni(II)-, and Cu(II)-montmorillonites. Applied Clay Science 19, 69–76.
- Khaorapapong, N., Kuroda, K., Ogawa, M., 2002a. Incorporation of thioacetamide into the interlayer space of montmorillonite by solid-solid reactions. Clay Science 11, 549-564
- Khaorapapong, N., Kuroda, K., Ogawa, M., 2002b. Intercalation of 8-hydroxyquinoline into Al-smectites by solid-solid reactions. Clays and Clay Minerals 50, 428–434.
- Khaorapapong, N., Ontam, A., Ogawa, M., 2008a. Formation of MnS particles in the interlayer space of montmorillonite. Materials Letters 62, 3722–3723.
- Khaorapapong, N., Ontam, A., Youngme, S., Ogawa, M., 2008b. Solid-state intercalation and in situ formation of cadmium sulfide in the interlayer space of montmorillonite. Journal of Physics and Chemistry of Solids 69, 1107–1111.
- Khaorapapong, N., Ontam, A., Khemprasit, J., Ogawa, M., 2009. Formation of MnS- and NiS-montmorillonites by solid-solid reactions. Applied Clay Science 43, 238–242.
  Khaorapapong, N., Ontam, A., Ogawa, M., 2010. Formation of ZnS and CdS in the inter-
- Khaorapapong, N., Ontam, A., Ogawa, M., 2010. Formation of ZnS and CdS in the interlayer spaces of montmorillonite. Applied Clay Science 50, 19–24.
- Khaorapapong, N., Ontam, A., Ogawa, M., 2011a. Very slow formation of copper sulfide and cobalt sulfide nanoparticles in montmorillonite. Applied Clay Science 51, 182–186.
- Khaorapapong, N., Pimchan, P., Ogawa, M., 2011b. Formation of mixed-ligand zinc(II) complex-montmorillonite hybrids by solid-solid reactions. 40, 5964–5970.
- Kshirsagar, V.S., Garade, A.C., Patil, K.R., Shirai, M., Rode, C.V., 2009. Liquid phase oxidation of *p*-cresol over cobalt saponite. Topics in Catalysis 52, 784–788.
- Lagaly, G., Ogawa, M., Dékány, I., 2006. Clay mineral organic intercalations. In: Bergaya, F., Theng, B.K.G., Lagaly, G. (Eds.), Handbook of Clay Science, Developments in Clay Science, vol. 1. Elsevier Science, Amsterdam, pp. 309–377.
- Lázár, K., Pál-Borbély, G., Beyer, H.K., Karge, H.G., 1994. Solid-state ion exchange in zeolites. Journal of the Chemical Society, Faraday Transactions 90, 1329–1334.

- Mahmoud, M.E., Haggag, S.S., Abdel-Fattah, T.M., 2009. Surface layer-by-layer chemical deposition reaction for thin film formation of nano-sized metal 8hydroxyquinolate complexes. Polyhedron 28, 181–187.
- Marchon, B., Bokobza, L., Cote, G., 1986. Vibrational study of 8-quinolinol and 7-(4-ethyl-1-methyloctyl)-8-quinolinol (Kelex100), two representative members of an important chelating agent family. Spectrochimica Acta 42A, 537–542.
- Ogawa, M., 2004. Photoprocess in clay-organic complexes. In: Auerbach, S.M., Carrado, K.A., Dutta, P.K. (Eds.), Handbook of Layered Materials. Marcel Dekker, New York, pp. 191–206.
- Ogawa, M., Kuroda, K., Kato, C., 1989. Preparation of montmorillonite-organic intercalation compounds by solid-solid reactions. Chemistry Letters 9, 1659–1662.
- Ogawa, M., Kato, K., Kuroda, K., Kato, C., 1990. Preparation of montmorillonite–alkylamine intercalation compounds by solid–solid reactions. Clay Science 8, 31–36.
- Ogawa, M., Hashizume, T., Kuroda, K., Kato, C., 1991. Intercalation of 2,2'-bipyridine and complex formation in the interlayer space of montmorillonite by solid–solid reactions. Inorganic Chemistry 30, 584–585.
- Ogawa, M., Nagafusa, Y., Kuroda, K., Kato, C., 1992a. Solid-state intercalation of acrylamide into smectites and Na-taeniolite. Applied Clay Science 7, 291–302.
- Ogawa, M., Shirai, H., Kuroda, K., Kato, C., 1992b. Solid-state intercalation of naphthalene and anthracene into alkylammonium-montmorillonites. Clays and Clay Minerals 40, 485–490.
- Ouyang, X., Zeng, H., Xie, Y., 2007. Synthesis and photoluminescence properties of 8-hydroxyquinoline derivatives and their metallic complexes. Frontiers of Chemistry in China 2, 407–413.
- Papadimitrakopoulos, F., Zhang, X.-M., Thomsen III, D.L., Higginson, K.A., 1996. A chemical failure mechanism for aluminum(III) 8-hydroxyquinoline light-emitting devices. Chemistry of Materials 8, 1363–1365.
- Pastre, I.A., Oliveira, I.D.N., Moitinho, A.B.S., de Souza, G.R., Ionashiro, E.Y., Fertonani, F.L., 2004. Thermal behaviour of intercalated 8-hydroxyquinoline (oxine) in montmorillonite clay. Journal of Thermal Analysis and Calorimetry 75, 661–669.
- Patil, A.O., Curtin, D.Y., Paul, I.C., 1984. Solid-state formation of quinhydrones from their components. Use of solid-solid reactions to prepare compounds not accessible from solution. Journal of the American Chemical Society 106, 348–353.
- Sapochak, L.S., Padmaperuma, A., Washton, N., Endrino, F., Schmett, G.T., Marshall, J., Fogarty, D., Burrows, P.E., Forrest, S.R., 2001. Effects of systematic methyl substitution of metal (III) tris(n-methyl-8-quinolinolato) chelates on material properties for optimum electroluminescence device performance. Journal of the American Chemical Society 123, 6300–6307.
- Shukla, V.K., Kumar, S., 2007. Study of optical properties and light induced effects on  $Inq_3$  thin film used in organic light emitting devices. Optical Materials 29, 1809-1816.
- Shukla, V.K., Kumar, S., Deva, D., 2006. Light induced effects on the morphology and optical properties of tris-(8-hydroxyquinoline) aluminium (Alq<sub>3</sub>) small molecular thin film. Synthetic Metals 156, 387–391.
- Toda, F., Tanaka, K., Sekikawa, A., 1987. Host-guest complex formation by a solid-solid reaction. Journal of the Chemical Society, Chemical Communications 279–280.
- Wada, K., 1961. Lattice expansion of kaolin minerals by treatment with potassium acetate. American Mineralogist 46, 78–91.
- Wang, M.H., Sawada, Y., Saito, K., Horie, S., Uchida, T., Ohtsuka, M., Seki, S., Kobayashi, S., Arii, T., Kishi, A., Takahashi, T., Nishimoto, Y., Wakimoto, T., Monzen, K., Kashima, I., Nishikiori, T., Sun, L.X., Ozao, R., 2007. Thermal change of Alq<sub>3</sub>, tris(8-hydroxy-quinolinato) aluminum(III) studied by TG and XRD-DSC. Journal of Thermal Analysis and Calorimetry 89, 363–366.

-Asian Clay Special Paper-

## SOLID-STATE INTERCALATION OF ORGANIC AND INORGANIC SUBSTANCES IN SMECTITES

NITHIMA KHAORAPAPONG<sup>a,\*</sup> and MAKOTO OGAWA<sup>b</sup>

<sup>a</sup>Department of Chemistry and Center of Excellence for Innovation in Chemistry, Faculty of Science, Khon Kaen University, Khon Kaen 40002, Thailand

<sup>b</sup>Department of Earth Sciences and Graduate School of Creative Science and Engineering, Waseda University, Nishiwaseda 1-6-1, Shinjuku-ku, Tokyo 169-8050, Japan

(Received September 6, 2010. Accepted November 30, 2010)

#### **ABSTRACT**

Our attempts in the preparation of smectite intercalation compounds by solid-solid reactions are reviewed. Various guest substances, including both cationic and nonionic species, metal complexes, and metal sulfide nanoparticles, have been immobilized in the interlayer spaces of smectites. Organoammonium ions were incorporated in the interlayer spaces by the solid-state cation exchange process. The adsorption of nonionic molecules into pristine and organically modified smectites was also possible. Solid-state intercalation was completed within a few minutes at room temperature. The interactions of sulfide ions with the interlayer cations of smectite via adsorption led to smectite-metal sulfide hybrids. Adsorption and *in situ* formation of both complexes and metal sulfides in smectites were observed, when homoionic (Na(I)-, K(I)-, Rb(I)-, NH4(I)-, Ca(II)-, Co(II)-, Cu(II)-, Ni(II)-, Cd(II)-, Al(III)-, Zn(II)- and Mn(II)-) smectites were ground with the appropriate ligands (diimines, 18-crown-6-ether, thioacetamide, thiourea, 8-hydroxyquinoline, as well as so-dium sulfide).

Key words: Intercalation, Smectite, Solid-solid reaction

#### INTRODUCTION

The intercalation of organic and inorganic cations, molecules or particles via ion exchange and adsorption processes into ordered architectures has attracted increasing interest from scientific and application studies (Ogawa, 2004; Ogawa and Kuroda, 1995, 1997; Lagaly et al., 2006). The physical and chemical properties of both guest and host species can be altered by the intercalation reactions (Whittingham, 1982). It is well known that intercalation proceeds by ion exchange of interlayer exchangeable cations, adsorption of polar molecules by ion-dipole interaction and/or hydrogen bonding, acid-base reaction or charge transfer complex formation (Ogawa and Kuroda, 1997). Various layered inorganic solids, including graphite, transition metal dichalcogenides, metal phosphates and phosphonates, transition metal oxides, layered double hydroxides, and clay minerals, have been used to accommodate guest species to form intercalation compounds (Ogawa, 2004; Ogawa and Kuroda, 1995, 1997; Lagaly et al., 2006).

In comparison with three dimensional network hosts such as zeolites, one of the advantages of layered solids is the expandability of their interlayer spaces, which make it possible to accommodate a wide variety of guest species.

Generally, the intercalation compounds are obtained by solid-liquid reactions and solid-gas reactions. The solid-solid reaction, including mechanochemical process, which occurs between powders in the solid state, can be achieved simply without large volume of solutions and long proceeding times. The formation of some organic host-guest complexes and the intercalation compounds of potassium acetate-kaolinite by solid-solid reactions at room temperature were reported (Wada, 1961; Rastogi et al., 1977; Toda et al., 1987). During our study on the preparation and properties of organic-layered inorganic solid hybrids, we have found that a solid-solid reaction is an effective way to intercalate various guest species into smectites. In the past two decades, we had reported the applications of solid-solid reactions to prepare intercalation compounds.

In this account, the solid-state intercalation of cationic and nonionic species, complexes, as well as metal sulfide semi-conductor particles in the interlayer spaces of smectites are summarized. The solid-state intercalation of guest species into smectites can be classified into four groups; (a) cation

<sup>\*</sup> Corresponding author: Nithima Khaorapapong, Department of Chemistry and Center of Excellence for Innovation in Chemistry, Faculty of Science, Khon Kaen University, Khon Kaen 40002, Thailand. e-mail: nithima@kku.ac.th

exchange reaction, (b) adsorption of polar molecules, (c) adsorption of organic ligands and *in situ* complexation and (d) formation of metal sulfides. The host-guest systems of the intercalation compounds prepared by solid-solid reactions are summarized in Tables 1, 2 and 3.

## INTERCALATION COMPOUNDS OF SMECTITES PREPARED BY SOLID-SOLID REACTIONS

Preparation of the solid-state intercalation compounds

The solid-state ion exchange reactions were conducted by grinding the dehydrated homoionic (Na(I)-, K(I)- and Rb(I)-) montmorillonite and dried organoammonium halides in an agate mortar under a dried air atmosphere in a glove box for a few minutes (Ogawa et al., 1990a, 1995a). The amounts of the organic salts were equivalent to the cation exchange capacity

of montmorillonite. The conventional ion exchange reaction of the same host-guest systems was also carried out as the references.

The adsorption of nonionic molecules such as acrylamide, methylacrylamide, *p*-aminoazobenzene, maleic and methylmaleic acids, fumaric and methylfumaric acids, naphthalene, anthracene, pyrene and so on was conducted by blending the powders of pristine or organically modified smectites with a mortar and a pestle under dried air atmosphere for a few minutes (Ogawa et al., 1989, 1990b, 1991a, 1992a, b, c, 1993, 1995b, 1996).

Macrocyclic ligand (18-crown-6-ether) was intercalated and formed complexes with the interlayer cations of homoion-ic-montmorillonite, kenyaite and fluortetrasilicic mica (Ogawa et al., 1997). Metal complexes including sodium-, calcium-, manganese-, cobalt-, copper- and/or nickel-diimines (2,2'-

Table 1. Basal spacings of the intercalation compounds of cationic guest species in smectites prepared by solid-state cation exchange reaction

Host	Cationic guest specie	$d_{(001)}$ (nm)	Reference
Na-montmorillonite	methylammonium chloride	1.19	2, 10)
	n-propylammonium chloride	1.31	
	n-hexylammonium chloride	1.31	
	n-octylammonium chloride	0.97*	
	n-decylammonium chloride	0.97*	
	n-dodecylammonium chloride	0.98*	
	n-octadecylammonium chloride	0.98*	
	dimethylammonium chloride	1.28	
	trimethylammonium chloride	1.34	
	tetramethylammonium chloride	1.40	
	tetramethylammonium bromide	1.38	
	tetramethylammonium iodide	_*	
K-montmorillonite	tetramethylammonium chloride	1.40	
	tetramethylammonium bromide	1.34	
	tetramethylammonium iodide	_*	
Rb-montmorillonite	tetramethylammonium chloride	1.39	
No monumormonic	tetramethylammonium bromide	1.37	
	tetramethylammonium iodide	_*	
Na-montmorillonite	tetraethylammonium bromide	1.40	
	tetrapropylammonium bromide	1.40	
	tetrabuthylammonium chloride	1.77	
	tetrabuthylammonium bromide	1.88***	
	tetrabuthylammonium iodide	_*	
K-montmorillonite	tetrabuthylammonium chloride	1.77	
	tetrabuthylammonium bromide	_*	
	tetrabuthylammonium iodide	_*	
Rb-montmorillonite	tetrabuthylammonium chloride	_*	
	tetrabuthylammonium bromide	_*	
	tetrabuthylammonium iodide	_*	
Na-montmorillonite	octyltrimethylammonium chloride	1.38	
	dodecyltrimethylammonium chloride	1.36	
	tetradecyltrimethylammonium chloride	0.96*	
	ethylenediammonium dichloride	1.20**	
	o-phenylenediammonium dichloride	1.37**	
	<i>m</i> -phenylenediammonium dichloride	1.32**	
	<i>p</i> -phenylenediammonium dichloride	1.26**	
	anilinium chloride	1.45	

<sup>\*</sup> No evidence of intercalation

Reference: Ogawa et al., 1990a<sup>2)</sup>, 1995a<sup>10)</sup>

<sup>\*\*</sup> Obtained after grinding for 30 min

<sup>\*\*\*</sup> Obtained after the reaction at 80°C for 1 day

Table 2. Basal spacings of the intercalation compounds prepared by solid-state adsorption of neutral molecules

Host	Neutral guest specie	$d_{(001)}$ (nm)	Reference
Na-montmorillonite	acrylamine	1.91	1)
	methylacrylamine	1.47	
	urea	1.71	
Ca-montmorillonite	urea	1.71	
Cu-montmorillonite	urea	1.68	
Na-montmorillonite/Kunipia	acrylamide	1.90 or 1.91	1, 7)
Na-montmorillonite/Gelwhite	acrylamide	1.90	
Na-saponite	acrylamide	2.00	
Na-hectorite	acrylamide	2.00	
Na-fluortetrasilicic mica	acrylamide	1.90	
Ca-fluortetrasilicic mica	acrylamide	1.90	
K-fluortetrasilicic mica	acrylamide	1.00*	
Al-fluortetrasilicic mica	acrylamide	_*	
Na-montmorillonite	n-tetradecylamine	4.80	3)
	n-hexadecylamine	5.10	
	n-octadecylamine	5.70	
Ca-montmorillonite	n-tetradecylamine	4.50	
	n-hexadecylamine	4.90	
Na-montmorillonite	n-octadecylamine	5.40	4)
	p-aminoazobenzene	1.90	4)
Ca-montmorillonite	<i>p</i> -aminoazobenzene	1.80	
Ni-montmorillonite	p-aminoazobenzene	2.00	0
Na-montmorillonite	maleic acid fumaric acid	1.25	6)
	methylmaleic acid	1.27	
	methylfumaric acid	_*	
DTMA-montmorillonite	naphthalene	3.00	8)
ODTMA-montmorillonite	naphthalene	3.50	,
DTMA-montmorillonite	anthracene	3.40, 1.80	
TDTMA-montmorillonite	anthracene	3.45, 1.89	
HDTMA-montmorillonite	anthracene	3.50, 2.00	
ODTMA-montmorillonite	anthracene	3.60 or 3.70	8, 9)
DMDODA-montmorillonite	anthracene	3.80	9)
ODTMA-montmorillonite	pyrene	3.60	- /
DMDODA-montmorillonite	pyrene	3.90	
ODTMA-saponite	pyrene	1.50	11)
DMDODA-saponite	pyrene	2.20	11)
ODTMA-fluortetrasilicic mica	pyrene	2.20	
DMDODA-fluortetrasilicic mica	**	2.20	
DA-montmorillonite	pyrene p aminoszobanzana	1.80-3.00	4)
DTMA-fluortetrasilicic mica	p-aminoazobenzene		4)
DIMA-nuortetrasilicic mica  DMEHA-fluortetrasilicic mica	p-aminoazobenzene	2.20	12)
	p-aminoazobenzene	3.30	
DMBHA-fluortetrasilicic mica	p-aminoazobenzene	3.40	
DA-fluortetrasilicic mica	p-dimethylaminoazobenzene	2.40	
DTMA-fluortetrasilicic mica	p-dimethylaminoazobenzene	2.30	
DMEHA-fluortetrasilicic mica	p-dimethylaminoazobenzene	3.40	
DMBHA-fluortetrasilicic mica	p-dimethylaminoazobenzene	3.50	

 $* No \ evidence \ of \ intercalation \\ Reference: Ogawa \ et \ al., \ 1989^{1)}, \ 1990b^{3)}, \ 1991a^{4)}, \ 1992a^{6)}, \ 1992b^{7)}, \ 1992c^{8)}, \ 1993^{9)}, \ 1995b^{11)}, \ 1996^{12)}, \ 1997^{13)}$ 

#### Abbreviation for Table 2

DA	Dodecylammonium (C <sub>12</sub> H <sub>25</sub> NH <sub>3</sub> <sup>+</sup> )
DDAM	Dodecyldimethylethylammonium (C <sub>12</sub> H <sub>25</sub> (CH <sub>3</sub> ) <sub>2</sub> C <sub>2</sub> H <sub>5</sub> N <sup>+</sup> )
DTMA	Dodecyltrimethylammonium (C <sub>12</sub> H <sub>25</sub> (CH <sub>3</sub> ) <sub>3</sub> N <sup>+</sup> )
TDTMA	Tetradecyltrimethylammonium (C <sub>14</sub> H <sub>29</sub> (CH <sub>3</sub> ) <sub>3</sub> N <sup>+</sup> )
HDTMA	Hexadecyltrimetylammonium (C <sub>16</sub> H <sub>33</sub> (CH <sub>3</sub> ) <sub>3</sub> N <sup>+</sup> )
ODTMA	Octadecyltrimetylammonium (C <sub>18</sub> H <sub>37</sub> (CH <sub>3</sub> ) <sub>3</sub> N <sup>+</sup> )
DMDODA	Dimethyldioctadecylammonium $((C_{18}H_{37})_2(CH_3)_2N^+)$
DMEHA	Dimethylethylhexadecylammonium (C <sub>16</sub> H <sub>33</sub> (CH <sub>3</sub> ) <sub>2</sub> C <sub>2</sub> H <sub>5</sub> N <sup>+</sup> )
DMBHA	Dimethylbenzylhexadecylammonium (C <sub>16</sub> H <sub>33</sub> (CH <sub>3</sub> ) <sub>2</sub> C <sub>6</sub> H <sub>6</sub> CH <sub>2</sub> N <sup>+</sup> )

Table 3. Basal spacings of the intercalation compounds prepared by solid-state adsorption and in situ formation

Host	Neutral guest specie	$d_{(001)}$ (nm)	Referenc
K-montmorillonite 18-crown-6-ether		1.95	13)
Rb-montmorillonite	18-crown-6-ether	1.93	
NH <sub>4</sub> -montmorillonite	18-crown-6-ether	1.92	
K-fluortetrasilicic mica	18-crown-6-ether	1.92	
K-kenyaite	18-crown-6-ether	3.04	
Co-montmorillonite	2,2'-bipyridine	1.81	5)
Na-montmorillonite	2,2'-bipyridine	no report of $d_{001}$	
Ca-montmorillonite	2,2'-bipyridine	no report of $d_{001}$	
Mn-montmorillonite	2,2'-bipyridine	no report of $d_{001}$	
Co-montmorillonite	4,4'-bipyridine	1.50	17, 18)
	1,2-di(4-pyridine)ethylene	1.50	
Cu-montmorillonite	4,4'-bipyridine	1.50	
	1,2-di(4-pyridine)ethylene	1.50	
Ni-montmorillonite	4,4'-bipyridine	1.50	
	1,2-di(4-pyridine)ethylene	1.50	
Cd-montmorillonite	thioacetamide	1.50, 1.75	19)
Cu-montmorillonite	thiourea	1.70	20)
Al-montmorillonite	8-hydroxyquinoline	1.70	21)
Al-saponite	8-hydroxyquinoline	1.50	
Li-montmorillonite	8-hydroxyquinoline	1.66	14, 16)
Li- saponite	8-hydroxyquinoline	1.66	16)
Mn-montmorillonite	8-hydroxyquinoline	1.66	
Zn-montmorillonite	8-hydroxyquinoline	1.65	14, 15)
Zn-saponite	8-hydroxyquinoline	1.35	
Cd-montmorillonite	sodium sulfide	1.24	23, 25)
Mn-montmorillonite	sodium sulfide	1.23	22, 24)
Ni-montmorillonite	sodium sulfide	1.23	24)
Zn-montmorillonite	sodium sulfide	1.23	25)
Co-montmorillonite	sodium sulfide	1.15	26)
Cu-montmorillonite	sodium sulfide	1.19	26)

 $Reference:\ Ogawa\ et\ al.,\ 1991b^{5)};\ Khaorapapong,\ 2010^{20)};\ Khaorapapong\ and\ Ogawa,\ 2007^{14)},\ 2008^{15)},\ 2010^{16)};\ Khaorapapong\ et\ al.,\ 2000^{17)},\ 2001^{18)},\ 2002a^{19)},\ 2002b^{21)},\ 2008a^{22)},\ 2008b^{23)},\ 2009^{24)},\ 2010a^{25)},\ 2010b^{26)}$ 

bipyridine, 4,4'-bipyridine and 1,2-di(4-pyridine)ethylene) (Ogawa et al., 1991b; Khaorapapong et al., 2000, 2001), cadmium-thioacetamide (Khaorapapong et al., 2002a), copperthiourea (Khaorapapong, 2010), as well as lithium-, aluminium-, zinc- and manganese-8-hydroxyquinoline (Khaorapapong and Ogawa, 2007, 2008, 2010; Khaorapapong et al., 2002b) were intercalated in smectites by adsorption of the organic ligands and *in situ* complexation between homoionic interlayer cations (Na(I), Ca(II), Co(II), Cu(II), Ni(II), Cd(II), Li(I), Al(III), Zn(II) and Mn(II)), and the ligands in the interlayer spaces. Metal complexes were formed in the interlayer spaces after the host and guest substances were mixed in an agate mortar for 10–15 min in air at room temperature.

The interactions of sulfide ions with the interlayer cations of smectite via adsorption and *in situ* formation led to smectite-metal sulfide hybrids (Khaorapapong et al., 2008a, b, 2009, 2010, 2011). Adsorption and *in situ* formation processes of metal sulfides in smectite were conducted by grinding the cation exchanged smectites with sodium sulfide in an agate mortar. Metal sulfides were obtained after the solid-solid reactions for 10–15 min and subsequent heat treatment at 200°C in air.

Characterization of the products

The intercalation of the guest species was confirmed by X-ray diffraction (XRD), thermal and thermogravimetric-mass spectroscopy analyses, elemental analysis (CHN), infrared spectroscopy and transmission electron microscopy. The formations of the complexes and/or metal sulfides into smectites were indicated by infrared, Raman, UV-visible and photoluminescence spectroscopies.

## ORGANOAMMONIUM-SMECTITE INTERCALATION COMPOUNDS

The organoammonium-smectites have been recognized and used in a wide variety of applications such as hosts of polymers and adsorbents (Ogawa and Kuroda, 1997). When the interlayer metal cations of smectites are replaced by cationic surfactants, the hydrophilic surfaces of the silicate layers are substantially modified to become strongly organophillic called organophillic clay or organoclay. The combination of the hydrophobic nature of surfactant and the stable layered structures of the silicate layers led to unique physicochemical properties. Although, most of the organophillic clays were investigated via a famous cation exchange method,

organoammonium-montmorillonites prepared by solid-solid reactions were also reported so far. The intercalation compounds were carried out by grinding powders of the reactants (montmorillonite and alkylammonium salts) together for a few minutes. The basal spacings of the products are listed in Table 1 (Ogawa et al., 1990a, 1995a). The results showed that the n-alkylammonium ions (from C1 to C10) were intercalated while the larger ions could not be intercalated in the interlayer spaces, suggesting that steric hindrance inhibited the solidstate ion exchange reactions. Generally, the intercalation compounds of organoammonium-smectites show the basal spacings in the range of ca. 1.4 to 2.2 nm (Lagaly, 1981). It is well known that the arrangements of the intercalated alkylammonium ions depend on the layer charge and the alkyl chain length. In the interlayer spaces of smectites, short chain alkylammonium ions are arranged in monolayer (ca. 1.4 nm) and long chain alkylammonium ions in bilayers (ca. 1.8 nm) with their alkyl chains parallel to the silicate layers. The transition from monolayer to bilayer arrangement can be occurred with increasing the alkyl chain length.

In the highly charged smectites, the intercalated alkylammonium ions, which exhibit a basal spacing of ca. 2.2 nm, are arranged in kinked alkyl chain layer and referred to as *pseudo*-trimolecular layers. For the products with the basal spacing larger than 2.2 nm, the alkylammonium ions form the monolayer or bilayer paraffin type arrangements in the interlayer spaces of some layered materials with higher layer charge density compared with those smectites (Ogawa and Kuroda, 1997).

Further study of the influence of the type of alkylammonium halides on the solid-state ion exchange reactions, the secondary (dimethyl), tertiary (trimethyl) and quaternary (tetramethyl) ammonium chlorides were used as the guest species. The basal spacings of the products (Table 1) (Ogawa et al., 1990a, 1995a) were consistent with those obtained by normal ion exchange methods using aqueous solutions of the organoammonium salts. The basal spacings of the products (ca. 1.2–1.4 nm) indicated that the alkylammonium ions were lying flat in between the silicate layers.

The effects of the counter anions and the interlayer cations on the reactivity were investigated by using the various quaternary ammonium salts (tetramethyl, tetraethyl, tetrapropyl, as well as tetrabutylammonium chlorides, bromides and iodides) as the guest species and sodium- potassiumand rubidium-montmorillonites as the host materials. When tetramethylammonium chloride and bromide were used, the intercalation was easily completed after grinding for a few minutes. The expansion of the interlayer spaces and the appearance of sodium chloride and bromide were also observed in the XRD patterns of the products (Table 1). On the other hand, when tetramethylammonium iodide was used, the intercalation was not observed even after grinding for 30 min. The solid-solid reaction between sodium- or potassiummontmorillonite and tetrabutylammonium chloride showed the increase in the basal spacing of to be ca. 1.8 nm (Table 1). In tetrabutylammonium bromide and sodium-montmorillonite system, the intercalation was observed after the reaction at 80°C under reduced pressure for 1 day. No reaction was observed for other systems even after the heat treatment. The

results suggested that counter anions and the interlayer cations had a certain effect for the solid-state ion exchange reactions probably due to thermodynamics.

Other types of organoammonium ions including diammoniums were also used as the guests. The solid-solid reactions between ethylenediammonium dichloride, o-phenylenediammonium dichloride, m-phenylenediammonium dichloride or p-phenylenediammonium dichloride and sodium montmorillonite led to the intercalation compounds. Besides the aliphatic ammonium ions, anilinium halides were also intercalated into montmorillonite. The basal spacings increased to 1.45 nm after grinding for 2 min by the solid-solid reaction of sodiummontmorillonite and anilinium chloride. The anilinium ions were intercalated as a monomolecular layer with the aromatic planes of anilinium ions perpendicular to the silicate layers. The formation of the intercalation compounds depended on sizes and types of counter anions used. The behavior observed in the solid-solid reactions was different from that in a conventional solution method. The preparation of aniliniummontmorillonites by solid-solid reactions was also reported by other group (Yoshimoto et al., 2005). The intercalation compounds obtained between montmorillonite and anilinium salts with different counter anions were investigated. The amounts of intercalated species depended on the types of counter anions and increased with decreasing the size of counter anions. Although, Vicente et al., reported that adsorbed water might be involved in solid-solid reaction (Vicente et al., 1989), our results showed that the water molecule was not essential (Ogawa et al., 1990a, 1995a).

## ADSORPTION OF ORGANIC MOLECULES IN SMECTITES

Adsorption on smectites

Normally, the exchangeable interlayer cations in smectites are inorganic ions such as sodium and calcium ions. The cations are strongly hydrated in the presence of water and the ion-dipole interactions inhibit the adsorption of poorly water soluble molecules such as organic molecules. Besides the conventional method, solid-solid reaction, which accessibly reacts without solution, is an easy way to intercalate nonionic molecules in the interlayer spaces under normal or restrictive condition. The molecular structures of some nonionic guests using in our works are shown in Tables 4 and 5. The adsorption of acrylamide on the surface of the dehydrated montmorillonites by solid-solid reaction was investigated so far (Ogawa et al., 1989, 1992b). The formation of the intercalation compounds was confirmed by the increase in the basal spacings of the products. The basal spacing of acrylamide-montmorillonites (ca. 1.9 nm) was close to that of the product prepared by treating montmorillonite with acrylamide in aqueous solution (2.0 nm). Judging from the observed basal spacings of the products and the estimated size of the acrylamide molecule (0.7  $\times$  0.6  $\times$ 3.7 nm), it was postulated that the intercalated acrylamide was arranged in bilayers with their molecular plane inclined to the silicate layers. Other types of smectites such as saponite and hectorite were also used as the host materials for acrylamide and their basal spacings are listed in Table 2.

Intercalation of methylacrylamide and urea into sodium-

Table 4. The molecular structures of some nonionic guest species for solid-state adsorption

sond-state adsorption	
Guest	Molecular structure
Acrylamide	o 
	NH <sub>2</sub>
Methylacrylamide	,0
	HN——
	/ \
Urea	
	NH <sub>2</sub>
. Total de evilencia e	$H_2N$
n-Tetradecylamine	\
H <sub>2</sub> N	
Maleic acid	о ОН О
	O—On
Fumaric acid	O II
	НО
	ОН
Madestratainesid	Ö
Methylmaleic acid	HO O
Methylfumaric acid	ОН
Methynumanic acid	
	НО
p-Aminoazobenzene	
	N NH2
	, , , , , , , , , , , , , , , , , , ,
p-Dimethylaminoazobenzene	
	N N
Naphthalene	
Anthracene	
D.	
Pyrene	
	<b>~ ~</b>

Table 5. The molecular structures of the organic ligands for solid-solid reaction and *in situ* complex formation

Guest	Molecular structure
18-Crown-6 ether	
2,2'-Bipyridine	N
4,4'-Bipyridine	N
1,2-Di(4-pyridine)ethylene	N N
Thioacetamide	H <sub>2</sub> N S
Thiourea	$H_2N$ $H_2N$
8-Hydroxyquinoline	OH

montmorillonite was also obtained by the solid-solid reactions. The basal spacings of methylacrylamide- and ureamontmorillonites were 1.47 and 1.71 nm, respectively. The intercalation compounds of urea with calcium- and copper(II)-montmorillonites gave the basal spacings of 1.71 and 1.68 nm. The solid-state intercalations of acrylamide, methylacrylamide and urea molecules were thought to be caused by the migration of the solid-solid interface and diffusion of acrylamide at the surface of montmorillonite particle to be intercalated in the interlayer spaces of montmorillonite, being the same as the solid-solid reactions of organic molecules (Rastogi et al., 1977; Toda et al., 1987).

In order to apply solid-state intercalation for large polar molecules, the intercalation of the long chain n-alkylamines (n-tetradecylamine, n-hexadecylamine and n-octadecylamine) into sodium and calcium montmorillonites (Ogawa et al., 1990b) was studied. The basal spacings of the products were ca. 4.8, 5.1 and 5.7 nm for n-tetradecylamine, n-hexadecylamine and n-octadecylamine in sodium montmorillonite, and at ca. 4.5, 4.9 and 5.4 nm for calcium montmorillonite. Alkylamines have widely been used as the guest species in intercalation chemistry and their arrangements in the interlayer

spaces of clay minerals were reported (Brindley, 1965; Lagaly, 1986; Sutherland and MacEwan, 1961; Aragon et al., 1959; Patil et al., 1984; Vicente et al., 1989). The basal spacings of the intercalation compounds prepared by the solid-solid reactions were consistent with those previously reported.

p-Aminoazobenzene was immobilized in the interlayer spaces of sodium-, calcium- and nickel(II)-montmorillonites by solid-solid reactions at room temperature (Ogawa et al., 1991a). The basal spacings were ca. 1.9, 1.8 and 2.0 for sodium-, calcium- and nickel(II)-montmorillonites. Photochemical behavior of azobenzene incorporated in homoionic montmorillonite was studied.

Another example of the solid-solid reactions is the intercalation of maleic and methylmaleic acids in the interlayer spaces of montmorillonite. After grinding the reactants for a few minutes, the maleic acid-montmorillonite showed the  $d_{001}$ diffraction peak at 1.25 nm. The basal spacing did not change after the heat treatment at 100°C, supporting the intercalation of maleic acid. A more intriguing result was the different reactivity between cis- and trans-isomers. In contrast to the solidsolid reaction of maleic acid in the interlayer space of sodiummontmorillonite, fumaric acid (trans-isomer of maleic acid) was not intercalated. On the contrary, both of them (maleic and fumaric acids) were intercalated into sodium-montmorillonite by conventional reaction from ethanolic solutions. Moreover, an intercalation compound of methylmaleic acidsodium-montmorillonite formed with the basal spacing of 1.27 nm, while methylfumaric acid (trans-isomer of methylmaleic acid) was not intercalated into sodium-montmorillonite. Their difference was caused by the crystal structures of the guests and the ability of cis-isomer geometries to form a chelate like structure with the interlayer exchangeable cations were concerned for the novel selectivity in the solid-state.

Adsorption of ionically neutral molecules into organically modified smectites

Smectites with metal cations in the interlayer spaces are hydrophilic and are often not a good adsorbent for poorly water soluble organic species, which do not compete with highly polar water for adsorption on the clay mineral surfaces. However, when the interlayer metal cations are replaced by organoammonium cations, the surface can be modified to be organophilic. The organically modified clays including alkylammonium montmorillonites have been studied widely as adsorbates, chromatographic stationary-phase, catalysts, rheology controlling agent and so on (Ogawa and Kuroda, 1997). Alkylammonium montmorillonites prepared by a conventional ion exchange reaction have been used as the host materials of nonionic species (Ogawa et al., 1991a, 1992a, b, c, 1993, 1995b, 1996). The immobilization of some neutral molecules such as photoactive species in the interlayer spaces of the alkylammonium montmorillonites was investigated and unique behaviors of the intercalated species were found.

Naphthalene-alkyltrimethylammonium  $(C_nH_{2n+1}(CH_3)N^+; n=8, 12, 14, 16 \text{ and } 18)$ -montmorillonites were obtained by solid-solid reactions at room temperature (Ogawa et al., 1992c). These reactions were completed within 10 min, showing that the mobility of the organic species was very high even in the solid-state. Octyltrimethylammonium (OTMA, C8)-

montmorillonite did not form the intercalation compound with naphthalene. While both dodecyltrimehylammonium (DTMA, C12)- and octadecyltrimethylammonium (ODTMA, C18)-montmorillonites gave the intercalation compounds with the basal spacings of 3.0 and 3.5 nm, respectively. Since the basal spacings of the original alkyltrimethylammoniummontmorillonites were different (1.8 nm for DTMA-montmorillonite and 2.3 nm for ODTMA-montmorillonite), the similarity in the expansion of the basal spacings indicated that the intercalated naphthalene was sandwiched by the alkyl chains of the alkyltrimethylammonium ions and closely packed in the interlayer spaces. The alkyl chain length of alkyltrimethylammonium ions affected the reactivity, supporting that the hydrophobic interactions between alkyltrimethylammoniummontmorillonites and aromatic compounds were the driving force for the solid-state intercalation.

The solid-state intercalation of azo-dyes, p-aminoazobenzene (p-AZ) and p-dimethylaminoazobenzene (p-MZ), into organoammonium montmorillonite and swelling fluortetrasilicic micas (TSMs) was conducted (Ogawa et al., 1991a, 1996). The basal spacings of the products are listed in Table 2. Photoisomerization of p-AZ in organoammonium montmorillonite and TSMs were investigated as follows; the products were embedded in poly(vinyl alcohol) film and the UV-visible absorption spectra of the films were recorded before and after the irradiation. In comparison with the absorption spectrum observed for a dilute benzene solution of trans-p-AZ (377 nm), the bands of p-AZ in organoammonium TSMs were redshifted, showing the partial aggregation, and/or the effects of the polarity and rigidity of p-AZ surroundings. The intercalated p-AZ showed reversible cis-trans photoisomerization upon UV irradiation and subsequent thermal treatment.

Intercalation of two arenes molecules, anthracene and pyrene, into alkylammonium-montmorillonites (ODTMA,  $C_{18}3C_1N^+$  and dimethyldioctadecylammonium,  $2C_{18}2C_1N^+$ , DMDODA types) was investigated by solid-solid reactions (Ogawa et al., 1992c, 1993). Anthracene-ODTMAmontmorillonite intercalation compounds showed the similar basal spacings for the ratios of host:guest were 1:1 and 1:2, indicating that the amount of anthracene intercalated into the ODTMA-montmorillonite was limited. In comparison with the reactions between alkylammonium-montmorillonites and naphthalene, the different reactivities of anthracene resulted from the variable hydrophobicity of the interlayer spaces of the alkylammonium-montmorillonites. Because of the bulkiness and more hydrophobic nature of anthracene compared to those of naphthalene, the anthracene intercalation was thought to require more hydrophobic host material.

The XRD patterns of the arene-alkylammonium-montmorillonite intercalation compounds showed the two different types of the adsorption of arene molecules. The arenes in the ODTMA-montmorillonite were aggregated and those in the DMDODA-montmorillonite were rather dispersed between the alkyl chains in the interlayer space. In the ODTMA-montmorillonite, the observed basal spacings showed that the alkylammonium ions were arranged as *pseudo*-trimolecular layers with their alkyl chains parallel to the silicate layers. For the DMDADA-montmorillonite, two types of arrangements were expected; one was monomolecular coverage with their

alkyl chains inclined to the silicate layers at ca. 53 degree and the other was bimolecular coverage with their alkyl chains inclined to the silicate layers at ca. 23 degree. The hydrophobic interactions between the guest species and the interlayer alkylammonium ions were the driving force for the solid-solid reactions.

Fluorescence spectra of the intercalated pyrene revealed an emission of monomer (at 400 nm) together with the broad band due to excimer (at 500 nm). The ratio of monomer to excimer emission intensity for the DMDADA-montmorillonite system was three times higher than that for the ODTMAmontmorillonite system, indicating that the intercalated pyrene molecules were isolated in the interlayer space of DMDADAmontmorillonite compared with those of the adsorbed pyrenes in ODTMA-montmorillonite. The intercalation behavior of arenes was different depending on a kind of the alkylammonium-montmorillonites that acted as organizing media with other adsorption states. The two organically modified montmorillonites not only showed different reactivity in the intercalation of the arene molecules but also provided different adsorption states (Ogawa et al., 1995b). Similar results were observed when fluortetrasilicic mica was used as the host substance. The basal spacing and the amount of the adsorbed organoammonium cations of the ODTMA- and DMDADA-TSMs were similar to those of the corresponding organoammonium-montmorillonites, indicating similar arrangements of the intercalated alkylammonium ions in the interlayer spaces. The changes of the XRD patterns for the reactions of the two organoammonium-TSMs with anthracene or pyrene were also similar to those observed for the montmorillonite systems.

Because of the lower layer charge density of synthetic saponite (CEC of 70 meg/100 g clay) compared with that of montmorillonite, the saponite was used as a host material in order to elucidate the difference of the adsorption states. The DMDADA-saponite showed the smaller basal spacing of 2.2 nm, indicating that the intercalated DMDADA ions arranged as a *pseudo*-trimolecular layer in the interlayer space of saponite similar to that observed for the ODTMA-montmorillonite. When pyrene was intercalated in the interlayer space of the DMDADA-saponite, the change in the fluorescence spectra as a function of the loaded amount was also similar to that observed for the ODTMA-montmorillonite system. The fluorescence spectrum showed the tendency of pyrene molecules to form excimer (or dimer) similar to those for the ODTMAmontmorillonite and TSM systems. On the other hand, the ratio of monomer to excimer intensity for the pyrene-DMDADA-TSM intercalation compound was two times higher than that for the ODTMA-TSM system.

The observations revealed that the arrangements of the intercalated alkylammonium ions are an important factor for the difference in the adsorption states of the guest species. When the interlayer alkylammonium ions arranged with the alkyl chain parallel to the silicate layers, the intercalated pyrene molecules tended to aggregate. On the other hand, the pyrene molecules dispersed effectively when the intercalated alkylammonium ions arranged as a paraffin type. All these results suggested that a wide variety of reaction environments can be created by selecting the hosts with different layer charge densities and guests with various sizes.

The photoluminescence results indicated that the intercalated pyrene molecules were separated molecularly by alkyl chains, and their motion was largely restricted. The nature of crystalline structure of the host materials played a role to isolate probe molecules effectively at such high concentration. To our knowledge, the incorporation of guest species in surfactant molecules with retaining an ordered structure is very difficult. Since the high concentration of photoactive centers is a merit for the application of such types of composite materials and their structural regularity, as well as the stability, the assembly of surfactant molecules formed in the layered materials is an important medium from both practical and scientific studies.

## IN SITU COMPLEXATION BY ADSORPTION OF ORGANIC LIGANDS

The immobilization of metal complexes in the constrained environment makes it possible to conduct reactions in the solid-state like in solutions and to minimize various technical limitations, which intrinsic in the homogenous system (Ogawa and Kuroda, 1995, 1997). Layered clay minerals possess the potential modifications of the selectivity and activity of the supported metal complexes. In some cases, the intercalation compounds of metal complex-clay minerals provide the unique selective property of a catalyst system or the unusual physicochemical properties of metal complexes. The ordered structure of smectites has played an important role in the synthetic design of heterogeneous catalysts and so on. The intercalation compounds of metal-2,2'-bipyridine-smectites have been studied and applied as catalysts and clay-modified electrodes (Pinnavaia, 1983). Solid-solid reaction is one of the effective methods to immobilize metal complexes in the interlayer spaces of smectites. When the interlayer sodium ions of pristine smectites are substituted by other metal cations, the charge transfer between the interlayer metal ions and organic ligands can be a driving force for the intercalation.

A typical property of macrocyclic polyethers such as 18-crown-6, benzo-12-crown-4, didenzo-18-crown-6 is the ability to form stable complexes with alkali, alkaline earth and transition metal ions. Intercalation compounds of macrocyclic polyether ligands may provide the useful applications for solid-electrolytes and ion selective membrane (Ruiz-Hitzky and Casal, 1978; Ruiz-Hitzky and Aranda, 1990; Ruiz-Hitzky et al., 1995). The intercalation compounds with the basal spacing of ca. 1.9 nm were obtained by solid-solid reactions between of 18-crown-6-ether and potassium-, rubidium- as well as ammonium-montmorillonites (Ogawa et al., 1996). The solid-solid reactions possessed the intercalation compounds with the basal spacings different from those prepared by a conventional method. The interactions between the interlayer cations and the ligands played an indispensable role for the reactions. The expansions of the interlayer spaces (ca. 1.0 nm) suggested that the intercalated 18-crown-6-ether molecules formed bilayers in the interlayer spaces with the molecular planes parallel to the silicate layers or monolayer with the molecular planes inclined to the silicate layers. Larger basal spacings observed for the products prepared by solidsolid reactions suggested that the greater amount of 18-crown-6-ether was intercalated in the interlayer spaces. Because the

arrangements of the guest species in the interlayer spaces are very important to determine the properties of the intercalation compounds, the present observation that the different reaction procedures led to the difference in the microstructures of intercalation compounds is worth mentioning.

2,2'-Bipyridine (abbreviated as bpy) was intercalated into montmorillonite (Ogawa et al., 1991b). The yellowish brown product, Co(bpy)3-montmorillonite, was obtained by solidsolid reactions between cobalt(II)-montmorillonite dried at 120°C under vacuum or air dried cobalt(II)-montmorillonite, and 2,2'-bipyridine at room temperature for a few minutes. The basal spacings of both hybrids were 1.81 nm, corresponding to the expansion of the interlayer spaces by 0.85 nm. The result indicated that the complex was arranged as a monolayer with the 3-fold axis of the complex perpendicular to the silicate layers (Fig. 1a). The product obtained by conventional ion exchange reaction of an aqueous dispersion montmorillonite and an aqueous solution of [Co(bpy)<sub>3</sub>]Cl<sub>3</sub> was also 1.81 nm, supporting that the intercalated 2,2'-bipyridine formed [Co(bpy)<sub>3</sub>]<sup>2+</sup> during the solid-solid reaction. The UVvisible diffuse reflectance spectrum of the product prepared by solid-solid reaction was identical to that of the product obtained by conventional ion exchange reaction. The IR spectrum also indicated that the intercalated 2,2'-bipyridine formed [Co(bpy)<sub>3</sub>]<sup>2+</sup> in montmorillonite. 2,2'-Bipyridine was also intercalated into sodium-, calcium- and magnesiummontmorillonites by solid-solid reactions and in situ complex-

Other diimines, 4,4'-bipyridine and 1,2-di(4-pyridine) ethylene were intercalated into the interlayer spaces of cobalt(II)-, nickel(II)- and copper(II)-montmorillonites by solid-solid reactions (Khaorapapong et al., 2000, 2001). 4,4'-Bipyridine and 1,2-di(4-pyridine)ethylene are the excellent bridging ligands, and so far a number of one-, two- and threedimensional frameworks of metal complexes of the ligands have already been generated (Slone et al., 1996; Hagrman et al., 1998a, b; Tong et al., 1999). The intercalation of 4,4'bipyridine and 1,2-di(4-pyridine)ethylene into montmorillonites was expected to exhibit novel structures and properties such as molecular recognitions and so on. Homoionic (Co(II)-, Ni(II)- and Cu(II)-) montmorillonites were prepared by conventional ion exchange reactions and subsequently reacted with 4.4'-bipyridine (or 1,2-di(4-pyridine)ethylene) by solid-solid reactions. The basal spacings of all products were 1.5 nm. The increase in the basal spacings was caused by the intercalation of 4,4'-bipyridine and 1,2-di(4-pyridine)ethylene through ligand displacement reactions between water and diimine molecules. The intercalated diimines formed complex cations with the formula of  $[M^{II}L_2]_n$  type coordination polymers in the interlayer spaces of montmorillonites (Fig. 1b), where M and L represented metal and ligand (4,4'-bipyridine and 1,2-di(4-pyridine)ethylene), respectively. Although the introduction of pre-synthesized coordination polymers in the interlayer spaces of layered solids is very difficult due to the low solubility of coordination polymers, the solid-state intercalation and in-situ complexation are an effective way to prepare planar coordination polymer-layered silicate hybrid

Intercalation of thioacetamide and thiourea molecules in

the interlayer spaces of Cd(II)- and Cu(II)-montmorillonites was also conducted by solid-solid reactions at room temperature (Khaorapapong, 2010; Khaorapapong et al., 2002a). One of the objects of the use of thioacetoamide and thiourea was a possible application as a precursor of metal sulfides. The intercalated thioacetamide with the basal spacing of 1.50 nm (Cd(II):thioacetamide = 1:3) formed a monolayer in the interlayer space and that of 1.75 nm (Cd(II):thioacetamide = 1:6) suggested that the intercalated thioacetamide formed a bilayer arrangement. The observed basal spacings decreased gradually to ca. 1.3 nm when the products were stored in air at room temperature for several months. Moreover, the reflections of thioacetamide crystal as well as those of cadmium sulfide particles were observed. The formation of cadmium sulfide was also confirmed by the change in the color of the products from white to yellow and the appearance of the UV-visible absorption bands owing to cadmium sulfide. The absorbance of the infrared bands due to thioacetamide and the organic contents of the products were reduced, indicating that thioacetamide molecules were partly decomposed to give cadmium sulfide, and the decomposition accompanied the deintercalation and sublimation of thioacetamide from the interlayer space of montmorillonite. Interestingly, thiourea reduced the interlayer copper(II) ion to copper(I) and was oxidized to formamimide disulfide in the interlayer space. The remained thiourea molecules formed copper(I) thioureamontmorillonite, which was the ESR silent. The intercalation compound showed the basal spacing of ca. 1.70 nm. The Raman bands at 221 and 249 cm<sup>-1</sup> indicated the formation of the four-coordinate copper, [Cu<sup>I</sup>(thiourea)<sub>4</sub>]<sup>+</sup>, and threecoordinate copper, [Cu<sup>I</sup>(thiourea)<sub>3</sub>]<sup>+</sup>, as the major and minor products in the interlayer space of montmorillonite.

The complexes studied widely for organic light emitting diodes (OLEDs) (Chen and Shi, 1998; Schmitz et al., 2000), including tris(8-hydroxyquinoline)aluminium(III) (abbreviated as Alq<sub>3</sub>), bis(8-hydroxyquinoline)zinc(II) (abbreviated as Znq<sub>2</sub>), bis(8-hydroxyquinoline)manganese(II) (abbreviated as Mng<sub>2</sub>), and mono(8-hydroxyquinoline)lithium(I) (abbreviated as Liq) complexes, were incorporated in the interlayer spaces of smectites by solid-solid reactions between homoionic (Al(III)-, Zn(II)-, Mn(II)- and Li(I)-) smectites and 8-hydroxyquinoline (8hq) at room temperature (Khaorapapong and Ogawa, 2007, 2008, 2010; Khaorapapong et al., 2002b). The intercalated Alq, complex took monolayer arrangement or the 8-hydroxyquinoline molecules formed bilayer arrangement in the interlayer spaces. Considering the expansions of the interlayer spaces (ca. 0.70 nm) of the Znq<sub>2</sub>-, Mnq<sub>2</sub>- and Liqmontmorillonites, as well as the molecular size and geometry of 8-hydroxyquinoline molecules, the hydrated complexes formed in montmorillonite and anhydrous Znq<sub>2</sub> complex in synthetic saponite. Since the expansion of the interlayer space of Liq-saponite (ca. 0.40 nm) was smaller than that observed for Liq-montmorillonite (ca. 0.70 nm), the coordinated 8Hq of Liq in saponite and montmorillonite formed a monolayer arrangement with the different molecular packing in the interlayer spaces due to the different in CEC of the two clay minerals.

The luminescence intensity of the Alq<sub>3</sub> (Fig. 2) and Znq<sub>2</sub> complexes in synthetic saponite was much higher than those

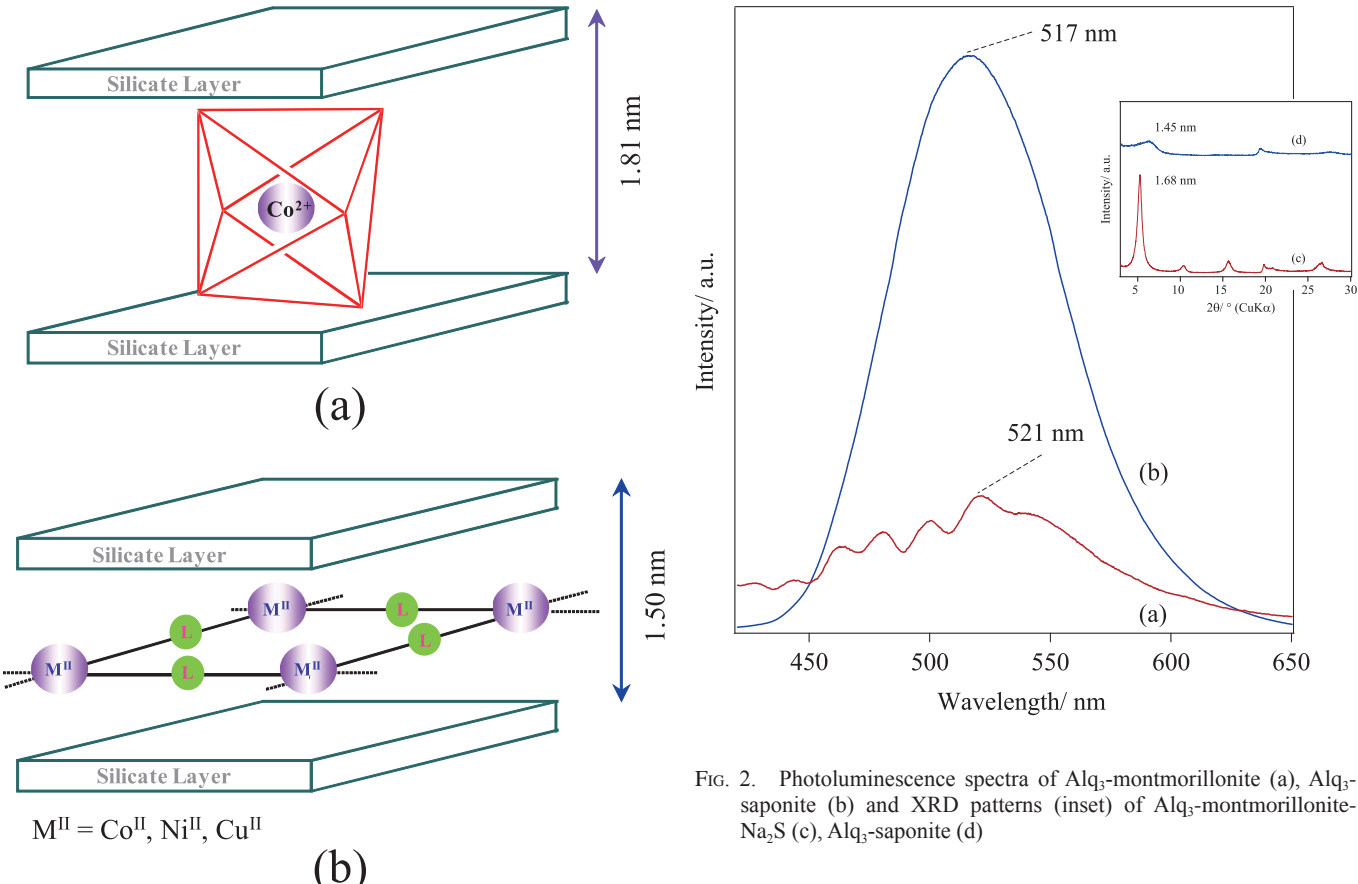


Fig. 1. The proposed molecular structures of (a) cobalt-2,2'-bipyridine and (b) metal-4,4'-bipyridine or 1,2-di(4-pyridine)ethylene

of corresponding complexes in montmorillonite, and this result was ascribed to the very small amount of the quenching impurities in synthetic saponite. The wavelength of the UV-visible and luminescent bands of the complexes varied slightly depending on the hosts, indicating the different molecular structure and packing of the complexes into smectites. The selection of appropriate host materials, interlayer cations, and guest species as a ligand are the quite promising methods for incorporating highly functional neutral complexes in the interlayer region by the solid-state intercalation.

#### FORMATION OF METAL SULFIDE NANOPARTICLES IN SMECTITE

Semiconductor particles including metal sulfides have been extensively studied due to their numerous potential applications such as catalysts for coal liquefaction, solid lubricants and electrooptical devices for rechargeable batteries, solar cell and coatings for microwave shields (Tian et al., 1995; Hu et al., 2002; Qin et al., 2005; Camacho-Bragado et al., 2008). The particle size and size distribution play the important roles in determining the unusual optical properties and activities of the semiconductors. The optimum size ranges from 10 to 20 nm (Tian et al., 1995). Control over the size and size distribution of metal sulfide particles are, therefore, of great saponite (b) and XRD patterns (inset) of Alq3-montmorillonite-

(d)

650

importance. Various methods have been developed to synthesize metal sulfides including adsorption of metal sulfide in restrictive systems such as MCM41 (Zhang et al., 2001), carbon nanotube (Du et al., 2005), zeolites (Iacomi et al., 2003) and layered metal oxide (Shangguan and Yoshida, 2002) partly because of their enhanced photoluminescence property and photocatalytic activity. The two dimensional nanospaces of pristine and organically modified smectites such as saponite and hectorite have been also utilized as the great supports to prohibit the aggregates of metal sulfide particles and their optical properties have been studied widely (Stramel et al., 1986; Kotov et al., 1993; Miao et al., 2006). Besides the conventional reaction, the so-called solid-solid reaction, an attractive method due to its simplicity and productivity, has been successfully applied to prepare metal sulfides in the interlayer spaces of montmorillonite and the resulting hybrids led to the unique optical properties.

Cadmium sulfide, zinc sulfide, magnesium sulfide, nickel sulfide, cobalt sulfide and copper sulfide were immobilized in the interlayer spaces of montmorillonite by solid-solid reactions and in situ formation between homoionic (Cd(II)-, Zn(II)-, Mn(II)- and Ni(II)-) montmorillonites and sodium sulfide with the molar ratio of 1:1 at room temperature (Khaorapapong et al., 2008a, b, 2009, 2010, 2011). The expansions of the interlayer spaces of the metal sulfide-montmorillonites were determined to be ca. 0.2-0.3 nm (Figs. 3a-3d and Table 1). The dark images of quantum sized cadmium sulfide particles with an average diameter of ca. 6-10 nm (Fig. 3e), as well as those of zinc sulfide, manganese sulfide,

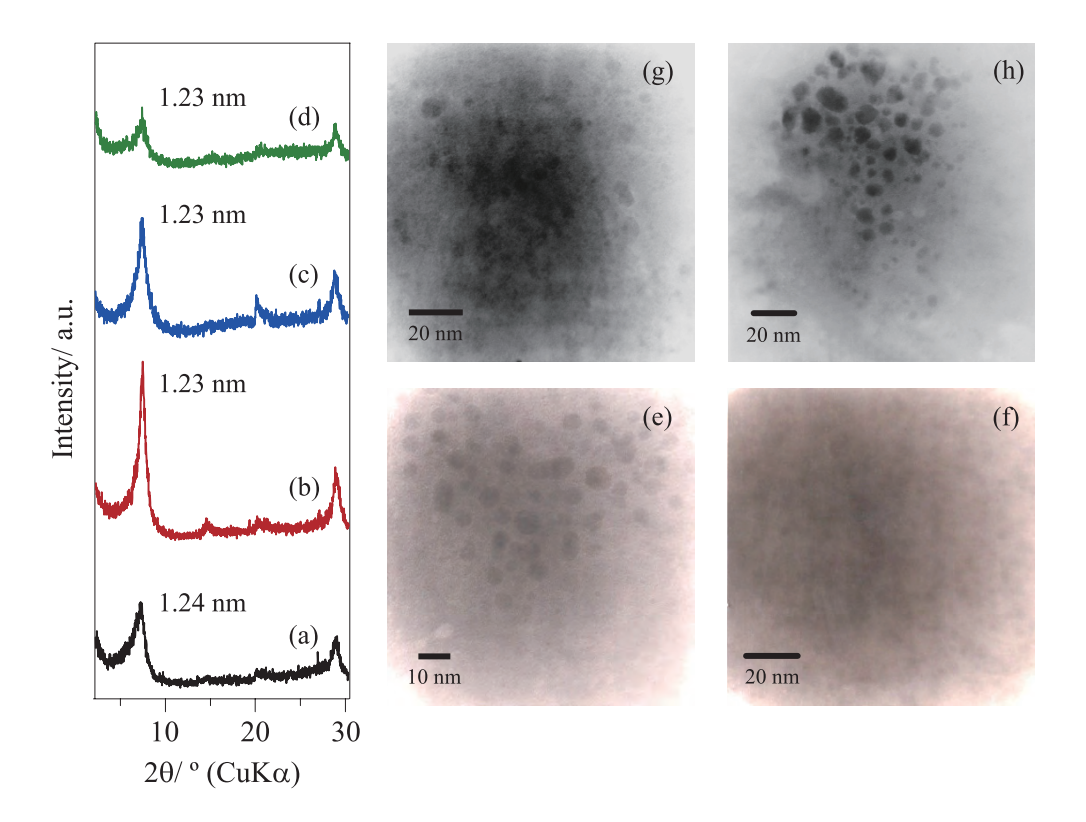


Fig. 3. XRD patterns and TEM images of CdS-montmorillonite (200°C) (a, e), ZnS-montmorillonite (200°C) (b, f), MnS-montmorillonite (200°C, 4 months) (c, g) and NiS-montmorillonite (200°C, 4 months) (d, h)

nickel sulfide (Figs. 3f–3h), cobalt sulfide and copper sulfide particles with an average size of 2–9 nm were well dispersed in the interlayer spaces of montmorillonite, where the disks or plate planes were oriented parallel to the silicate layers. Spectral shifts of the Raman and UV-visible absorption suggested the formation of metal sulfides. The semiconductor particles showed quantum size effects as suggested by in the blue shifts of UV-visible absorption onsets relative to the bulk semiconductors.

Metal sulfide-montmorillonite hybrids showed the difference of the appearance of photoluminescence behaviors. Cadmium sulfide and zinc sulfide in montmorillonite exhibited the emission bands after solid-solid reactions and the bands still maintained after subsequent heat treatment at 200°C (Figs. 3a and 3b). On the other hand, no luminescence band was observed for manganese sulfide-, nickel sulfide-, cobalt sulfide- and copper sulfide-montmorillonites prepared by solid-solid reactions and subsequent heating at 200°C, however, the emission bands were seen in the photoluminescence spectra of the products after storage for several months. The very slow processes were concerned for the states of the formed particles.

The photoluminescence intensities of the products were weak due to the presence of quenching impurities in montmorillonite. The present solid-state intercalation and *in situ* formation of metal sulfides in the interlayer spaces of montmorillonite are promising synthetic methods to prepare metal sulfide-montmorillonite hybrid materials with novel nanostructure and properties.

#### CONCLUSIONS AND FUTURE PERSPECTIVE

The solid-solid reaction summarized here is unique and may be applied as a facile method for preparation of the novel layered silicate hybrids. In addition, it led to the formation of nanohybrid products, which cannot be obtained by the conventional ion exchange method.

The organization of organic and inorganic substances in the interlayer spaces of smectites has been reviewed. The intercalation compounds of organic cations and nonionic species were conducted by solid-state cation exchange and adsorption methods. Solid-state modification of smectites by metal chelates and metal sulfides was carried out by adsorption and *in situ* formation between homoionic exchanged-smectites and the appropriate ligands.

Modification of solid surface with organoammonium ions gave the strongly organophillic products that be able to immobilize nonionic molecules in the interlayer spaces. Hydrophobic guest species with photoactivities such as azo-dyes were intercalated in the nanospaces of the organically smectites.

The introduction of metal complexes and metal sulfides was achieved by adsorption of the ligands and *in situ* formation in the interlayer spaces. The confined environment of low dimensional layered materials was used to produce the novel microstructures and properties of the materials.

The successes in preparation of intercalation compounds with specific microstructures and properties by solid-solid reactions might motivate researchers for designing novel low dimensional nanohybrid materials from the other layered host

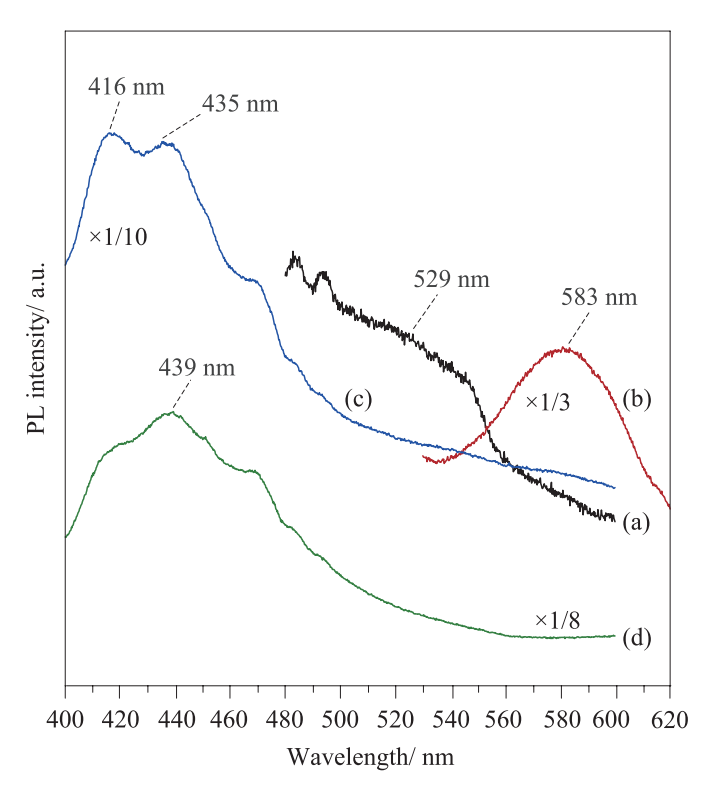


Fig. 4. Photoluminescence spectra of CdS-montmorillonite (200°C) (a), ZnS-montmorillonite (200°C) (b), MnS-montmorillonite (200°C, 4 months) (c) and NiS-montmorillonite (200°C, 4 months) (d)

and guest species.

#### **ACKNOWLEDGEMENTS**

This work was partially supported by the Hitachi Scholarship Foundation, Japan, the Thailand Research Fund and Commission on Higher Education (Grant no. MRG5080261), the Thailand Research Fund and Khon Kaen University (Grant no. DBG5380004), as well as the Center of Excellence for Innovation in Chemistry (PERCH-CIC), Commission on Higher Education, Ministry of Education, Thailand. One of the authors (N.K.) thanks to the invitation of the present paper from the Clay Science Society of Japan.

#### REFERENCES

- Aragon, F., Cano-Ruiz, J. and MacEwan, D.M.C. (1959)  $\beta$ -Type interlamellar sorption complexes. *Nature*, **183**, 740–741.
- Brindley, G.W. (1965) Complexes of primary amines with montmorillonite and vermicufite. *Clay Miner.*, **6**, 91–96.
- CAMACHO-BRAGADO, G.A., Luis Elechiguerra, J. and Jose Yacaman, M. (2008) Characterization of low dimensional molybdenum sulfide nanostructures. *Mater. Character.*, 59, 204–212.
- CHEN, C.H. and SHI, J. (1998) Metal chelates as emitting materials for organic electroluminescence. *Coord. Chem. Rev.*, 171, 161–174.
- Du, J., Fu, L., Liu, Z., Han, B., Li, Z., Liu, Y., Sun, Z. and Zhu, D. (2005) Facile route to synthesize multiwalled carbon nanotube/zinc sulfide heterostructures: Optical and electrical properties. *J. Phys. Chem. B*, 109, 12772–12776.
- HAGRMAN, D., HAMMOND, R.P., HAUSHALTER, R. and ZUBIETA, J. (1998a) Organic/inorganic composite materials: Hydrothermal syntheses and structures of the one-, two-, and three-dimensional copper(II) sulfate-

- organodiamine phases  $[Cu(H_2O)_3(4,4'-bipyridine)(SO_4)]\cdot 2H_2O$ ,  $[Cu(bpe)_2][Cu(bpe)(H_2O)_2(SO_4)_2]\cdot 2H_2O$ , and  $[Cu(bpe)(H_2O)(SO_4)]$  (bpe = trans-1,2-bis(4-pyridyl)ethylene). *Chem. Mater.*, **10**, 2091–2100.
- HAGRMAN, D., HAUSHALTER, R.C. and ZUBIETA, J. (1998b) Three-dimensional organic/inorganic hybrid materials constructed from one-dimensional copper diamine coordination polymers linked by bridging oxoanion tetrahedra: [Cu(dpe)(MoO<sub>4</sub>)] and [Cu(dpe)(SO<sub>4</sub>)(H<sub>2</sub>O)] (dpe = 1,2-trans-(4-pyridyl)ethene). *Chem. Mater.*, **10**, 361–365.
- Hu, H., Bai, J., Guo, S. and Chen, G. (2002) Coal liquefaction with in situ impregnated Fe<sub>2</sub>(MoS<sub>4</sub>)<sub>3</sub> bimetallic catalyst. *Fuel*, **81**, 1521–1524
- IACOMI, F., VASILE, A. and POLYCHRONIADIS, E.K. (2003) MnS clusters in natural zeolites. *Mater. Sci. Eng. B*, 101, 275–278.
- KHAORAPAPONG, N. (2010) In situ complexation of thiourea in the interlayer space of copper(II)-montmorillonite. Appl. Clay Sci., 50, 414–417.
- Khaorapapong, N. and Ogawa, M. (2007) Solid state intercalation of 8-hydroxyquinoline into Li(I)-, Zn(II)- and Mn(II)-montmorillonites. *Appl. Clay Sci.*, **35**, 31–38.
- KHAORAPAPONG, N. and OGAWA, M. (2008) In situ formation of bis(8-hydroxyquinoline) zinc(II) complex in the interlayer spaces of smectites by solid–solid reactions. J. Phys. Chem. Solids, 69, 941–948.
- Khaorapapong, N. and Ogawa, M. (2010) Formation of mono(8-hydroxyquinoline) lithium(I) complex in smectites by solid-solid reactions. *J. Phys. Chem. Solids*, **71**, 1644–1650.
- KHAORAPAPONG, N., KURODA, K., HASHIZUME, H. and OGAWA, M. (2000) Solid state intercalation of 4,4'-bipyridine into the interlayer space of montmorillonites. *Mol. Cryst. Liq. Cryst.*, 341, 351–356.
- Khaorapapong, N., Kuroda, K., Hashizume, H. and Ogawa, M. (2001) Solid-state intercalation of 4,4'-bipyridine and 1,2-di(4-pyridine) ethylene into the interlayer space of Co(II)-, Ni(II)-, and Cu(II)-montmorillonites. *Appl. Clay Sci.*, **19**, 69–76.
- Khaorapapong, N., Kuroda, K. and Ogawa, M. (2002a) Incorporation of thioacetamide into the interlayer space of montmorillonite by solid-solid reactions. *Clay Sci.*, **11**, 549–564.
- KHAORAPAPONG, N., KURODA, K. and OGAWA, M. (2002b) Intercalation of 8-hydroxyquinoline into Al-smectites by solid-solid reactions. *Clays Clay Miner.*, 50, 428–434.
- KHAORAPAPONG, N., ONTAM, A., YOUNGME, S. and OGAWA, M. (2008a) Solid-state intercalation and in situ formation of cadmium sulfide in the interlayer space of montmorillonite. J. Phys. Chem. Solids, 69, 1107–1111.
- KHAORAPAPONG, N., ONTAM, A. and OGAWA, M. (2008b) Formation of MnS particles in the interlayer space of montmorillonite. *Mater. Lett.*, 62, 3722–3723
- KHAORAPAPONG, N., ONTAM, A., KHEMPRASIT, J. and OGAWA, M. (2009) Formation of MnS- and NiS-montmorillonites by solid-solid reactions. Appl. Clay Sci., 43, 238–242.
- Khaorapapong, N., Ontam, A. and Ogawa, M. (2010) Formation of ZnS and CdS in the interlayer spaces of montmorillonite. *Appl. Clay Sci.*, **50**, 19–24.
- Khaorapapong, N., Ontam, A. and Ogawa, M. (2011) Very Slow Formation of Copper Sulfide and Cobalt Sulfide Nanoparticles in Montmorillonite. *Appl. Clay Sci.*, **51**, 182–186.
- KOTOV, N.A., PUTYERA, K., FENDLER, J.H., TOMBÁCZ, E. and DÉKÁNY, I. (1993) Cadmium sulfide particles in organomontmorillonite complexes. *Colloids Surf. A*, 71, 317–326.
- Lagally, G. (1981) Characterization of clays by organic compounds. *Clay Miner.*, **16**, 1–21.
- LAGALY, G. (1986) Interaction of alkylamines with different types of layered compounds. Solid State Ionics, 22, 43-51.
- Lagaly, G., Ogawa, M. and Dékány, I. (2006) Clay mineral organic intercalation, pp. 309–377 in: Bergaya, F., Theng, B.K.G. and Lagaly, G. (Eds.), Handbook of Clay Sciences Volume 1 Developments in Clay Science. Elsevier, The Netherlands.
- MIAO, S., LIU, Z., HAN, B., YANG, H., MIAO, Z. and SUN, Z. (2006) Synthesis and characterization of ZnS-montmorillonite nanocomposites and their application for degrading eosin B. *J. Colloid Inter. Sci.*, **301**, 116–122
- Ogawa, M. (2004) Photoprocess in clay-organic complexes, pp. 191-260

- in: Auerbach, S.M., Carrado, K.A. and Dutta, P.K. (Eds.), Handbook of Lavered Materials. Marcel Dekker. New York.
- OGAWA, M. and KURODA, K. (1995) Photofunctions of intercalation compounds. Chem. Rev., 95, 399–438.
- Ogawa, M. and Kuroda, K. (1997) Preparation of inorganic-organic nanocomposites through intercalation of organoammonium ions into layered silicates. *Bull. Chem. Soc. Jpn.*, **70**, 2593–2618.
- Ogawa, M., Kuroda, K. and Kato, C. (1989) Preparation of montmorillonite-organic intercalation compounds by solid-solid reactions. *Chem. Lett.*, 1659–1662.
- OGAWA, M., HANDA, T., KURODA, K. and KATO, C. (1990a) Formation of organoammonium-montmorillonites by solid-solid reactions. *Chem. Lett.*, 71–74.
- OGAWA, M., KATO, K., KURODA, K. and KATO, C. (1990b) Preparation of montmorillonite-alkylamine intercalation compounds by solid-solid reactions. *Clay Sci.*, 8, 31–36.
- OGAWA, M., FUJII, K., KURODA, K. and KATO, C. (1991a) Preparation of montmorillonite-p-aminoazobenzene intercalation compounds and their photochemical behavior. *Mater. Res. Soc. Symp. Proc.*, **233**, 89–94
- OGAWA, M., HASHIZUME, T., KURODA, K. and KATO, C. (1991b) Intercalation of 2,2'-bipyridine and complex formation in the interlayer space of montmorillonite by solid-solid reactions. *Inorg. Chem.*, **30**, 584–585
- Ogawa, M., Hirata, M., Kuroda, K. and Kato, C. (1992a) Selective solid-state intercalation of *cis-trans* isomers into montmorillonite. *Chem. Lett.*, 365–368.
- OGAWA, M., NAGAFUSA, Y., KURODA, K. and KATO, C. (1992b) Solid-state intercalation of acrylamide into smectites and Na-taeniolite. *Appl. Clay Sci.*, 7, 291–302.
- OGAWA, M., SHIRAI, H., KURODA, K. and KATO, C. (1992c) Solid-state intercalation of naphthalene and anthracene into alkylammoniummontmorillonites. *Clays Clay Miner.*, 40, 485–490.
- OGAWA, M., AONO, T., KURODA, K. and KATO, C. (1993) Photophysical probe study of alkylammonium-montmorillonites. *Langmuir*, 9, 1529–1533.
- OGAWA, M., HAGIWARA, A., HANDA, T., KATO, C. and KURODA, K. (1995a) Solid state ion exchange reactions between homoionic-montmorillonites and organoammonium salts. *J. Porous Mater.*, 1, 85–89.
- Ogawa, M., Wada, T. and Kuroda, K. (1995b) Intercalation of pyrene into alkylammonium-exchanged swelling layered silicates: The effects of the arrangements of the interlayer alkylammonium ions on the states of adsorbates. *Langmuir*, 11, 4598–4600.
- OGAWA, M., KIMURA, H., KURODA, K. and KATO, C. (1996) Intercalation and the photochromism of azo dye in the hydrophobic interlayer spaces of organoammonium-fluor-tetrasilicic micas. *Clay Sci.*, **10**,
- OGAWA, M., KADOMOTO, H., KATO, C. and KURODA, K. (1997) Intercalation of a crow-ether into layered silicates. *Clay Sci.*, **10**, 185–194.
- PATIL, A.O., CURTIN, D.Y. and PAUL, I.C. (1984) Solid-state formation of quinhydrones from their components. Use of solid-solid reactions to prepare compounds not accessible from solution. *J. Am. Chem. Soc.*, 106, 348–353.
- PINNAVAIA, T.J. (1983) Intercalated clay catalysts. *Science*, **220**, 365–371. QIN, A.-M., FANG, Y.-P., OU, H.-D., LIU, H.-Q. and SU, C.-Y. (2005) For-

- mation of various morphologies of covellite copper sulfide submicron crystals by a hydrothermal method without surfactant. *Cryst. Growth Design*, **5**, 855–860.
- RASTOGI, R.P., SINGH, N.B. and SINGH, R.P. (1977) Organic solid-state reactions. J. Solid State Chem., 20, 191–200.
- RUIZ-HITZKY, E. and CASAL, B. (1978) Crown ether intercalation with phyllosilicates. *Nature*, 276, 596–597.
- RUIZ-HITZKY, E. and ARANDA, P. (1990) Polymer-salt intercalation complexes in layer silicates. Adv. Mater., 2, 545-547.
- RUIZ-HITZKY, E., ARANDA, P., CASAL, B. and GALVÁN, J.C. (1995) Nanocomposite materials with controlled ion-mobility. Adv. Mater., 7, 180–184.
- SCHMITZ, C., SCHMIDT, H.-W. and THELAKKAT, M. (2000) Lithium-quinolate complexes as emitter and interface materials in organic light-emitting diodes. *Chem. Mater.*, **12**, 3012–3019.
- SHANGGUAN, W. and YOSHIDA, A. (2002) Photocatalytic hydrogen evolution from water on nanocomposites incorporating cadmium sulfide into the interlayer. J. Phys. Chem. B, 106, 12227–12230.
- SLONE, R.V., HUPP, J.T., STERN, C.L. and ALBRECHT-SCHMITT, T.E. (1996) Self-assembly of luminescent molecular squares featuring octahedral rhenium corners. *Inorg. Chem.*, 35, 4096–4097.
- STRAMEL, R.D., NAKAMURA, T. and THOMAS, J.K. (1986) Cadmium sulfide on synthetic clay. Chem. Phys. Lett., 130, 423–425.
- Sutherland, H.H. and MacEwan, D.M.C. (1961) Organic complexes of vermiculite. *Clay Miner. Bull.*, **4**, 229–233.
- TIAN, D., SHARMA, R.K., STILLER, A.H., STINESPRING, C.D. and DADYBUR-JOR, D.B. (1995) Direct liquefaction of coal using ferric-sulfide-based, mixed-metal catalysts containing Mg or Mo. *Fuel*, **75**, 751–758.
- Toda, F., Tanaka, K. and Sekikawa, A. (1987) Host-guest complex formation by a solid-solid reaction. *J. Chem. Soc., Chem. Commun.*, 279–280.
- Tong, M.-L., Lee, H.-K., Chen X.-M., Huang, R.-B. and Mak, T.C.W. (1999) A novel three-dimensional triangular organic-inorganic hybrid network self-assembled by mononuclear [Mn(4,4'-bipyridine)<sub>2</sub> (H<sub>2</sub>O)<sub>4</sub>]<sup>2+</sup> cations and rich solvate 4,4'-bipyridine molecules through hydrogen-bonding and  $\pi$ -π interactions. *J. Chem. Soc., Dalton Trans.*, 3657–3659.
- VICENTE, M.A., SÁNCHEZ-CAMAZANO, M., SÁNCHEZ-MARTÍN, M.J., DEL ARCO. M., MARTÍN, C., RIVES, V. and VICENTE-HERNÁNDEZ, J. (1989) Adsorption and desorption of N-methyl 8-hydroxyquinoline methyl sulfate on smectite and the potential use of the clay-organic product as an ultraviolet radiation collector. Clays Clay Miner., 37, 157–163.
- Yoshimoto, S., Ohashi, F. and Kameyama, T. (2005) X-ray diffraction studies of intercalation compounds prepared from aniline salts and montmorillonite by a mechanochemical processing. *Solid State Commun.*, **136**, 251–256.
- WADA, K. (1961) Lattice expansion of kaolin minerals by treatment with potassium acetate. Am. Miner., 46, 78–91.
- Whittingham, M.S. (1982) Intercalation Chemistry: An introduction, in: Whittingham, M.S. and Jacobson, A.J. (Eds.), Intercalation Chemistry, Academic Press, New York, pp. 1–18.
- ZHANG, W.-H., SHI, J.-L., CHEN, H.-R., HUA, Z.-L. and YAN, D.-S. (2001) Synthesis and characterization of nanosized ZnS confined in ordered mesoporous silica. *Chem. Mater.*, 13, 648–654.

# Journal of Materials Chemistry



Cite this: J. Mater. Chem., 2012, 22, 20001

www.rsc.org/materials PAPER

# Immobilization of cadmium telluride nanoparticles on the surface of hexadecyltrimethylammonium-montmorillonite†

Areeporn Ontam, Nithima Khaorapapong and Makoto Ogawa

Received 27th January 2012, Accepted 16th July 2012

DOI: 10.1039/c2jm33327a

A novel hybrid material of cadmium telluride, one of the II–VI group of semiconductors, and hexadecyltrimethylammonium-montmorillonite was prepared by the intercalation of cadmium telluride into hexadecyltrimethylammonium-montmorillonite. The resulting hybrids were characterized by X-ray diffraction, FT-IR, HRTEM, TG-DTA, UV-visible and photoluminescence spectroscopies. The size and size distribution of cadmium telluride were stabilized by hexadecyltrimethylammonium-montmorillonite, which can greatly affect the optical properties. High resolution transmission electron micrographs showed that cadmium telluride particles with the diameter of 1.30–2.50 nm were well-separated and uniformly distributed in the interlayer spaces of hexadecyltrimethylammonium-montmorillonite.

#### Introduction

The development of fluorescent semiconductor nanoparticles is a current topic of great interest for both fundamental and practical applications because of their strongly size-dependent optical properties that make them usable as nonlinear optical materials, photocatalysts, sensing and so on. 1.2 Generally, the nanosized semiconductors are inherently unstable, they tend to grow larger than the quantum size domain. 1 Therefore, the preparation of semiconductor nanoparticles has been conducted under restricted environments or controlled conditions for the possible molecular design at a nanometer scale. 2 Inorganic matrices are one of the possible supports for nanoparticles owing to their stability and defined nanostructures. The incorporation of semiconductor nanoparticles within the inorganic matrices so as to generate a hybrid material is one successful method for stabilizing quantum size semiconductors.

Smectite, which is a group of layered clay minerals, including montmorillonite, is an inorganic solid which has attractive features such as large surface area, swelling behaviour, adsorptive and ion exchange properties, biocompatibility, as well as null toxicity for a wide range of applications.<sup>3–5</sup> The interlayer spaces of layered inorganic materials can be modified by organoammonium cations and their colloidal properties make them

Highly emissive cadmium telluride (CdTe) nanoparticles show great potential in biological labelling and so on due to their unique optical properties such as narrow emission band associated with tunable particle size and size distribution. 2,12,13 It was previously reported that the use of organic and organometallic capping agents<sup>14,15</sup> as well as polymers<sup>16</sup> for the synthesis of CdTe resulted in the aggregation of CdTe clusters by the hydrophobic interactions between the capping agents. There are a few complicated methods for the preparation of CdTe nanoparticles that use three-dimensional microstructures, for instance, CdTe-PAMAM (poly(amidoamine))-MWNT (multi-walled carbon nanotube)<sup>17</sup> and CdTe-zeolite-A.<sup>18</sup> In the present study, a simple process under mild conditions was used to prepare CdTe nanoparticles in a two-dimensionally restricted environment, the interlayer spaces of organically modified montmorillonite. Although a method for controlling the particle size of CdTe within zeolite A has been reported, the small 6-ring window (0.22 nm) of the matrix limited encapsulation of CdTe particles due to the large size of Te anion (0.44 nm).<sup>18</sup> Because the interlayer space of montmorillonite is expandable for a variety of small and large sizes of guest species, the incorporation of CdTe in between the silicate layers seems to be possible to give novel hybrids of CdTe nanoparticles confined in the two dimensional nanospace.

possible to produce novel hybrid materials of various semiconductors. The examples include formation of metal sulfide nanoparticles in smectites that efficiently limited nucleation and growth conditions to provide uniformly dispersed nanoparticles, decrease surface energy, inhibit molecular diffusion, as well as control the particle size.<sup>6-9</sup> The preparation of semiconductor and metal nanoparticles in layered materials, montmorillonite, as well as layered alkali silicate and titanate, is a focus of our work to achieve useful materials such as luminescent materials and photocatalysts.<sup>10,11</sup>

<sup>&</sup>quot;Department of Chemistry and Center of Excellence for Innovation in Chemistry, Faculty of Science, Khon Kaen University, Khon Kaen 40002, Thailand. E-mail: nithima@kku.ac.th; Fax: +66 43 202373; Tel: +66 43 202222-41 ext. 12370-2

<sup>&</sup>lt;sup>b</sup>Department of Earth Sciences and Graduate School of Creative Science and Engineering, Waseda University, 1-6-1 Nishiwaseda, Shinjuku-ku, Tokyo 169-8050, Japan

<sup>†</sup> Electronic supplementary information (ESI) available. See DOI: 10.1039/c2jm33327a

Recently, *in situ* formation of CdTe in the layered clay mineral has been reported.<sup>19</sup> However, the release of the large amount of CdTe under UV radiation is harmful for biological application and the environment. To the best of our knowledge, the intercalation of pre-synthesized CdTe in layered materials has not been investigated yet. Here, cadmium telluride was prepared and inserted in the hydrophobic surface of hexadecyltrimethylammonium-montmorillonite by a facile solid–liquid reaction in order to control its thermal and optical properties. The effect of hexadecyltrimethylammonium-montmorillonite on the particle size and size-distribution of CdTe nanoparticles was also examined.

#### **Experimental section**

#### Materials

Sodium-montmorillonite (Kunipia F, Kunimine Industries, the reference clay sample of the Clay Science Society of Japan; JCSS-3101) was used as a host material. The cation exchange capacity (CEC) is 119 meq. per 100 g of clay. Hexadecyltrimethylammonium (HDTMA) bromide (C<sub>19</sub>H<sub>42</sub>NBr), tellurium (Te) powder and thioglycolic acid (TGA) were purchased from Sigma-Aldrich. Cadmium chloride (CdCl<sub>2</sub>·H<sub>2</sub>O) was obtained from Carlo Erba Reagenti. Sodium borohydride (NaBH<sub>4</sub>) was supplied by Univar. All chemicals are of analytical grade and were used without further purification.

#### Synthesis of CdTe-HDTMA-montmorillonite hybrids

Hexadecyltrimethylammonium-montmorillonite was prepared by a conventional ion exchange reaction between an aqueous solution of HDTMA bromide and an aqueous suspension of montmorillonite. The amount of the loading HDTMA ions was equal to the CEC of Na-montmorillonite. The mixture was allowed to react by magnetic stirring at 70 °C for one day. An aqueous solution of thioglycolic acid-stabilized cadmium telluride (TGA-stabilized CdTe) was prepared by refluxing an aqueous solution of cadmium chloride, sodium hydrogentelluride (NaHTe) and thioglycolic acid in a nitrogen atmosphere for 2 hours<sup>20</sup> and subsequently reacted with the dispersion of HDTMA-montmorillonite. The mixture was stirred until the CdTe solution was totally adsorbed in HDTMA-montmorillonite. The resulting solids were separated by centrifugation, washed with distilled water and dried in a desiccator at room temperature for 4 days. The amounts of TGA-stabilized CdTe reacted with the HDTMA-montmorillonite were 12, 36 and 60 meq. per 100 g of montmorillonite.

#### Instrumentation

X-ray diffraction data were collected on a Bruker D8 ADVANCE diffractometer using monochromatic CuK $\alpha$  radiation. A Perkin-Elmer Spectrum One Fourier transform-infrared (FT-IR) spectrophotometer was employed for recording the spectra using the KBr pellet method. TEM images were taken using a Tecnai  $G^2$  20 transmission electron microscope operating at 200 kV (FEI). TG-DTA curves were obtained with a Perkin-Elmer Pyris Diamond TG-DTA at a heating rate of 10 °C min<sup>-1</sup> under dried air flow using  $\alpha$ -alumina ( $\alpha$ -Al<sub>2</sub>O<sub>3</sub>) as a standard

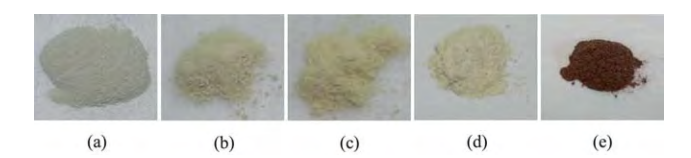


**Fig. 1** The solid samples of (a) HDTMA-montmorillonite, (b) CdTe(12)–HDTMA-montmorillonite, (c) CdTe(36)–HDTMA-montmorillonite, (d) CdTe(60)–HDTMA-montmorillonite and (e) TGA-stabilized CdTe.

material. Diffuse reflectance spectra were recorded with a Shimadzu UV-VIS-NIR-3101PC scanning spectrophotometer using an integrated sphere. Luminescence spectra were recorded with a Hitachi F-4500 fluorescence spectrofluorophotometer with the excitation at 380 nm. Fluorospectroscopic photographs were taken using a Nikon ECLIPSE E600 fluorescence microscope. Photoluminescence quantum yields of the powder samples were measured by a Hamamatsu photonics C9920-02.

#### **Results and discussion**

As a result of conventional solid–liquid reaction between an aqueous solution of TGA-stabilized CdTe and a dispersion of HDTMA-montmorillonite, yellow solids were obtained (Fig. 1) and the supernatant liquid was colourless. This result suggested that the CdTe was adsorbed by HDTMA-montmorillonite during the reaction. Hereafter, the hybrids are denoted as CdTe(n)–HDTMA-montmorillonite, where n in the parenthesis indicates the amount of TGA-stabilized CdTe at the loading amounts of 12, 36 and 60 meq. per 100 g of montmorillonite.

The XRD patterns of the three hybrids are shown in Fig. 2 together with that of HDTMA-montmorillonite. Before the incorporation of TGA-stabilized CdTe the hydrophilic interlamellar surface of montmorillonite was recovered by the alkyl

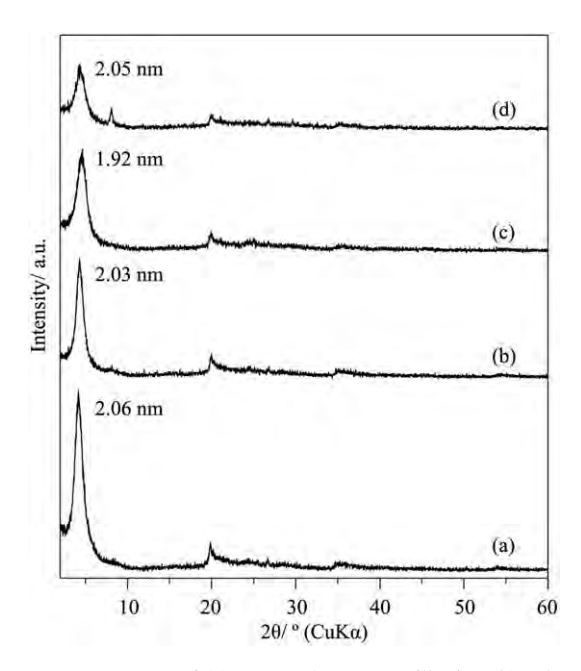


**Fig. 2** XRD patterns of (a) HDTMA-montmorillonite, (b) CdTe(12)—HDTMA-montmorillonite, (c) CdTe(36)–HDTMA-montmorillonite and (d) CdTe(60)–HDTMA-montmorillonite.

chains of HDTMA ions, resulting in the organophilic surface.<sup>5</sup> The basal spacing of HDTMA-montmorillonite was 2.06 nm (Fig. 2a). The expansion of the interlayer space was determined to be 1.10 nm by subtracting the thickness of the silicate layer (ca. 0.96 nm) from the observed basal spacing, suggesting that alkylammonium ions arranged in the kinked alkyl chain or paraffin type monolayer in between the silicate layers. The basal spacing of HDTMA-montmorillonite was large enough to incorporate CdTe particles in the interlayer space. The XRD pattern of TGA-stabilized CdTe revealed the three broad diffraction peaks, corresponding to the (111), (220) and (311) lattice planes of zinc blende CdTe (JCPDS 75-2086) (ESI, Fig. S1†). The basal spacings of CdTe(12)-, CdTe(36)- and CdTe(60)-HDTMA-montmorillonites were 2.03, 1.92 and 2.05 nm (Fig. 2b-d), corresponding to the gallery heights of 1.07, 0.96 and 1.09 nm, respectively. The XRD patterns of the hybrids did not show the reflection due to CdTe crystal or the other components, confirming that the CdTe was intercalated in the interlayer spaces. The basal spacing of HDTMA-montmorillonite did not increase further even when a large amount of CdTe was mixed. It was considered that even with such a large number of CdTe being loaded, HDTMA-montmorillonite could support the semiconductor particles and maintain the structural features of the host. This indicated that the size and/or the thickness of CdTe nanoparticles were independent from the amount of the intercalated CdTe nanoparticles. There is a possibility that the CdTe could adsorb at the external surface of montmorillonite, but the relative contribution of the external surface to the interlayer space should be very small and could not be detected by the conventional XRD measurement. We assumed that the adsorption of neutral CdTe on the organophilic surface of montmorillonite occurred through the hydrophobic interactions, namely the water soluble TGA-stabilized CdTe nanoparticles were first attached to the sodium cations in the suspension of HDTMA-montmorillonite and subsequently interacted with the hydrophobic surface of HDTMA-montmorillonite. In order to confirm that the CdTe was indeed intercalated into the interlayer spaces of HDTMA-montmorillonite, the suspension of sodium montmorillonite (pale gray powder) was reacted with an aqueous solution of TGA-stabilized CdTe (vellow colour solution). After the reaction, the precipitate was pale gray (not coloured) and the supernatant liquid contained the yellow colour of TGA-stabilized CdTe still. This observation indicated that the CdTe semiconductor was not intercalated into sodium montmorillonite, which was in contrast to the reaction with HDTMAmontmorillonite.

The FT-IR spectra of the hybrids were compared with that of TGA-stabilized CdTe (ESI, Fig. S2†). The FT-IR spectra of the hybrids showed the characteristic bands due to HDTMA ion including a CH<sub>2</sub> symmetric stretching vibration at around 1482 cm<sup>-1</sup>. By comparison with the band assigned to the CH<sub>2</sub> vibrations of the alkyl chain of HDTMA (at 2918, 2850 and 1480 cm<sup>-1</sup>; not shown), it was thought that the absorption bands observed in the hybrids almost remained at the same frequencies, suggesting that the interactions between the HDTMA ion and the silicate layer did not affect the orientation of HDTMA. The presence of the CdTe nanoparticles in HDTMA-montmorillonite was confirmed by the appearance of the absorption bands due to the surface stabilizing agent, thioglycolic acid, such as a

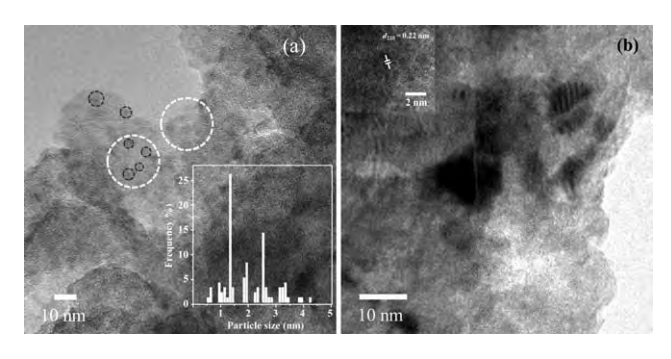


**Fig. 3** (a) TEM micrographs of CdTe(36)–HDTMA-montmorillonite (inset: particle size distribution of CdTe(36)–HDTMA-montmorillonite) and (b) high-magnified TEM micrograph of CdTe(36)–HDTMA-montmorillonite.

C=O stretching vibration band of the carboxylate group at around 1384 cm<sup>-1</sup>. In the FT-IR spectra of the hybrids, a sharp absorption band was observed at around 1380–1385 cm<sup>-1</sup>, showing the co-adsorption of the CdTe in the interlayer spaces.<sup>15</sup>

The size and size distribution of the CdTe nanoparticles in HDTMA-montmorillonite were studied by high resolution transmission electron microscopy (HRTEM). The TEM micrograph of CdTe(36)-HDTMA-montmorillonite is shown in Fig. 3 as an example. The darker contrast observed on the micrograph was due to the effect of the reflection of CdTe nanoparticles as the average atomic number of the nanoparticles is higher than that of the silicate layer, indicating the presence of the CdTe nanoparticles in the interlayer space. The TEM micrograph also showed that the round-shaped CdTe nanoparticles with a diameter of about 1.30-2.50 nm (Fig. 3a, inset) distributed uniformly in between the silicate layers. Taking the gallery height of CdTe(36)-HDTMA-montmorillonite (0.96 nm) and the average size of the nanoparticles (ca. 1.30–2.50 nm) into account, it was thought that the absorbed CdTe nanoparticles were disklike in shape with the thickness of  $\leq ca$ . 1.00 nm and the lateral size of 1.30-2.50 nm. The crystal structure of the intercalated CdTe was further analyzed using the HRTEM micrograph and selected area electron diffraction (SAED) pattern. Although the lattice plane of the intercalated CdTe was not clearly seen by HRTEM due to the interaction of the electron beam with the intercalated HDTMA ion in montmorillonite,21 it showed the lattice plane spacing of about 0.22 nm (Fig. 3b), corresponding to the zinc blende CdTe. The selected area electron diffraction (SAED) pattern of CdTe(36)-HDTMA-montmorillonite displayed both a (220) ring assigned to the zinc blende phase of the intercalated CdTe, and a ring-pattern of montmorillonite (ESI, Fig. S3†). Fig. 3b revealed a characteristic of Moiré fringes that are affected by the interaction between the externally adsorbed CdTe and HDTMA-montmorillonite, indicating the existence of the CdTe on the surfaces. The results confirmed the presence of the CdTe nanoparticles in the interlayer space and the small amount at the external surface of montmorillonite. The restricted microenvironment of HDTMA-montmorillonite greatly controlled the separation and distribution of the CdTe nanoparticles.

In order to confirm the stability, thermogravimetric analysis of all hybrids was performed. The TG-DTA curves of CdTe(36)–HDTMA-montmorillonite are shown as an example in Fig. 4 together with those of TGA-stabilized CdTe and

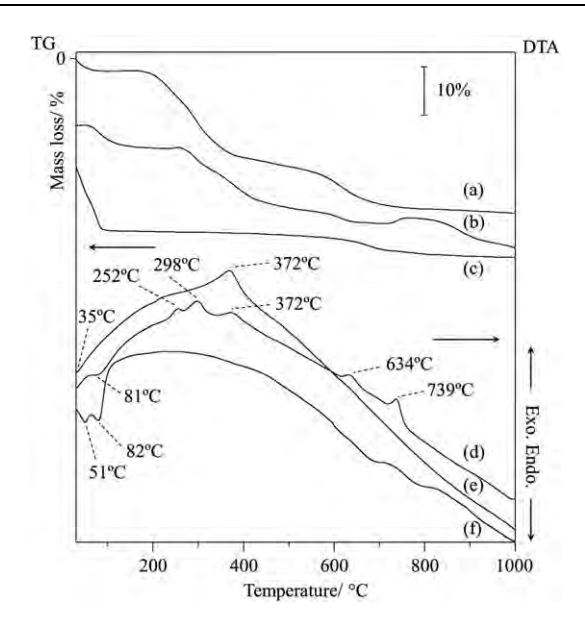


**Fig. 4** TG-DTA curves of (a and d) CdTe(36)–HDTMA-montmorillonite, (b and e) TGA-stabilized CdTe, and (c and f) montmorillonite.

montmorillonite. In the DTA curve of HDTMA (ESI, Fig. S4 and S5†), the endothermic (at 109 °C) and the exothermic peaks (at 205, 312 and 467 °C), which accompanied a mass loss observed between room temperature and 500 °C in the corresponding TG curve, were interpreted to be due to the melting and oxidative decomposition of the alkyl chain of HDTMA bromide, respectively. For the TG-DTA curves, the first mass loss step of TGA-stabilized CdTe (Fig. 4b) revealed below 220 °C was due to the removal of physically adsorbed water. 15 The weight gain observed from 220 to 270 °C corresponding to the exothermic peaks at 252 °C in the DTA curve (Fig. 4e) was interpreted to be due to the oxidation of the CdTe. The mass loss between 270 and 700 °C, which accompanied the exothermic peaks at 298, 372 and 634 °C, was ascribed to the decomposition of thioglycolic acid<sup>15</sup> and the oxidation of the charcoal.<sup>22</sup> In the final step, the weight gain at about 720-750 °C indicated the oxidation of the oxidized specie of CdTe.<sup>23</sup> In the TG-DTA curves of the hybrids, three steps of mass losses were observed. The first mass loss steps observed at room temperature to 180 °C for CdTe(12)-HDTMA-montmorillonite (ESI, Fig. S4†), CdTe(36)-HDTMAmontmorillonite (Fig. 4a) and CdTe(60)-HDTMA-montmorillonite (ESI, Fig. S5†), corresponding to the endothermic reactions at 32, 35 and 32 °C were attributed to the dehydration. No endothermic (at 109 °C) and exothermic peaks (at 205, 312 and 467 °C) due to melting and vaporization of the alkyl chain of HDTMA ion were detected, suggesting the thermal stability of the alkyl chain that is protected by the silicate layers. The second mass loss steps occurred between 180 and 420 °C for CdTe(12)-HDTMA-montmorillonite, 180 and 437 °C for CdTe(36)-HDTMA-montmorillonite, as well as 180 and 450 °C for CdTe(60)–HDTMA-montmorillonite and were interpreted to be due to the decomposition of HDTMA and/or thioglycolic acid. The last mass loss steps observed above 420, 437 and 450 °C for CdTe(12)-, CdTe(36)- and CdTe(60)-HDTMA-montmorillonites were due to the thermal decomposition of the intercalated CdTe and the hydroxylation of structural OH groups of

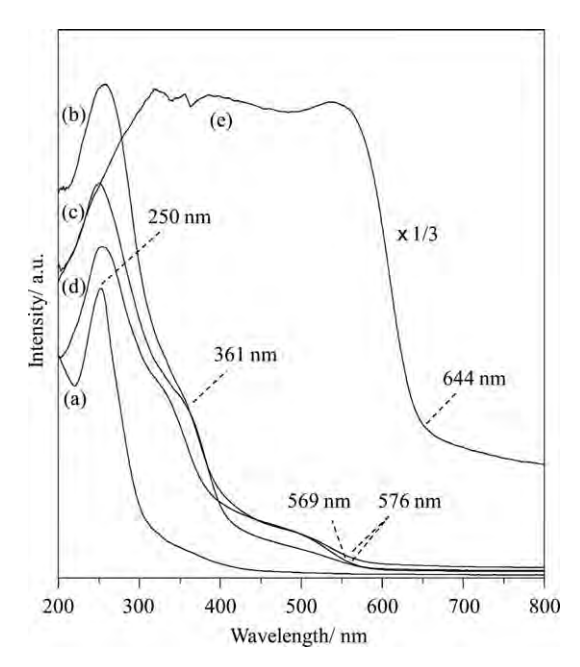


**Fig. 5** Diffuse reflectance absorption spectra of (a) montmorillonite, (b) CdTe(12)–HDTMA-montmorillonite, (c) CdTe(36)–HDTMA-montmorillonite, (d) CdTe(60)–HDTMA-montmorillonite and (e) TGA-stabilized CdTe.

montmorillonite. It was noted that the degradation of the hybrids in each step was quite different from that of TGA-stabilized CdTe. Moreover, no weight gain was seen in the TG curves of the hybrids, as well as the evaporation of TGA-stabilized CdTe occurred at lower temperature compared to the intercalated ones, supporting a higher stability of the intercalated CdTe nanoparticles to evaporation and sublimation. The increase of the thermodynamical stability of the hybrids proved that the evaporation of the CdTe nanoparticles could be prevented by the microenvironment of montmorillonite.

The absorption spectra of the hybrids are shown in Fig. 5 together with those of montmorillonite and TGA-stabilized CdTe. The broad absorption band of TGA-stabilized CdTe was fitted by Gaussian function. Two absorption peaks due to CdTe were seen at 368 and 554 nm (Table 1 and ESI, Fig. S6†). The

Table 1 UV-visible and photoluminescence data of montmorillonite and the hybrids

	Absorption		г	
Hybrid	Band (nm)	Onset (nm)	Emission wavelength (nm)	FWHM (nm)
CdTe(12)–HDTMA- montmorillonite	361	405, 576	499, 514, 536, 555, 575	79
CdTe(36)–HDTMA- montmorillonite	336	386, 569	551	50
CdTe(60)–HDTMA- montmorillonite	361	405, 576	502, 517, 538, 553	68
TGA-stabilized CdTe	368 <sup>a</sup> 554 <sup>a</sup>	644	591	43
Montmorillonite	250	_	_	_

<sup>&</sup>lt;sup>a</sup> The fitted Gaussian curve of the absorption spectrum.

diffuse absorption spectra of the hybrids showed the two absorption bands at around 336-361 nm and 500 nm, as well as two absorption onsets at around 386-405 nm and 569-576 nm (Table 1). The absorption peak of mercaptopropionic acidstabilized CdTe nanoparticles exhibited at 611 nm, 20 while that of CdTe/ZnO@SiO<sub>2</sub> nanocomposites exhibited at 550 nm.<sup>24</sup> The absorption bands of all hybrids occurring in the present system were ascribed to the presence of the CdTe nanoparticles in the hybrids. It is well known that a smaller-sized CdTe nanoparticle shows a blue-shift of the absorption onset compared with a larger one. All of the absorption onsets of the hybrids (Table 1 and ESI, Fig. S6†) appeared at the shorter wavelength regions than that of TGA-stabilized CdTe, showing the existence of smaller size CdTe particles in the interlayer spaces. The blue-shifts of the onsets reflected that the silicate layers prevented the aggregation and assisted the distribution of the intercalated CdTe nanoparticles. The onset values of CdTe(36)-HDTMA-montmorillonite were less than those of CdTe(12)- and CdTe(60)-HDTMA-montmorillonites indicating that the average size of the intercalated CdTe nanoparticles contained in the hybrid was the smallest. The two absorption onsets observed in each UVvisible spectrum of the hybrids were thought to be related to the presence of two different types of the CdTe particles. We assumed that the smaller-sized CdTe particles were internally incorporated in the interlayer spaces and the bigger-sized CdTe particles were externally adsorbed on the clay surfaces, which was consistent with the TEM image of CdTe(36)-HDTMAmontmorillonite (Fig. 3b). In the absorption spectrum of CdTe(12)-HDTMA-montmorillonite (Fig. 5b), the prominent band centered at around 361 nm, which was first reported in this work, was thought to originate from the main specie that should be the intercalated CdTe nanoparticles. As a result of the absorbed CdTe in the hybrids, a small tail at around 500 nm, which is a typically optical feature of CdTe, arose. As the loading amount of the CdTe increases from 12 to 36 meg. per 100 g of montmorillonite, the intensity of the visible absorption band at around 336 nm was slightly decreased due to the decrease of the size of the intercalated CdTe, and that at around 500 nm enhanced, which meant that the amount of the adsorbed CdTe increased. This observation was consistent with the XRD result mentioned above. For CdTe(60)-HDTMA-montmorillonite, the absorption intensity at around 361 nm increased with increasing the loading amount of the CdTe and that at around 500 nm remained constant, interpreted to be due to the increase of the intercalated CdTe specie, that may lead to the narrow distance between the CdTe particles, which would subsequently result in the growth of particles. This interesting phenomenon was consistent with the decrease of the PL intensity mentioned below. The observations clearly indicated that the two different particle sizes of the CdTe particles present in the hybrids, and the particle size of the intercalated CdTe could be tuned by loading different amounts of the CdTe in the interlayer spaces.

The photoluminescence (PL) spectra of the three hybrids revealed the emission peaks at 499-575 nm (Fig. 6a-c). In contrast, the photoluminescence spectrum of TGA-stabilized CdTe showed a weak and broad emission peak at 591 nm (Fig. 6d) that was near the edge of its diffuse reflectance absorption spectrum (555 nm), indicating a characteristic of near-band edge emission. The PL spectra of CdTe in the glass

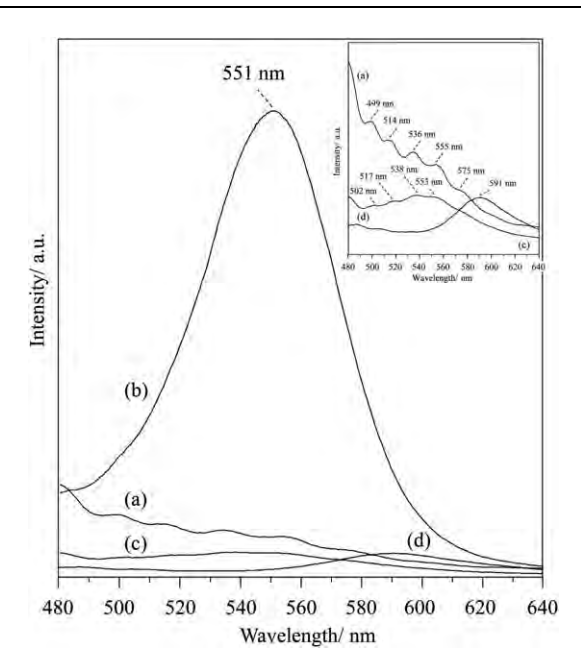
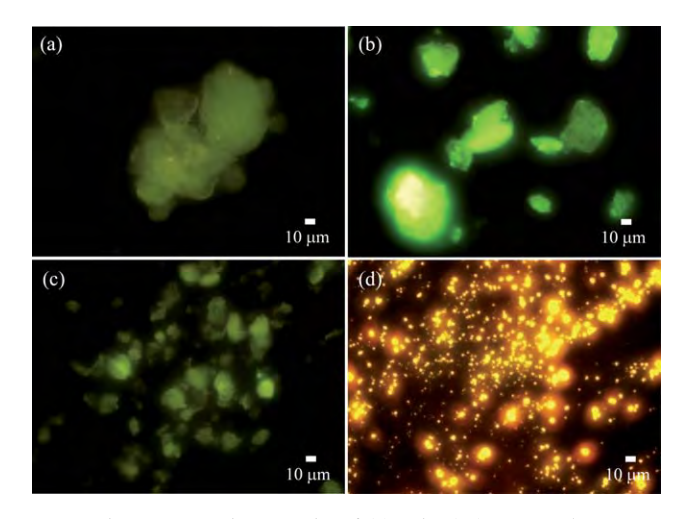


Fig. 6 Photoluminescence spectra of (a) CdTe(12)-HDTMA-montmorillonite, (b) CdTe(36)-HDTMA-montmorillonite, (c) CdTe(60)-HDTMA-montmorillonite and (d) TGA-stabilized CdTe.

matrix exhibited the emission peaks at 543–650 nm<sup>25</sup> and those of CdTe-PAMAM (poly(aminoamine)) showed an emission peak at 550 nm. 17 The maximum emission peak of thioglycolic acidstabilized CdTe nanoparticles was observed at ca. 559 nm. <sup>26</sup> The emission spectrum at 77 K of CdTe-zeolite showed the broad peaks centered at 563 and 750 nm that arose from defects. 18 The observed emission peaks of all hybrids occurred at 499–575 nm were ascribed to the presence of the CdTe nanoparticles in HDTMA-montmorillonite. Based on this result, the position of the visible emission band was blue-shifted by introducing the CdTe nanoparticles in the matrix, attributed to the deaggregation and/or the uniform dispersion of particles. Besides the possibility to tune the wavelength of visible emission, it is also able to tailor the luminescent intensity of the hybrids. As shown in Fig. 6, the emission peak of CdTe(36)–HDTMA-montmorillonite was of good symmetry with a full width at half-maximum (FWHM) of 50 nm, which was narrower than those values of CdTe(12)- and CdTe(60)–HDTMA-montmorillonites (Table 1). It is well known that a narrow FWHM of emission band reflects a narrow size-distribution, which leads to the high luminescent intensity.25 With the difference in loading amount of the CdTe that would affect the PL intensity, the emission band of CdTe(36)-HDTMA-montmorillonite served as the prominent photoluminescence of all hybrids. The luminescent intensity was lowered by 10–12 times when the loading amount of the CdTe in the hybrids was higher and lower than 36 meg. per 100 g of montmorillonite. The photoluminescence quantum yield of CdTe(36)-HDTMA-montmorillonite was 3.1% while those of CdTe(12)- and CdTe(60)-HDTMA-montmorillonites were 0.1%. The above observations showed that CdTe(36)-HDTMAmontmorillonite is a greatly luminescent material with intensely visible emission. As obviously seen in the fluorescence micrographs, TGA-stabilized CdTe exhibited red fluorescence (Fig. 7d), while those of the hybrids showed the green



**Fig. 7** Fluorescence photographs of (a) CdTe(12)–HDTMA-montmorillonite, (b) CdTe(36)–HDTMA-montmorillonite, (c) CdTe(60)–HDTMA-montmorillonite and (d) TGA-stabilized CdTe.

fluorescence (Fig. 7a-c), which was consistent with the position of their PL bands. In addition, among all of the hybrids, CdTe(36)-HDTMA-montmorillonite showed the highest emission peak and brightest green fluorescence, supporting the uniform and narrow size-distribution of the intercalated CdTe nanoparticles. Interestingly, the emission spectrum of CdTe(12)– HDTMA-montmorillonite and that of CdTe(60)-HDTMAmontmorillonite showed numerous emission bands (Fig. 6, inset). We believed that the appearance of the separated emission bands was related to the presence of the heterogeneous particle sizes of the intercalated CdTe nanoparticles. This result was consistent with the larger values of FWHM (Table 1). The low emission intensity of CdTe(12)- and CdTe(60)-HDTMAmontmorillonites due to the wide size-distribution of the intercalated CdTe suggested the combination of some adjacent CdTe nanoparticles that existed in the interlayer spaces, and that of TGA-stabilized CdTe was caused by the particle aggregation. The unique optical properties of the hybrids were thought to be closely related to the nature of the CdTe surface. The interaction between TGA-stabilized CdTe and microenvironment of montmorillonite led to the modification of the CdTe surface that resulted in the enhancement of PL intensity and the blue-shifts of the absorption onsets and emission bands. The excellent efficiency of the photoluminescence may provide the potential application in many fields including photocatalyst, biotechnology and so on.

#### **Conclusions**

The cadmium telluride nanoparticles prepared with the assistance of thioglycolic acid were intercalated into hexadecyltrimethylammonium-montmorillonites by a simple and low cost solid—liquid reaction. The incorporation of cadmium telluride in the interlayer spaces was confirmed by the appearance of absorption and emission peaks. The role of tailoring the amount of cadmium telluride in/on the clay surfaces was presented by changing the loading amount of cadmium telluride. The experimental results showed that the photoluminescence intensity was

quenched severely when the intercalated cadmium telluride increased, whereas the luminescent intensity was enhanced as the intercalated cadmium telluride decreased. The main reason for the enhancement of the photoluminescence was ascribed to the well separated intercalated cadmium telluride nanoparticles in the hybrids. On the basis of our results, it was conceivable that the microenvironment of montmorillonite was another stabilizing material for cadmium telluride nanoparticles to prevent the aggregation, control the size and size distribution, as well as to improve the thermal stability.

#### Acknowledgements

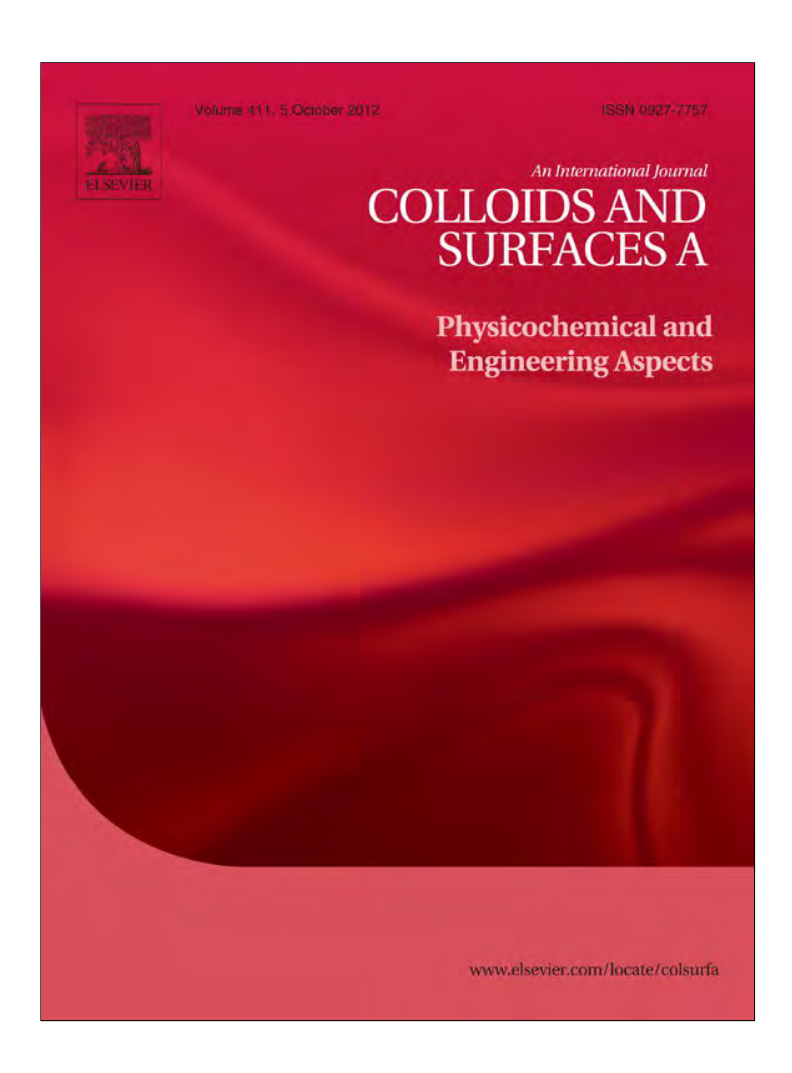
One of the authors (A.O.) thanks the Office of the Higher Education Commission, Thailand for support by grant fund under the program Strategic Scholarships for Frontier Research Network for the Join Ph.D. Program Thai Doctoral degree for this research, as well as Rajamangala University of Technology Isan, Thailand. This project was financially supported by the Thailand Research fund (TRF) and Khon Kaen University (grant no. DBG5380004), as well as the Center of Excellence for Innovation in Chemistry (PERCH-CIC), Commission on Higher Education, Ministry of Education, Thailand.

#### References

- 1 V. I. Klimov, J. Phys. Chem. B, 2006, 110, 16827-16845.
- 2 (a) E. A. Turner, Y. Huang and J. F. Corrigan, Eur. J. Inorg. Chem., 2005, 4465–4478; (b) A. L. Rogach, T. Franzl, T. A. Klar, J. Feldmann, N. Gaponik, V. Lesnyak, A. Shavel, A. Eychmüller, Y. P. Rakovich and J. F. Donegan, J. Phys. Chem. C, 2007, 111, 14628–14637; (c) R. J. Byers and E. R. Hitchman, Prog. Histochem. Cytochem., 2011, 45, 201–237.
- 3 M. Ogawa, in *Handbook of Layered Materials*, Marcel Dekker, New York, 2004, pp. 191–259.
- 4 M. Ogawa and K. Kuroda, Chem. Rev., 1995, 95, 399-438.
- 5 M. Ogawa and K. Kuroda, Bull. Chem. Soc. Jpn., 1997, 70, 2593– 2618.
- 6 O. Enea and A. J. Bard, J. Phys. Chem., 1986, 90, 301-306.
- I. Dékány, L. Turi, E. Tombácz and J. H. Fendler, *Langmuir*, 1995, 11, 2285–2292.
- 8 I. Dékány, L. Turi, A. Szücs and Z. Király, *Colloids Surf.*, A, 1998, 141, 405–417.
- 9 Z. Han, H. Zhu, S. R. Bulcock and S. P. Ringer, J. Phys. Chem. B, 2005, 109, 2673–2678.
- 10 (a) Y. Ide, A. Fukuoka and M. Ogawa, Chem. Mater., 2007, 19, 964–966; (b) Y. Ide, Y. Nakasato and M. Ogawa, Bull. Chem. Soc. Jpn., 2008, 81, 757–760; (c) Y. Ide, M. Matsuoka and M. Ogawa, J. Am. Chem. Soc., 2010, 132, 16762–16764.
- 11 (a) N. Khaorapapong, A. Ontam, S. Youngme and M. Ogawa, J. Phys. Chem. Solids, 2008, 69, 1107–1111; (b) N. Khaorapapong, A. Ontam and M. Ogawa, Mater. Lett., 2008, 62, 3722–3723; (c) N. Khaorapapong, A. Ontam, J. Khemprasit and M. Ogawa, Appl. Clay Sci., 2009, 43, 238–242; (d) N. Khaorapapong, A. Ontam and M. Ogawa, Appl. Clay Sci., 2010, 50, 19–24; (e) N. Khaorapapong, A. Ontam and M. Ogawa, Appl. Clay Sci., 2011, 51, 182–186; (f) N. Khaorapapong, N. Khumchoo and M. Ogawa, Mater. Lett., 2011, 65, 657–660; (g) A. Ontam, N. Khaorapapong and M. Ogawa, J. Colloid Interface Sci., 2011, 357, 554–557.
- 12 J. M. Tsay, M. Pflughoefft, L. A. Bentolila and S. Weiss, J. Am. Chem. Soc., 2004, 126, 1926–1927.
- 13 Z. Tang, N. A. Kotov and M. Giersig, Science, 2002, 297, 237-240.
- 14 X. Feng, Q. Shang, H. Liu, H. Wang, W. Wang and Z. Wang, J. Phys. Chem. C, 2009, 113, 6929–6935.
- 15 M. S. Abd El-sadek and S. Moorthy Babu, *Phys. B*, 2010, **405**, 3279–3283
- 16 Z. Kang, Y. Zhang, H. Menkara, B. K. Wagner, C. J. Summers, W. Lawrence and V. Nagarkar, Appl. Phys. Lett., 2011, 98, 181914.

- 17 Y. Zeng, C. Tang, H. Wang, J. Jiang, M. Tian, G. Shen and R. Yu, Spectrochim. Acta, Part A, 2008, 70, 966–972.
- 18 E. S. Brigham, C. S. Weisbecker, W. E. Rudzinski and T. E. Mallouk, Chem. Mater., 1996, 8, 2121-2127.
- 19 F. Gao, C. Lv, J. Han, X. Li, Q. Wang, J. Zhang, C. Chen, Q. Li, X. Sun, J. Zheng, L. Bao and X. Li, J. Phys. Chem. C, 2011, 115, 21574-21583.
- 20 H. Zhang, Z. Zhou, B. Yang and M. Gao, J. Phys. Chem. B, 2003, **107**, 8–13.
- 21 O. Kozák, P. Praus, K. Kočí and M. Klementová, J. Colloid Interface Sci., 2010, 352, 244-251.
- 22 I. A. Pastre, I. D. N. Oliveira, A. B. S. Moitinho, G. R. de Souza, E. Y. Ionashiro and F. L. Fertonani, J. Therm. Anal. Calorim., 2004, 75, 661-669.
- 23 G. Matuschek, A. Finke, W. Thumm and A. Kettrup, Thermochim. Acta, 1995, 263, 23-28.
- 24 Y. Song, X. Cao, Y. Guo, P. Chen, Q. Zhao and G. Shen, Chem. Mater., 2009, 21, 68-77.
- 25 C. L. Li, M. Ando and N. Murase, J. Non-Cryst. Solids, 2004, 342, 32 - 38.
- 26 M. Gao, S. Kirstein, H. Möhwald, A. L. Rogach, A. Kornowski, A. Eychmüller and H. Weller, J. Phys. Chem. B, 1998, 102, 8360–8363.

Provided for non-commercial research and education use. Not for reproduction, distribution or commercial use.



This article appeared in a journal published by Elsevier. The attached copy is furnished to the author for internal non-commercial research and education use, including for instruction at the authors institution and sharing with colleagues.

Other uses, including reproduction and distribution, or selling or licensing copies, or posting to personal, institutional or third party websites are prohibited.

In most cases authors are permitted to post their version of the article (e.g. in Word or Tex form) to their personal website or institutional repository. Authors requiring further information regarding Elsevier's archiving and manuscript policies are encouraged to visit:

http://www.elsevier.com/copyright

#### Author's personal copy

Colloids and Surfaces A: Physicochem. Eng. Aspects 411 (2012) 27-33



Contents lists available at SciVerse ScienceDirect

# Colloids and Surfaces A: Physicochemical and Engineering Aspects

journal homepage: www.elsevier.com/locate/colsurfa



## An incorporation of cadmium selenide at organophillic surface of clay mineral

Areeporn Ontama, Nithima Khaorapaponga,\*, Makoto Ogawab

- a Department of Chemistry and Center of Excellence for Innovation in Chemistry, Faculty of Science, Khon Kaen University, Khon Kaen 40002, Thailand
- b Department of Earth Sciences and Graduate School of Creative Science and Engineering, Waseda University, 1-6-1 Nishiwaseda, Shinjuku-ku, Tokyo 169-8050, Japan

#### HIGHLIGHTS

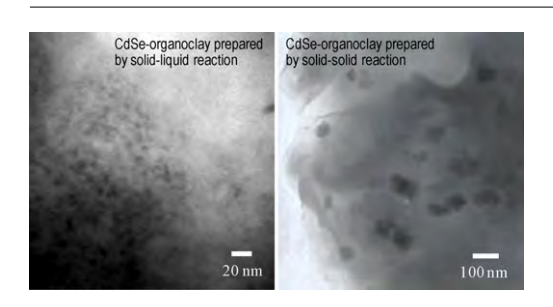
- ► Hybridization of CdSe and organoclay was investigated by a colloidal process.
- CdSe nanoparticles in organoclay showed blue-shift of onset and emission band.
- ► Size of CdSe in organoclay prepared by colloidal method was smaller than other one.

#### ARTICLE INFO

Article history: Received 26 April 2012 Received in revised form 27 June 2012 Accepted 30 June 2012 Available online 16 July 2012

Keywords: Cadmium selenide Hybrid Montmorillonite Optical property Photoluminescence

#### GRAPHICAL ABSTRACT



#### ABSTRACT

hybridization cadmium selenide and organically modified cetyltrimethylammonium-montmorillonite, was investigated by a simply colloidal process. The hybrid was characterized by powder X-ray diffraction, thermal analysis, transmission electron microscopy, as well as Raman, UV-visible and photoluminescence spectroscopies. The blue-shift of the absorption onset and the appearance of the luminescence band at the wavelength of 565 nm for cadmium selenide-cetyltrimethylammonium-montmorillonite were thought to be caused by the restricted microenvironment of cetyltrimethylammonium-montmorillonite that affected the particle size and growth of the cadmium selenide nanoparticles. Transmission electron micrograph showed that the cadmium selenide nanoparticles with the diameters of 7.00–10.10 nm were intercalated in the interlayer space. The enhancement of the emission intensity of the stored hybrid indicated that solid surface of cadmium selenide in the adsorbed state could be tailored by cetyltrimethylammonium-montmorillonite.

© 2012 Elsevier B.V. All rights reserved.

#### 1. Introduction

The study of semiconductor nanoparticles is one of the intensive topics in nanochemistry and nanotechnology over the past several years. The nanoparticles have sized-tunable emissions due to quantum size effect and may lead to novel optical and electrical properties. Hybridization of semiconductors with ordered structures is a promising way to investigate novel functional materials though the controlled fabrication of one-, two- and three-dimensional nanostructures [1]. The utilization of two- and

three-dimensional inorganic materials such as layered inorganic materials, mesoporous silica, SBA-15 and MCM-41, for surface modification of semiconductors including metal chalcogenides and metal oxides has been investigated [2–7].

Among possible layered inorganic solids, smectite, a group of layered clay minerals including montmorillonite, provides attractive features such as large surface area, swelling behaviour, adsorptive and ion-exchange properties for organizing organic and/or inorganic guest species. The organic modification of smectites leads to a novel functional material by further accommodation of functional units including semiconductors into the organically modified smectites [8,9]. A large variety of layered inorganic-semiconductor hybrids is available depending on the host-guest and guest-guest interactions [2,3,10–12]. One of our

<sup>\*</sup> Corresponding author. Tel.: +66 899405490; fax: +66 43202373. E-mail address: nithima@kku.ac.th (N. Khaorapapong).

research interests has been focused on hybrids of metal clusters and semiconductors [13–28]. The confinement of semiconductor nanoparticles in the interlayer spaces of montmorillonite has been reported by colloidal method and solid–solid reaction. The optical properties of the hybrids were found to be dependent on the microenvironment, the interlayer space of montmorillonite [6,22–28].

Cadmium selenide (CdSe), one of the II–VI group semiconductors, has attracted increasing attention due to their promising applications in optical and optoelectric devices, as well as biological imaging [29,30]. For the realization, the modification of the optical properties of cadmium selenide arose from their size, morphology, matrix, dispersion, and most importantly, the surface modification by the interactions with surrounding media [29–31]. Accordingly, the organization of cadmium selenide semiconductor on layered inorganic materials is worth studying to tailor the size, the shape, and the surface chemistry of the nanoparticle via the host–guest and guest–guest interactions.

This work presents a relatively simple and low cost process to prepare cadmium selenide nanoparticle in a two dimensionally restricted environment, the interlayer space of organically modified montmorillonite. There are a number of methods for the preparation of cadmium selenide nanoparticle, such as solvothermal, ultrasonic irradiation and organometallic precursor methods in order to control size, shape and surface of semiconductor nanoparticles [2,3,32-34]. However, the former processes required the complicated equipments or expensive organometallic precursors. It was also reported that the optical properties of entrapped cadmium selenide in synthetic clays, layered double hydroxide (LDH) and Laponite, were different from the bulk materials [2,3]. Our hybrid materials used a natural clay mineral, montmorillonite, which has district microenvironment, for immobilizing cadmium selenide nanoparticles by changing methodology. The increase of luminescent intensity of organically stabilized cadmium selenide immobilized on hydrophilic surface of montmorillonite was reported in our preliminary communication [28]. To obtain more insight into the sized-tunable phenomena of cadmium selenide, in this study, we extended our work to incorporation of neutral cadmium selenide nanoparticles, which was obtained by simple solid-liquid reaction using cadmium(II) ion and disodium selenosulfite as cadmium selenide precursors, in organophillic montmorillonite, cetyltrimethylammonium-montmorillonite. We also studied the effect of the organophillic montmorillonite on the optical behavior of cadmium selenide in the adsorbed states up to 29 weeks because the pristine cadmium selenide is unstable to aggregate upon exposure to air, in LDH and Laponite systems [2,3], no such behavior was observed. Additionally, during the encapsulation of cadmium selenide, the effect of cetyltrimethylammonium-montmorillonite on the particle size, size distribution and surface of cadmium selenide nanoparticles was comparatively examined between different reactions. The hybrid, cadmium selenide-cetyltrimethylammonium-montmorillonite, is expected to have a greatly potential application as a new generation of photoluminescent materials.

#### 2. Experimental

#### 2.1. Materials

Sodium–montmorillonite (Kunipia F, Kunimine Industries, the reference clay sample of the Clay Science Society of Japan) was used as a host material. The cation exchange capacity (CEC) is 119 meq/100 g of clay. Cetyltrimethylammonium bromide (CTAB) and selenium (Se) powder were purchased from Sigma–Aldrich. Cadmium(II) sulfate octahydrate (CdSO<sub>4</sub>·8H<sub>2</sub>O) was obtained by

Carlo Erba Reagenti. Disodium sulfite (Na<sub>2</sub>SO<sub>3</sub>) was supplied by APS Finechem. All chemicals are analytical grade and were used without further purification.

#### 2.2. Preparation of CdSe-CTA-montmorillonite hybrid

Cetyltrimethylammonium–montmorillonite was prepared by a conventional ion exchange reaction between an aqueous solution of cetyltrimethylammonium (CTA) bromide and an aqueous suspension of montmorillonite. The amount of the added CTA cations was equal to the CEC of Na-montmorillonite. The mixture was allowed to react by magnetic stirring at 70 °C for one day. Then, the dispersion of CTA–montmorillonite was added with an aqueous solution of cadmium(II) sulfate (molar ratio of Cd<sup>2+</sup>:CTA was 1:1) and that of disodium selenosulfite (Na<sub>2</sub>SeSO<sub>3</sub>) synthesized by refluxing an aqueous solution of disodium sulfite and selenium power under stirring for one day. The reactants were stirred for 2 h at room temperature. The resulting solid was separated by centrifugation and washed with deionized water. The product was dried in a desiccator with silica gel at room temperature for 3 days.

#### 2.3. Characterization

Powder X-ray diffraction data were collected on a Bruker D8 ADVANCE diffractometer using monochromatic CuK $\alpha$  radiation. TG–DTA curves were obtained on a Perkin Elmer Pyris Diamond TG–DTA instrument at a heating rate of  $10\,^{\circ}\text{C}\,\text{min}^{-1}$  under a dried air flow using  $\alpha$ -alumina ( $\alpha$ -Al $_2$ O $_3$ ) as the standard material. TEM image was taken on a Hitachi H-7650 transmission electron microscope with an accelerating voltage of 120 kV. Raman spectrum was measured on a Jobin Yvon T64000 System Raman spectrometer with a 30 mW argon ion laser operating at 514.50 nm for excitation. Diffuse reflectance spectra of the solid samples were performed on a Shimadzu UV–VIS–NIR–3101PC scanning spectrophotometer using an integrated sphere. Photoluminescence spectra were recorded on a Shimadzu RF–5301PC spectrofluorophotometer in the wavelength range of 300–900 nm with the excitation at 450 nm.

#### 3. Results and discussion

#### 3.1. Adsorption of CdSe into CTA-montmorillonite

As a result of conventional solid-liquid reaction, the color of CTA-montmorillonite changed from white to orange. The change in the color of CTA-montmorillonite suggested the presence of CdSe in the product. Hereafter the product was denoted as CdSe-CTA-montmorillonite. The basal spacing of CTA-montmorillonite was 2.06 nm (not shown). The gallery height was obtained by subtracting the thickness of the silicate layer, dehydrated montmorillonite, (ca. 0.96 nm) from the observed basal spacing to be 1.10 nm. Considering the expansion of the interlayer space of CTA-montmorillonite and the size of CTA cation, the CTA cations arranged in kinked alkyl chain layer or monolayer paraffin type in the interlayer space of montmorillonite [9]. The XRD pattern of pure CdSe revealed the broad diffraction peaks due to cubic CdSe (JCPDS 19191) at  $2\theta$  = 25, 41, 48 degree (Fig. 2, inset). The XRD pattern of the hybrid, CdSe-CTA-montmorillonite, did not show the reflections due to CdSe crystal, suggesting that smaller sized CdSe was intercalated in the interlayer space and/or the amount of CdSe was too small to be detected by the XRD. The basal spacing of CTA-montmorillonite (2.06 nm) was not increased further after adding CdSe in the interlayer space of CTA-montmorillonite (Fig. 1a), indicating that the intercalation of CdSe did not affect the gallery height of CTA-montmorillonite. Since the XRD pattern of the hybrid showed the basal spacing similar to that of CTA-montmorillonite, the incorporation of CdSe nanoparticles in

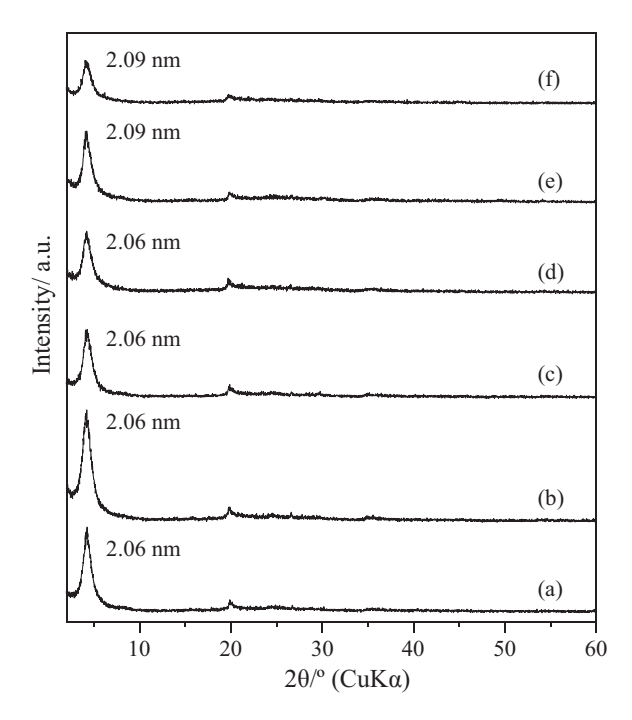


**Fig. 1.** XRD patterns of (a) CdSe-CTA-montmorillonite, (b) CdSe-CTA-montmorillonite after storage for 4 weeks, (c) 13 weeks, (d) 20 weeks, (e) 28 weeks, (f) 29 weeks.

the interlayer space of CTA-montmorillonite was controlled by the restricted microenvironment of CTA-montmorillonite. In addition, we assumed that the adsorption of neutral CdSe nanoparticles in between the silicate layers was promoted by the interactions with the hydrophobic surface of CTA-montmorillonite. When the product was stored for longer periods (4–29 weeks), the basal spacings of the stored CdSe-CTA-montmorillonite were not significantly changed (ca. 2.06–2.09 nm) (Fig. 1b–f) and there was no reflection due to CdSe or the other compounds was observed in the XRD patterns of the stored product, indicating to the stability of CdSe-CTA-montmorillonite under the ambient conditions.

In comparison, the intercalation of pre-synthesized CdSe powder (deep red color) prepared by the previous method [35] into CTA-montmorillonite was investigated by solid-solid reaction. The mixture of CTA-montmorillonite and CdSe (molar ratio of Cd<sup>2+</sup>:CTA was 1:1) was ground manually with an agate mortar and a pestle at room temperature for 10-15 min. The product obtained by solid-solid reaction was abbreviated as CdSe-CTA-montmorillonite(s). The basal spacing of CdSe-CTA-montmorillonite(s) was 2.13 nm (Fig. 2a), indicating the expansion of the interlayer space of 1.17 nm. No diffraction peak of CdSe was detected in the X-ray diffraction pattern of CdSe-CTA-montmorillonite(s), supporting that the pre-synthesized CdSe was adsorbed into CTA-montmorillonite and/or the amount of the un-intercalated CdSe was very little to show the reflection on the XRD pattern. When CdSe-CTA-montmorillonite(s) was stored in a desiccator with silica gel for 4 weeks, the basal spacing was observed at  $d_{001} = 2.01 \,\mathrm{nm}$  without the reflections due to CdSe crystal. The slight decrease of the basal spacing of CdSe-CTA-montmorillonite(s) (4 weeks) was thought to be caused by the removal of adsorbed water during storage in the desiccator. The result indicated that the intercalated species including CTA and/or CdSe still maintained in the interlayer space or a small amount of CdSe existed at the outer surface of CTA-montmorillonite. This could be confirmed further by the TEM image.

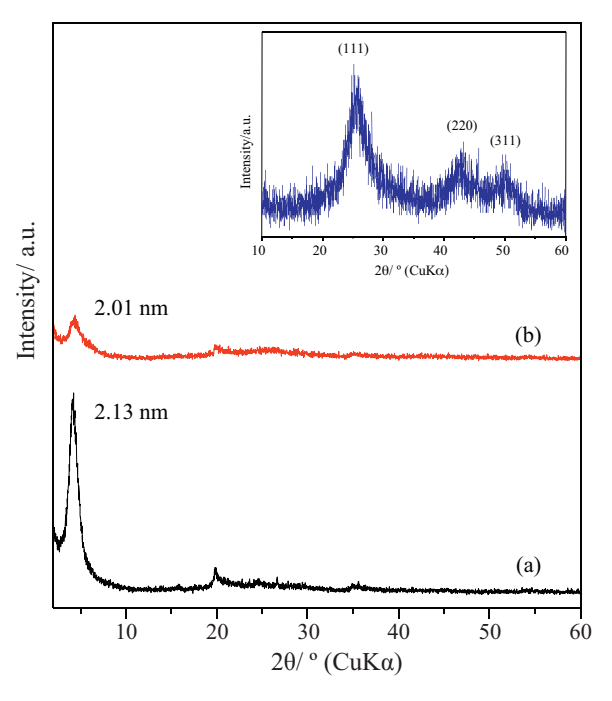


**Fig. 2.** XRD patterns of (a) CdSe-CTA-montmorillonite(s), (b) CdSe-CTA-montmorillonite(s) after storage for 4 weeks, (inset) pure CdSe.

#### 3.2. Formation of CdSe-CTA-montmorillonite hybrid

The TEM observation was performed to investigate the size and size distribution of CdSe in CTA-montmorillonite. The CdSe nanoparticles, which showed the darker contrast than the silicate layer due to the effect of reflection, were observed in the micrograph of the hybrid (Fig. 3). It was seen that the round shape CdSe nanoparticles with the average size of ca. 7.00-10.10 nm were homogeneously dispersed in the interlayer space of CTA-montmorillonite. Taking the gallery height of the hybrid (1.10 nm) and the average size of the nanoparticles (ca. 7.00–10.10 nm) into account, it was thought that the intercalated CdSe nanoparticles were flat in shape with the thickness of 1.10 nm as well as the diameter of around 7.00-10.10 nm, and have the planar orientation parallel to the silicate layers. We have reported that the CTA modified CdSe nanoparticles prepared in montmorillonite by self assembly method [28] gave CdSe nanoparticles, which have the average size a bit smaller than the immobilized CdSe prepared in this work (the thickness of 0.99 nm and the diameter of 3.00–6.00 nm). It was thought that the growth of CdSe particles obtained by the present solid-liquid reaction could occur before the intercalation process, which was also supported by the TEM image of CdSe-CTA-montmorillonite(s). On the contrary, the TEM image of CdSe-CTA-montmorillonite(s) (4 weeks) (Fig. S1, Supporting Information) showed the small amount of the intercalated CdSe (10.00–30.00 nm, not shown) and the large amount of cubic-shaped CdSe crystal with the average size of around 50.00–70.00 nm, which was in agreement with the particle size of the pristine CdSe, indicating that most of the pre-synthesized CdSe aggregated easily before grinding with CTA-montmorillonite. Therefore, CdSe could be interacted with the modified montmorillonite only on the external surface. These results supported that the aggregation and/or size distribution of CdSe were controlled by the restricted microenvironment of CTA-montmorillonite. Moreover, we have found that the encapsulation time of CdSe into CTA-montmorillonite is also very important for avoiding the growth of CdSe particles. The average size of CdSe nanoparticles in CTA-montmorillonite prepared by solid-liquid reaction was almost ten times smaller than those

A. Ontam et al. / Colloids and Surfaces A: Physicochem. Eng. Aspects 411 (2012) 27-33

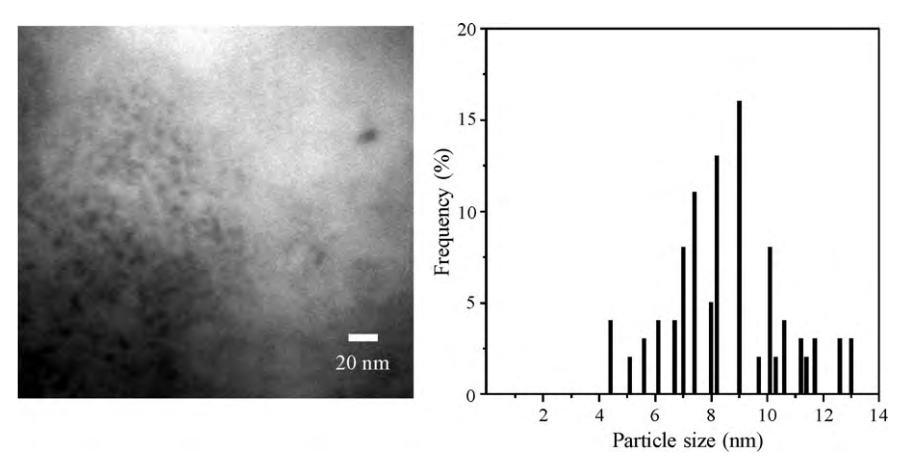
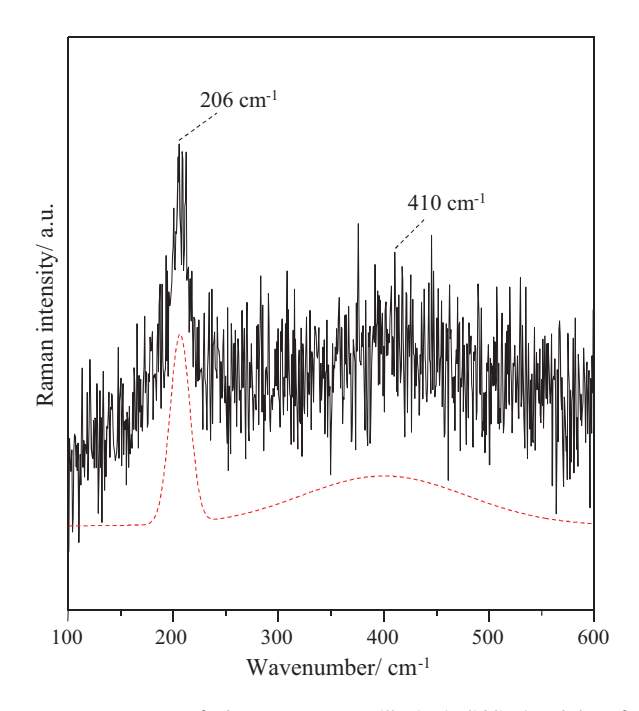


Fig. 3. TEM image of CdSe-CTA-montmorillonite.

obtained by solid-solid reaction. It was thought that by solid-liquid reaction, CdSe particles had short time to grow up because the formation of CdSe and the intercalation were occurred in the same reacting flask, while by solid-solid reaction, the pristine CdSe took a few days to dry and aggregate before the encapsulation.

The Raman spectrum of CdSe–CTA–montmorillonite exhibited the bands at 206 and 410 cm<sup>-1</sup> (Fig. 4). The two Raman bands were due to the first-harmonic longitudinal optical phonon (1LO) and the second-harmonic longitudinal optical phonon (2LO) of CdSe particles [36]. It was reported that as a decrease of the size of nanocrystals, more red-shift and more broadening of the peak width were observed in the Raman spectra [37]. Compared with the 1LO band of pure CdSe (210 cm<sup>-1</sup>) as well as the 2LO band of CdSe–CTA–montmorillonite(s) (414 cm<sup>-1</sup>) (not shown), the red-shift and also significant broadening of the 1LO and 2LO bands were observed for CdSe–CTA–montmorillonite (206 and 410 cm<sup>-1</sup>), suggesting that the particle size of CdSe in CTA–montmorillonite prepared by solid–liquid reaction was smaller than that of CdSe obtained by solid–solid reaction and pure CdSe. The observed



**Fig. 4.** Raman spectrum of CdSe–CTA–montmorillonite (solid line) and that of the spectrum fitted by Gaussian (dashed line).

Raman bands of the hybrid were assigned to the immobilization of CdSe particles in CTA-montmorillonite.

The TG curve of pure CdSe exhibited three evident mass losses (Fig. S2, Supporting Information); namely, the removal of adsorbed water occurred below 410 °C, the oxidation and formation of individual metal oxides detected between 410 and 800°C and the sublimation of the oxide compounds revealed from 800-1000 °C [38,39]. Three steps of mass losses were also seen in the TG curve of CdSe-CTA-montmorillonite. The first mass loss observed below 200 °C corresponding to the endothermic peaks at 46 and 150 °C in the DTA curve was interpreted to the removal of water adsorbed at the clay surface of CdSe-CTA-montmorillonite. The second mass loss occurred between 200 and 570 °C corresponding to the exothermic peaks at 311 and 366 °C suggested the decomposition of the intercalated organic matter in montmorillonite. The last mass loss detected between 570 and 800 °C was interpreted to the thermal decomposition of CdSe and dehydroxylation caused by breaking of the hydroxyl group of montmorillonite. This result confirmed the presence of CdSe particles in the hybrid material. The intercalated CdSe was destroyed at the temperature higher than pure CdSe, suggesting that the decomposition of CdSe nanoparticles was protected by the microenvironment of montmorillonite.

#### 3.3. Optical properties of the hybrid

spectrum The diffuse reflectance absorption CdSe-CTA-montmorillonite is shown in Fig. 5 together with those of pristine CdSe and montmorillonite. The absorption spectrum of the as-prepared CdSe-CTA-montmorillonite (Fig. 5b) showed an absorption onset at 593 nm, as well as two shoulders at around 365 and 532 nm, and that of pure CdSe (Fig. 5c) revealed an onset at 632 nm. While no absorption peak in visible region was observed for montmorillonite (Fig. 5a). The shoulders showed the blue- or red-shift compared with the absorption bands of CdSe-LDH composites with various compositions (531-562 nm) [2], Laponite/CdSe-aniline film due to aniline tetramer (560 nm) and CdSe-aniline (440 and 350 nm) [3], as well as those of CdSe/SBA-15 composites obtained at different reaction times (512, 530 and 542 nm) [40]. The spectral shifts supported our successful immobilization of CdSe in the hybrid and the host-guest interactions. It is well known that the smallersized CdSe nanoparticles showed the blue-shift of the absorption onset compared with the larger ones. The absorption onset of CdSe-CTA-montmorillonite (593 nm) was blue-shifted compared with that of pure CdSe (632 nm), suggesting that the particle size of CdSe incorporated in the interlayer space of CTA-montmorillonite was smaller than the size of pure CdSe. Since CdSe prepared in an

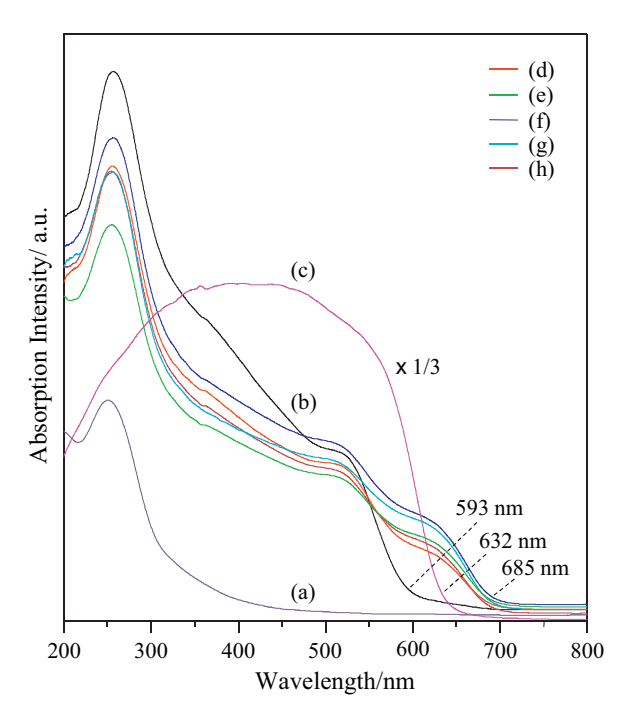


**Fig. 5.** Diffuse reflectance absorption spectra of (a) Na-montmorillonite, (b) CdSe–CTA–montmorillonite, (c) as-prepared CdSe, (d) CdSe–CTA–montmorillonite after storage for 4 weeks, (e) 13 weeks, (f) 20 weeks, (g) 28 weeks, (h) 29 weeks.

aqueous medium trended to aggregate [41], an aggregation of CdSe particles in the hybrid prepared by the present solid–liquid reaction could be prevented by the restricted microenvironment of CTA–montmorillonite. Thus the immobilization of CdSe in the interlayer space of CTA–montmorillonite provided the smaller-sized CdSe particles that could cause the change in the optical behavior.

To confirm the effect of CTA-montmorillonite on the absorption onset, the products were allowed to stand in desiccator at room temperature for longer periods (4-29 weeks), after the storage, CdSe-CTA-montmorillonite exhibited a new absorption onset at the higher wavelength (685 nm) as can be seen in Fig. 5. The two absorption onsets observed in UV-visible spectrum of CdSe-CTA-montmorillonite were thought to be related to two species of CdSe particles; namely, the specie of smaller-sized CdSe particles revealed the absorption onset in the shorter wavelength and that of the bigger-sized CdSe in the longer region. The redshift of the new absorption onset of CdSe-CTA-montmorillonite indicated that the size of CdSe gradually increased most likely due to guest-guest interactions. The absorption onset of the asprepared CdSe (632 nm) was red-shifted to 680 nm after the storage for 20-29 weeks, indicating that the aggregation of pure CdSe particles took place faster than the CdSe nanoparticles in the adsorbed state (Fig. S3, Supporting Information). The aggregation of pre-synthesized CdSe semiconductor resulted in the delocation of energy states, and it could be prevented by the restricted environment of montmorillonite. Therefore, it was believed that montmorillonite played a major role in controlling the growth and/or aggregation of CdSe particles.

In the photoluminescence spectrum of CdSe–CTA–montmorillonite (Fig. 6), the luminescence band was observed at 565 nm. On the other hand, no emission band was seen in the luminescence spectra of pure CdSe and CdSe–CTA–montmorillonite(s) due to the formation of bulk CdSe. The band due to the incorporated CdSe observed at around 565 nm for CdSe–CTA–montmorillonite was also displayed for other CdSe-organic/inorganic composites and comparatively blue- or red-shifted by changing the

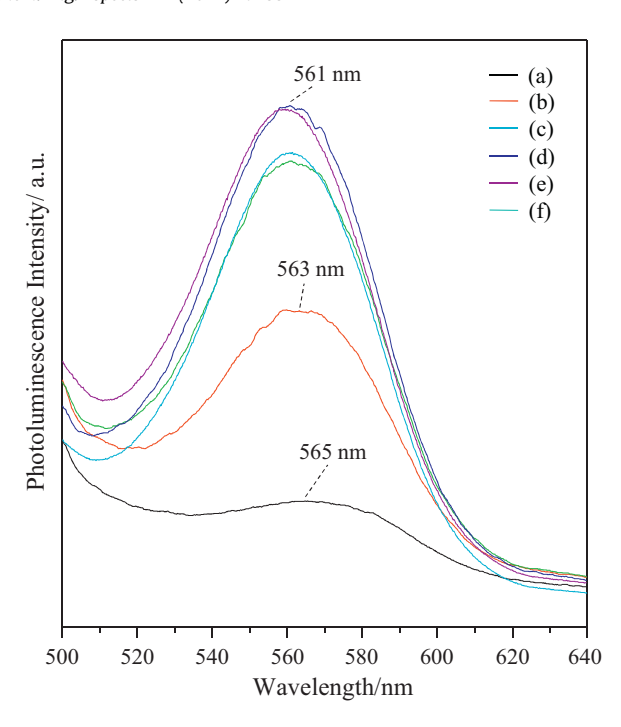


**Fig. 6.** Luminescence spectra of (a) CdSe–CTA–montmorillonite, (b) CdSe–CTA–montmorillonite after storage for 4 weeks, (c) 13 weeks, (d) 20 weeks, (e) 28 weeks, (f) 29 weeks.

matrix and/or the preparation conditions [40,42-44]. We have reported that the photoluminescence band of the CTA modified CdSe-montmorillonite hybrid obtained by self assembly appeared at 507 and 550 nm [28]. The emission band of CdSe-CTA-montmorillonite prepared in this study (565 nm) was red-shifted compared to those observed in our previous report, supporting the formation of a bit bigger-sized CdSe in CTA-montmorillonite, which was consistent with the particle size estimated from the expansion of the interlayer space and the TEM image mentioned above. The emission band was not seen in the photoluminescence spectra of pure CdSe and CdSe-CTA-montmorillonite(s), showing the emission quenching of bulk CdSe [45]. This result supported that the aggregation of CdSe particle could be prevented by the surrounding environment of montmorillonite and the anti-aggregation itself caused the changes in the optical properties of CdSe, which was consistent with the UV-visible result mentioned above.

The luminescence intensity of CdSe-CTA-montmorillonite observed at around 561-563 nm increased (four times) when the hybrid was stored in the desiccator up to 20 weeks, indicating that the growth of some CdSe particles in the stored hybrid (as mentioned above) did not seem to quench the photoluminescence intensity, and the intensity slightly decreased after storage longer. We assumed that the increase of the luminescence intensities supported the surface modification of the adsorbed CdSe nanoparticles, which was caused by the microenvironment of CTA-montmorillonite. Surprisingly, CdSe-CTA-montmorillonite(s) stored for 4 weeks showed a very weak emission peak centered at 583 nm and the photoluminescence intensity of the product gradually increased for two times after 10 months (Fig. S4, Supporting Information), indicating that the photoluminescence efficiency of CdSe was improved by the confinement of CTA-montmorillonite. While no emission band was observed for pure CdSe even after storage for 29 weeks or longer periods. The appearance of the emission band (583 nm) and the enhancement of the photoluminescence intensity observed for CdSe-CTA-montmorillonite(s) were ascribed to be related to the

errors in structure creation such as stoichiometric defect (Cd<sup>2+</sup> and Se<sup>2-</sup> vacancies) and dangling bond [46] due to the interaction between CdSe and CTA-montmorillonite. Because montmorillonite can act as both electron acceptor and donor, we supposed that the emission efficiency may be affected by the charge transfer from montmorillonite, which has dangling bonds on its crystal edges [47], to Cd<sup>2+</sup> and/or Se<sup>2-</sup> vacancies, otherwise, it resulted from the transition of electrons from the immobilized free radicals or dangling bonds of the adsorbed CdSe to montmorillonite.

The aggregation of cadmium selenide particles resulted in quenching of photoluminescence intensity, and the quenching was lost when cadmium selenide was immobilized in CTA-montmorillonite. Thus, these present results proved that CTA-montmorillonite is a greatly potential matrix for preventing the aggregation and modifying the surface of the semiconductor particles that can change the optical properties. Further studies are being made in order to control the size, distribution and surface of semiconductors by using other inorganic matrices for development of photofunctional materials and photocatalysts.

#### 4. Conclusions

Cadmium selenide–cetyltrimethylammonium–montmorillonite hybrid was prepared via a simple adsorption of cadmium selenide nanoparticles from colloidal solution. The hybrid in which the adsorbed cadmium selenide nanoparticles were well-dispersed in the interlayer space of cetyltrimethylammonium–montmorillonite showed the blue-shift of the absorption onset and emission maximum. The increase in the luminescence intensity of the stored products was ascribed to host–guest and guest–guest interactions. The average size of the semiconductors incorporated in cetyltrimethylammonium–montmorillonite by the colloidal method was smaller than that obtained by solid–solid reaction. It is feasible that the modified montmorillonite could tune the size, distribution and surface of cadmium selenide by tailoring the reaction processes.

In the study of cadmium selenide-mesoporous SBA15, the size of cadmium selenide insides the matrix channels can be controlled easily by varying the reaction times [40]. Venugopal et al. have reported that the absorption maxima and band gap energy of cadmium selenide can be tailored by altering the composition of the composites [2]. Kehlbeck and colleagues have shown that the density of polymer (polyaniline) covered on the cadmium selenide nanoparticles for Laponite/cadmium selenide-polyaniline can optimize photoefficiencies [3]. To date, our group has reported the effect of layered clay mineral, montmorillonite, on size, distribution and surface modification of cadmium selenide upon different reaction procedures. The controllability of the properties and the variation of the optical behaviors of cadmium selenide in the absorbed states owing to the effect of natural clay mineral and preparation method may lead to development of attractive nanohybrids using other layered inorganic matrices and/or semiconductors for such application of photocatalyst, optoelectrical device, biological imaging and so on.

#### Acknowledgements

One of the authors (A.O.) thanks the Office of the Higher Education Commission, Thailand, for supporting by a grant fund under the program Strategic Scholarships for Frontier Research Network for the Join Ph.D. Program Thai Doctoral degree for this research. The financial supports from the Thailand Research fund (TRF) and Khon Kaen University (Grant DBG5380004), and the Center of Excellence for Innovation in Chemistry (PERCH-CIC), Commission on Higher Education, Ministry of Education, Thailand are acknowledged. We

also thank the Hitachi High-Technologies for partial support of the TEM instrument.

#### Appendix A. Supplementary data

Supplementary data associated with this article can be found, in the online version, at http://dx.doi.org/10.1016/j.colsurfa. 2012.06.038.

#### References

- [1] M. Ogawa, Photoprocess in clay-organic complexes, in: S.M. Auerbach, K.A. Carrado, P.K. Dutta (Eds.), Handbook of Layered Materials, Dekker, New York, 2004, pp. 191–206.
- [2] B.R. Venugopal, N. Ravishankar, C.R. Perrey, C. Shivakumara, M. Rajamathi, Layered double hydroxide-CdSe quantum dot composites through colloidal processing: effects of host matrix-nanoparticle interaction on optical behavior, J. Phys. Chem. B 110 (2006) 772–776.
- [3] J.D. Kehlbeck, M.E. Hagerman, B.D. Cohen, J. Eliseo, M. Fox, W. Hoek, D. Karlin, E. Leibner, E. Nagle, M. Nolan, I. Schaefer, A. Toney, M. Topka, R. Uluski, C. Wood, Directed self-assembly in laponite/CdSe/polyaniline nanocomposites, Langmuir 24 (2008) 9727–9738.
- [4] B.G. Trewyn, S. Giri, I.I. Slowing, V.S.-Y. Lin, Mesoporous silica nanoparticle based controlled release, drug delivery, and biosensor systems, Chem. Commun. (2007) 3236–3245.
- [5] W. Xu, Y. Liao, D.L. Akins, Formation of CdSe nanoparticles within modified MCM-41 and SBA-15, J. Phys. Chem. B 106 (2002) 11127-11131.
- [6] K. Mogyorósi, I. Dékány, J.H. Fendler, Preparation and characterization of clay mineral intercalated titanium dioxide nanoparticles, Langmuir 19 (2003) 2938–2946.
- [7] O.P. Tkachenko, K.V. Klementiev, E. Löffler, I. Ritzkopf, F. Schüth, M. Bandyopadhyay, S. Grabowski, H. Gies, V. Hagen, M. Muhler, L. Lu, R.A. Fischer, W. Grünert, The structure of zinc and copper oxide species hosted in porous siliceous matrices, Phys. Chem. Chem. Phys. 5 (2003) 4325–4334.
- [8] M. Ogawa, K. Kuroda, Photofunctions of intercalation compounds, Chem. Rev. 95 (1995) 399–438.
- [9] M. Ogawa, K. Kuroda, Preparation of inorganic-organic nanocomposites through intercalation of organoammonium ions into layered silicates, Bull. Chem. Soc. Jpn. 70 (1997) 2593–2618.
- [10] N.A. Kotov, K. Putyera, J.H. Fendler, E. Tombácz, I. Dékány, Cadmium sulfide particles in organomontmorillonite complexes, Colloids Surf., A: Physicochem. Eng. Aspects 71 (1993) 317–326.
- [11] I. Dékány, L. Turi, E. Tombácz, Preparation of size-quantized CdS and ZnS particles in nanophase reactors provided by binary liquids adsorbed at layered silicates, Langmuir 11 (1995) 2285–2292.
- [12] I. Dékány, L. Turi, Z. Király, CdS, TiO<sub>2</sub> and Pd<sup>0</sup> nanoparticles growing in the interlamellar space of montmorillonite in binary liquids, Appl. Clay Sci. 15 (1999) 221–239.
- [13] N. Khaorapapong, In situ complexation of thiourea in the interlayer space of copper(II)-montmorillonite, Appl. Clay Sci. 50 (2010) 414–417.
- [14] N. Khaorapapong, M. Ogawa, Solid state intercalation of 8-hydroxyquinoline into Li(I), Zn(II)- and Mn(II)-montmorillonites, Appl. Clay Sci. 35 (2007) 31–38.
- [15] N. Khaorapapong, M. Ogawa, In situ formation of bis(8-hydroxyquinoline) zinc(II) complex in the interlayer spaces of smectites by solid-solid reactions, J. Phys. Chem. Solids 69 (2008) 941–948.
- [16] N. Khaorapapong, M. Ogawa, Formation of mono(8-hydroxyquinoline) lithium(I) complex in smectites by solid-solid reactions, J. Phys. Chem. Solids 71 (2010) 1644–1650.
- [17] N. Khaorapapong, K. Kuroda, H. Hashizume, M. Ogawa, Solid state intercalation of 4,4'-bipyridine into the interlayer space of montmorillonites, Mol, Cryst. Liq. Cryst. 41 (2000) 351–356.
- [18] N. Khaorapapong, K. Kuroda, H. Hashizume, M. Ogawa, Solid state intercalation of 4, 4'-bipyridine and 1, 2-di(4-pyridine)ethylene into the interlayer space of Co(II)-, Ni(II)-, and Cu(II)-montmorillonites, Appl. Clay Sci. 19 (2001) 69-76.
- [19] N. Khaorapapong, K. Kuroda, M. Ogawa, Intercalation of 8-hydroxyquinoline into Al-smectites by solid-solid reactins, Clays Clay Miner. 50 (2002) 428–434.
- [20] N. Khaorapapong, K. Kuroda, M. Ogawa, Incorporation of thioacetamide into the interlayer space of montmorillonite by solid-solid reactions, Clay Sci. 11 (2002) 549–564.
- [21] N. Khaorapapong, P. Pimchan, M. Ogawa, Formation of mixed-ligand zinc(II)complex-montmorillonite hybrids by solid-solid reactions, Dalton Trans. 40 (2011) 5964–5970.
- [22] N. Khaorapapong, N. Khumchoo, M. Ogawa, Preparation of zinc oxide-montmorillonite hybrids, Mater. Lett. 65 (2011) 657–660.
- [23] N. Khaorapapong, A. Ontam, S. Youngme, M. Ogawa, Solid-state intercalation and in situ formation of cadmium sulfide in the interlayer space of montmorillonite, J. Phys. Chem. Solids 69 (2008) 1107–1111.
- [24] N. Khaorapapong, A. Ontam, M. Ogawa, Formation of MnS particles in the interlayer space of montmorillonite, Mater. Lett. 62 (2008) 3722–3723.
- [25] N. Khaorapapong, A. Ontam, J. Khemprasit, M. Ogawa, Formation of MnSand NiS-montmorillonites by solid-solid reactions, Appl. Clay Sci. 43 (2009) 238–242.

- [26] N. Khaorapapong, A. Ontam, M. Ogawa, Formation of ZnS and CdS in the interlayer spaces of montmorillonite, Appl. Clay Sci. 50 (2010) 19–24.
- [27] N. Khaorapapong, A. Ontam, M. Ogawa, Very slow formation of copper sulfide and cobalt sulfide nanoparticles in montmorillonite, Appl. Clay Sci. 51 (2011) 182–186.
- [28] A. Ontam, N. Khaorapapong, M. Ogawa, Simple preparation of a cadmium selenide-montmorillonite hybrid, J. Colloid Interface Sci. 357 (2011) 554–557.
- [29] L.K. Teh, V. Furin, A. Martucci, M. Guglielmi, C.C. Wong, F. Romanato, Electrodeposition of CdSe on nanopatterned pillar arrays for photonic and photovoltaic applications, Thin Solid Films 515 (2007) 5787–5791.
- [30] B. Xing, W. Li, H. Dou, P. Zhang, K. Sun, Systematic study of the properties of CdSe quantum dots synthesized in paraffin liquid with potential application in multiplexed bioassays, J. Phys. Chem. C 112 (2008) 14318–14323.
- [31] G. Kalyuzhny, R.W. Murray, Ligand effects on optical properties of CdSe nanocrystals, J. Phys. Chem. B 109 (2005) 7012–7021.
- [32] Y. Liu, H.-Y. Qiu, Y. Xu, D. Wu, M.-J. Li, J.-X. Jiang, G.-Q. Lia, Selective synthesis of wurtzite CdSe nanorods and zinc blend CdSe nanocrystals through a convenient solvothermal route, J. Nanopart. Res. 9 (2007) 745–752.
- [33] D.V. Talapin, A.L. Rogach, İ. Mekis, S. Haubold, A. Kornowski, M. Haase, H. Weller, Synthesis and surface modification of amino-stabilized CdSe, CdTe and InP nanocrystals, Colloids Surf., A: Physicochem. Eng. Aspects 202 (2002) 145-154
- [34] M. Behboudnia, Y. Azizianekalandaragh, Synthesis and characterization of CdSe semiconductor nanoparticles by ultrasonic irradiation, Mater. Sci. Eng. B 138 (2007) 65–68.
- [35] S. Yochelis, G. Hodes, Nanocrystalline CdSe formation by direct reaction between Cd ions and selenosulfate solution, Chem. Mater. 16 (2004) 2740–2744.
- [36] S. Levichev, P. Basa, Zs.J. Horváth, A. Chahboun, A.G. Rolo, N.P. Barradas, E. Alves, M.J.M. Gomes, Memory effect on CdSe nanocrystals embedded in SiO<sub>2</sub> matrix, Solid State Commun. 148 (2008) 105–108.

- [37] Y.-T. Nien, B. Zaman, J. Ouyang, I.-G. Chen, C.-S. Hwang, K. Yu, Raman scattering for the size of CdSe and CdS nanocrystals and comparison with other techniques, Mater. Lett. 62 (2008) 4522–4524.
- [38] R. Sathyamoorthy, V. Manjuladevi, P. Sudhagar, S. Senthilarasu, U. Pal, Surfactant-assisted room-temperature synthesis of CdSe nanoclusters, Mater. Chem. Phys. 105 (2007) 20–24.
- [39] M. Kristl, I. Ban, A. Danč, V. Danč, M. Drofenik, A sonochemical method for the preparation of cadmium sulfide and cadmium selenide nanoparticles in aqueous solutions, Ultrason. Sonochem. 17 (2010) 916–922.
- [40] J. Bao, Y. Shen, Y. Sun, J. Wu, X. Chen, N. Dai, J.C. Zhang, Controlled assembling of CdSe nanoparticles into the mesopores of SBA-15 via hot soap method, Physica E 40 (2008) 907–910.
- [41] O. Kozák, P. Praus, K. Kočí, M. Klementová, Preparation and characterization of ZnS nanoparticles deposited on montmorillonite, J. Colloid Interface Sci. 352 (2010) 244–251.
- [42] J.H. Li, C.L. Ren, X.Y. Liu, Z.D. Hu, D.S. Xue, Green synthesis of starch capped CdSe nanoparticles at room temperature, Mater. Sci. Eng. A 458 (2007) 319–322.
- [43] S.H. Liu, X.F. Qian, J.Y. Yuan, J. Yin, R. He, Z.K. Zhu, Synthesis of monodispersed CdSe nanocrystals in poly(styrene-alt-maleic anhydride) at room temperature, Mater. Res. Bull. 38 (2003) 1359–1366.
- [44] P. Wang, Y. Zhu, X. Yang, C. Li, H.L. Du, Synthesis of CdSe nanoparticles into the pores of mesoporous silica microspheres, Acta Mater. 56 (2008) 1144–1150.
  [45] M. Noh, T. Kim, H. Lee, C.-K. Kim, S.-W. Joo, K. Lee, Fluorescence quenching
- [45] M. Noh, T. Kim, H. Lee, C.-K. Kim, S.-W. Joo, K. Lee, Fluorescence quenching caused by aggregation of water-soluble CdSe quantum dots, Colloids Surf., A: Physicochem. Eng. Aspects 359 (2010) 39–44.
- [46] B. Kang, S.-Q. Chang, Y.-D. Dai, D. Chen, Synthesis of green CdSe/chitosan quantum dots using a polymer-assisted-radiation route, Radiat. Phys. Chem. 77 (2008) 859–863.
- [47] N. Kakegawa, T. Kondo, M. Ogawa, Variation of electron-donating ability of smectites as probed by photoreduction of methyl viologen, Langmuir 19 (2003) 3578–3582.